Design and Evaluation of Compact, Low SAR and EBG based Fractal Wearable Antennas for WBAN Applications

Submitted in partial fulfillment of the requirements for

the award of the degree

DOCTOR OF PHILOSOPHY

By

Mallavarapu Sandhya

(Roll No. 718045)

Under the guidance of

Prof. L. Anjaneyulu

Department of Electronics & Communication Engineering

NATIONAL INSTITUTE OF TECHNOLOGY WARANGAL, INDIA

December – 2022

APPROVAL SHEET

This Thesis entitled **"Design and Evaluation of Compact, Low SAR and EBG based Fractal Wearable Antennas for WBAN Applications"** by **MALLAVARAPU SANDHYA** is approved for the degree of **Doctor of Philosophy.**

Examiners

Supervisor

Dr. L. Anjaneyulu

Professor, ECE Dept., NIT WARANGAL

Chairman

Dr. P. Srihari Rao

Professor & HOD, ECE Dept.,

NIT WARANGAL

Date:

DECLARATION

I hereby declare that the matter embodied in this thesis entitled "**DESIGN AND EVALUATION OF COMPACT, LOW SAR AND EBG BASED FRACTAL WEARABLE ANTENNAS FOR WBAN APPLICATIONS**" is based entirely on the results of the investigations and research work carried out by me under the supervision of **Dr. L. Anjaneyulu**, Professor, Department of Electronics and Communication Engineering, National Institute of Technology Warangal, India. I declare that this work is original and has not been submitted in part or full, for any degree or diploma to this or any other University, and was not submitted elsewhere for the award of any degree.

I declare that this written submission represents my ideas in my own words and where others ideas or words have been included. I have adequately cited and referenced the original sources. I also declare that I have adhered to all principles of academic honesty and integrity and have not misrepresented or fabricated or falsified any idea/date/fact/source in my submission. I understand that any violation of the above will be cause for disciplinary action by the institute and can also evoke penal action from the sources which have thus not been properly cited or from whom proper permission has not been taken when needed.

(Mallavarapu Sandhya)

(718045)

Date:

Place: Warangal

National Institute of Technology, Warangal

(Deemed University)

CERTIFICATE

This is to certify that the thesis entitled "**DESIGN AND EVALUATION OF COMPACT, LOW SAR AND EBG BASED FRACTAL WEARABLE ANTENNAS FOR WBAN APPLICATIONS**" being submitted by **Mrs. Mallavarapu Sandhya** in partial fulfillment for the award of the degree of *Doctor of Philosophy in Department of Electronics and Communication Engineering* of National Institute of Technology Warangal, is a record of bonafide research work carried out by her under my supervision. To the best of our knowledge, the work incorporated in this thesis has not been submitted elsewhere for the award of any degree.

Prof. L. Anjaneyulu,
(Supervisor)
Dept. of Electronics & Communication Engineering,
National Institute of Technology Warangal
Warangal, India – 506004.

Dedicated To

My Guru Prof. Lokam. Anjaneyulu, who taught me, constantly encourages me and the one who always make me confortable in his presence.

To my dear (late) father Mallavarapu. Brahmanachari
"Though you never got to see this, you're on every page"
&
To my loving and caring husband Karaka. Satya Bhaskar, for your patience, friendship, and letting me experience the kind of love that people freely die for.

ACKNOWLEDGEMENTS

It gives me immense pleasure to express my deep sense of gratitude and sincere thanks to my supervisor and mentor, **Dr. L. Anjaneyulu**, Professor, Department of Electronics & Communication Engineering, National Institute of Technology, Warangal, for his perpetual encouragement, invaluable guidance, and suggestions. His steady influence throughout my Ph.D. career has oriented me in a proper direction and supported me with promptness and care. His knowledge, logical and thought-provoking advice, and discussions both technically and morally helped me to become a capable researcher. He not only gave me the required knowledge to pursue my research through the subjects he taught but also always gave the required moral support during my hard times. He inculcated in me a never-ending motivation and zeal towards my research efforts, as well as encouraged my presentation skills regularly. His encouragement helped me to overcome the difficulties encountered in my research as well as in my personal life.

I wish to express my thanks to **Prof. P.Srihari Rao**, Head, Dept. of E.C.E., as chairman of the DSC for his kind support. I would like to thank **Prof. D. Vakula,** one of my doctoral Scrutiny Committee members, for sharing her extensive experience in Antenna, RF/microwave design and his invaluable assistance in academic work and extend my thanks to **Dr. Gopi Ram,** Assistant Professor, one of my Doctoral Scrutiny Committee member, for his valuable suggestions throughout my semester presentations.

I take this privilege to thank my external Doctoral Scrutiny Committee member, **Prof. D. Srinivasacharya**, Professor of Mathematics Department, for his detailed review, constructive suggestions, and excellent advice during the progress of this research work.

I am thankful to **Prof. Bheemarao**, former Head, Dept. of E.C.E., for his help and cooperation. I thank all the faculty and non-teaching staff of the Dept. of ECE, especially Microwave lab assistant T. Venkateshwarlu at NIT Warangal, who helped me during the research period.

I thank my nation India, for giving me the opportunity to carry out my research work at the NIT Warangal. A special thanks to **MHRD** for its financial support. I wish to express my sincere thanks to **Prof. N.V. Ramana Rao**, Director, NIT Warangal, for his official support and encouragement.

I want to mention my sincere and special thanks to **Mr. Pingali. Vikram Kumar**, Science communicator, Hyderabad, and his team for his continuous support that has helped me so much during this period. Also, I would like to extend my thanks to the team of **Cosmic Enterprises,** Hyderabad, for supporting the fabrication of Patch antennas.

I take this opportunity to convey my regards to my closest friends for always being next to me. Thanks to Dr. B.Surekha, Dr.Ch.Sulakshana, Dr.D.Kiran, Dr.R.Sahoo, Dr.B.pranitha, Dr.R.Swetha, Dr. Umar Farooq and Adi Surendra Mohana Raju, Department of Electronics and Communication Engineering, for their constant motivation throughout the work. With all your support and encouragement, my study life has become happy in all respects!

I acknowledge my gratitude to all my teachers and colleagues at various places for supporting and cooperating with me to complete the work. I'm very grateful to my mother, Padma Priya, and father Brahmanachari (Late) for successfully carrying out my research work. Finally, I render my respect and acknowledge my biggest debt to my mother-in-law K. Jogiratnam, who wished to see me as Dr. Sandhya, and my father-in-law for supporting me financially and mentally. They have motivated and helped me to complete my research work successfully. I would like to thank my beloved daughter Adya Girvani for her support. Last but not least, I am very much grateful to my dear husband, K. Satya Bhaskar, for his support, encouragement, understanding, and sacrifices, which helped and motivated me a lot throughout the time of my research. I could not have done it without you.

Mallavarapu Sandhya

Abstract

Recently, body-centric communication has become one of the most attractive fields of study. The versatile applications of Wireless Body Area Network (WBAN) communications are not only being used for health monitoring but also real-time communication purposes in special occupations. An inevitable part of any such system is antennas, which are required to ensure the wireless transfer of the signal, either within or outside the body, depending on the application. The wearable antenna embedded into clothing finds its use in wireless communications, including tracking and navigation, mobile and wearable computing, and public safety and security. For user accessibility, there is a growing requirement for incorporating antennas on or in clothing. Given the constraints in power, size, weight, conformity, and deformability, one of the most challenging parts is the designing antenna for such communication systems. In the process of designing a textile antenna, the availability of electromagnetic properties such as permittivity and loss tangent of the fabrics is pivotal to mounting the radiator on regularly worn clothes. On the other hand, the wearable antennas must operate near the human body scenario and undergo several deformations depending on the dynamic movements of the human body. To ensure robust performance, the aforementioned factors must be accounted for in the design of the wearable antenna.

Consequently, prior to the designing of the body wearable antennas, these supplementary issues must be addressed. One of which is the realization of the electromagnetic properties of the fabrics used in the design. Accordingly, the thesis addressed the issue by the Microstrip Ring Resonator (MRR) method. The achieved result is verified by the second method focused on the simulation of the patch radiator. The second and third subsidiary issues are related to deformations and near human scenarios. The wearable antennas are likely to undergo deformations such as bending and crumpling while worn on the human body with its curvatures and complexities. The structural deformations, mismatches, and losses associated with the human body affect the performance of the wearable antenna. To get more insights, an electrical equivalent model is also designed to realize the potentials inside the geometry of the wearable

antenna under a bending environment. In this regard, it is important to appreciate the effect of the human body and deformations on the performance of body-worn antennas, which is also addressed in this thesis. The structural bending of the wearable antennas proposed in this thesis is situated on the foam cylinders of radii 40 mm, 50 mm, and 70 mm, whose radii are carefully picked to represent the model hand, arm, and chest of the human body. Further, the proposed wearable antennas are tested on a real human volunteer instead of relying on simulation models, which adds practicality and robustness to the thesis.

Nevertheless, it is essential to achieve superior performance wearable antennas for less impact of frequency detuning, improved Front to Back Ratio (FBR), high radiation efficiency, and reduced Specific Absorption Rate (SAR) for WBAN application. This doctoral thesis deals with the design of compact, multiband wearable antennas with the use of Fractal technology and studying their performance by integrating with Electromagnetic bandgap (EBG) and Defected Ground Structures (DGS) in the body-centric environment by focusing on the specific characteristics of such an environment compared to free space. The Novel EBG structures can act as reflective surfaces and tend to improve the isolation between the human body and the antenna, and DGS can provide compact antenna designs with enhanced performances at required frequencies. Subsequently, it is vital to select appropriate topologies for the wearable antenna in WBAN applications. Though microstrip patch antennas are simple in design and very useful for wearable applications, they have limitations like narrow bandwidth, lower radiation efficiency, and surface wave losses. An alternative to such antennas is found by incorporating radiating elements of different shapes and feeds, such as microstrip line fed patch and CPW fed patch, as they exhibit high performance with a simple fabrication process. Additionally, designing dual-band or multiband wearable antennas is a challenging task as the frequency of operation is determined by the fixed ratios. In regards to these challenges, this thesis anticipated and authenticates the following solutions:

1. A Microstrip Ring Resonator (MRR) method is employed in estimating the electromagnetic properties of the textile substrates due to its feasible geometry, ease in prototyping, low price, small volume, and adaptability. Also, two wearable antennas with inset and aperture coupled feeding methods are designed, fabricated, and experimentally validated the performance under flat and deformation scenarios. To get the insight

behavior of the proposed antennas, an equivalent circuit is derived and analyzed using the ADS software package. The antennas are designed to operate at 2.5 GHz frequency in WLAN standards.

2. A Robust, Efficient, and Low Profile Fractal Enabled EBG Incorporated Wearable Antenna for WLAN Standards is proposed and validated. Avoiding vertical vias of conventional EBGs, the new topology of uniplanar configuration EBG (UC-EBG) is shown to be robust and comfort to the effect of the human body and mechanical deformations. The antenna is targeted to cover ISM band frequencies with a center frequency of 2.45 GHz. A salient feature of this antenna is achieving a low SAR, enhanced gain, and FBR, while maintaining optimum performance for the deformations and near human body.
3. A Fully Flexible, High Gain Saw-tooth Shaped Boundary Fractal Wearable Patch Antenna for WBAN Applications is anticipated and validated experimentally. The striking feature of this antenna topology is that it is compact and simple to design and easy to fabricate on flexible substrates while achieving high gain with low SAR.
4. A Dual-band EBG-DGS incorporated wearable antenna for Emergency services and responses in WBAN is proposed and validated. A noticeable feature of this antenna is improved gain and SAR along with the co & cross-polarized fields with the utilization of DGS in the ground plane of EBG. The DGS improves Cross-polarization and co-polarization by changing the fields in the ground plane at the back of EBG.
5. An Improved wearable, breathable, triple band EBG loaded CPW fed fractal textile antenna for WBAN applications is proposed and validated. The porous ground plane of EBG not only improves the bandwidth of the final antenna but also improves the breathability and wearability of the design. The outstanding feature of this antenna is that it is highly breathable, triple band with optimum gain performance. Additionally it shows stable performance for the deformation and human tissue loading.
6. A flexible, compact and triple band step shaped Sierpinski fractal antenna on a Hilbert patterned ground plane is proposed and experimentally validated for Wearable-Wireless Body Sensor Networks (W-WBSN) applications. The remarkable features of this antenna are high efficient, high gain while resonating at multiple bands. Further, it is highly radiation safe to use in near human scenario.

7. A Compact, Flexible, Circularly polarized wearable antenna for wireless applications is proposed and validated. A significant feature of this antenna is achieving the circular polarization with a simple defected and insertion of two rectangular stubs ground plane of the anticipated antenna. Further, the proposed antenna has high axial ratio bandwidth, and SAR is within standards.

Overall, this thesis holistically explores a range of issues related to the realization and utilization of wearable antennas for body-worn applications. Hence the contribution of the thesis laid a strong foundation for future wearable antenna deployment.

Contents

ACKNOWLEDGEMENTS **vi**

ABSTRACT **viii**

LIST OF FIGURES **xvii**

LIST OF TABLES **xxii**

LIST OF ABBREVATIONS **xxv**

LIST OF SYMBOLS **xxvii**

Chapter 1- Introduction 1

1.1. Definitions and basic concepts **9**

1.1.1. S-parameters 11

1.1.2. Impedance Bandwidth 13

1.1.3. Gain and antenna efficiency 14

1.1.4. Radiation pattern 15

1.1.5. Specific Absorption Rate (SAR) 16

1.2. Wearable technology **16**

1.2.1. Examples of Wearable Technology 18

1.2.2. Applications of wearable antennas 18

1.3. Basic antennas for wearable communication systems **20**

1.3.1. Dipole Antenna 21

1.3.2. Monopole Antennas 21

1.3.3. Loop Antennas 21

1.3.4. Slot Antennas 21

1.3.5. Microstrip Antennas 22

1.4. Interpretation of Microstrip Patch antenna **22**

1.4.1. Microstrip patch antenna feeding techniques 25

1.4.1.1. Microstrip line feed 25

1.4.1.2. Coaxial Feed 26

1.4.1.3. Aperture coupled feed 26

1.4.1.4. Proximity coupled patch antenna 27

1.4.1.5. Coplanar waveguide (CPW) feed 28
1.5. Overview of the previous work on wearable antennas 29
1.6. Wearable antenna fabrication 34
1.7. Wearable antenna measurement 37
1.7.1. Commercial simulation software packages 37
1.7.2. Measurement of various parameters 41
1.7.1.1. Return loss 41
1.7.1.2. Anechoic chamber 42
1.7.1.3. Specific Absorption Rate (SAR) 43
1.8. Motivation and problem formulation 44
1.9. Objectives and scope of the research 46
1.10. Contribution to the knowledge 46
1.11. Organization of thesis 47

Chapter 2- Wearable antennas: Electrical equivalents 51

2.1. Introduction 51
2.2. Theoretical analysis of wearable antennas 52
2.3. Textiles and their EM characteristics 56
2.3.1. Dielectric fabrics 58
2.3.2. Conductive fabrics 59
2.3.3. Dielectric properties of fabrics 60
2.4. Design of Wearable antenna using various feeding methods 63
2.4.1. Inset-fed wearable patch antenna and its electrical equivalent 63
2.4.2. Aperture coupled patch antenna and its electrical equivalent 66
2.5. Bending characterization and Electrical modeling 69
2.6. Effect of Bending on the performance of the Antenna 71
2.6.1. Effect on Resonant frequency and impedance match 72
2.6.2. Effect on Electric field intensity 74
2.6.3. Effect on the Radiation pattern 75
2.7. Summary 76

Chapter 3- Microstrip line fed Wearable antennas for On-Body Applications **78**

3.1. Introduction **78**
3.2. Saw-tooth Shaped Boundary Fractal Wearable Patch Antenna **79**
3.2.1. Geometrical evolution of the proposed antenna 79
3.3. Performance of the antenna under flat and deformations **81**
3.3.1. Reflection coefficient under Flat condition 81
3.3.2. Reflection coefficient under deformation 82
3.3.3. Radiation characteristics 85
3.4. Gain measurement **88**
3.5. Antenna performance on human tissue loading **89**
3.5.1. Electromagnetic Characteristics of Human Tissue 89
3.5.2. Numerical phantoms 90
3.1.1.1. Theoretical phantoms 90
3.1.1.2. Voxel phantoms 90
3.6. Inferences from Results and Discussions **90**
3.7. Wearable step-shaped Sierpinski Fractal antenna **94**
3.7.1. Anticipated antenna structure 95
3.7.2. Free space analysis 97
3.7.3. On-Body Analysis 99
3.7.4. SAR simulations 101
3.8. Summary **102**

Chapter 4- Flexible monopole antenna incorporated with EBG structure **104**

4.1. Introduction **104**
4.2. Design considerations and operating principles of EBG **108**
4.3. Characterizations of EBG **110**
4.3.1. Reflection phase method 110

4.3.2. Suspended transmission line method 111
4.3.3. Dispersion diagram 112
4.4. Fractal Enabled EBG Incorporated Wearable Antenna 113
4.4.1. Design and configuration 113
4.4.2. Electrical Equivalent 116
4.4.3. Proposed EBG Design and Electrical Equivalent 118
4.5. Performance of the integrated antenna in free space 119
4.5.1. Reflection coefficient 119
4.5.2. Radiation pattern 120
4.5.3. Banding effects 121
4.6. Performance of the integrated antenna on the human body 124
4.7. SAR analysis 126
4.8. Summary 126

Chapter 5 – Dual-band, EBG-DGS Wearable antenna for WBAN Applications 128

5.1. Introduction 128
5.2. Design and configuration of the proposed dual-band antenna 130
5.3. Proposed EBG structure 132
5.3.1. Reflection phase characteristics 133
5.3.2. Transmission characteristics 134
5.4. Defected Ground Structures (DGS) 135
5.4.1. Characteristics of DGS 135
5.4.1.1. Slow wave Propagation in Pass Band 135
5.4.1.2. Band Stop Characteristics 134
5.4.2. Advantages of defected ground structure 136
5.4.3. Proposed DGS array 137
5.5. Performance of the integrated antenna in free space 138
5.5.1. Reflection coefficient 138
5.5.2. Radiation pattern 139

5.5.3. Gain and Radiation efficiency 141
5.5.4. Co-polarization and cross-polarization 141
5.6. Deformation effects 143
5.6.1. On reflection coefficient 143
5.6.2. On radiation pattern 144
5.7. Summary 145

Chapter 6- Improved wearable, breathable triple band antenna integrated with porous EBG 147

6.1. Introduction 147
6.2. Triple band CPW fed wearable antenna 148
6.3. Triple band porous EBG design 149
6.4. Performance of Perforated EBG Loaded CPW Antenna 152
6.4.1. Under Flat state 152
6.4.2. Under Deformations 154
6.5. Integrated antenna performance on-body 156
6.6. SAR 158
6.7. Summary 159

Chapter 7- Conclusions and Future scope 161

7.1. Conclusion 161
7.2. Future Scope 162
List of publications out of this research work 164
References 166

LIST OF FIGURES

Figure No	Title	Page No
Fig.1.1	Basic mechanism of Radiation for a single conducting wire	10
Fig.1.2	Radiation from an antenna	11
Fig.1.3	Reflection coefficient curve of microstrip patch antenna showing usable bandwidth and resonant frequency	13
Fig.1.4	3D radiation pattern of a directional antenna	15
Fig.1.5	The most sophisticated wearable devices available in the present market (a) AI based hearing aids (b) Google glass (c) Microsoft's HoloLens (d) Disposable skin patch with sensors	17
Fig.1.6	Applications of wearable antennas	20
Fig.1.7	Different shapes of Patch radiator	22
Fig.1.8	Rectangular microstrip patch antenna showing the fringing effect	23
Fig.1.9	Microstrip patch antenna with inset feed	25
Fig.1.10	Coaxial probe feed microstrip patch antenna	26
Fig.1.11	Aperture coupled microstrip patch antenna	27
Fig.1.12	Proximity couple patch antenna	28
Fig.1.13	CPW fed patch antenna	28
Fig.1.14	Fabrication process of an antenna pattern	35
Fig.1.15	Inkjet printing	35
Fig.1.16	Common manufacturing techniques of conductive textiles	36
Fig.1.17	(a) Scalpel cutting tool set (b) Foam cylinders represent the human body parts	37
Fig. 1.18	Various solvers offered in CST MW Studio	39
Fig.1.19	CST Design Environment	40
Fig.1.20	(a) Measurement setup for the radiation pattern measurement (b) Inside the Anechoic chamber at NITW	42
Fig.1.21	Textile antennas wrap around the foam cylinder along E, H-plane directions	43

Fig.1.22	Simulated SAR of the example antenna (a) on standard four layer human phantom (b) on HUGO Voxel model	44
Fig.2.1	(a) Slot-loaded patch and (b) Equivalent circuit model of the slot-loaded patch	54
Fig.2.2	(a) Slot and notches loaded on the patch and (b) Equivalent circuit model of the slot and notch loaded patch antenna	56
Fig.2.3	Flow chart of the wearable antenna design flow	58
Fig. 2.4	(a) Schematic of the MRR (b) Prototype	60
Fig.2.5	S21 (dB) Vs. Frequency of MRR	62
Fig. 2.6	(a) Geometrical profile (b) Fabricated prototype of the inset fed wearable patch antenna	64
Fig. 2.7	(a) Simulated equivalent circuit in ADS (b) Reflection coefficient plot of inset fed microstrip patch antenna	65
Fig. 2.8	(a) Scheme of Aperture coupled wearable patch antenna (b) Front view (c) Back view of fabricated prototype (d) Experimental setup	67
Fig.2.9	(a) Circuit model (b) Reflection coefficient curve of aperture coupled patch antenna	69
Fig.2.10	(a) Antennas wrapped around foam cylinders in E, H-plane directions (b) Equivalent circuit of a bent patch antenna	71
Fig.2.11	Return loss variations for different bending cases for (a) AC-WPA on E-plane (b) Inset fed patch antenna on E-plane (c) AC-WPA on H-plane (d) Inset fed patch antenna on H-plane	73
Fig.2.12	Electric field variations of (a) Inset fed (b) Aperture coupled wearable antenna on different bending fixtures.	74
Fig.2.13	2D Radiation pattern variations of (a) Aperture coupled (b) Inset fed wearable patch antenna in different bending situations	76
Fig.3.1	S11 curves for various iterations of the anticipated fractal boundary patch antenna	80
Fig.3.2	(a) Scalpel cutting tools set (b) Front view of the fabricated antenna	81
Fig. 3.3	Reflection coefficient of the anticipated antenna	82

Fig.3.4	Proposed antenna bends on foam cylinders along E; H-plane (a) simulated (b) Practical	83
Fig.3.5	Effect of bending on the anticipated antenna under various bending scenarios (a) E-plane bending (b) H-plane bending	84
Fig.3.6	Simulated Radiation patterns (dB) along (a) E-plane (b) H-plane, Measured radiation patterns (dBm) along (c) E-plane (d) H-plane	87
Fig.3.7	Measurement setup inside the anechoic chamber for radiation pattern	87
Fig.3.8	Simulated and measured peak gain of the anticipated antenna	88
Fig. 3.9	Positioning of the proposed antenna on (a) Chest (b) arm along Y-axis (c) arm along X-axis	91
Fig.3.10	S11 curves of the proposed antenna when located on the chest and arm	92
Fig.3.11	Radiation patterns of the proposed antenna when placed on the human body	92
Fig.3.12	The geometry of the proposed antenna (a) Front view (b) Back view (c) Photograph of the fabricated prototype (c) Front view (d) Back view	96
Fig.3.13	Comparison of the simulated and measured S11 curves of the proposed antenna	97
Fig.3.14	Surface current distribution at (a) 3.3 GHz (b) 5.2 GHz (c) 5.8 GHz	98
Fig.3.15	Radiation patterns of the proposed antenna in free space at (a) 3.3 GHz, (b) 5.2 GHz, (c) 5.8 GHz	99
Fig.3.16	Model of the four-layered human phantom with the proposed antenna along with specified dimensions	99
Fig.3.17	(a) Simulated and measured S11 on the Human body (b) Proposed design on chest and arm	100
Fig.3.18	Simulated and measured radiation patterns on the body at (a) 3.3 GHz, (b) 5.2 GHz, (c) 5.8 GHz	101
Fig.3.19	SAR of the proposed antenna for 10g of average Human tissue at	102

	(a) 3.3 GHz, (b) 5.2 GHz, (c) 5.8 GHz	
Fig.4.1	(a) A woodpile 3-D EBG structure (b) A mushroom 2-D EBG surface (c) A Uniplanar (UC-EBG) structure	106
Fig.4.2	Identifying bandgap of EBG surface using (a) Dispersion diagram (b) Reflection phase	107
Fig.4.3	(a) Parameters of via-EBG (b) Equivalent circuit of EBG unit cell	109
Fig.4.4	(a) Antenna situated close to ground plane (b) Antenna situated far from the ground plane (c) Antenna integrated with EBG surface in very close proximity with the ground plane	111
Fig. 4.5	Suspended transmission line method of EBG	112
Fig. 4.6	Numerical model of a mushroom type EBG unit cell in CST MW Studio for dispersion diagram calculation	113
Fig. 4.7	(a) S11 of evolution process (b) Front view (c) Back view of the anticipated geometry of the monopole antenna	114
Fig.4.8	(a)Fabricated prototype (b) S11 evaluation of simulated and measured antenna.	115
Fig.4.9	Equivalent circuit of (a) Simple monopole patch (b) notch loaded patch (c) DGS equivalent (d) proposed antenna	117
Fig.4.10	(a) The layout of EBG array of unit cells (b) Equivalent circuit (c) Reflection phase diagram (d) Dispersion diagram of the proposed EBG unit cell	119
Fig.4.11	(a) Reflection coefficient of EBG integrated antenna, (b) The current distribution of antenna alone (c) Current distribution of EBG integrated antenna	120
Fig.4.12	Radiation properties of the proposed antenna along (a) y-z (b) x-z plane at 2.45 GHz	121
Fig.4.13	S11 variations of the anticipated antenna on various bend diameters along (a) x-z (b) y-z planes (c) On Human equivalent hand and chest tissue	123

Fig.4.14	Radiation patterns of the proposed antenna under various banding situations along (a) x-z (b) y-z planes at 2.45 GHz	124
Fig.4.15	(a) Variation of S11 on the human body (b) radiation pattern at 2.45 GHz (c) Variation of gain along with the frequency for the anticipated antenna	125
Fig.4.16	Evaluation of SAR for 10 g of tissue on (a) Chest (b) Arm	126
Fig.5.1	Geometry of the anticipated dual band antenna	131
Fig.5.2	Prototype of the proposed antenna (a) Front view (b) Back view (c) Comparison between simulated and measured S_{11} curves	132
Fig.5.3	(a) Proposed configuration of the EBG unit cell (b) Fabricated EBG array	133
Fig.5.4	Reflection phase and impedance diagram of proposed EBG unit cell	134
Fig.5.5	Transmission characteristics of the proposed EBG surface	135
Fig.5.6	(a) Suspended line method of DGS; Surface current distribution of the proposed DGS array at (b) 2.45 GHz, (c) 5.85 GHz, (d) DGS array etched on the ground plane of EBG structure	137
Fig.5.7	(a) The configuration of the proposed antenna; (b) Fabricated prototype front and back view; (c) Reflection coefficient of the anticipated antenna	139
Fig.5.8	Radiation patterns (a) E-plane; (b) H-plane at 2.45 GHz; (c) E-plane; (d) H-plane at 5.85 GHz	140
Fig.5.9	Simulated co- and cross-polarization of the proposed antenna in (a) H-plane; (b) E-plane at 2.45 GHz, 5.85 GHz, respectively	142
Fig. 5.10	Photograph of the proposed antenna when wrapped around the foam cylinders of different radii R along (a) E-plane and (b) H-plane	143
Fig. 5.11	Bending performance of the anticipated antenna on reflection coefficient (a) E-plane; (b) H-plane	144
Fig.5.12	Influence of bending on radiation pattern at (c) 2.45 GHz; (d) 5.85	145

	GHz	
Fig.6.1	(a) Geometrical configuration (b) Fabricated prototype (c) Evolution of the proposed design in terms of reflection characteristics	149
Fig.6.2	Schematic of Porous EBG Structure (a) Frontal (b) Backward View, Snapshot of the fabricated prototype (c) Frontal (d) Backward view	150
Fig.6.3	Simulated Reflection characteristics of Perforated EBG unit cell	151
Fig.6.4	Surface current distribution on EBG unit cell at (a) 2.45 GHz (b) 3.5 GHz (c) 5.4 GHz	151
Fig.6.5	Fabricated prototype of the proposed antenna	152
Fig.6.6	a) Measured and simulated S_{11} of the proposed antenna, Radiation patterns comparison of the CPW antenna and PEBG antenna in free space at (b) 2.45 GHz (c) 3.5 GHz (d) 5.5 GHz	154
Fig.6.7	(a) S11 curves of the deformed integrated antenna under bending for various radii along (a) y-axis (b) x-axis	155
Fig.6.8	Radiation patterns of the integrated antenna under bending of radius 70 mm along the y-axis	156
Fig.6.9	(a) Numerical model of chest developed in CST (b) S11 curves of the integrated antenna on real human	157
Fig.6.10	Comparison of Radiation performance of the integrated antenna on the body at (a) 2.45 GHz (b) 3.5 GHz (c) 5.5 GHz	158
Fig.6.11	SAR analysis for an average 10g tissue at (a) 2.45 GHz (b) 3.5 GHz (c) 5.5 GHz	159

LIST OF TABLES

Table No	Title	Page No
Table.1.1	Radio frequency spectrum- applications	3
Table.1.2	Diverse Communication bands	5
Table.1.3	Features of WBAN (IEEE 802.15.6 Standard)	7
Table.1.4	Various frequency bands in WBAN	7
Table.2.1	Optimized dimensions of the MRR	61
Table. 2.2	Resultant dielectric properties of Jeans Substrate using the method of Ring Resonator	62
Table. 2.3	Dimensions of the inset fed wearable patch antenna	63
Table.2.4	Optimized dimensions of the Aperture coupled wearable patch antenna	68
Table.2.5	Gain and efficiency variations of the proposed antennas for various bending radii	75
Table.3.1	Assessment of bending behavior of the anticipated antenna with the regular square shape of the radiator	83
Table.3.2	Electromagnetic Properties of Some of Human Tissues at 2.45 GHz	89
Table.3.3	Simulated SAR value	93
Table.3.4	Comparison of the proposed antenna with the state art designs	93
Table.3.5	The optimized dimensions of the proposed antenna	96
Table.3.6	Simulated SAR values of the proposed antenna	102
Table.4.1	SAR evaluation for chest and Arm models	126
Table.4.2	Comparison of the proposed antenna against the previously published literature	127
Table.5.1	Comparison of modern wireless technologies	128
Table.5.2	Optimized Dimension of the Dual-Band Monopole Antenna	131
Table. 5.3	Detailed Dimensions of the Proposed EBG Unit Cell	133
Table.5.4	Comparison of Gain and Radiation Efficiency of a Monopole Antenna, EBG Based Monopole Antenna, Monopole Antenna with	141

	DGS Loaded EBG Structure	
Table.5.5	Comparison of the Proposed Work against the Previously Published Literature	146
Table.6.1	Parameters of the proposed antenna	148
Table.6.2	Simulated SAR of the proposed antenna	159
Table.6.3	Comparison of wearable breathable antenna against previously published literature	160

LIST OF ABBREVIATIONS

ADS	Advanced Design System
AMC	Artificial magnetic conducting
AR	Axial Ratio
AUT	Antenna Under Test
ARBW	Axial ratio bandwidth
BW	Bandwidth
CAD	Computer Aided Design
CP	Circularly Polarized
CPW	Coplanar waveguide
CST	Computer Simulation Technology
DS	Dumbbell Shape
DGS	Defected Ground Structures
EBG	Energy band gap
EM	Electromagnetic
FCC	Federal Communications Commission
FDTD	Finite Difference Time Domain
FEM	Finite Element Method
FOM	Figure of merit
FSS	Frequency Selective Surface
GPS	Global Positioning System
GSM	Global System for Mobile Communication
HF	High Frequency
HFSS	High Frequency Structure Simulator
HP	Hewlett Packard
IEEE	Institute of Electrical and Electronics Engineering
IL	Insertion Loss
IOT	Internet of things
ISM	Industrial, Scientific and Medical
LF	Low Frequency

MIMO	Multiple-Input Multiple -Output
MoM	Method of Moments
PCB	Printed Circuit Board
PCS	Personal Communication Service
PRS	Partially Reflective Surface
RF	Radio Frequency
RFID	Radio Frequency Identification
RL	Return Loss
RMPA	Rectangular microstrip patch antenna
SAR	Specific Absorption Rate
UWB	Ultra Wideband
VNA	Vector Network Analyzer
VSWR	Voltage Standing Wave Ratio
WLAN	Wireless Local Area Network
Wi-Bro	Wireless Broadband
Wi-Fi	Wireless Fidelity
WiMAX	Worldwide Interoperability Microwave Access
WBAN	wireless Body area network

List of Major Symbols

εr	:	Dielectric constant
εeff	:	Effective relative permittivity
C_0	:	Speed of light in free space
γ	:	Propagation constant
®	:	Phase constant
⎫	:	Angular frequency
k	:	Wave number (/m)
α	:	Attenuation constant
λ_g	:	Guided Wavelength
λ_0	:	Wavelength in air
Z_0	:	Characteristic impedance
f_0	:	Center frequency
S	:	Scattering parameters

Chapter 1.

Introduction

Technology is persistently experiencing a principal expansion instigated by the emergence of many innovative interconnected “things” and their fortress in our day-to-day life [1]. The wearables set forth its footprint with the creation of eyeglasses in the 13th century by English friar Roger Bacon who drew the operating mechanisms behind the use of corrective lenses in his experiment Opus Majus [2]. Later, the lenses were towering in the smart glasses industry. In the early 16th century, the first pocket mechanical watch was found, which is easily carried anywhere. The journey of wearables toward modern smart rings and smart computers started with the Abacus ring in the 17th century [3]. This helps the traders for calculations and hence becomes the compact smart computer. The initial wireless systems were redesigned during the reign and were heavy, usually carried by cavalry horses.

A revolution started with the invention of the “packest system,” also known as the “Walkie-talkie,” employed by Donald Hings in 1937 [4]. Later, the trends of wristwatches were initiated and are necessitated for planning and co-ordination of various functions of military operations, thus, adopted wristwatches universally [5]. In 1961, Edward O. Thorpe and Claude Shannon hid a timing device in the shoe which can precisely forecast the location of the ball on a roulette table [6]. In 1968, Ivan Sutherland discovered the first ever virtual reality Head Mounted Display (HMD) system supporting the wearer to submerge them in a 3D virtual environment [7]. A momentous development in the smart watch industry occurred with the invention of the Pulsar Calculator Watch in 1975 [8]. The Private Eye head-mounted display devised in 1989 which is the second great-grandfather of Google Glass.

The start of the 90s came to the limelight with the invention of the Active Badge to track locations [9]. In 1998, the wearable payment era started, still existing in Apple and Android

watches. The year 2001 is renowned for the emergence of the very first Plantronics M1000 Wireless Headset, which has been accompanied by the rollout of the lightweight M1500 [10]. The first GoPro camera was presented to the globe in 2004 [11]. James Park and Eric Friedman originated Fitbit at the beginning of 2007 [12]. 2014 could be considered the year of the personal activity tracker surge. Apple unveiled its 1st wearable device, the Apple Watch, in 2015, urged by the technological race [13]. Conventional activity trackers were insufficient for monitoring patient conditions on a routine basis, which is why Apple created the Watch.

Recently, flexible wearable electronics have towered cutting-edge technologies in both academia and industry. The long-established broadcasting systems to the latest spacecraft systems and wireless communications have unfolded a requisite part of daily human lives. Radio frequency and wireless communications encompass the utilization of electromagnetic waves of diverse frequencies. Various frequency ranges are used in diverse applications. Since the thesis focused on the design of wearable antennae for various WBAN applications, it is significant to comprehend various frequency ranges and facilities that are employed at these frequencies in RF and wireless communications. WBAN systems have been assigned a number of frequency bands, such as medical implantable communications systems (MICS), Industrial, Scientific, medical (ISM) bands, and Ultra-wideband (UWB). The network made by IEEE 802.15.6 compliant devices is recognized as WBAN (Wireless Body Area Network). It is instigated to emerge communication models for low-power devices that can install on or inside the human body for numerous applications such as medical, consumer electronics, entertainment, etc. The electromagnetic spectrum specifying the band designations wave propagation characteristics and applications are summarized in Table.1.1.

Table 1.1. Radio frequency spectrum- applications

Frequency range	**Wavelength**	**Class**	**Characteristics**	**Services**
3 Hz-30 Hz	10-100 Mm	Extremely low frequency (ELF)	High atmospheric noise, inefficient antennas	In seismic studies, researchers use this frequency range to analyse natural

				processes occurring in the earth's atmosphere.
30 Hz-300 Hz	1-10 Mm	Super low frequency (SLF)	High atmospheric noise	Power transmission and submarine communications.
300 Hz-3 kHz	0.1-1 Mm	Ultra-low frequency (ULF)	High atmospheric noise	Telephone and audio.
3–30 kHz	10-100 km	Very low frequency (VLF)	High atmospheric noise	Navigation positioning and SONAR
30–300 kHz	1-10 km	Low frequency (LF)	High atmospheric noise	Long-range navigation beacons.
300–3,000 kHz	0.1-1 km	Medium frequency (MF)	High atmospheric noise and good ground wave propagation.	AM broadcasting, navigation, and maritime communication.
3–30 MHz	10-100 m	High frequency (HF)	Moderate atmospheric noise, ionosphere reflections for long-distance links, influenced by solar flux	Amateur radio, telephone, telegraphy, long-distance aircraft communication, international short-wave broadcasting, and ship-to-shore communication.
30–300 MHz	1-10 m	Very high frequency (VHF)	Ionosphere reflections, line of sight propagation.	Radio navigational assistance for mobile devices, FM broadcasting, air traffic

				control, and television.
300–3,000 MHz	10-100 cm	Ultra-high frequency (UHF)	line of sight propagations, efficient portable antennas	Satellite communications, land mobile communications, radar, GPS, PCS, mobile phones, and wireless local area networking.
3–30 GHz	1-10 cm	Super high frequency (SHF)	line of sight propagations	UWB, fixed broadband, 3G PCS, microwave connections, land mobile communications, wireless LANs, and PANs.
30–300 GHz	0.1-1 cm	Extremely high frequency (EHF)	Line of sight propagation, atmospheric absorption.	Satellite links, mm-wave personal area networking, radar, and military and secure communications
300–3,000 GHz	1-10 mm	Terahertz or tremendously high frequency (THF)	Line of sight propagation, atmospheric absorption.	Astronomy, meteorology.

The communication bands, per the Federal communications commission (FCC) website, are presented in table 1.2.

Table 1.2. Diverse Communication bands

S.No	Applications	Frequency bands
1	Cordless Telephones	46-49 MHz
2	CDMA	420-495 MHz
3	AMPS Downlink	824-849 MHz
4	AMPS Uplink	864-894 MHz
5	GSM 850 MHz 900 MHz	824-890 MHz 880-960 MHz
6	DCS 1800	1710-1880MHz
7	PCS 1900	1850-1990MHz
8	UMTS	1725-2055 MHz 1950-2170 MHz
9	Air traffic control Radar	0.96-1.215 GHz
10	GPS	1.227-1.575 GHz
11	Wi-Fi IEEE 802.11 b/g – 2.4 GHz IEEE 802.11 a- 5 GHz	2.4-2.485 GHz 5.15-5.35 GHz 5.47-5.725 GHz 5.725-5.875 GHz
12	Bluetooth, Microwave oven-2.45 GHz	2.3-2.5 GHz
13	WBAN IEEE 802.15.6 2.4 GHz 800 MHz 900 MHz	2.36-2.4 GHz 2.4-2.483 GHz 863-870 MHz 902-928 MHz

	400 MHz	950-956 MHz 402-405 MHz 420-450 MHz
14	WiMAX IEEE 802.16 2.3 GHz 2.5 GHz 3.3 GHz 3.5 GHz 3.7 GHz 5.8 GHz	2.3-2.4 GHz 2.5-2.69 GHz 3.3-3.4 GHz 3.4-3.6 GHz 3.6-3.8 GHz 5.75-5.85 GHz
15	LTE 700 4G LTE	746-798 MHz 2.5-2.69 GHz
16	WiBro IEEE 802.16 e	2.3-2.4 GHz
17	ISM	2.412-2.484 GHz
18	WLAN IEEE 802.11 2.4 GHz 5.2 GHz 5.8 GHz Universal	2.4-2.5 GHz 5.15-5.35 GHz 5.725-5.875 GHz 5.1-5.8 GHz
19	C-band satellite communication Systems	3.7-4.2 GHz
20	RFID- LF HF UHF SHF	125 KHz- 134 KHz 13.56 MHz 860 MHz- 960 MHz 2.45 GHz, 5.8 GHz
21	UWB	3.1-10.6 GHz

The wearable technology raises the application of perceptively organizing individuals' daily wear and implanted several sensing, recognition, connection, and cloud services into individuals' eyeglasses, wristwatches, jewels, clothing, shoes and socks, and other leisure wear. Wearable devices are conventional hardware devices and cross-border equipment that establish a data and cloud interaction through mobile or the internet. Antennas are the supreme element in developing contemporary wireless devices, extending from mobiles to handy GPS trackers and from the network cards of laptops to the receivers of satellite televisions. The present era of wireless communications tends to cultivate cheap, light weight and small broadcasting antennas that are high-performance efficient from wearable electronics, demanding antenna researchers and motivating the evolution of novel designs. Unswervingly, flexible electronic systems necessitate the incorporation of textile antennas functioning in designated frequency ranges to offer wireless connectivity, which is an extreme requisite in present-day meticulous society. Unsurprisingly, the characteristics of the incorporated antenna decide the efficiency and performance. Simultaneously, these antennas are expected to be mechanically robust and efficient and have reasonable performance.

A wearable antenna is defined as "an antenna particularly designed to operate while being worn on the human body." It can exchange communication, including on-body antennas and lateral antennas. The tangible incorporation of antennas into other devices has been important for antenna designers due to additional features like security and guideline constraints. Well-being, health, and lifestyle are the major concerns during the design and development of such systems. Several specialized activity segments apply body-centric communication systems, such as paramedics, firefighters [14], spacesuits [15], and aircraft, military, and public safety. Moreover, wearable antennas can also be applied for teenagers, the aged, and athletes to monitor vital signs of health care, such as temperature sensing, BP checking, and heart rate measuring. Etc.

Designing a textile antenna requires knowledge of electromagnetic properties such as permittivity and loss tangent of the textile material. The Microstrip Ring Resonator (MRR) method [16] is used to deduce the electromagnetic characteristics of the substrates with their realistic profile, effortlessness in fabrication, low cost, compactness, and compliance. Microstrip antennas can be utilized in the design of wearable antennas [17] as they are easily embedded in

garments for continuous monitoring with increased safety levels and comfort of the wearer. With the proper use of textile materials, low-cost and low-profile antennae can achieve maximum efficiency and high performance.

1.1. Definitions and basic concepts

The antenna is the basic building block of any electronic system that depends on a free space propagation medium. An antenna is described as a "transducer that converts electrical power into electromagnetic waves and vice versa"[18]. In other words, an antenna is a device that radiates or receives radio waves. Electromagnetic waves are also designated as radio waves. Generally, many antennas available show a resonant behavior and can provide a narrow bandwidth with less efficiency. The antenna is designed in such a way that it can match the same frequencies in the radio system to which it is applied. The antenna's sole purpose is to transmit or receive power. Fig.1.1 shows the basic principle of radiation for a single conducting wire. It is understood from the figure that any transmission line has current flow with uniform velocity, and a straight line with infinity length has no radiation. On the other hand, for a transmission line to radiate has to be meeting the following conditions.

- The line with uniform velocity should be bent, truncated, or terminated
- The line with time-varying currents can radiate power even though the line is straight.

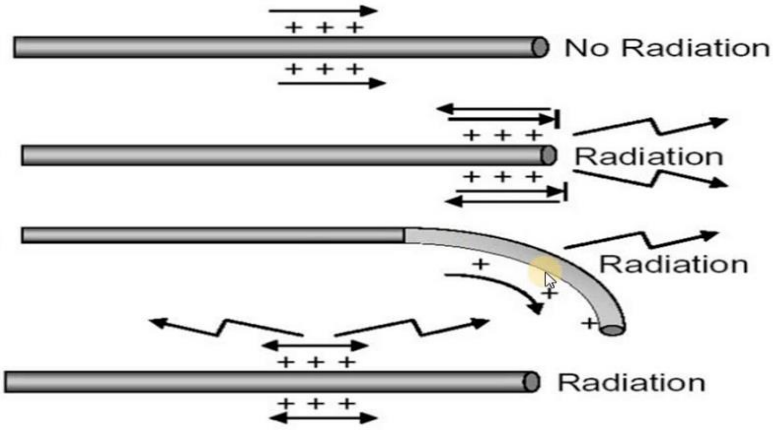

Fig.1.1. Basic mechanism of Radiation for a single conducting wire

The mechanism of the radiation from an antenna has demonstrated in Figure 1.2. A sinusoidal voltage source is linked to a transmission line that can generate the electric field E and magnetic field H. The time-varying nature of these fields tends to the creation of electromagnetic waves. When these waves move towards infinite space, free space waves are created by connecting the two ends of the lines. While the source continues to excite, causing the electric disturbance leading to continuous generation of electromagnetic waves, which travel all the way over the line, and radiated into the free space. The continuous electromagnetic waves appear within the transmission line due to the continuous source. However, once they encounter free space, they establish closed loops and are radiated.

Some physical parameters are essential to estimate the antenna's performance that are independent of time and acknowledged as fundamentals of the antenna. These parameters are significant while constructing an antenna. When it comes to the design of wearable antennas, there must be special requirements in shape and size subjected to the wearable location of the human body. For example, if the wearable antenna is mounted on the chest/back of the human body, it can be a little larger and not restricted in shape as there is a large area available on the chest/back. If it is situated on the arm/hand/waist, the appearance can be in the form of a belt/watch/ bangle. However, by appearance, thin wearable antennas are preferable. Additionally, the dynamic movements of the human body put forward the bending and crumpling, which alters the antenna's basic performance. All these requirements restrict the freedom of the antenna designer.

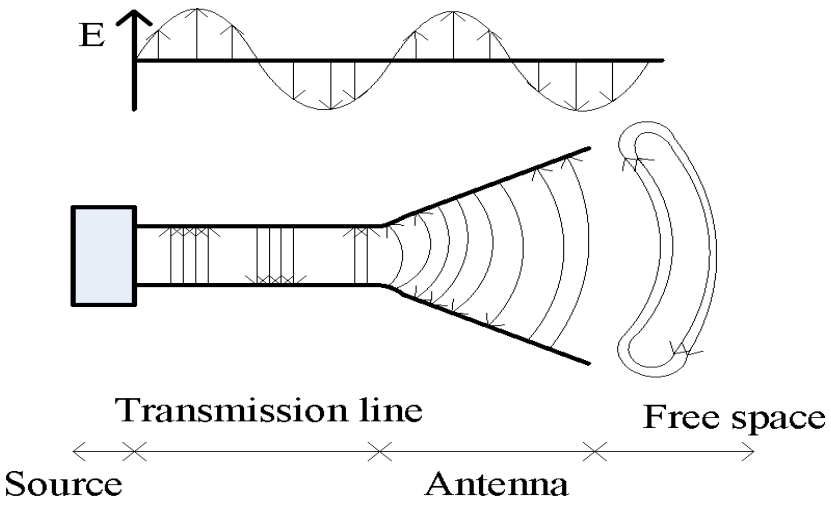

Fig.1.2. Radiation from an antenna

To comprehend the challenges encountered while designing the wearable antenna and describe the performance, it is indispensable to provide some key parameters. Some of these parameters: *S*-parameters, input impedance, Impedance bandwidth, Gain, radiation pattern, efficiency, Front-to-back ratio, and SAR will be conferred in brief with special consideration regarding wearable antenna designs.

1.1.1. S-parameters

S-parameters, also referred to as scattering parameters in RF engineering, describe the input-output relation between the terminals of an electrical system. For instance, in a communication system with two radios, radio1 and radio 2, the two radio terminals would be the two ports. The incident RF signal at one port and a portion of the signal gets reflected and trying to deliver to antenna 1 is referred to be S_{11}. Similarly, S_{22} is the radio 2 power trying to be delivered to antenna 2. Generally, S-parameters can vary along the frequency. A two-port network model is frequently employed for the S-parameter measurement of an antenna. Port 1 represents the feed port of the antenna under test (AUT), and S_{11} characterizes the voltage reflection ratio at that port. It is shown in Equation 1.1.

$$S_{11} = \frac{V_{\text{Reflected}-\text{at}-\text{port1}}}{V_{Toward-port-1}} \tag{1.1}$$

In practice, S_{11} gives the reflected power from the terminals. If S11=0 dB, all power is reflected from the antenna and no radiation occurs. Therefore, practically, intercepted power is either radiated or absorbed as losses within the system. The power reflected leads to poor efficiency and can be mitigated using matched feed circuits. S_{11} is often denoted in dB as in Equation 1.2.

$$S_{11}(dB) = 10\log S_{11}{}^{2} = 20\log S_{11} \tag{1.2}$$

For a typical antenna, S_{11} less than -10 dB is considered. It denotes that the antenna receives 3 dB of power while reflecting the rest 7 dB. In other words, 10% of reflection takes place, which is considered the usable bandwidth. This is also known as impedance bandwidth and can assess the antenna's impedance matching. A typical return loss plot of the microstrip patch antenna is shown in Figure 1.3.

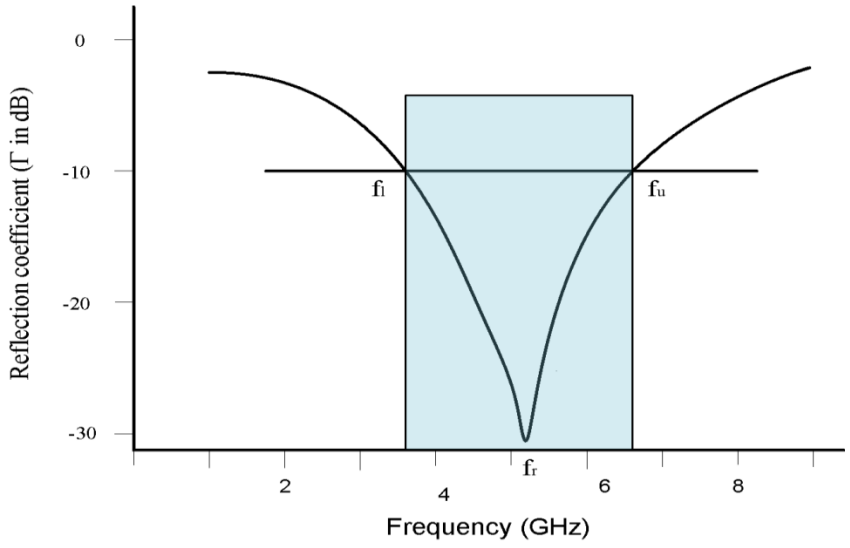

Fig.1.3. Reflection coefficient curve of microstrip patch antenna showing usable bandwidth and resonant frequency

1.1.2. Impedance Bandwidth

The bandwidth is another key fundamental parameter of the antenna [19]. It signifies the frequency range over which the antenna can emit or receive energy. The impedance bandwidth is defined as,

$$BW = \frac{f_u - f_l}{f_r} \times 100 \tag{1.3}$$

The antenna's bandwidth is the range of frequencies within which it complies with the given parameter requirements. Polarization, radiation pattern, and VSWR are the commonly specified parameters. If the VSWR is chosen for the bandwidth consideration, then the bandwidth is called impedance bandwidth. Next, an anticipated radiation pattern guarantees low or high-energy radiation in a specified direction. Lastly, inside the operable bandwidth, a distinct polarization of an antenna reduces the potential losses due to polarization mismatch.

The impedance bandwidth for an S_{11} of less than -10 dB is labelled light blue in Fig. 1.3. Practically, the bandwidth is specified on VSWR. For example, if the antenna is working at 100-400 MHz for VSWR<1.5, it means that the reflection coefficient is < 0.2, and Only 4% of the power is returned to the transmitter by reflection.

1.1.3. Gain and antenna efficiency

The antenna gain describes the transmitted power in the peak direction concerning the isotropic source. For instance, if a transmitting antenna has a gain of 3 dB, it indicates that for the same input power, the received power at a distance from the antenna is 3 dB greater than the received power from an isotropic antenna. The antenna gain or power gain is described as “the ratio of radiation intensity in the desired direction ‘I’ to the radiation intensity of an isotropic antenna ‘I_{iso}’ for the same distance”. This ratio is typically stated in decibels, and these units are known as decibels-isotropic (dBi)

$$Gain = 10\log\left(\frac{I}{I_{iso}}\right) \tag{1.4}$$

In practice, antenna efficiency refers to total efficiency. Generally, the antenna efficiency losses are due to reflection losses and dielectric and conductor losses. Then the total power delivered to the antenna is equal to the antenna ohmic losses P_{ohmic} (Conduction loss + dielectric loss) and the power radiated by the antenna P_r. The antenna radiation efficiency η_{cd} is given by

$$\eta_{cd} = \frac{P_r}{P_{in}} = \frac{P_r}{P_{ohmic} + P_r} \tag{1.5}$$

Total efficiency η_0, which includes the losses due to mismatch and is given by

$$\eta_0 = \eta_{cd}\eta_r, \eta_r = 1 - |\Gamma|^2 \tag{1.6}$$

Antenna efficiency commonly relates to radiation efficiency in the case of a properly matched antenna design. Specifically, the wearable antenna functioning near the human body, the reflection coefficient, and the efficiency of the antenna are affected due to its lossy nature. The only solution to improve efficiency is to reduce the losses. Choosing a substrate material with an appropriate dielectric constant will aid in reducing the loss caused by the antenna material.

1.1.4. Radiation pattern

The radiation pattern is described as "a mathematical function or graphical representation of radiation properties as a function of space coordinates." An isotropic radiator is a lossless antenna that radiates equally in all directions. It is not physically realizable. However, it is frequently used to express the radiation properties of actual antennas. Usually, the radiation pattern is considered at a distance > $\lambda_0/4$, known as a far field. The parts of radiation patterns are called lobes. Many practical antenna radiation patterns have a main lobe along with minor lobes. As a consequence of the interference between the radio waves radiated by the antenna's several sections, the highest radiation can be possible at angles in which the radio waves show up in-

phase and minimum at all other angles where they show up out-of-phase. Fig. 1.4 shows the 3D radiation pattern of a directional antenna.

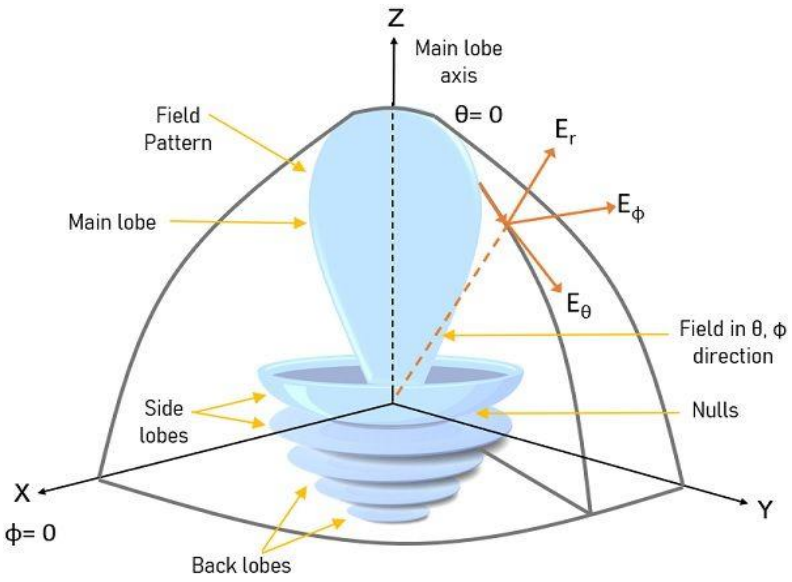

Fig.1.4. 3D radiation pattern of a directional antenna

In the view of wearable antennas, the back radiation is significant in the near human scenario. The front-to-back ratio (FBR) is described as the quality indicator that can refer to the back radiation from the directional antenna. Fundamentally, the FBR is "The ratio of the peak gain in the forward direction to the gain 180^0 behind the peak". It is just the difference between the gains in the forward direction to the backward direction in a dB scale, shown in equation 1.7.

$$\text{FBR} = \frac{\text{Forward Power}}{\text{Backward Power}} \tag{1.7}$$

1.1.5. Specific Absorption Rate (SAR)

Civic apprehension and awareness about the health hazards of radiation and legal necessities around the world have insisted researchers continuously consider the quantity of radiation engrossed by the human body. When the antenna operates near the human body, the side and back lobe radiations penetrate and are absorbed by the human tissue. The amount of absorbed power per unit mass of human tissue can be evaluated in terms of a Specific Absorption Rate (SAR). The SAR can be calculated from equation 1.8.

$$SAR = \frac{\sigma |E|^2}{2\rho} \tag{1.8}$$

Where σ and ρ are the electrical conductivity and mass density of the human tissue

The greatest secure bound of SAR articulated by “The US standard is 1.6 W/kg for 1 g of tissue [20], and the International Commission of Non-Ionization Radiation Protection (ICNIRP) for Europe has set a maximum level of SAR as 2 W/kg for any 10 g of tissue [21]”.

1.2. Wearable technology

Wearable technology is an evolving interdisciplinary field. Intelligence in bioengineering, electrical engineering, software engineering, and mechanical engineering is essential to construct and implement wearable communication systems. It is intended to be worn on the body and may be in any form, including jewellery, accessories, medical devices, and clothing. The most cutting-edge wearable technology includes holographic computers in the form of virtual reality (VR) headsets, Google Glass, Microsoft's HoloLens, and artificial intelligence (AI) hearing aids. Detachable skin patches with sensors that electronically broadcast patient data to a control unit in a health system is an examples of less complex wearable technology. Some of the available wearable devices are exposed in Fig. 1.5.

(a)

(b)

(c)

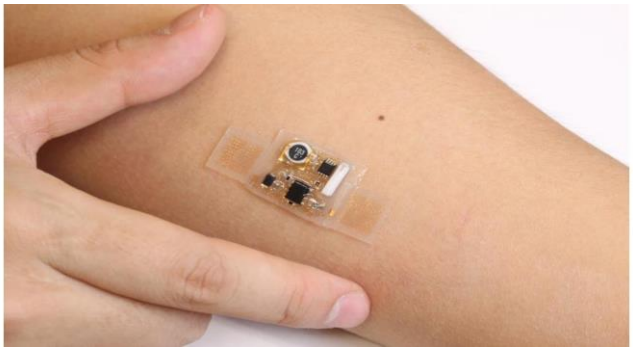

(d)

Fig.1.5. The most sophisticated wearable devices available in the present market (a) AI-based hearing aids (b) Google glass (c) Microsoft's HoloLens (d) Disposable skin patch with sensors [22]

The wearable antennas function according to the applications based on the category they belong to, such as health, fitness, or entertainment. Mostly, wearable technologies collect data from various nodal points using an internet connection to different smart devices. These can be hidden sensors attached/embedded in the accessories to track the body movements. For instance, fit bands and activity trackers wrapped around the wrist can monitor the activities throughout the day. Some wearables can function even without physical contact with the body. Other wearables track movement and speed by employing remote smart sensors and accelerometers; some use optical sensors to measure heart rate or glucose levels. But the very communal feature amongst the wearables is that they all monitor the real-time data in variable environments. Hence, wearable devices will become important components to enhance the quality and comfort of one’s life in the next decade.

1.2.1. Examples of Wearable Technology

In the last few years, wearable technology products with applications in medicine and healthcare have developed quickly. These consist of:

- In Louisville, Kentucky, AIR Louisville's wearable technology is being used to assess pollutants, track air quality, and pinpoint areas where locals with respiratory issues are most likely to congregate.

- An intelligent patch called Cyrcadia Breast Monitor was created by Cyrcadia Health. It can identify early indications of breast cancer and send the data to a lab for evaluation.
- Greater freedom and flexibility are being facilitated for the aged and disabled by wearable medical alert monitors.
- It is being developed to monitor heart and brain activity, sleep issues, and muscle function through smart tattoos that have flexible electrical sensors. Even inks are being investigated, albeit these are only transitory.
- Parkinson's disease sufferers can track their symptoms with a smart watch that sends the information so that more individualized treatment regimens can be created.

1.2.2. Applications of wearable antennas

Wearable antennas are designed to communicate to their source station while worn and moving. To attain this, wearable antennas are made with textile materials. Fig.1.6 indicates the major applications of wearable antennas. When analogized with present-day smartphones and tablets, the wearable devices primarily focused on different added features for monitoring and scanning biofeedback or other sensory physiological functions like biometry related. Even while consumer wearable technology has advanced significantly since their conception, it is still in its development. The majority of individuals still use a smart phone together with an activity tracker, which only allows them to see their heart rate and number of steps. In fact, the variety of data that is gathered and processed in the context of a wearable ecosystem can bring an unprecedented user experience for humanity.

Wearable antennas are widely used in medical applications to remotely monitor the patient's health status. The ingestible antennas are employed for endoscopy studies, giving a better result than the conventional probe-based techniques. However, the quality of the endoscopy images majorly depends upon the efficiency of the connected antenna structures. The on-body wearable antennas are used to observe and transmit the body parameters like heart rate, temperature, and blood pressure with the help of sensors. Implantable antennas are the other wearable antenna that keeps the device inside the human body. Such antennas are used for retinal prostheses, brain activity monitoring, and oral implants.

The wearable sensors are even applied to entertainment-based applications for gaming and virtual reality interactions. In some places, the sensors and antennas are incorporated into watches and shoes to make the wearables intelligent devices. The wearable bands are also utilized for detecting the location of the users through a global positioning system (GPS).

With the advance of wearable technology, space suits have become sophisticated, high-tech components of astronauts' equipment embedded with multiple antennas. These antennas perform various functions that require tests and measurements to prepare them for optimal performance in harsh space environments. Also, wearable sensors can be attached to the people working in the borders, mines, and chemical industries for their safety and to keep track of their activities. The prime element in the sensor device is the wearable antenna.

The miniaturized wearable antennas are used in military applications for microphone and camera modules for transferring data. However, the compactness, manageability, wirelessly exchange, energy-efficient computing, and innovative display technologies have united to produce state-of-the-art smart devices.

1.3. Basic antennas for wearable communication systems

It is essential to select an antenna that is appropriate for the application, as a one-design-fits-all strategy does not satisfy all requirements. An antenna is one of wireless wearable devices' most significant and crucial components. They need to be particularly designed to work while worn on and off the body. Usually, wearable antenna desires for all modern applications must be lightweight, economical, almost maintenance-free, and not require installation. Some frequently used antenna types include microstrip antennas, dipole, monopole, loops, slot antennas, and planar inverted F antennas.

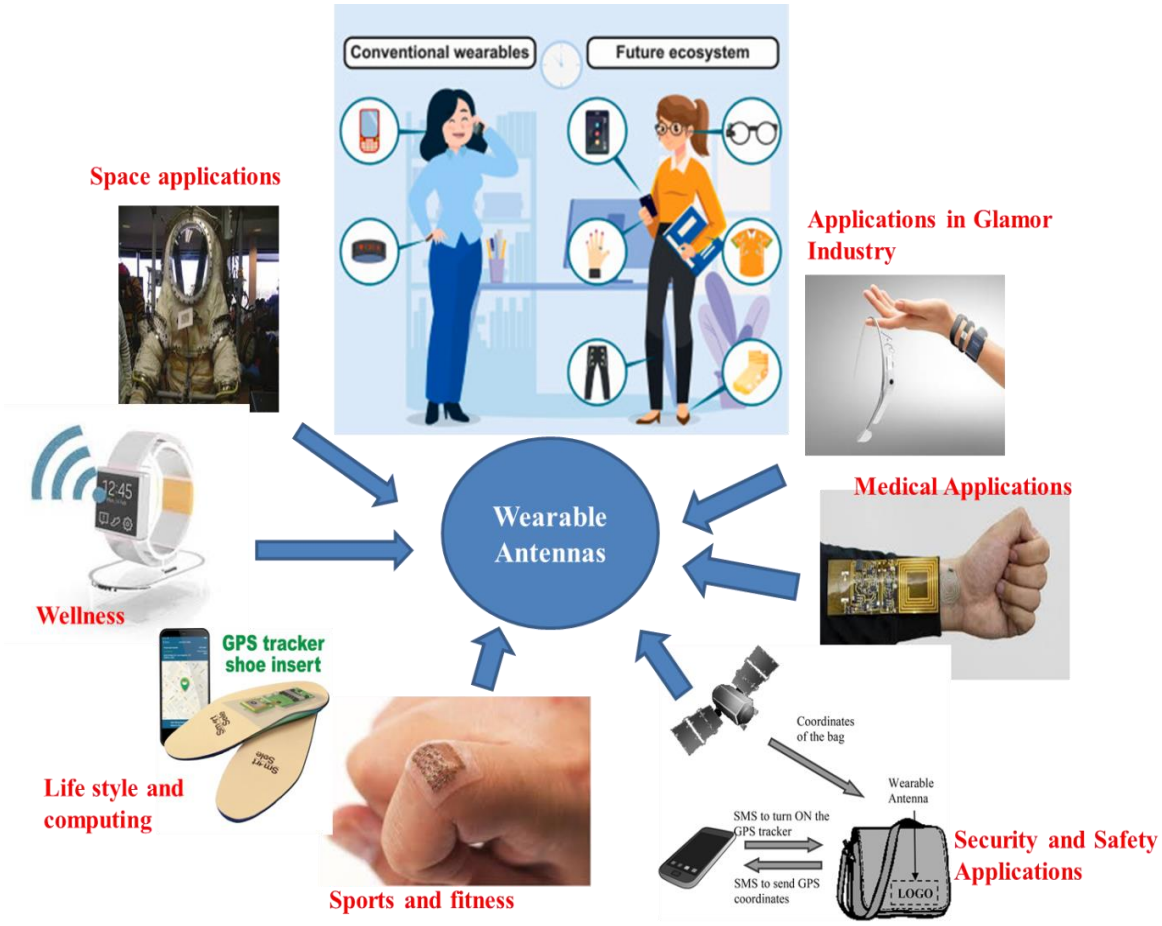

Fig.1.6. Applications of wearable antennas

1.3.1. Dipole Antenna

A dipole antenna is a short-circuited wire fed at the center and is the simplest of all other antennas. These are more prevalent subjected to their small-profile, simple fabrication, low price, polarisation purity, and extensive frequency coverage. The only disadvantage is its large size. Moreover, the donut-shaped pattern poses difficulties in less form factor profiles. Dipole antennas are widely used in various wireless and mm-Wave applications.

1.3.2. Monopole Antennas

The size of a monopole antenna is half that of a dipole antenna and are regularly straddling above the ground planes. These antennas are less in size and can be useful where compactness is a

must. The advantages of low profile, low cost, and ease of fabricating make them ideal for integrating into clothes. When combined with high-impedance surfaces, the performance of these antennas is further improved.

1.3.3. Loop Antennas

A single or several loops in the form of a circle, square, or any other closed geometric shape make up the Loop antenna. To make sure the in phase current throughout the loop, the size of the loop antenna should be lesser than a wavelength. The key advantages of these antennas are light-weight, simple, and small. The disadvantage of loop antennas is their poor efficiency, which results in power loss. These antennas are perfect for small radio devices and body-worn communication systems utilized in military applications.

1.3.4. Slot Antennas

The Slot antenna contains a metal patch imprinted with narrow slots. The slot antennas are multipurpose and usually function for frequencies 300 MHz - 24 GHz. The performance of the antenna is depends on the slot size, shape, and substrate material utilized. Its simple structure and flexibility makes it appropriate for medical and military wearables. This antenna transmits wireless data effectively even when the human position changes.

1.3.5. Microstrip Antennas

Notably, in the modeling of the wearable antenna, the planar patch antenna is more prevalent in the research community as it is made conformal for integration into clothing and also because of its benefits like reduced dimensions, lightweight, high operating frequency, capable of supporting multiple frequencies, dual-polarization, and lower fabrication cost. Despite these advantages, it suffers disadvantages like lower gain and low power handling capacity.

1.4. Interpretation of Microstrip Patch antenna

The elementary form of a microstrip antenna contains a metallic patch on top and a ground plane on bottom surface of the substrate. Microstrip antennas are also known as "Patch" antennas [23]. The radiating patch is generally made of a conductive material such as copper. It can take any potential shape, as in Fig. 1.7. Typically, the feed lines and radiating patch are photo-etched onto the dielectric substrate. The conventional microstrip patch antennas are fed by microstrip, probe, proximity, and aperture-coupled feeding techniques. The operating frequency is usually determined by the size and shape of the patch, so the antennas are categorized as resonant antennas.

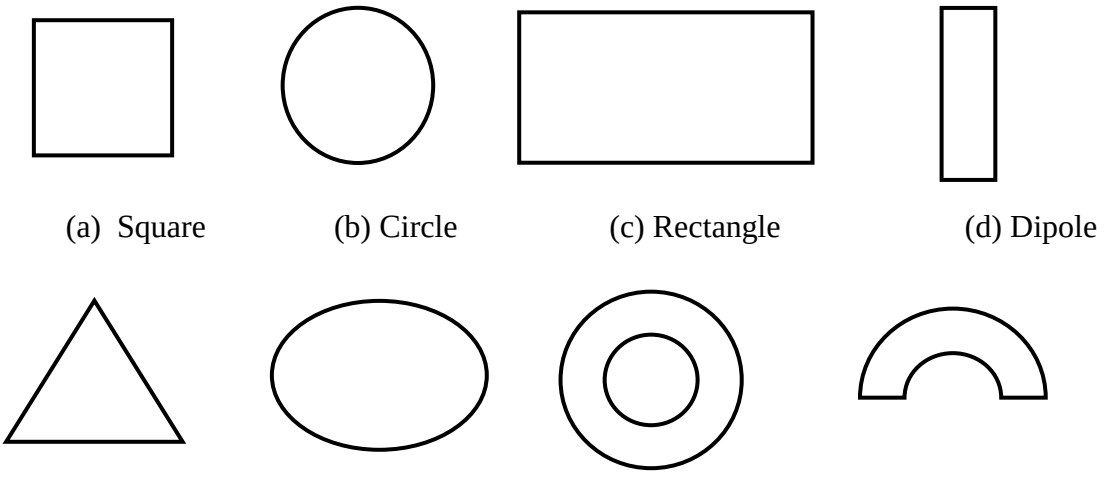

Fig.1.7. Different shapes of Patch radiator

Conventionally, numerous substrates are available to design the microstrip antennas whose dielectric constant is between $2.2 \leq \varepsilon_r \leq 12$. However, for wearable applications, man-made or casual cloth materials are utilized as dielectric substrates such as polyester, wet cotton, dry cotton, liquid crystal polymer (LCP), fleece fabric, Nomex, nylon, foam, and jeans materials, etc. The dielectric constant of these flexible substrate materials is in the range of $1 \leq \varepsilon_r \leq 2$.

The transmission line model is the simplest of all and represents the patch antennas as a parallel plate transmission line connecting two radiating slots. The slots act as high-impedance terminals on both sides of the transmission line. Hence, the patch has highly resonant properties

depending on the length of the patch. However, the physical length is not the same as the electrical length due to the effect of fringing phenomena, which is the major reason for the radiation. Therefore, efficient and high bandwidth antennas can be evolved by utilizing a thick, low permittivity substrate in the design of the patch antennas. As in Fig.1.8, the edge located electric field normal components are moving in opposite directions and are out of phase since the patch length is λ/2. Subsequently, on the broadside, they cancel-out one another. The tangential components that are in phase will assemble at the structure's surface to provide maximum radiation. The microstrip patch is a line with heterogeneous mediums, typically air and substrates. Due to the different mediums, the phase velocities of the waves will differ, and the propagation of pure TEM waves is not possible. As in the figure, the fringing fields are not confined to the substrate but spread into the air. Hence, the effective permittivity is slightly less than ε_r. Note that the small the ε_r, the more fringing lines are bowed and extending away from the patch, contributing to better radiation.

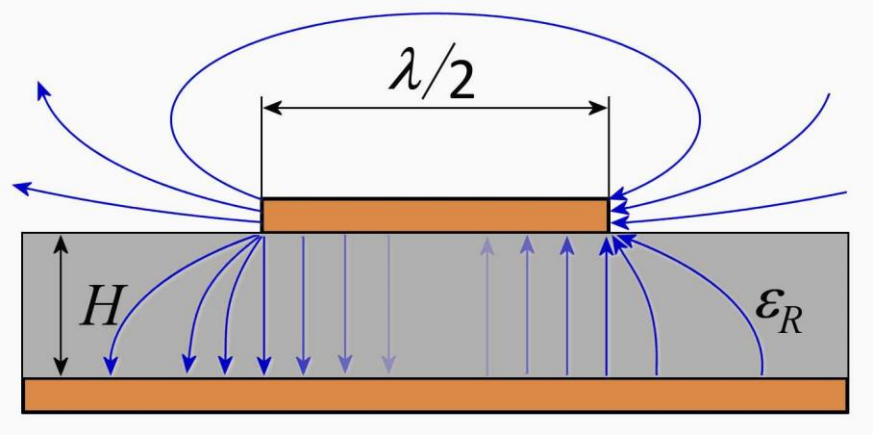

Fig.1.8. Rectangular microstrip patch antenna showing the fringing effect

The resonant frequency fr is determined using the width (W) of the patch, which has a small impact on it and is calculated using [24]

$$W = \frac{C}{2 f_r} \sqrt{\frac{2}{\varepsilon_r + 1}} \tag{1.9}$$

Where C is the light velocity and ε_r is the relative permittivity of the material

The field lines are inside the substrate for the microstrip line, and some are extended to outer space. For this, an effective dielectric constant (ε_{reff}) is introduced to account for fringing and the wave propagation in the line. The effective permittivity (ε_{reff}) given by

$$\varepsilon_{reff} = \left[\frac{\varepsilon_r + 1}{2}\right] + \left[\frac{\varepsilon_r - 1}{2}\right] + \left[1 + \left(\frac{12h}{W}\right)\right]^{\frac{1}{2}} \tag{1.10}$$

Generally, the patch length (L) governs the resonant frequency, which is an essential parameter in design of the patch antenna, and value of L is provided by

$$L = \frac{C}{2 f_r \sqrt{\varepsilon_{reff}}} - 2\Delta L \tag{1.11}$$

The extended length of the patch due to the fringing is given by

$$\frac{\Delta L}{h} = 0.412\left[\frac{\varepsilon_{reff} + 0.3}{\varepsilon_{reff} - 0.258}\right]\left[\frac{\frac{W}{h} + 0.264}{\frac{W}{h} + 0.8}\right] \tag{1.12}$$

Where h is the height of the substrate

The effective patch length can be calculated as

$$Le = L + \nabla L \tag{1.13}$$

1.4.1. Microstrip patch antenna feeding techniques

There are four distinct techniques available for exciting the patch antenna. They are categorized into two: contacting and non-contacting methods. In the contacting methods, the feedline is directly connected to the radiating element, whereas in the non-contacting type, the feedline and the radiating patch are electromagnetically coupled. Aperture-coupled and proximity-coupled techniques are non-contacting type feeding techniques.

1.4.1.1. Microstrip line feed

In this method, a conducting line is attached directly to the edge of the patch, as displayed in Fig. 1.9. The width of the feed line is small compared to the patch and is imprinted on the same substrate to form a planar structure. To match the line impedance to the patch without using any additional matching components, the insets are scraped away from the patch. This technique suffers from poor surface wave efficiency and spurious feed radiations.

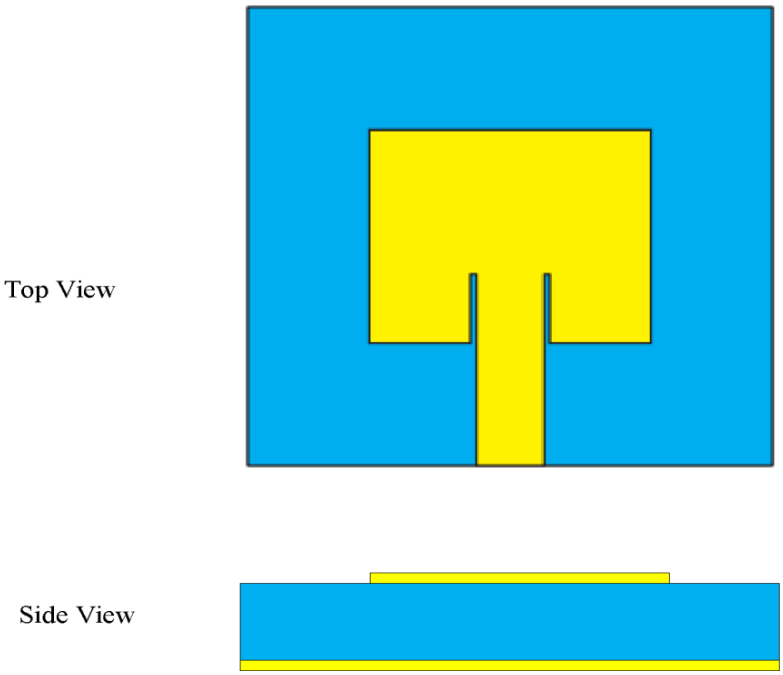

Fig.1.9. Microstrip patch antenna with inset feed [25]

1.4.1.2. Coaxial Feed

The probe feed is one of the most popular and non-planar feeding techniques in which a coaxial cable is used to feed the patch. The inner conductor of the coaxial cable is connected to the patch by protruding into the substrate, whereas, the outer conductor is attached to the ground, as shown in Fig.1.10. The probe is placed at the point where the antenna's input impedance is 50Ω. This technique suffers from several limitations. The major disadvantages are that it is

difficult to model because holes have to drill into the substrate and in the thicker substrates, leading to matching problems.

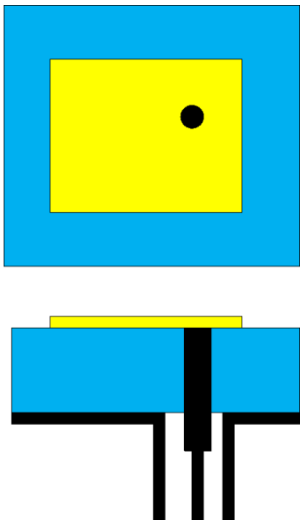

Fig.1.10. Coaxial probe feed microstrip patch antenna [25]

1.4.1.3. Aperture coupled feed

The aperture feed technique involves two substrates: the antenna substrate and the feed substrate. The metal patch is situated on the top of the antenna substrate, and the feed line is situated at the back of the feed substrate. The ground plane with an aperture located exactly at the center below the patch is sandwiched between the antenna substrate and feed substrates, as in Fig.1.11. This feeding method achieves excellent polarization purity, which is something unattainable with other feed techniques. Usually, a thin high dielectric feed substrate and thick low dielectric antenna substrate is utilized in the design of the aperture coupled antenna.

1.4.1.4. Proximity coupled patch antenna

The proximity feed uses two-layer substrates, where the feed line is placed lower layer, and the patch is placed on the upper layer, as shown in Fig.1.12. Here the feed line is terminated in an open end, and the power transfer from the feed to the patch takes place through electromagnetic field coupling. Feed line radiation has significantly decreased as a result of the feed line's relocation to a lower level. In comparison to other approaches, it also offers higher bandwidth efficiency. The only disadvantage using this technique is its poor polarization purity.

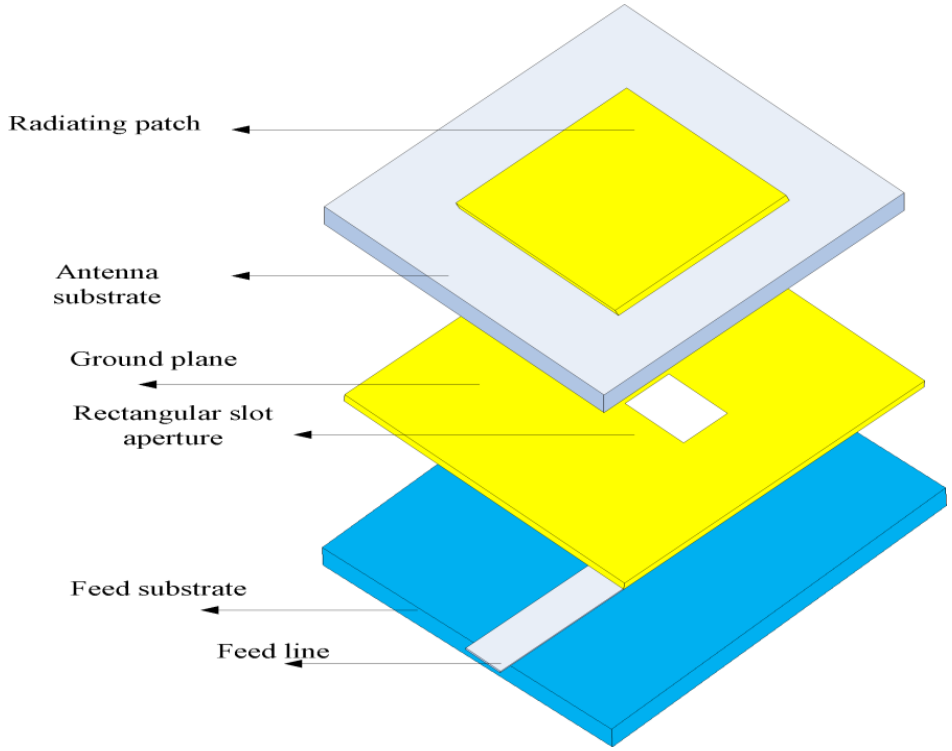

Fig.1.11. Aperture-coupled microstrip patch antenna[26]

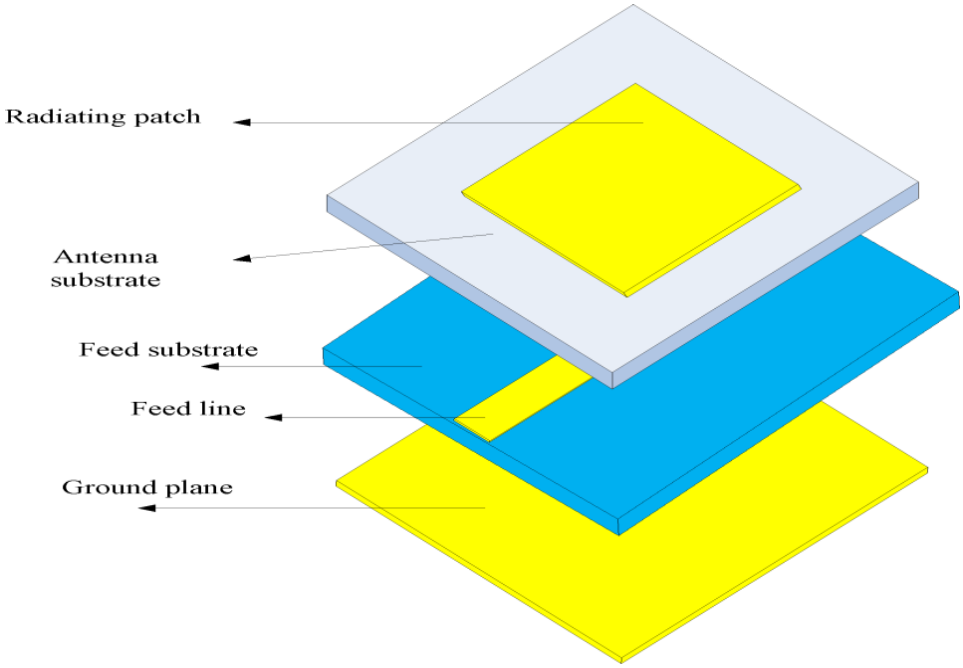

Fig.1.12. Proximity couple patch antenna

1.4.1.5. Coplanar waveguide (CPW) feed

In this method, the side plane conductor is the ground, and center strip line carries the signal. By adjusting the gap between the ground and the feedline, the performance of the antenna can be improved. The patch is excited by a 50 ohm microstrip line situated at the center. Therefore, an antenna can be directly matched to the CPW feed, as depicted in Fig. 1.13.

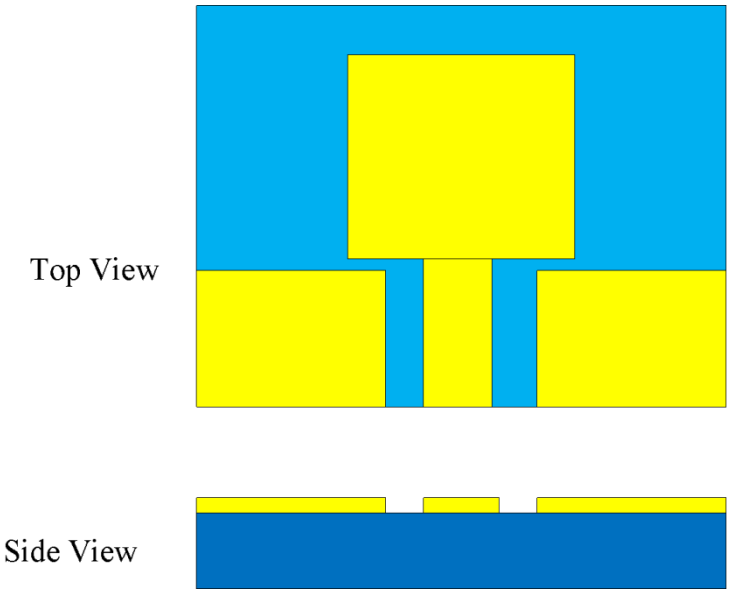

Fig.1.13. CPW-fed patch antenna [27]

To mitigate some of the difficulties of microstrip antennas as specified earlier and to accomplish better performance, microstrip line and coplanar waveguide feeding techniques are utilized in this research work. The CPW feed has negligible radiation due to the excitation of odd modes because of the coupled slot line. Due to this mode, the magnetic currents on both CPW slots have equal magnitudes and are out of phase, which cancels each other leading to insignificant radiations attained from the feed.

For wearable applications, always user comfort is ahead of all the features. Therefore, utmost care must be taken while selecting the feed type, type of substrate, and fabrication process of the antenna. The probe is connected to the radiating patch in the coaxial probe feed by making holes in the substrates. This causes fabrication issues and looks awkward and uncomfortable when worn on the body. On the other hand, the non-contacting feeding methods, namely aperture, and proximity coupled feeding methods have coupled the power to the radiating patch by an aperture

inside the ground plane, which is sandwiched between two substrates resulting in higher thickness and fabrication problems. Keeping all those parameters in mind, the microstrip feedline and CPW feeds are chosen as appropriate feeding methods in this thesis for wearable applications. The two feeding methods have several advantages over the conventional coaxial probes and non-contacting feeding methods. These methods will simplify the fabrication, facilitate comfort to the wearer and, eliminates the need for wraparound and via holes, reduces the radiation losses, provides larger bandwidth, lower conduction and dispersion losses. Etc.

1.5. Overview of the previous work on wearable antennas

This section briefly gives an account of the published literature on wearable antennas, Wearable wireless applications in WBAN, impedance bandwidth, gain, and SAR enhancement techniques used for wearable antennas. The techniques existing in the published research are studied, and their drawbacks are highlighted.

Lingnan Song et al. developed and investigated the influence of bending on wearable antennas situated above cylindrical surfaces [28]. The deviations of resonant frequency and radiation characteristics are investigated with simulations and validated experimentally for various bending angles. The relative deviation of the resonant frequency in regard to the bending radius is plotted to focus on numerous wireless applications.

Xiu Yin Zhan et al. designed a dual-band button antenna for body-worn systems [29]. In the inferior band, the proposed antenna is configured for on-body communication. In the superior band, the higher-ordered modes are exploited along with the copper reflector surface to appreciate eight-shaped patterns for off-body applications. The extreme transferred power in the SAR guideline of 1.6 W/Kg is 26.4 dBm, which means the projected antenna is a potential contender for body-centric communications.

Ali Arif et al. constructed a triangular patch antenna with a low-cost, extensively accessible Rogers 5880 flexible substrate [30], [31]. The anticipated antenna configuration is attained with the amalgamation of Koch fractal, meander line cuts, and DGS to comprehend an innovative geometry having a compact footprint, decent physical conformability, and better

impedance matching to function in the Industrial, Scientific, and Medical (ISM) band at 2.45GHz. The anticipated antenna shows a gain of 2 dBi and has undergone structural deformations, which lead to frequency detuning and bandwidth variations. For the validation of SAR, the anticipated antenna is simulated on a genuine heterogeneous HUGO voxel model.

Sangeetha Velan et al. designed a dual-band wearable fractal monopole antenna combined with EBG [32]. The fabricated antenna is intended to resonate at 1.8 GHz and 2.45 GHz frequencies. The EBG surface not only reduces the radiation into the human body by 15 dB but also decreases the detuning of resonance because of the human body. The deformation properties of the antenna and on-body conditions are considered and found that the SAR is within the standards.

Guoping GAO et al. designed a planar monopole antenna assisted by a new uni-planar electromagnetic bandgap surface for 2.4 GHz WBAN [33]. The anticipated antenna has experienced a reduced size of up to 50% if the EBG is optimized from 3 × 4 to 2× 3, whereas the radiation characteristics are nearly unchanging. With the utilization of 2×3 UC-EBG beneath the antenna, a unidirectional pattern resulted, and the gain has seen improvement from 2.1 to 5.6 dB. In the meantime, the EBG surface surpasses the cross-polarization of the monopole antenna, apparently. The simulated SAR results are 0.0536 W/kg for 1 g and 0.0296 W/kg for 10 g of tissue, which is within the standard limits of the USA and Europe.

Alford Chauraya et al. developed Frequency Selective Surfaces (FSS) for wearable applications [34]. The FSS surface is constructed on the felt substrate of thickness 0.8 mm, fabricated by a speed and cost-efficient embroidery method using conducting threads. The anticipated FSS surface, operable at 2 GHz frequency, has a transmission coefficient of lesser than 10 dB. At first, the FSS structure is simulated by utilizing the available commercial simulation tools. This anticipates the direction of textile FSS surfaces for body-worn systems.

Cheng Huang et al. demonstrated a technique to accomplish high transmission efficiency and wideband reduced scattering at two distinguishing frequencies by uniting FSS and EBG surfaces [35]. The FSS-EBG surfaces comprise two layers with metal arrangements. The lowest FSS layer acts as a filter that can permit the in-band signals and reflect the signals that fall out of

the band, whereas the topmost EBG layer embraces the 0^0 and 180^0 reflection phase with a chessboard pattern to decrease the back wave. The integrated antenna operates in S- and X–Ku bands, which is appropriate in the stealth antenna radomes.

Wissem El May et al. designed a co-planar triple band EBG-based wearable antenna for sub-6 GHz 5G and WLAN applications [36]. The presence of the EBG surface made the anticipated antenna susceptible effect on the human body. The experimental results demonstrated that the anticipated antenna had exhibited tolerance to several deformations along with human tissue loading. Further, the SAR has shown a drop of > 95%, which fulfills international regulations.

Abdul Wahab Memon et al. conferred the structure of a breathable textile antenna for enhanced water vapour permeability [37]. The water vapor permeability of the anticipated antenna has increased by loading holes of 1 mm diameter in the conduction parts of the antenna proposed. The results accomplished the water vapor permeability of 5296.70 g/m2 per day, air permeability of 510 mm/s, and the forward gain of 4.2 dBi, 5.4 dBi in the E-plane and H-plane, correspondingly at 2.45 GHz.

B. Zoubiri et al. describe a scheme to control the propagation of the surface wave, leading to an enhanced gain of a microstrip antenna by a novel EBG [38]. The anticipated structure comprises punctured cylindrical holes periodically dispersed around the boundary of two ellipses with dissimilar radii. The characteristics of the anticipated antenna simulated using the full-wave method are demonstrated and assessed with a traditional microstrip for the same functioning frequency, and found that the accomplished results exhibit an improved gain of 1.9 dB in the E-plane.

Bashyam Sugumaran et al. designed a flexible antenna supported by FSS for wireless body area communications [39]. A monopole antenna with a rectangular slit in the ground plane operates at a 2.45 GHz ISM band with a bandwidth of 550 MHz. The integrated antenna with FSS witnessed a fractional bandwidth of 22.44% and a peak gain of 7.76 dBi with dimensions of 120x120x30 mm3. The addition of FSS diminishes the back radiation, thereby reducing the SAR level, accomplished from 3.197 W/kg to 0.164 W/kg.

Mengjun Wang et al. designed a metamaterial-based dual-band flexible antenna [40]. A thin bendable polyimide substance is utilized as the substrate for the construction of the antenna. With the presence of metamaterial situated betwixt the antenna and the human's forearm, the antenna's gain has improved from 9.3 dB and 5.37 dB, and the radiation efficiency has enhanced by 48.4% and 35.7%, at 2.45 and 5.8 GHz, correspondingly. Furthermore, electromagnetic exposure is reduced by above 70%, keeping the limits enforced by the standard authorities for the specified frequencies.

Dileepan Dhanasekaran et al. designed a small decagon ring fractal antenna for multiple bands [41]. The decagon ring boosts the bandwidth when analogized to existing structures and has an overall volume of 26.5 × 23.5 ×1.6 mm3. The proposed antenna has a maximum impedance bandwidth of 2.4 GHz at 5.27 GHz and is intended to operate at 2.4 GHz, 3.775 GHz, and 5.27 GHz frequencies and finds applications in various wireless local area network channels.

Debatosh Guha et al. demonstrated the application of DGS to inhibit cross-polarization from a microstrip patch antenna [42]. A pair of arc-shaped defects embedded symmetrically on the ground plane positioned under a circular patch. The existence of defects demonstrates the isolation of 30 dB and hence reduces the cross-pol level from its maximum radiation and is juxtaposed with traditional patch antenna without DGS. This identified an enhancement of 12 dB. The XP values achieved around 7–12 dB on the E-plane of the patch.

Mohamed El Atrash et al. designed a great gain, low SAR monopole antenna [44]. It is assisted by a 3 × 3 array of EBG unit cells. By controlling the distance betwixt the grounds of the CPW feed and the anticipated shape of the monopole antenna, a coupling current resulted, leading to gain enhancement. When the monopole antenna is situated on the human body at a distance of 30 mm, it resonates at 2.45 GHz. With the integration of the EBG surface, for a gap of 3 mm from the human body, the gain shows 2.68 dB and 11.54 dB at 2.45 GHz, correspondingly. Additionally, the SAR exhibited a reduction of 99.5%, averaging over 1 and 10 g of tissue.

Helin Yang et al. designed a small-sized, wearable antenna working in frequency bands 5.15 ∼ 5.25 GHz and 5.72 ∼5.83 GHz [45]. The simulated results confirm the EBG-incorporated

antenna has an impedance bandwidth of 4.09% and 4.14%, enlarged gains of 7.9 dB and 8.2 dB, and a front-to-back ratio of 20 dB and 18 dB at the two frequencies, correspondingly. The experimental results are very close to the simulated results. In general, the metasurface acts as a ground plane meant for improved isolation as well as the radiator that allows a maximum drop in the SAR.

In the present work, it is attempted to investigate various compact, flexible, and highly radiation-safe wearable antennas WBAN and W-WBSN applications. In addition, EBG and DGS structures are added beneath the radiating patch to accomplish isolation betwixt the antenna and the human body while giving the optimum performance to the gain and the presence of deformations and human tissue loading. The EBG structures are incorporated at the back of the antenna to enhance the FBR, leading to improved isolation betwixt the antenna and the human body. Further, a defective ground structure is etched in the ground plane of EBG to enhance the bandwidth without altering the other parameters.

MATLAB 2018 is used for the design of the antennas numerically, while CSTMW Studio 2019 is used for optimization and simulation purposes. The ADS electromagnetic software is used for the estimation of the equivalent circuits of the designed antennas. The flexible substrate materials Jeans of thickness 0.7 mm, and 2.5 mm, and RT Duroid 5880 of thickness 0.508 mm, and 1.57 mm are used to fabricate prototype antennas throughout the research work. Agilent N5247AVector network analyzer and anechoic chambers are used for measurement purposes.

1.6. Wearable antenna fabrication

The key considerations for any antenna working for WBAN applications is the electrical stability when placed on the human body and the novel fabrication procedures that offers enlarged mechanical strength to handle with various body postures, motion artefacts, subject specificity, and moisture (dampness/sweat). An additional concern is the attractiveness of the antenna. The antennas are integrated with clothing that never brings about any disturbance to the usual routine of the wearer. By contemplating this, the fabrication process of the wearable antenna must be adaptable and simple. Some of the available techniques are

- Line Patterning

- Flexography
- Screen-printing
- Photolithography
- Thermal evaporation
- Sewing and embroidering
- Inkjet printing

The Line patterning technique is the easiest and most reasonable fabrication methods for RFID and flexible electronics. In this method, the conductive patterns are imprinted by the following procedure, as seen in Fig.1.14. First, the silver nanowire (SNW) ink is released on the ditches with the help of a syringe. Allow the ink to flow into the tracks until full, then sinter at 125^0C for 30 minutes. Lastly, the PDMS template can be peeled off easily using forceps, and the desired antenna pattern is attained.

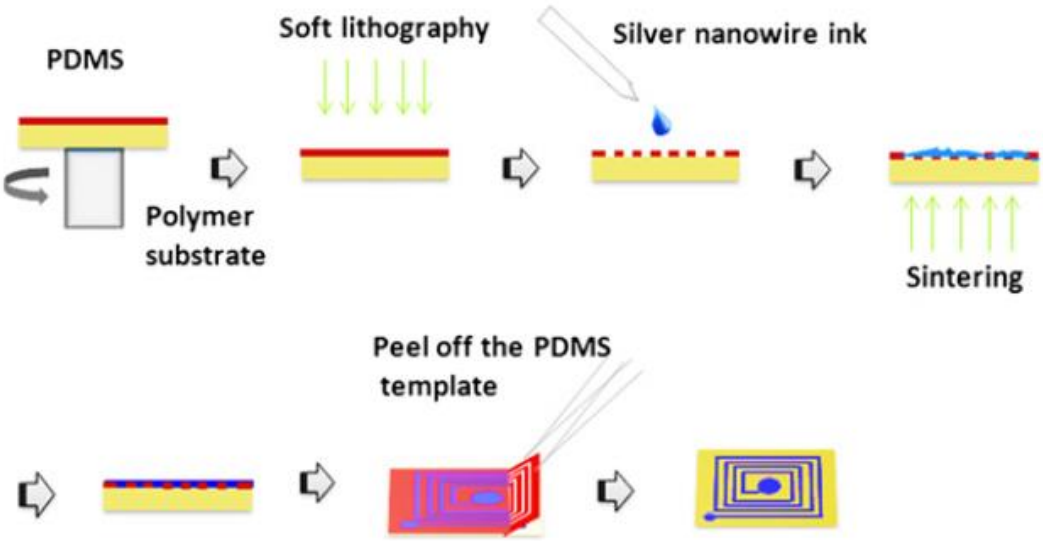

Fig.1.14. The fabrication process of an antenna pattern [46], [47]

In flexography, a high conductive ink is utilized, and only the protuberant surface has inked while other recessed areas are free of ink. The antenna's efficiency depends on the electrical conductivity of the radiating element. Screen printing begins with the creation of a mask with the desired pattern, which is then applied directly to a flexible substrate/film, where the conductive ink is applied and thermally treated to evaporate the excess solvent.

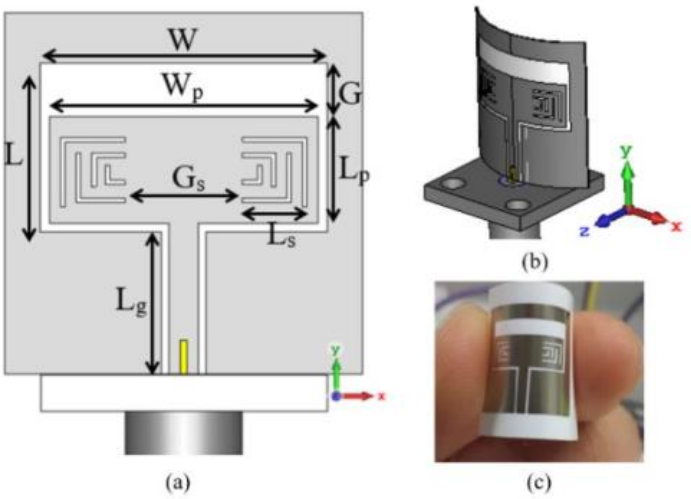

Fig.1.15. Inkjet printing [48], [49]

The highly conductive ink based on nanostructural materials is used in the inkjet printing of antennas. Inkjet material printers work on pico-liter-sized ink droplets, which lead to high-resolution patterns and compact designs. Photolithography method encompasses a photoresist and chemical agents to etch the undesired regions. The preferred template is extracted by engraving areas of either or both sides of a single or double-sided substrate.

Latest, the sewing or embroidery technique of prototyping wearable antennas has gained attention due to its unobtrusiveness. They also have a vigorous physical capability to withstand monotonous deformations due to dynamic movements of the human body. Furthermore, the computer-based fabrication process leads to faster production, which is useful, especially for mass production. To make embroidered antennas, a CAD software-controlled sewing machine is usually used. A digitised design is created from the design images that are entered into the CAD software and transferred to the sewing machine to serve as the embroidery guide. The following Fig. 1.16 shows the prototype of the textile antenna fabricated using the embroidery technique.

Fig.1.16. Common manufacturing techniques of conductive textiles [50]

In this thesis, the radiator scheme is refined over a low-cost jeans material, with a dielectric constant of 1.7 and a permittivity of 0.02. Adhesive copper tape is utilized for the radiating patch on the top of the substrate and the full ground plane below the substrate. The extent of flexibility and simple adhesive copper layer allows for improving the degree of comfort level to the user. The fabrication process of a flexible antenna starts with the prototype using adhesive copper tape. The jeans layers are stacked one by one and stitched to get the required thickness, and then the copper tape is attached in accordance with the proposed shape. Attaching a conducting copper tape of a different shape to a flexible fabric substrate is challenging. It may lead to errors and inaccuracy when dealing with sharp edges and complex shapes of a radiator. Scalpel cutting tools or stencil tools are utilized to maintain accurate and precise parts of antenna prototypes. Later, direct soldering connects the microstrip patch on top and the ground plane to the SMA connector. The cutting tool utilized for the fabrication and foam cylinders of the particular curvature is depicted in Fig.1.17.

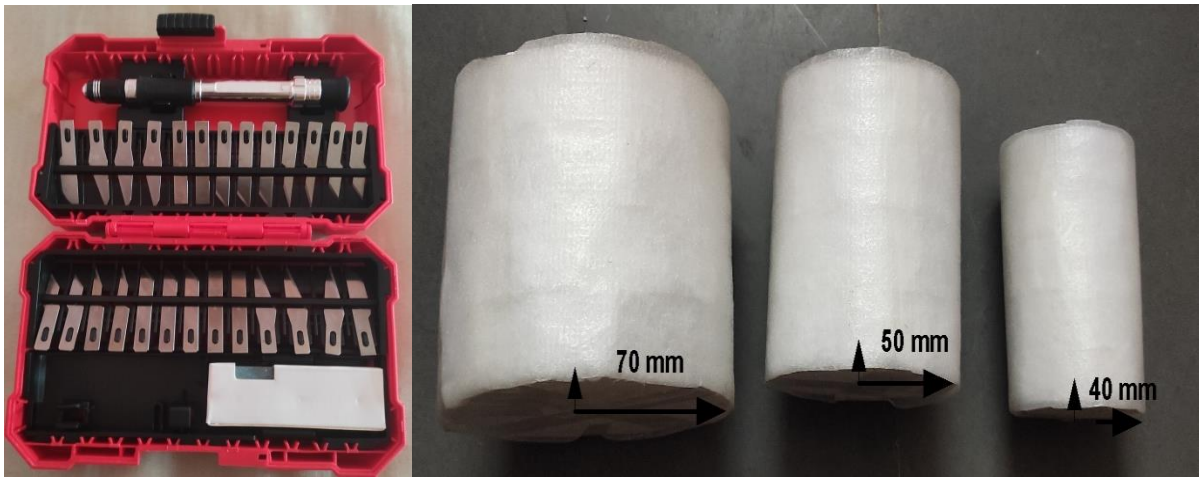

(a) (b)

Fig.1.17. (a) Scalpel cutting tool set (b) Foam cylinders represent the human body parts

1.7. Wearable antenna Measurement

The next step is to characterise the wearable antenna after it has been manufactured. Designed and optimize the antenna and analyzed its performance in free space and on the body utilizing the full-wave simulations later verified experimentally.

1.7.1. Commercial simulation software packages

Simulation software is the foremost part of designing an antenna with optimum performance because it is an intermediate stage between the antenna model and the fabrication process. After the fabrication process, the antenna model has the performance characteristics to be accurate and possible through simulation tools, and it helps save money and time. The simulation software is selected in such a way that it gives accurate antenna performance with accuracy. Hence simulation tool plays a key role in designing a microstrip antenna.

There are many electromagnetic (EM) simulation software packages available for designing an antenna, such as IE3D (Integral Equation 3-Dimension), HFSS (High-Frequency Structure Simulator), CST Studio (Computer Simulation Technology), ADS (Advanced Design System), FEKO, Antenna Magus, etc. Each simulation software is characterized in time or

frequency domain based on numerical techniques. For the opted antenna geometry, the selection of simulation tools plays a key role in giving the best performance.

Accordingly, the best EM simulation is based on optimum performance with respect to the minimal simulation run time. Based on the antenna design chosen and its complexity, simulation run time, and accurate performance, the antenna prototype is constructed from these inputs, and also, a maximum match of results of simulated and measured data is taken care of.

CST MW Studio: CST MICROWAVE STUDIO is a professional tool for modeling high-frequency structures. It also can provide fast and accurate analysis. For the specialized applications, various solver modules are inbuilt and enable the industry-standard workflow through the CST user interface. Multiple simulation solvers are available using the finite integration technique (FIT) method and finite element method (FEM). The CST Studio Suite's seamless integration of the solvers into a single user interface makes it simple to choose the best simulation approach for a particular issue class, resulting in better simulation performance and previously unheard simulation dependability through cross-verification. CST offers accurate computational solutions for electromagnetic design and analysis, and the solver offered by CST MW Studio is shown in Fig.1.18.

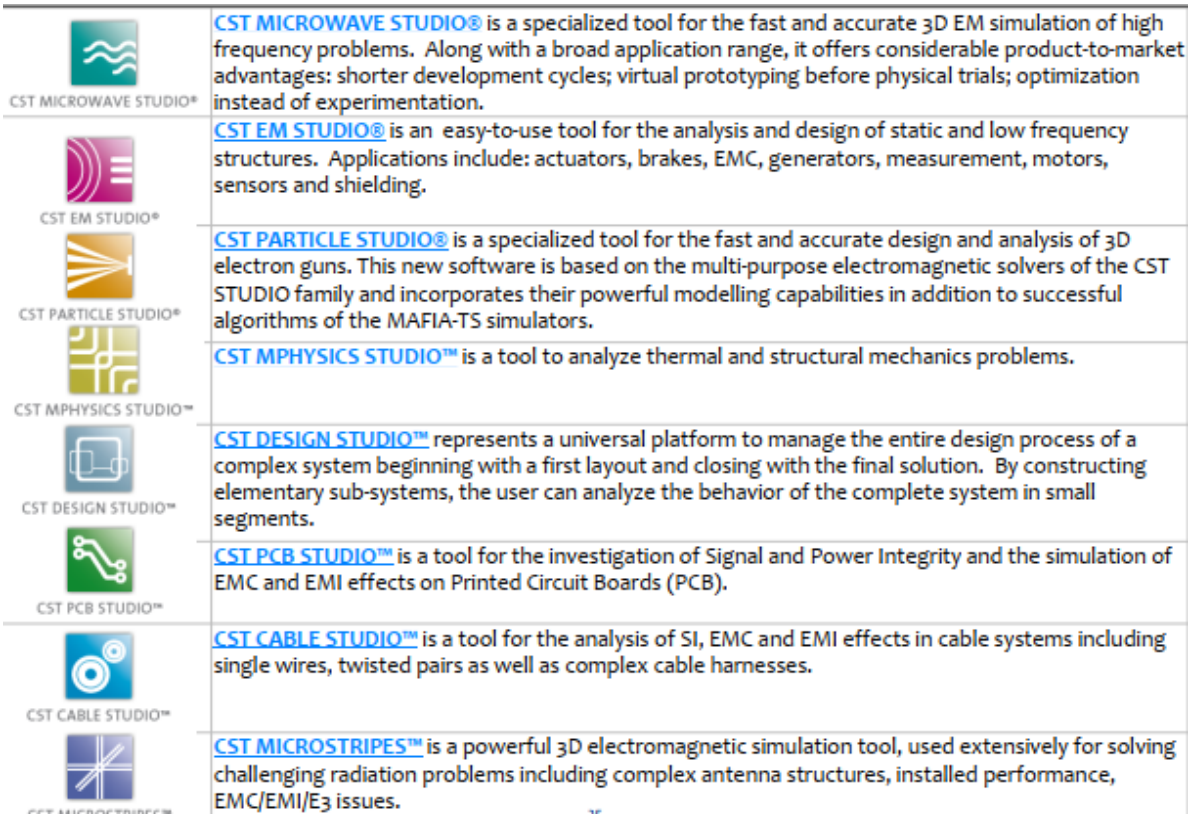

Fig. 1.18. Various solvers offered in CST MW Studio

Key Features of CST Design Studio:

The following are the primary features of CST Design Studio for high-frequency simulations.

- The construction can be observed in 3D model as well as schematic.
- Numerous independent solver approaches (depending on hexahedral and tetrahedral meshes) permit accurate analysis for high-frequency applications.
- Feasibility to import 2D CAD data from DXF GDSII and Gerber file formats
- Numerous bio models and voxel models for import and analysis.
- Vast substrate material database
- Supports frequency domain, Eigenmode, integral equation, and Asymptotic solvers
- plane wave excitation
- Characteristic mode analysis

Every CST simulation involves six basic steps to create the structure and to solve using the appropriate EM Solvers.

1. Selecting a template
2. Adjusting working plane properties
3. Create the proposed geometry
4. Define ports at the appropriate locations
5. Assign boundaries
6. Simulate using the suitable solver

After getting the solver run for the defined structure, post-processing is required to acquire the achieved results. The CST design environment is shown in Fig. 1.19.

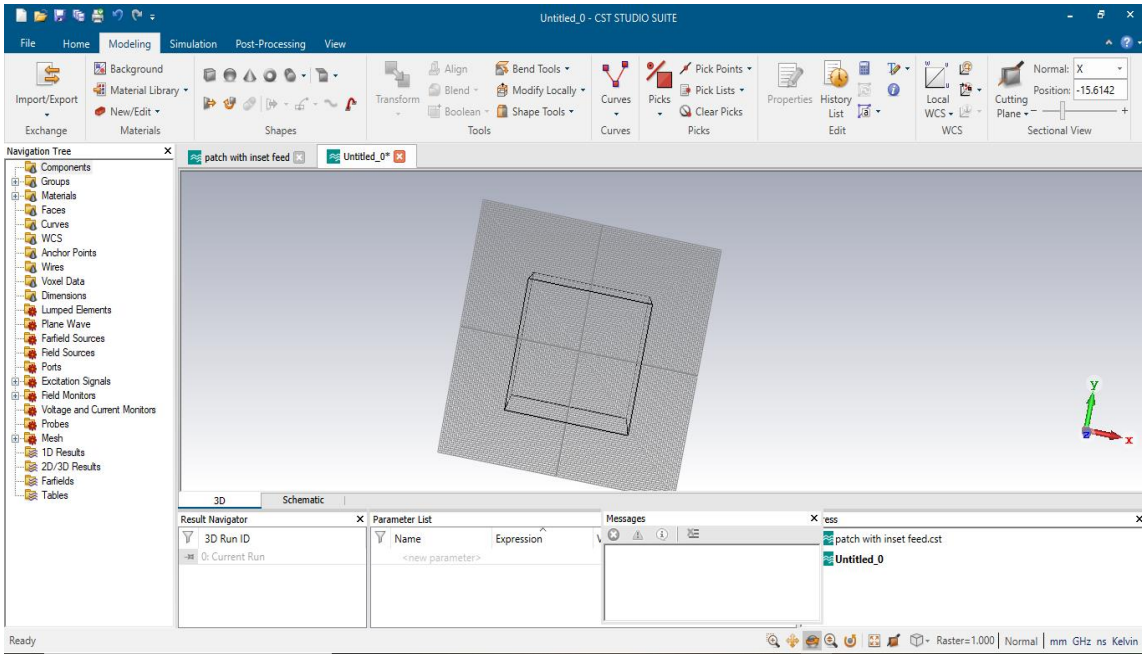

Fig.1.19. CST Design Environment

ADS Software

Advanced Design System (ADS) software is useful for designers, engineers, and businesses to quickly design and produce high-quality components and systems. ADS has revolutionized the world of circuit designing and system designing for electronics, automotive, and other industries, which are rapidly adopting this unique solution with out-of-the-box features and functionalities. ADS software is the leading electronic circuit design, simulation, and automation software developed by Path Wave Design, which comes under Keysight

Technologies. ADS software offers an integrated environment to design RF electronic systems like wireless networks, mobile phones, satellite communications, pagers, high-speed data links, and radar systems. Its initial release surfaced in 1985 named – Microwave Design System (MDS). ADS software was introduced in 2016 with improvements in its speed, performance, and design flexibility.

Some of the features of ADS are as follows:

- Keysight's ADS helps reduce hardware failure and associated costs by intelligently integrating modules interconnecting circuit design systems such as radio-frequency integrated circuits (RFIC), laminate, antennas, and monolithic microwave integrated circuits (MMIC), wafer-level packaging, and PCBs into dense 3-dimensional structures.
- ADS also helps you simulate EVM for optimization and tuning to help you verify industry-level wireless standards like automotive radar, 5G, Wi-Fi, etc. With comprehensive and rigorous amplifier-stability analysis, ADS replaces traditional techniques to provide enhanced amplifier stability under non-linear and linear conditions.

1.7.2. Measurement of various parameters

An experimental apparatus such as a Vector network analyzer and the anechoic chamber is required to validate the simulation results. Care must be taken for the accurate measurement of the parameters. The deformation tests can be conducted by utilizing a cylindrical foam fixture of the required curvature.

1.7.2.1. Return loss

The return loss is measured using Vector Network Analyzer (VNA). In this work, Agilent N5247A Network analyzer (10 MHz- 40 GHz) and Hewlett Packard 8719A vector network analyzer are used. For the measurement, one port, or both ports, is/are connected to the network analyzer, which performs S-parameter analysis.

The fabricated antennas are wrapped around the foam cylinders of various curvatures to validate the bending effect, as shown in Fig. 1.20, to impersonate human body parts while it is connected to the network analyzer.

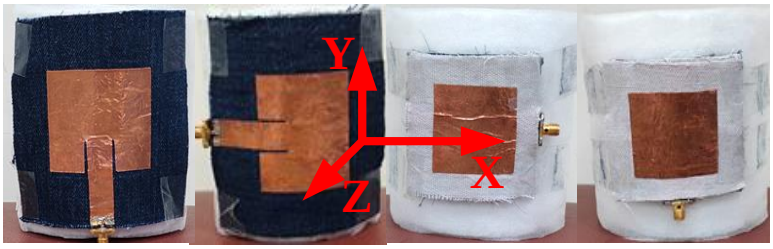

Fig.1.20. Textile antennas wrap around the foam cylinder along E, H-plane directions

1.7.2.2. Anechoic chamber

Generally, the principal plane patterns can be measured in a far-field test setup (preferably in an anechoic chamber) with a standard gain antenna as a transmitter and the antenna under test (AUT) as a receiver placed over a pedestal that can turn the antenna around all axis. The chamber is isolated from the outside, absorbing most of the radiation from the antenna. The measurement is done by letting the antenna radiate over a frequency sweep with a uniform selection of all possible angles. By comparing results to a calibration run, the radiation pattern of the antenna is obtained. Finally, together with the knowledge of the input power of the antenna, it is possible to calculate the efficiency of the antenna.

The measurement facility used to verify the results in this thesis is an anechoic chamber at the Indian Institute of Technology Roorkee (IITR) and the National Institute of Technology Warangal (NITW), India. The model of the measurement facility is displayed in Fig. 1.21.

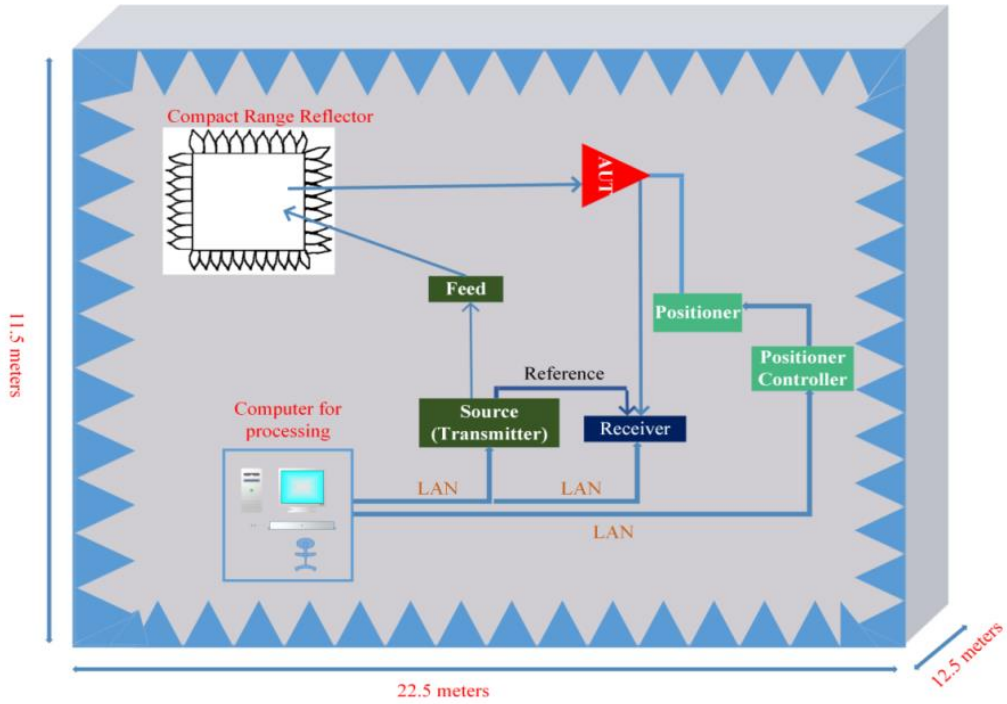

(a)

(b)

Fig.1.21. (a) Measurement setup for the radiation pattern calibration (b) Inside the Anechoic chamber

1.7.2.3. Specific Absorption Rate (SAR)

For wearable applications, the impact of antennas on the human body must be assessed. Fig. 1.22 shows the sample antennas simulated SAR on a flat four-layer human body and on the HUGO voxel model from the CST Voxel family.

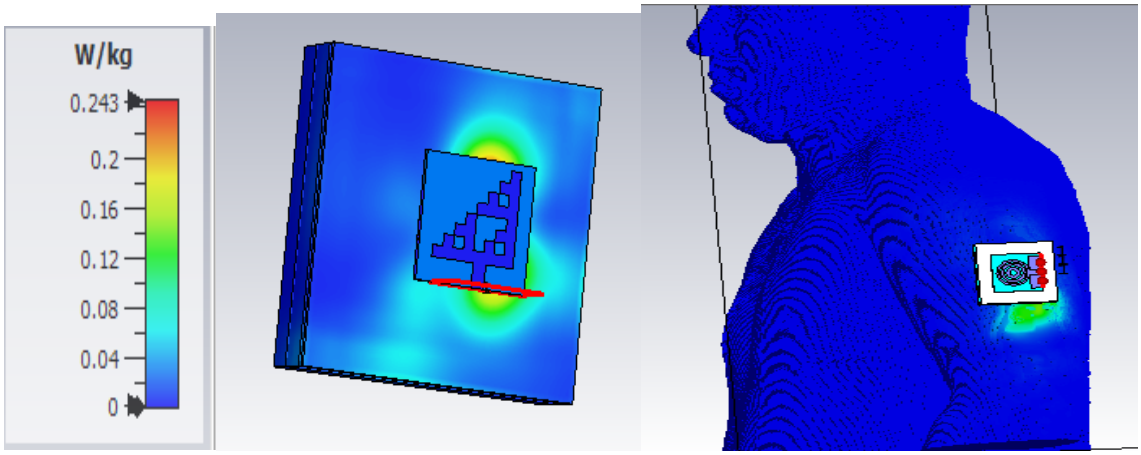

(a) (b)

Fig.1.22. Simulated SAR of the example antenna (a) on standard four-layer human phantom (b) on HUGO Voxel model

1.8. Motivation and problem formulation

1.8.1. Motivation

Body-centric systems refer to communication systems encompassing the interactions in the existence of the human body. They may be considered as the perpetuation of the development in progress with the expansion of mobile phones, while their possible applications range from military communication systems to medical telemetry or commercial use. The antenna is an indispensable part of any body-centric device. Thus, its design requirements need to be modified to adapt to the particular demands and features of the body-centric environment. They must be principally considered to function while put on and off the body. Microstrip patch antennas have been extensively utilized in wearable applications with their merits like low cost, small size, simple structure, and easy incorporation into clothing. However, they suffer from narrow bandwidth, low gain, and less power. While wireless equipment emphasizes the exchange of data and interconnection between devices, the antenna has to be multipurpose. Henceforth the size, multiband operation, impedance bandwidth, fewer radiation losses, high gain, and high efficiency

are the extremely inspiring characteristics in antenna design, which is the motivation for this research.

The objective is to design a type of antennas that are appropriate for on-body applications in WLAN and WBAN standards. The following are the desired characteristics of the anticipated antennas

1. It must be conformal and convenient to elude any disconcertment.
2. Diminishing electromagnetic exposure into the human body for safety apprehension and guaranteeing maximum on-body radiation efficiency.
3. Employing realistic substrates and production procedures to minimize the global cost and uphold convinced robustness levels.
4. The simple and compact profile of the antenna for its efficient usage in various devices

To achieve these properties, the Microstrip antennas incorporated with EBG and DGS structures are developed for achieving compactness, bandwidth enhancement, improved isolation, and SAR for wireless communication applications. The goal is to design a wearable antenna with less complexity for its efficient usefulness in several wireless devices.

Many wearable antenna designs published in the literature are using semi-flexible substrates [51]–[53], large in size, small gain, less isolation from the body, not tolerable to bending, and high specific absorption rates [44], [54], [55]. The novel contributions of this thesis proposed a solution to each unsolved challenges by introducing an EBG surfaces and defective EBG structures to not only enhance the performance characteristics of the wearable antennas, but also provides the wearability, breathability and conformability to the wearer.

1.8.2. Problem Statement

To design, fabricate and validate a wearable antenna with improved gain, bandwidth, FBR, cross-polarization properties, and highly radiation safe while maintaining low-profile characteristics even in the deformation and human tissue environment in ISM and MBAN frequency bands.

1.9. Objectives and scope of the research

The objectives of the research work are mentioned below:

- Design, fabricate and test compact, flexible, highly radiation-safe, wearable antennas for WBAN applications.
- Use simple fractal structures and a tranquil fabrication process.
- Compact dimensions with microstrip line feed and compared with the existing literature
- Incorporation of the EBG structures beneath the antennas to enhance the bandwidth, gain, FBR, and isolation.
- Simultaneous improvement of gain, impedance bandwidth, SAR, and co-polarization of the wearable antenna by introducing defects in the ground plane of EBG.
- To enhance the breathability and wearability with the use of perforated ground plane EBG along with the other desirable parameters.

1.10. Contribution to the knowledge

The key contributions of this work are summarized as follows:

a) Various techniques to improve the gain and bandwidth of wearable antennas for WBAN applications are studied, and designed a simple step-shaped Sierpinski fractal antenna for WBAN applications [2**], [1**].

b) Designed microstrip patch antennas using inset and aperture coupled feeding techniques on the flexible jeans and wash cotton substrates and experimentally verified the bending for various diameters for wearable applications in WBAN. A circuit modeling of the patch antennas loaded with fractal slots and notches is obtained using the ADS simulator. Also, the electromagnetic properties of the substrates used in the design are estimated and measured experimentally using the Microstrip ring resonator method [2*].

c) A novel, robust, efficient, and highly radiation-safe wearable antenna backed by EBG substrate at 2.45 GHz is designed, fabricated (Rogers RT 5880 with a thickness of 0.508 mm), and measured experimentally. The purpose of the design is to provide a high gain, improved FBR, and Specific Absorption Rate (SAR) [3*].

d) A high gain, low SAR saw-tooth shaped fractal boundary wearable patch antenna is designed and fabricated for ISM band frequencies. The purpose of the proposed design is to withstand the deformations when worn on the human body while maintaining the optimum performance in terms of gain and SAR [4*].

e) A dual-band EBG-DGS wearable antenna for emergency search services and responses in WBAN applications is designed, fabricated, and measured. The purpose of the design is to create a compact, high gain and an efficiency of about 70% under the various bending scenarios while influencing the co-& cross-polarization at WLAN bands (2.4-2.485GHz and 5.1-5.9GHz) [5*].

f) A triple band, breathable, improved wearable CPW-fed antenna backed by a porous EBG structure for WBAN applications is designed. The performance of the designed antennas is verified experimentally in an anechoic chamber. The purpose of the design is to improve breathability while maintaining the other characteristics of the designed antenna [6*].

g) A flexible, compact, Sierpinski step-shaped fractal antenna on the Hilbert patterned ground for Wearable-wireless body sensor networks (W-WBSN) is designed, fabricated, and measured for 3.3 GHz/5.2 GHz/5.8 GHz frequencies [1*].

* indicates Author's Joint Journal Publications and, ** indicates Author's Joint Conference Publications

1.11. Organization of thesis

The thesis is organized as follows

Chapter 1: Introduction

This chapter presents a brief introduction to antennas and explains the importance of wearable antennas in the present-day wireless body area environment. It also presents the importance of Wireless Body Area Networks (WBAN) in the day-to-day application and their uses. This is followed by an introduction to simulation software packages used to design and predict the performance of the antennas. The motivation behind this research work and thesis

objectives and contributions are also mentioned. In the end, the organization of the thesis is elaborated.

Chapter 2: Wearable antennas: Electrical equivalents

In this chapter, the electrical equivalent of the wearable antennas (when loaded with the notches and slots) has been estimated and validated using the software ADS. Also, the deformation effects on the wearable antennas when bent on a certain radius have been presented. Two exciting feeding methods were adopted and fabricated on Jeans and wash cotton substrate materials, experimentally validated, and bending analysis is also presented.

Chapter 3: Microstrip line fed Wearable antennas for On Body applications

This chapter presents a detailed overview and review of the previously published work in the area of wearable antennas for WBAN and W-WBSN applications with their limitations. Also presents the techniques applied for the improvement of bandwidth, gain, FBR, Co-& Cross-polarization, and specific absorption rate (SAR). Three prototypes of compact, multiband, and high gain wearable antennas using fractal boundary are designed, fabricated, and validated experimentally for WBAN application, and the prototypes are compared with the existing wearable antennas. The compactness, multiband characteristics, gain, and SAR are obtained by incorporating various techniques like Sierpinski fractals, Hilbert patterned ground planes, and fractal boundary shapes, respectively.

Chapter 4: Flexible Monopole Antenna Incorporated with Electromagnetic Bandgap (EBG) structures

This chapter explains the design and performance evaluation of compact, flexible wearable antennas incorporated with electromagnetic bandgap structures. The proposed Koch fractal boundary monopole antenna is applicable for wearable applications in WLAN. A robust, compact, and high radiation efficiency antenna backed by an EBG structure is designed, fabricated, and validated experimentally for wearable applications in WLAN standards, and the prototype is compared with the existing literature. The compactness, maximum gain

characteristics, and SAR are obtained by incorporating the Electromagnetic bandgap (EBG) structures beneath the patch antenna and Koch fractal, meander slits parallel to the feed line of the patch, respectively.

Chapter 5: Dual-band, EBG-DGS Wearable antenna for Emergency services and responses in WBAN

This chapter presents the design and performance evaluation of a Dual-band EBG-DGS incorporated wearable antenna for Emergency services and responses in WBAN. The gain and SAR, along with the co & cross-polarized fields, are improved with the utilization of DGS in the ground plane of EBG. The defect in the form of DGS improves Cross-polarization and co-polarization by changing the fields in the ground plane at the back of EBG.

Chapter6: Improved wearable, breathable triple antenna integrated with porous EBG

This chapter presents the design and performance evaluation of a multiband wearable antenna backed by perforated EBG structures as a reflective surface for improving the wearability and breathability of WBAN and W-WBSN applications.

Chapter 7: Conclusions & Future Scope

A consolidation of the results achieved is presented. Compact and radiation-safe wearable antennas using various techniques are designed for WBAN applications to increase the impedance bandwidth, gain, and SAR. Consequently, the achieved results demonstrated that the designed wearable antennas are potential candidates for WBAN and W-WBSN applications. Also, concludes the thesis and the open issues for future work are also mentioned.

Chapter 2.

Circuit Modelling and Effect of Deformations on Wearable Antennas

This chapter presents the methods to evaluate and experimentally calculate the dielectric characteristics of the flexible substrates that are utilized in the wearable antenna design. Later, two microstrip antennas with inset feed and aperture coupled feed are designed, fabricated, and on Jeans and wash cotton substrates. Also, the electrical equivalent circuits of the designed antennas for different feeding methods are drawn and validated the equivalent circuits are using ADS software. Later, the deformation effects on the wearable antennas for various bending curvatures and equivalent circuit simulations are performed.

2.1. Introduction

Electrical equivalents are advantageous for antenna design, as the EM simulations are time consuming, and require a huge computational effort. Presently, microstrip antennas are advanced due to their features like lightweight, low volume, and compactness in size. Despite their low gain and bandwidth, these are found effective in short-range communications, system on chip and antenna in the package, etc. Generally, the compact and efficient antenna designs came from several antenna techniques such as meander line, looping, shorting pins, fractals, loading with reactive elements, embedding slots, electromagnetic bandgap (EBG), and structures and defected ground structures (DGS). When it comes to the design of a wearable antenna, it should possess highly flexible, have almost no installation requirements, have high durability, and support bending and stretching at certain strain levels, but simultaneously it must be able to still function efficiently without compromising its RF characteristics. However, all these requirements might

induce certain design complexities while achieving the desired specifications. On the other hand, this can be made very easy by introducing the circuit models and potentials to estimate the insights of the physical designs of the antennas.

2.2. Theoretical analysis of wearable antennas

The electrical equivalent circuit of the rectangular patch antenna is the parallel combination of resistance (R1), inductance (L1), and capacitance (C1), and their parametric values are given by [56]

$$C_1 = \frac{\varepsilon_0 \varepsilon_e L W}{2h} \cos^{-2}\left(\frac{\pi y_0}{L}\right) \tag{2.1}$$

$$L_1 = \frac{1}{\omega^2 C_1} \tag{2.2}$$

$$R_1 = \frac{Q_r}{\omega C_1} \tag{2.3}$$

$$\varepsilon_e = \frac{\varepsilon_r + 1}{2} + \frac{\varepsilon_r - 1}{2}\left(1 + \frac{10h}{W}\right)^{\frac{-1}{2}} \tag{2.4}$$

Where ε_r = relative permittivity and ε_e= effective permittivity, h = height of the substrate.

$$Q_r = \frac{\sqrt[C]{\varepsilon_e}}{4fh} \tag{2.5}$$

Where Q_r= quality factor, f = resonating frequency, and c = speed of light.

The impedance of a simple patch can be calculated in the following manner, which is presented in Equation (2.6)

$$Z_{patch} = \frac{1}{\frac{1}{R_1} + \frac{1}{j\omega L_1} + j\omega C_1} \tag{2.6}$$

This antenna is excited by a 50-ohm microstrip line feed, and its parameter values are evaluated by Equations (2.7), (2.8)

$$C_a = W_1\left[\left(10.1\log\varepsilon_r + 2.33\right).\frac{W_1}{W_2} - 12.6\log\varepsilon_r - 317\right] \tag{2.7}$$

$$L_a = H\left[40.5\left(\frac{W_1}{W_2} - 1\right) - 75\log\left(\frac{W_1}{W_2}\right) + 0.2\left(\frac{W_1}{W_2} - 1\right)^2\right] \tag{2.8}$$

In general, the antenna designs are optimized to get the desired solutions for particular applications. In the process, the basic shape of the patch is loaded with slots and notches. If the slots are inserted in the patch, then the resistance and reactance of the slot are added in series with the already existing patch, which is given by Equations (2.9), and (2.10).

$$Z_{slot} = R_{slot} + jX_{slot} \tag{2.9}$$

$$R_{slot} = 60C + \ln\left(kL_{sl}\right) + \frac{1}{2}\sin\left(kL_{sl}\right)\left[s_i\left(2\left(kL_{sl}\right)2S_i\left(kL_{sl}\right)\right)\right] + \frac{1}{2}\cos\left(kL_{sl}\right)C + \ln\frac{\left(kL_{sl}\right)}{2} \tag{2.10}$$

$$X_{slot} = 30\cos^2\alpha\left\{2S_i\left(kL_{sl}\right) + \cos\left(kL_{sl}\right)\left[2S_i\left(kL_{sl}\right) - S_i\left(2kL_{sl}\right) - \sin\left(kL_{sl}\right)\right]\left[2C_i\left(kL_{sl}\right) - C_i\left(2kL_{sl}\right) - C_i\left(\frac{2kW_{sl}^2}{L_{sl}}\right)\right]\right\} \tag{2.11}$$

Where

$$S_i\left(x\right) = \int_0^x \frac{\sin\left(x\right)}{x}dx,\ C_i\left(x\right) = -\int_x^\infty \frac{\sin\left(x\right)}{x}dx$$

L_{sl} = length of the slot, C = 0.5772 (Euler's constant), and k = propagation constant.

The equivalent circuit of the basic microstrip line-fed patch antenna with the slot-loading is shown in Fig. 2.1.

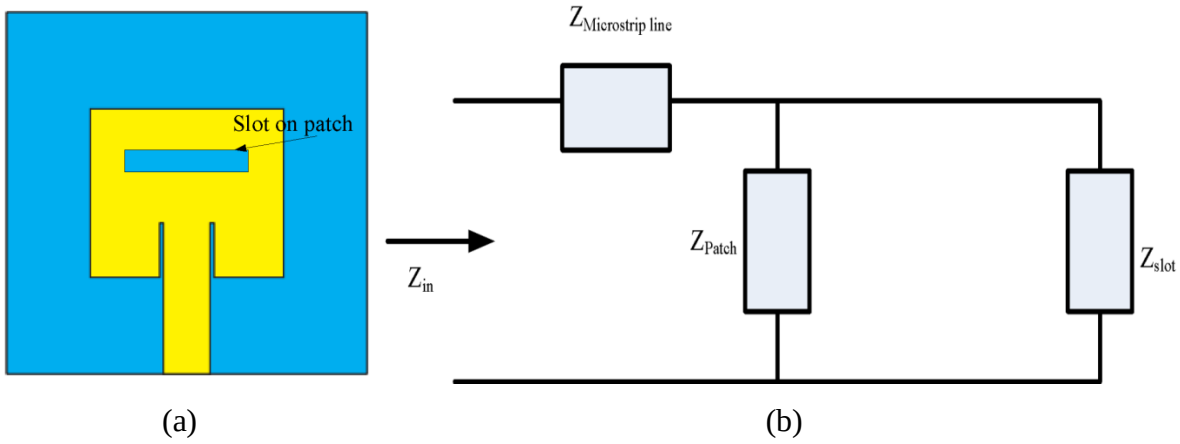

Fig.2.1. (a) Slot-loaded patch and (b) Equivalent circuit model of the slot-loaded patch

Cutting a slit on the patch's edge is seen as a notch, that can embraces a parallel combination of R2, L2, and C2, whereas L2 is the series inductance value of L1, ΔL1, and ΔL2. Similarly, C2 is also the series capacitance value of C_1, ΔC_1, and ΔC_2 [57].

$$L_2 = L_1 + \Delta L_1 + \Delta L_2 \tag{2.12}$$

$$C_2 = \frac{C_1 \Delta C_1 \Delta C_2}{C_1 + \Delta C_1 + \Delta C_2} \tag{2.13}$$

$$\Delta L = \frac{h \mu_0 \pi}{8} \left(\frac{W_{patch}}{w_{notch}} \right) \tag{2.14}$$

$$\Delta C = \left(\frac{W_{patch}}{w_{notch}} \right) C_{gap-capacitance} \tag{2.15}$$

$$Z_{notch} = \frac{1}{\frac{1}{R_2} + \frac{1}{j\omega L_2} + j\omega C_2} \tag{2.16}$$

When the patch antenna is loaded with notches, a coupling capacitance is presented in the equivalent circuit, given by Equations (2.17) and (2.18).

$$C_c = \frac{-(C_1 + C_2) + \sqrt{(C_1 + C_2)^2 - C_1 C_2 \left(1 - \frac{1}{k_c^2}\right)}}{2} \tag{2.17}$$

$$Z_c = \frac{1}{j\omega C_c} \tag{2.18}$$

When the patch is loaded with the combination of slots and notches, then the equivalent impedance between the slot and notch is evaluated by the following Equations. The equivalent circuit is shown in Fig. 2.2.

$$Z = \frac{Z_{notch} Z_{slot}}{Z_{notch} + Z_{slot}} \tag{2.19}$$

$$Z_{in} = \frac{Z_{patch}(Z_c + Z)}{Z_{patch} + Z_c + Z} \tag{2.20}$$

$$\Gamma = \frac{Z_0 - Z_{in}}{Z_0 + Z_{in}} \tag{2.21}$$

$$VSWR = \frac{1 + |\Gamma|}{1 - |\Gamma|} \tag{2.22}$$

$$\text{Returnloss} = 20 \log |\Gamma| \tag{2.23}$$

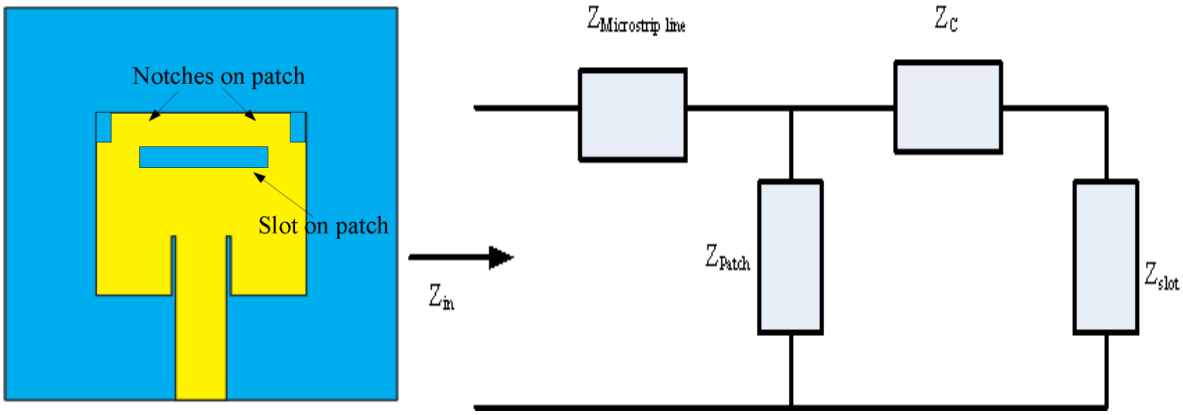

(a) (b)

Fig.2.2. (a) Slot and notches loaded on the patch and (b) Equivalent circuit model of the slot and notch loaded patch antenna

Further, every design is verified and simulated using the circuit theory in the EM simulator Advanced Design System (ADS), a keysight circuit simulator, from which the optimization and elemental electrical parameters are evaluated.

2.3. Textiles and their EM characteristics

There are significant ramifications to understanding how internal textile components modify the dielectric characteristics of textile materials. The advancement of the textile antenna depends on the unique features of the dielectric textile materials used in the design. The same has drawn ever-increasing interest due to the collective features of electronics and traditional fabrics. The electromagnetic properties of the textiles include electrical conductivity, dielectric properties such as permittivity and loss tangent, and electrostatic and magnetic properties. Etc. Textiles typically have poor electromagnetic (EM) properties, such as low conductivity, low dielectric constants, and low magnetic constants, which reduce surface wave losses and broaden the impedance bandwidth of the antenna.

In recent times, electro textiles (e-textiles) have drawn a lot of interest as potentially useful materials for the construction of wearable antennas that are entirely flexible and enable free wireless communication for smart clothing. Usually, in the wearable antenna design, e-textiles are utilized for the radiating parts whereas the dielectric materials for the substrates. The electromagnetic properties of the substrates like dielectric constant and loss tangent need to be measured, as they play a key role in deciding the antenna characteristics. For instance, the bandwidth and efficiency of the patch antenna depends on the permittivity and thickness of the substrate

The design procedure of the wearable antennas can be explained with the following flow chart shown in Fig. 2.3. As in Fig.2.3, The design of the wearable antenna starts with the selection of the conductive and dielectric materials according to the requirements. In this thesis, adhesive copper tape is used for the conductive parts of the antenna, and a casual jeans material is used as

the substrate material. Then the electromagnetic properties of the dielectric material, such as permittivity and loss tangent, must be obtained. Later, the antenna profile and feeding methods are specified and simulated using the Electromagnetic simulator CST MW Studio and optimize the dimensions before fabrication. At last, the fabrication method is selected based on the availability of materials used and antenna topology. Further, a series of measurements have been performed for S-parameters, radiation patterns, and gain, along with bending behavior. Specific Absorption Rate (SAR) should be conducted and compared with the standards to conform to the wearable applications.

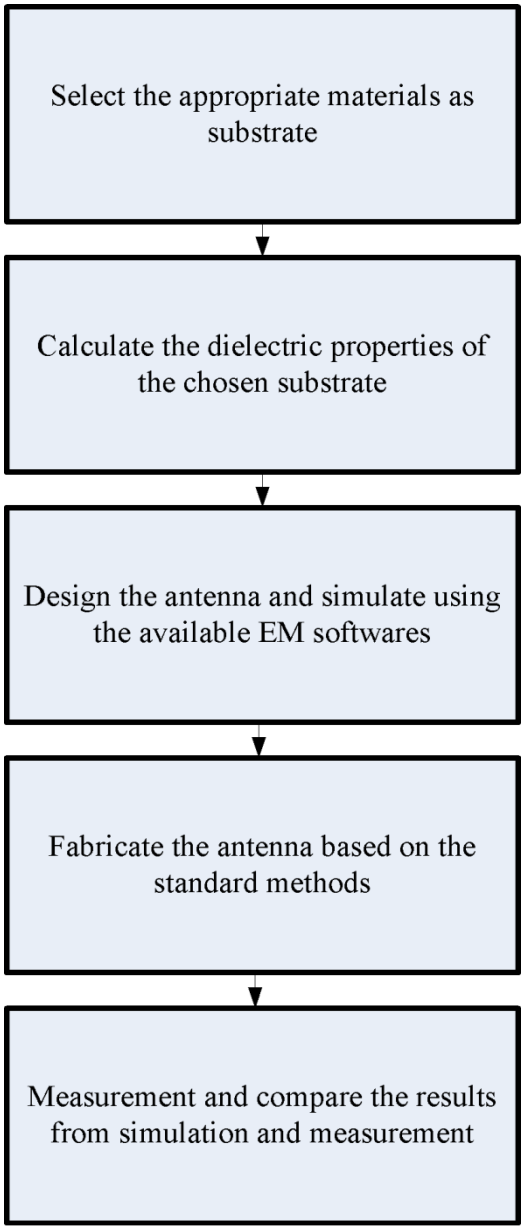

Fig.2.3. Flow chart of the wearable antenna design flow

2.3.1. Dielectric fabrics

Dielectric substrate materials are typically employed to support the conductive antenna elements. There are many different types of flexible substrate materials existing in the present-day market, and these are approved based on the properties of conductive materials exploited in the design of the antenna. Some of them are Polymid films, Polyester (Also referred to as Polyethylene Terephthalate, PET), Liquid crystal films (LCP), and Kapton. The Kapton material, as a high-performance PI film, shows good soldering tolerance for flexible antenna fabrication and withstands high temperatures, which is required in the thermal annealing of inkjet printed antennas [58].

However, the non-conductive fabrics or fabrics used in clothing are also utilized for the design of flexible antennas. Various textile materials are employed, such as wash cotton, silk, wool, viscose, felt, and jeans materials. Etc. The dielectric properties of such materials highly depend on the type of construction, like knitted or woven, and the thickness of the materials. Hence, obtaining the electromagnetic properties of such textiles is quite important before the design and simulation. Other types of substrates, such as paper, PDMS, and foam materials, can be utilized for special purposes. For instance, the paper substrate is used in inkjet printing or screen printing as paper is a low-cost and widely available material. But the only disadvantage is that it is lossy and frequency dependent. The PDMS substrates are waterproof and show stable behavior for high temperatures. Also, the substrates whose dielectric constant is approximately equal to air can be utilized for embroidering within the clothing.

2.3.2. Conductive fabrics

Similar to conventional antennas, wearable antennas are also utilizing pure metallic materials for the conducting parts of the antenna. These can include Silver paste, Copper foils, and copper gauze. If the wearable antenna can adopt these materials in the design process, then adhesive copper laminates or supporting foams can be utilized instead of the embroidery or sewing methods. The only advantage of using these materials is that they have high conductivity, low price, and fabrication simplicity. On the other hand, e-textiles or electro-textiles are the other options for the conductive parts of the antenna design. Adopting these metal-plated textiles in the

design enables the sewing into clothing by conductive threads. Some of these materials are Nora, FlecTron, and Zelt materials.

The conductive ink, which is made of carbon or metal particles, is also a promising material for the flexible antenna design. This made the antenna fabrication simple and effortless, compatible with standard screen printing and inkjet printing method of fabrication.

2.3.3. Dielectric properties of fabrics

Several techniques are available in the literature to identify the dielectric properties of fabrics. One simple technique adopted here is the Microstrip Ring Resonator (MRR), which is useful for Analyzing the electromagnetic properties of the materials due to its feasible geometry, ease in prototyping, low price, small volume, and adaptability [59], [60]. The proper usage of the fabric material as substrate while designing wearable low-profile antennas makes them efficient. The MRR method uses the resonant frequency and the quality factor to calculate the permittivity and loss tangent of the substrate, which gives accurate results due to the absence of end effects and the high Q factor. This makes the proposed method advantageous compared to previously published [61].

A straightforward resonant technique to characterize sample fabric's electromagnetic properties is based on the MRR, and another method is based on the patch radiator, which is used to validate the results of the first. The geometry of the MRR involves the ring and two feed lines separated by a gap(Δ), which are placed on top of the substrate of size $50\times50mm^2$.On the back of the substrate, the ground plane is placed. Adhesive copper foil is utilized for the metal parts, such as the ring and the two feed lines, whereas flexible jean is the substrate, as shown in Figure 2.4. The optimized dimensions are obtained with the help of traditional equations (Table 2.1).

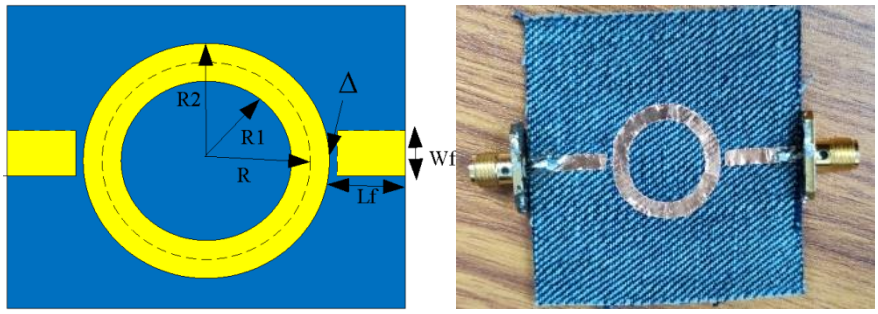

(a) (b)

Fig. 2.4. (a) Schematic of the MRR (b) Fabricated Prototype

Table.2.1. Optimized dimensions of the MRR

Ring Dimensions	Mean Radius (R)	R1	R2	feed line Width (W_f)	Feed line Length (L_f)	Gap (Δ)
Value (mm)	8.5	6.5	10.5	3	14	1

Theoretically, the nth resonance peak takes place at [62]

$$F_n = \frac{nc}{2\pi R\sqrt{\varepsilon_r}} \tag{2.24}$$

Where R is the average radius, c is the speed of light in a vacuum, and ε_r is the required dielectric constant.

Also, the insertion loss S_{21} (dB) is given by

$$IL = 20\log\left[1-\frac{Q_l}{Q_u}\right] \tag{2.25}$$

Where Q_l and Q_u are the loaded and unloaded quality factors, respectively

From the S_{21} curve, the loaded quality factor given by

$$Q_l = \frac{f_0}{\Delta f} \tag{2.26}$$

Where f_0 = Resonance frequency

Δf = Difference frequency from upper to lower in the S_{21} (dB) curve.

The loss tangent can be calculated by determining the unloaded quality factor Q_u from equation (2.25) and substituting in the following equation (2.27)

$$\frac{1}{Q_u} = \frac{1}{Q_c} + \frac{1}{Q_d} \tag{2.27}$$

$$Q_c = h\sqrt{f_0 \mu_0 \pi \sigma_c} \tag{2.28}$$

Where Q_d and Q_c are the quality factors of dielectric and conductor, respectively.
And then, the loss tangent is calculated from the equation

$$\tan \delta = \frac{1}{Q_d} \tag{2.29}$$

Fig.2.5 shows the measurement setup on the network analyzer and the transmission coefficient of the proposed method. From Figure.2.5, it is observed that there are two resonance peaks obtained at 4.27GHz and 8.9 GHz, respectively, with a corresponding return loss of -35.94 and -22.48 dB for the jeans textile. Based on the resonant peaks that appeared in S_{21}, the dielectric properties are calculated by substituting equations (2.24-2.29) and tabulated in Table.2.2. The simulated and measured values are in good agreement with each other. This result is also verified by the second method, which is focused on designing the patch antenna on the desired substrate that was done in [63].

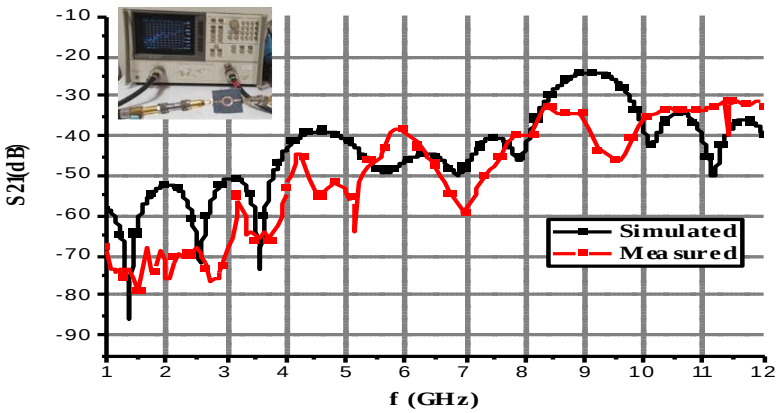

Fig.2.5. S_{21} (dB) Vs. Frequency of MRR

Table. 2.2. Resultant dielectric properties of Jeans Substrate using the method of Ring Resonator

Mode	Resonant Frequency (GHz)	Insertion loss (S_{21} (dB))	dielectric constant (ε_r)	loss tangent (tanδ)
n=1	4.2716	-35.94322	1.729	0.078
n=2	8.916	-24.9838	1.687	0.025

In general, the fabric material is said to be lossless when the loss tangent is significantly less. According to the obtained results, the dielectric constant and loss tangent are taken to be 1.729, 0.025, respectively [64]-[65]. Usually, the substrate's relative permittivity plays a substantial part in the design of the antenna, and variations in its value tend to change the operating frequency of the antenna to more or less of the desired center frequency. However, the variation in loss tangent has a negligible effect on the antenna resonant frequency, affecting mostly the magnitude of return loss.

2.4. Design of Wearable antenna using various feeding methods

Ideally, a wearable antenna should be highly flexible, lightweight, and small in volume, have no installation requirements, and have high durability and supports bending, and stretching at certain strain levels but still function efficiently without compromising its RF characteristics.

Here, two wearable antennas are designed with different feeding mechanisms, and their equivalent circuits are obtained.

2.4.1. Inset-fed wearable patch antenna and its electrical equivalent

The elementary form of a microstrip patch antenna consists of two metallic layers and a dielectric layer sandwiched between them, as in Fig.2.6. The full ground plane attached to the back of the substrate shields the user from unwanted radiations. The radiating patch and the feed line are attached to the top of the substrate. Here patch antenna with inset feed is designed on flexible jeans as substrate and adhesive copper foil as the radiating patch. The proposed wearable patch antenna is designed to resonate at 2.5 GHz Wi-Max applications as it can be used for various applications. The transmission line model is used to find the input impedance of the inset-fed microstrip patch antenna. The microstrip patch antenna operates on the same principle where the length of the patch has a greater influence in deciding the resonant frequency. The fringing fields' forms at both ends along the patch length tend to increase their effective length. Therefore, the impedance at the edges is very high and decreases as the inset distance moves toward the center of the patch. By adjusting the inset distance, proper impedance matching is achieved. The optimized dimensions are obtained from the standard equations [66], as shown in Table.2.3.

The textile antenna can be described in its electrical equivalent to get more insight. Using the transmission line model [66], the equivalent circuit of the inset-fed patch element is modeled as a parallel RLC resonant network with a series inductance representing the near-field effect of the microstrip feed line. The electromagnetic fields' parameters L and C can be determined in the antenna's near field, representing the ability to deposit magnetic and electric energy in the circuit throughout resonance. The circuit simulations are carried out in ADS software. The optimized parameter values are directly shown with the elements in the circuit, as shown in Fig.2.7.

Table. 2.3. Dimensions of the inset-fed wearable patch antenna

Parameter	Lp	Wp	W	L	Feed width	Thickness (h)
Dimensions (mm)	46.6	53.6	100	100	13	3.5

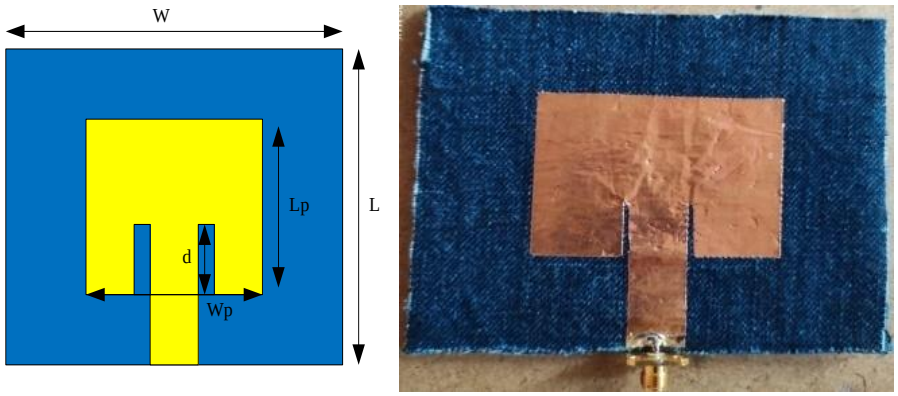

(a) (b)

Fig. 2.6 (a) Geometrical profile (b) Fabricated prototype of the inset-fed wearable patch antenna

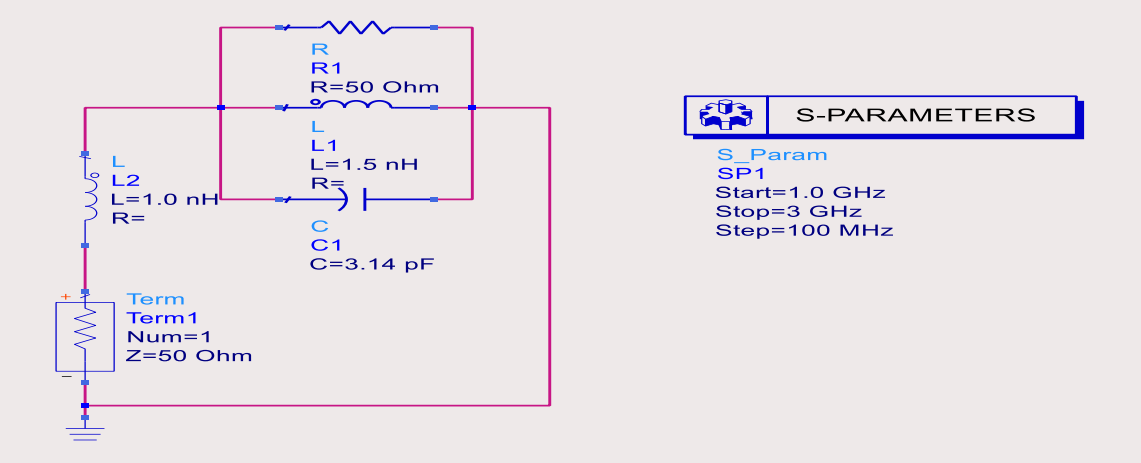

(a)

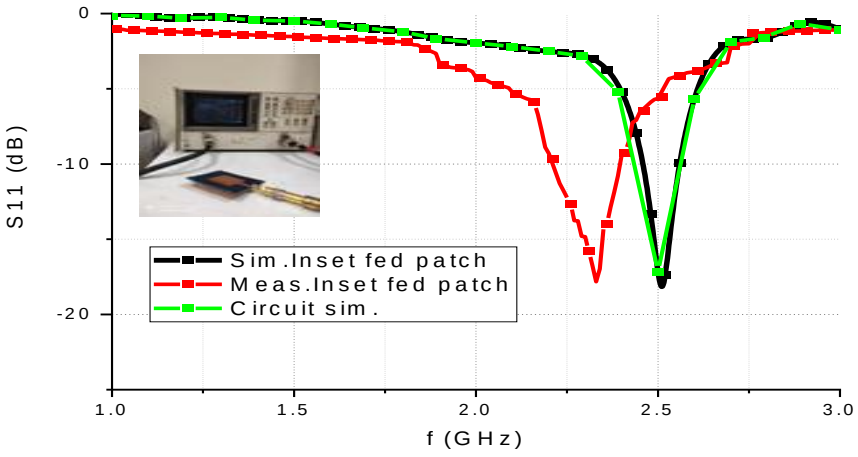

(b)

Fig. 2.7 (a) Simulated equivalent circuit in ADS (b) Reflection coefficient plot of inset-fed microstrip patch antenna

From the circuit, the feed point impedance at the specific frequency band can be modeled as an inductance (L) at high-frequency and a capacitor at low frequency (which is neglected and not shown in the circuit) in series. The circuit parameters R_a, L_a, and C_a are the equivalent resistance; inductance and capacitance are given by the standard relations [56] given below

$$C_a = \frac{\varepsilon_e \varepsilon_0 L_p W_p}{2h} . \frac{1}{\cos^2(\beta)}, \ \beta = \frac{\pi Zo}{L_p} \tag{2.30}$$

$$La = \frac{1}{2\pi f_r C_a} \tag{2.31}$$

$$Ra = \frac{Q}{2\pi f_r C_a} \tag{2.32}$$

The input impedance at the feed location from the circuit noted as

$$Z_{in}(f) = \frac{1}{\frac{1}{R_a} + \frac{1}{jwL_a} + jwC_a} + X_f \tag{2.33}$$

Where L_p = length of patch, W_p = width of patch, h= substrate thickness and Z_0 = feed location impedance

From Fig.2.7 (b), it is observed that there is a good agreement between the simulated and measured values. However, a small discrepancy is accountable for the fabrication errors. Being a flexible substrate, it is always challenging to shape the material in the obtained dimensions with the help of scalpel/ cutting tools. While cutting the edges of the substrate, due to parallax error, the slides and edges may not be straightly cut, or some threads are coming out. All these complications may affect antenna matching and performance. Therefore the wearable antenna is fabricated with the right tools and with utmost care.

2.4.2. Aperture coupled patch antenna and its electrical equivalent

The present generation of clothing can monitor the biosignals of the wearer and enables continuous communication between the antenna attached to it and the outer world regarding the person's state of health. Though many of the existing models involve a single-layer design, and regularly a coaxial feed [67]-[68] is utilized to attach the antenna to the transceiver. This type of feed structure is firm and is often annoying to the wearer. Similarly, using microstrip feed to the antenna is not the greatest solution because of unnecessary parasitic radiations from the feed line and radiating element. However, these problems can be mitigated by situating the feed line beneath the antenna ground plane, which can protect the feed line and the transceiver from the radiating antenna. The power is transferred from the feed line to the radiating element through an aperture in the ground plane that leads to an aperture-coupled patch antenna.

The AC-WPA (aperture-coupled Wearable patch antenna) serves the purpose due to its advantages. The aperture couple wearable patch antenna structure involves a ground plane sandwiched between two different substrates. The radiating patch is placed on the antenna substrate, and a feed line is seated on the base of the feed substrate, as shown in Fig.2.8.

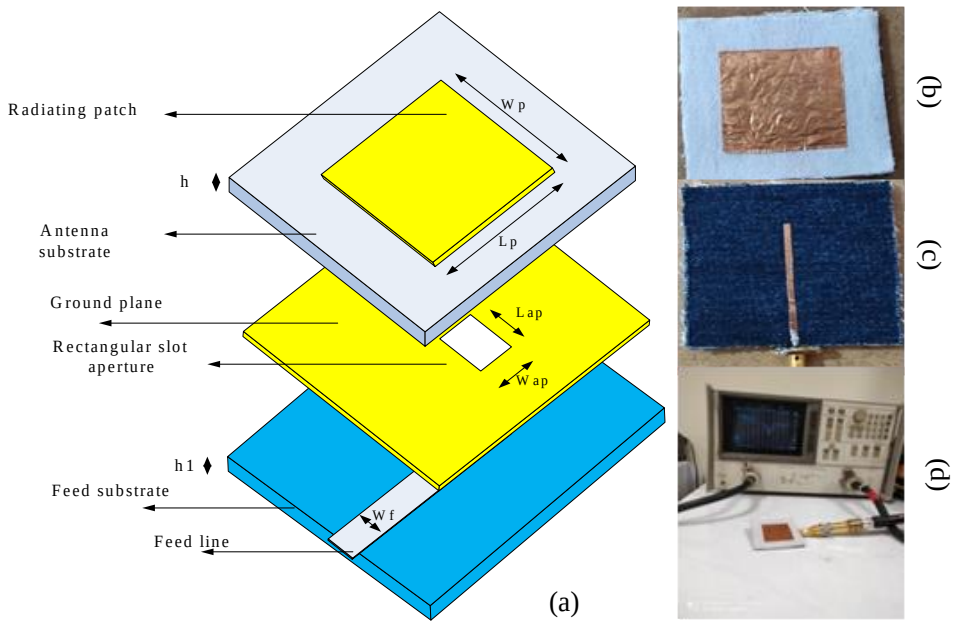

Fig. 2.8. a) Scheme of Aperture coupled wearable patch antenna (b) Front (c) Back view of the prototype (d) Experimental setup

All the rigid cables are replaced with a simple transmission line, and the power is coupled through a small aperture of arbitrary shape in the ground plane, which justifies the name of the aperture coupled patch antenna. Flexible jeans and wash cotton were chosen as the feed and antenna substrates since these are typical, durable, inelastic, and low-cost. The design studies are carried out using the electromagnetic simulator CST MW Studio and the optimized dimensions are tabulated in Table.2.4. The adopted feeding method produces a high bandwidth compared to other methods of feeding because of its impedance transformation behavior. In practical applications, the transceiver is directly connected to the feed line, which will couple the power to the patch through an aperture placed exactly in the middle under it. The prototype is built according to the specifications shown in Fig.2.8.

Table.2.4. Optimized dimensions of the Aperture coupled wearable patch antenna

Patch	Adhesive copper	W_p (mm)	L_p(mm)	
		43	40	
Antenna substrate	Wash Cotton	h(mm)	ε_r	tanδ
		2.56	1.5	0.025
Ground plane	Adhesive copper	W_g(mm)	L_g(mm)	
		65	65	
Aperture		W_{ap}(mm)	L_{ap}(mm)	
		3.5	20	
Feed substrate	Jeans	h(mm)	ε_r	tan δ
		1.15	1.7	0.02
Feed line	Adhesive copper	W_f(mm)	l_f(mm)	
		1.5	22.5	

The AC-WPA is represented in its electrical equivalent circuit model to gain insight into the underlying electromagnetic behavior. The equivalent circuit of AC-WPA is practically complex and consists of lumped RLC elements, an ideal transformer, and a transmission line segment to represent the radiating patch and coupling slot. A simple equivalent model is adopted here, in which the optimized parameter values are shown directly in the circuit. The circuit simulations are carried out in ADS, whereas an electromagnetic simulator CST MWS was applied to achieve the AC-WPA design and optimization, which are shown in Fig.2.9 (a).

It is observed that there is a close relationship between the simulated and measured values. However, proper care and attention must be needed while assembling the multilayer structure manually because even small misalignment between the feed line, slot, and patch results in performance variations. Moreover, high fabrication tolerances exist while working on textiles compared to traditional substrates. All these circumstances lead to some measurement deviation in the resonance frequency, as in Fig.2.9 (b).

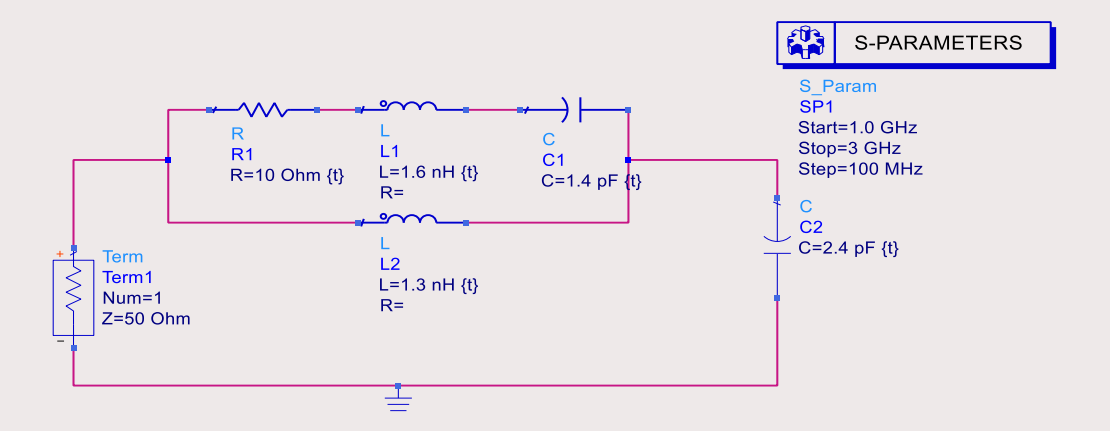

(a)

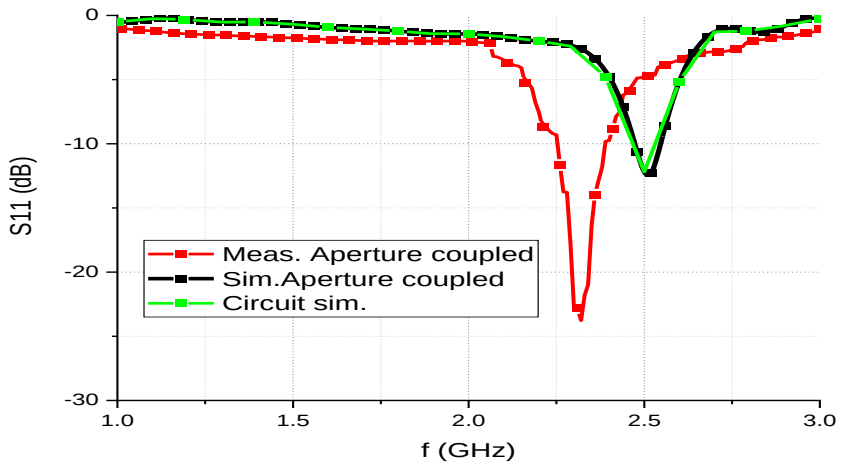

(b)

Fig.2.9. (a) Circuit model (b) Reflection coefficient curve of aperture coupled patch antenna

2.5. Bending characterization and Electrical modeling

The bent wearable patch antenna's geometry is modeled as a cylindrical cavity [69]. The geometry of the foam cylinders upon which the textile antennas are wrapped around is shown in Fig.2.10 (a). For both inset-fed and aperture-coupled antennas, patch and ground planes were modeled as perfect electric conductors and the remaining four sides as perfect magnetic conductors. Hence this arrangement forms a cavity bounded by electric and magnetic walls at $\rho = r, \rho = r + h$ and

$$\varphi = \pm\frac{\beta}{2},\ Z = \pm\frac{L}{2} \tag{2.34}$$

The field equations from MAXWELL'S equations are

$$E = -\nabla XF - jw\mu A + \frac{1}{jw\varepsilon}\nabla\left(\nabla.A\right) \tag{2.35}$$

$$H = -\nabla XA - jw\mu F + \frac{1}{jw\varepsilon}\nabla\left(\nabla.\mathrm{F}\right) \tag{2.36}$$

The fields inside the cylindrical cavity are obtained by imposing the boundary conditions on Maxwell's equations. By solving these equations, one can get the relations for T.E. and T.M. modes, from which a relation between resonant frequency and bending radius was found analytically. To give an outlook on WBAN applications, it is essential to explore certain bending radii/angles per antenna width/length. From the circuit analysis point of view, the bending of the patch antenna changes length, thereby altering the antenna's E-field, which can be validated by changing the capacitance between the antenna element and the ground plane. In general, the bending of the antenna brings discontinuity, i.e., the electric field becomes strongest in that particular part, and the magnetic field shows minimal effect. This indicates that inductive loading doesn't get affected, whereas capacitive loading is known as a tuning capacitor, denoted by C_t. With increasing the bending radius, the capacitive loading becomes small [70]. The simulated circuit parameters for the patch antenna bent in the E-plane are shown in Fig.2.10 (b). Comparing the flat case with bent cases, it is observed that the capacitance C2 decreases and L2 increases. The

product L.C. increases when bending becomes critical, which means the resonance frequency shifts to a lower frequency band.

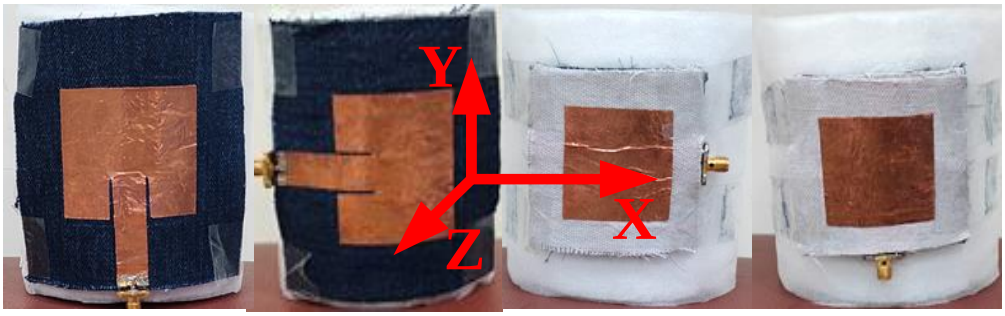

(a)

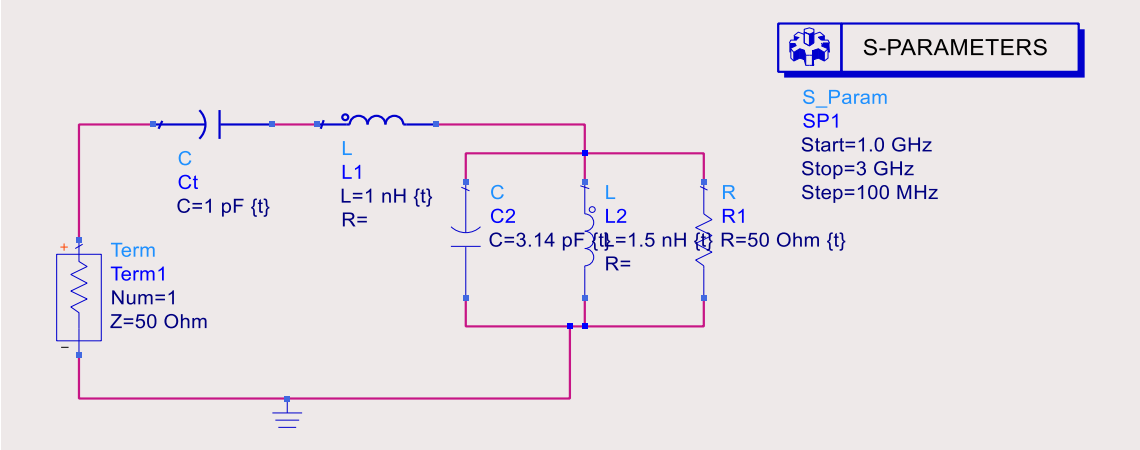

(b)

Fig.2.10. (a) Antennas wrapped around foam cylinders in E, H-plane directions (b) Equivalent circuit of a bent patch antenna

2.6. Effect of Bending on the performance of the Antenna

Although the performance of flexible antennas can be upgraded with united solutions for wearable applications, developing and optimizing such materials still require further characterization and improvement. Here a comparison is made for bending variations for different feeds of patch antennas where four different scenarios are considered. These radii are sensibly considered to mimic the chest and arm sizes in the human body [71]. These deformations were conducted to test their capability to resist a certain amount of structural bending.

2.6.1. Effect on Resonant frequency and impedance match

Simulations are carried out over the frequency range of 1.0–3.0 GHz. The anticipated textile antennas have been fabricated, and the resultant reflection coefficient is measured using the Vector Network Analyzer (VNA) HEWLETT PACKARD 8719A. When these antennas are wrapped around the cylindrical foam surfaces, the simulated resonant frequency appears to be dependent on the antenna curvature, more particularly for the antenna bending in the direction of length as the fact that for a microstrip radiator, the electric field lines are oriented along the length and magnetic field lines along the width. Therefore a shift in resonant frequency appeared as the effective length of the patch decreased when it was bent lengthwise. If the tendency of detuning of simulated resonant frequency is considered and graphed for different bending cases (for varying bending radius, R), it is remarkable to know that the more the antenna is bent in E-plane, in general, the more effective length gets reduced, and so the resonant frequency gets shifted to the higher band as shown in Fig.2.11 (a),(b) for AC-WPA and Inset fed patch antenna respectively [72]. On the other hand, the H-plane bending shows minute variations in resonant frequency that is almost negligible and is shown in Fig.2.11 (c), (d). Next, it is seen that the reflection coefficient increases as the bending become critical, i.e., the antenna operates ordinarily.

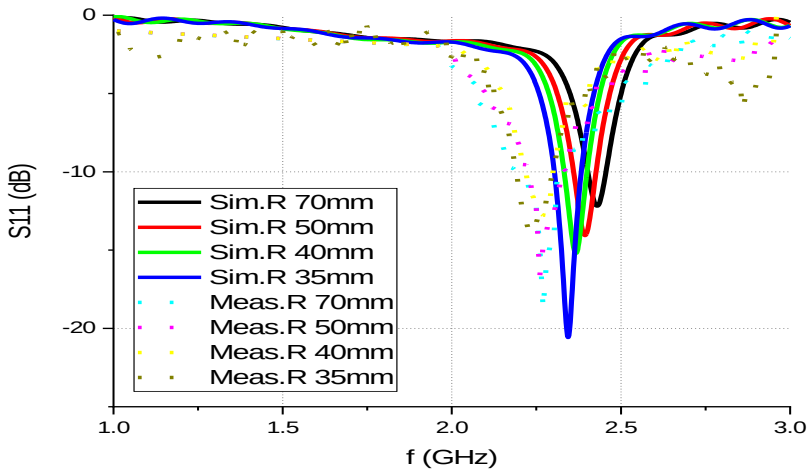

(a)

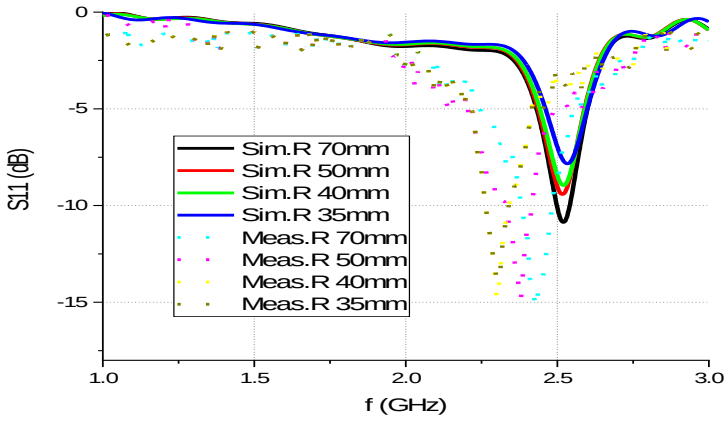

(b)

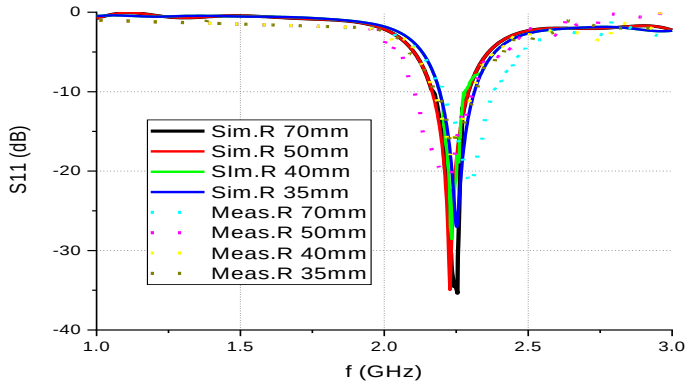

(c)

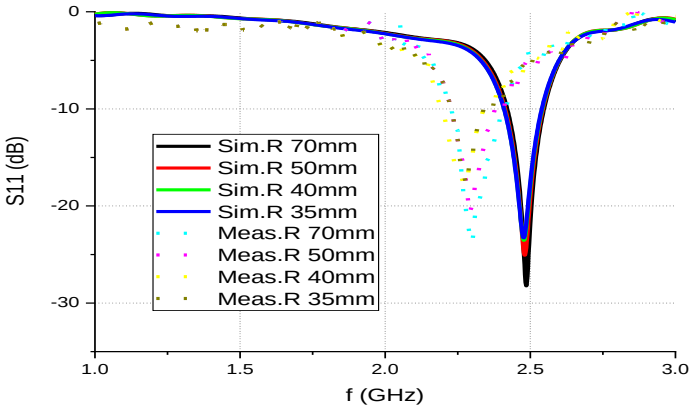

(d)

Fig.2.11. Return loss variations for different bending cases for (a) AC-WPA on E-plane (b) Inset fed patch antenna on E-plane (c) AC-WPA on H-plane (d) Inset fed patch antenna on H-plane

2.6.2. Effect on Electric field intensity

The electric field intensity can be better understood when the antenna is bending on a foam cylinder. The distribution of the E-field for both the proposed antennas under different bending radii is shown in Fig.2.12. From Fig.2.12, it is observed that the E-field is small at the center, and the maximum exists at the sides of the patch for flat antenna candidates. Instead, for both the antenna candidates, there is an insignificant effect on the E-field behavior of the antennas under bending situations, in which maximum occurs at the sides of the patch. Generally, for the inset-fed patch antennas, the electric field and, thus, the current flow is associated with the length, whereas the magnetic field is with the width. When exposing antennas to the bending in the length direction, it is easy to expect the current flow and electric field influences while it impacts marginally when bending in the width direction. The kind of performance is due to a change in the distance traveled by the current between opposing ends of the patch antenna because of the bending of the materials leading to a reduction in patch length.

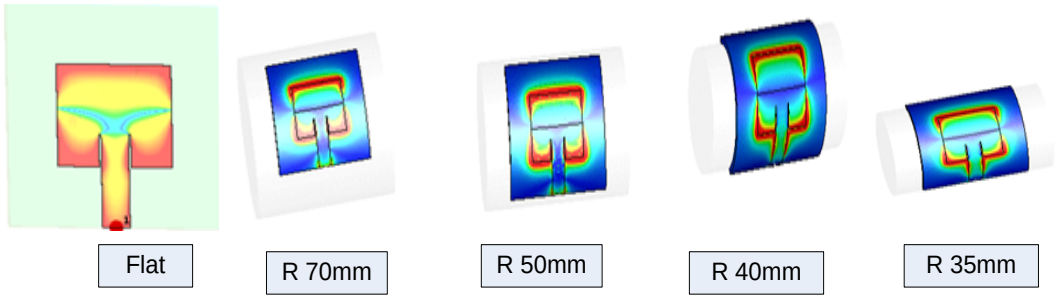

(a)

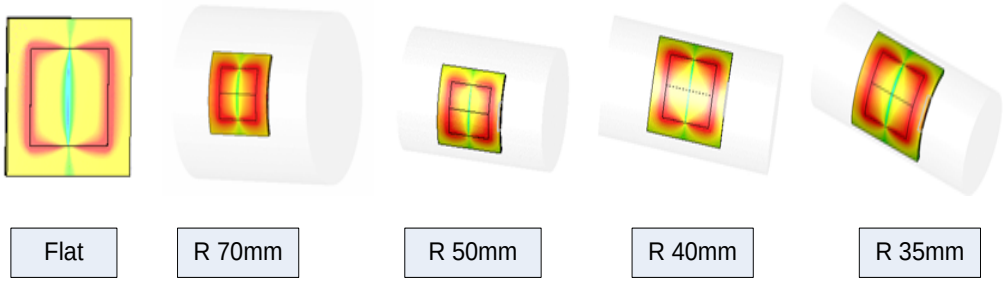

(b)

Fig.2.12. Electric field variations of (a) Inset fed (b) Aperture coupled wearable antenna on different bending fixtures.

2.6.3. Effect on the Radiation pattern

The effects of bending on radiation patterns are explored. Fig.2.13 shows the E-plane 2D radiation patterns for the planar and bent antennas. Meanwhile, for all the bending cases, the forward gain shows slight variations due to the high bending radius, which gives some difficulties for the antenna to radiate appropriately. It is instinctively clear that antenna bending widens the radiation pattern in the bending plane, which leads to a reduction in gain. Different bending radii do not have a significant effect on the antenna radiation pattern. However, the efficiency of the proposed antenna is marginally reduced as the antenna bending is increased, but the antenna still operates efficiently and is at an acceptable level, as shown in Table.2.5. Another main consequence was obtained in terms of 3dB angular beam width, which is experienced as an increment when bending becomes critical.

Table.2.5. Gain and efficiency variations of the proposed antennas for various bending radii

Cylinder Radius(mm)	Gain (dBi)		Efficiency (%)	
	Inset fed	Aperture coupled	Inset fed	Aperture coupled
Flat	6.12	4.84	58.61	53.95
70	6.01	4.50	58.34	46.02
50	5.74	4.46	58.47	55.08
40	5.41	4.41	59.56	55.08
35	5.03	4.13	60.06	52.72

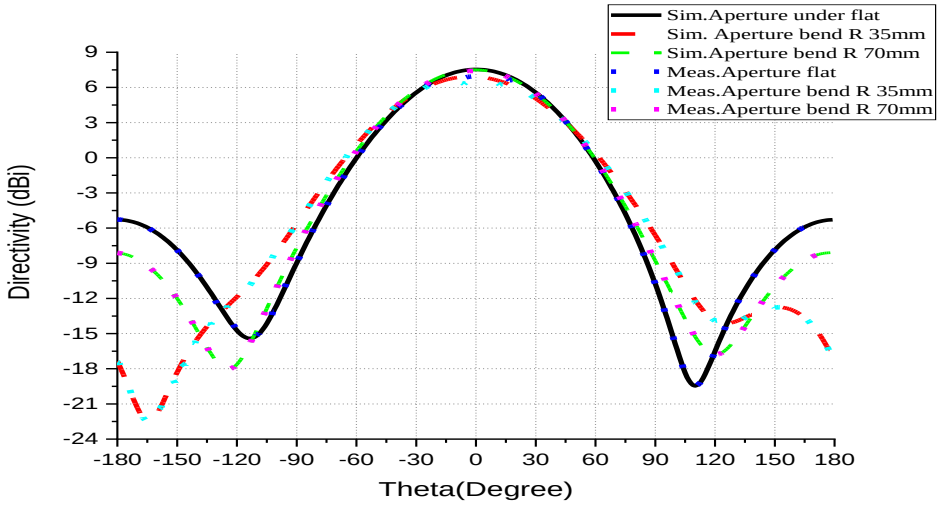

(a)

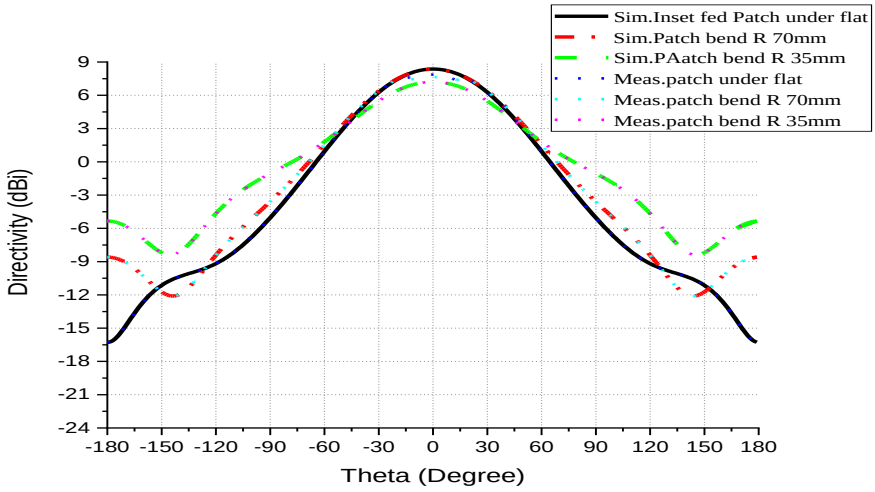

(b)

Fig.2.13. 2D Radiation pattern variations of (a) Aperture coupled (b) Inset fed wearable patch antenna in different bending situations

2.7. Summary

To start with, two wearable antennas with two different feeding methods, as given below, are designed, fabricated, and experimentally validated.

- A microstrip line-fed wearable antenna operating at 2.5 GHz
- Aperture-coupled wearable antenna operating at 2.5 GHz

Further, to get insights, electrical equivalents are developed and simulated using ADS software and compared with the already achieved results. Later, the fabricated antennas wrapped around foam cylinders of different radii (chosen to mimic the human body parts) and identified the performance characteristics.

It was found that the E-Plane bending has a dominant impact on the impedance matching for both textile antennas. The achieved results showed that the aperture-coupled antenna has a minimal bending influence on the impedance matching and resonant frequency, proving the robustness of the antenna under these effects at the cost of complexity. Moreover, the feed type removes the usage of rigid cables and unnecessary radiation from the feeds. The lower cross-polar level makes it a better candidate for wearable applications. Also, the electric field intensity and gain have minimal effect on bending for both antenna candidates.

S. Mallavarapu and A. Lokam, “Circuit Modeling and Analysis of Wearable Antennas on the Effect of Bending for Various Feeds”, **Eng. Technol. Appl. Sci. Res**., vol. 12, no. 1, pp. 8180–8187, Feb. 2022.https://doi.org/10.48084/etasr.4699

Chapter 3.

Microstrip Line Fed Fractal Wearable Antennas for On-Body Applications

This chapter introduces two microstrip line-fed wearable antennas for various WBAN applications. At first, a compact, high gain flexible antenna based on a saw-tooth shaped boundary fractal is designed and verified on/off body and deformation, and human tissue loading behavior for WBAN application, and secondly, a step-shaped Sierpinski fractal antenna is proposed, fabricated and validated for W-WBSN applications.

3.1. Introduction

In modern wearable wireless communication systems, compact, wider bandwidth and high gain antennas have huge demand for both commercial and personal body area applications. The utilization of Fractal technology has significantly influenced many areas of science and engineering, especially in RF and antennas domain. The fractal geometries in antennas have been revealed to improve several antenna features to varying extents. B. Mandelbrot invented the term "fractal," which is used to describe structures with non-integer aspects [73]. Fractal geometry incorporates natural geometrical attributes. It has the potential to characterize the branching of tree leaves and plants, rugged terrain, the spikiness of the shorelines, and many other natural phenomena. Fractal geometric objects have several fascinating properties specifically; they can have a finite area while having an infinite perimeter, which is known as the self-similarity property, or an infinite area for a finite volume object, which is known as the space-filling nature. With the incorporation of structural complexity and self-similarity, wide and multi band antennas are accomplished. By employing fractals to antenna designs [74]

1. Antenna become compact

2. Can resonate at multiple frequencies
3. Maximum gain achieved
4. Accomplish wideband

Examples of fractals are contour sets, Koch snow flacks, Sierpinski carpet, and Sierpinski gasket. Nature is full of estimated fractals. These objects have self-similar structures across a wide but finite scale range. Examples include clouds, snowflakes, crystals, mountain ranges, lightning, river networks, cauliflower or broccoli, and systems of blood vessels and pulmonary vessels. Coastlines may be loosely considered fractal in nature.

The dimension of the Fractal can be approximated by the Hausdorff dimension. Assume that a fractal has 'N' identical components that, when scaled by L, are similar to the entire fractal, and then the Hausdorff dimension of the fractal is given by Eq (3.1)

$$Dimension = \frac{\log N}{\log L} \tag{3.1}$$

3.2. Saw-tooth Shaped Boundary Fractal Wearable Patch Antenna

The textile was susceptible to discontinuities and other factors. To allow deformation and flexibility, a typical compact-sized microstrip antenna design is one solution [69], [75], [76]. But there is a trade-off between the deformation and compactness allowed for the wearable applications at WLAN standards. Also, thick flexible substrates or semi-flexible substrates susceptible to deformations can be utilized while designing the wearable antenna. The rigid/semi-flexible substrates are not the purpose choice in conformal applications. Therefore a wearable antenna design involves choosing a shape to compromise the effective length/width during bending.

3.2.1. Geometrical evolution of the anticipated antenna

Fig.3.1 exhibits the evolution process of the anticipated antenna. The antenna geometry is primarily derived from the regular square and circular-shaped patches. First, a square shape is chosen as the initial shape, and the dimensions are calculated using traditional methods [56]. The

anticipated antenna profile is realized by the successive spin and intersection of a similar length square patch shape, leading to an increased electrical length, thereby, and an equivalent area of the patch. The slots and notches on the patch enhance the current path length and decrease the resonant frequency further. The motivation behind the design principle is to expand the current path length by making a fractal-like boundary that takes sharp edges and produces a compact antenna with better gain. The initial square patch is rotated at an angle of 45^0 and overlaid on the initial shape to get iteration 1. The procedure is repeated for up to three iterations. Further, a rectangular slot of size 2X18 mm^2, rotated with 45^0 angles, is inserted in the center of the saw-tooth boundary fractal antenna to attain the required frequency of 2.45 GHz. A 50 Ω microstrip line is utilized to feed the antenna at the edge of the fractal boundary to achieve proper matching.

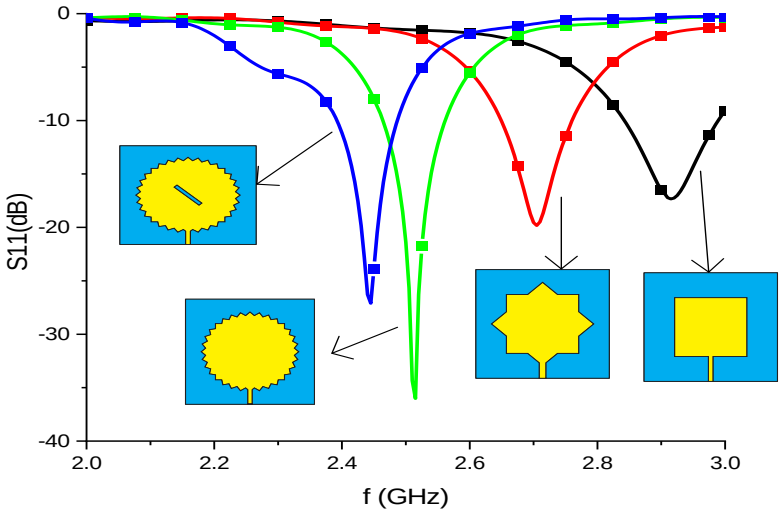

Fig.3.1. S_{11} curves for various iterations of the anticipated fractal boundary patch antenna

Theoretically, the length of the initial patch is determined using the traditional formula

$$L = \frac{C_0}{2 f_r \sqrt{\varepsilon_{reff}}} \tag{3.2}$$

Where C_0 is the speed of light in free space, ε_{reff} is the effective permittivity.

This square patch is converted to a fractal boundary patch by sequential rotation and combination. The detail in the generated pattern can be expressed with the fractal dimension, and the dimension is estimated as

$$D = -\frac{\log N}{\log \frac{1}{\theta}} \tag{3.3}$$

Where N is the number of copies, θ is the initial scaling angle.

The dimension of the fractal need not be an integer. The boundary can apply to those values of ɵ perfectly divisible by 360^0. Parametric simulations are executed to optimize the dimensions of the proposed wearable antenna. The initial length of the patch is determined as 38 mm, with a resonant frequency of 2.91GHz. After three iterations, the frequency of resonance shifts to the desired 2.5 GHz. Additionally, the resonance frequency is shifted to 2.45 GHz by cutting a rectangular slot. The etched rectangular slot in the radiator enhances the quality factor that contributes to good impedance matching, which reduces bandwidth, and a better impedance matching results in the desired resonance peak at 2.45 GHz. The prototype is illustrated in Fig. 3.2.

Fig.3.2. Front view of the fabricated antenna

3.3. Performance of the antenna under flat and deformations

3.3.1. Reflection coefficient under Flat condition

The parameters are measured with the help of an Agilent N5247A Network analyzer. Fig.3.3depicts the measurement setup and reflection coefficient curve for simulated and measured under the flat condition in free space. It is realized that the simulated reflection coefficient shows -

26.10 dB at 2.45 GHz, whereas the measured shows -30.75 dB at 2.43 GHz with slightly increased bandwidth. The simulated and measured bandwidths are 4.2 % and 5 %, individually. The slight discrepancy between the measured and simulated is due to prototyping tolerances and losses associated with the flexible substrate.

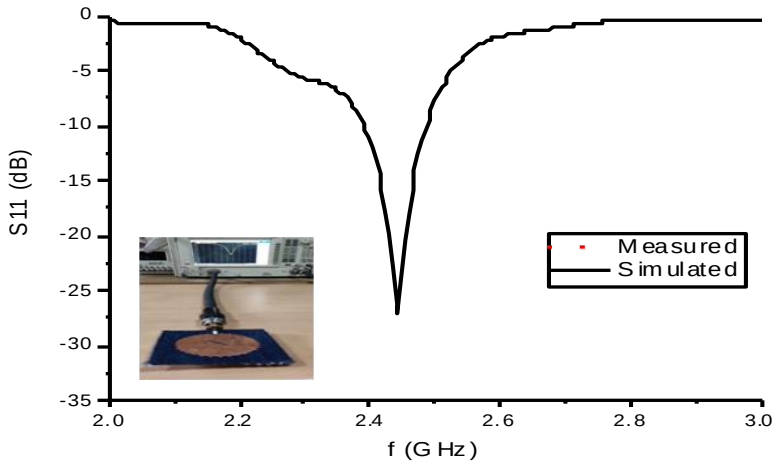

Fig. 3.3. Reflection coefficient of the anticipated antenna

3.3.2. Reflection coefficient under deformation

The major prerequisite of WBAN applications is that the antenna proposed should be operable under deformation, such as bending and crumpling, when functioning near or around the human body or any other rough surface. To authenticate the bending, the anticipated antenna is bent in E-plane and H-plane directions with radii of curvature of 70 mm and 50 mm, respectively. For measurements, 3D fixtures of foam are built to provide selected curvature, as shown in Fig. 3.4. A minor, almost insignificant frequency shift is observed when bent in the E-plane direction, whereas in the H-plane direction, a small change in the bandwidth is observed.

It is very consistent compared to the simulation reflection coefficient. From Fig.3.5, the reflection coefficient slightly increases when the antenna is bent, maintaining almost the same resonant frequency as the antenna on a flat surface. This proves that the bending effect on the saw-tooth-shaped boundary patch antenna is almost negligible. It is the consequence of the antenna being bent in the length/width direction. The change in the effective length/width of the

proposed shape is almost equal to the original length/width. Therefore, the proposed shape can hold the original dimensions during bending. Under deformation conditions, the measured reflection coefficient gives almost the same results as the simulated results. Hence this type of antenna can be very flexible to utilize in wearable WBAN applications.

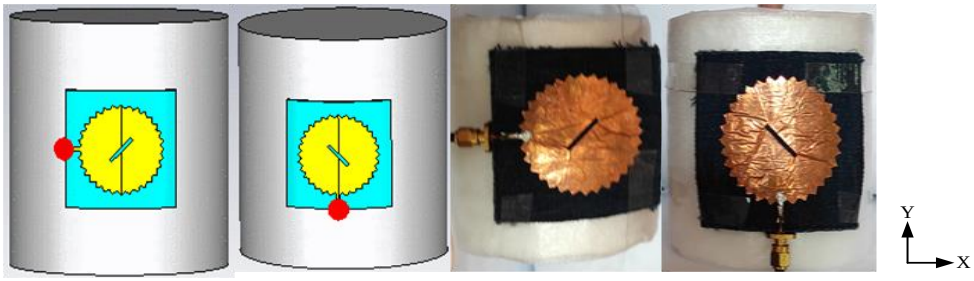

(a) (b)

Fig.3.4. Proposed antenna bends on foam cylinders along E; H-plane (a) simulated (b) Practical

A comparative study is also done to verify the critical bending for different shapes, namely the proposed and initial square patch. The deviation in frequency shift for both the proposed and square-shaped antenna is considered and arranged in Table.3.1.

Table.3.1. Assessment of bending behavior of the anticipated antenna with the regular square shape of the radiator

Deviation in Resonant Frequency (GHz) $\Delta f = f_{r(\text{flat})} - f_{r(\text{bent})}$								
Bending Radius (mm)	**Proposed Antenna**				**Square shaped antenna**			
	Deviation (GHz)		***Reflection coefficient (dB)***		***Deviation (GHz)***		***Reflection coefficient (dB)***	
	E-plane	H-plane	E-plane	H-plane	E-plane	H-plane	E-plane	H-plane
70	0.061	0.02	-16.75	-22.94	0.195	0.025	-27.20	-20.64
50	0.085	0.03	-13.98	-29.44	0.210	0.02	-29.24	-22.32

It is observed from Table.3.5 that E-plane bending has a considerable effect on square-shaped antennas, whereas it is almost negligible on the saw-tooth-shaped antenna. However, the H-plane bending shows a negotiable effect on both antennas. This proves that the proposed shape performs well even in a deformation environment, satisfying the requirement of wearable applications in WBAN.

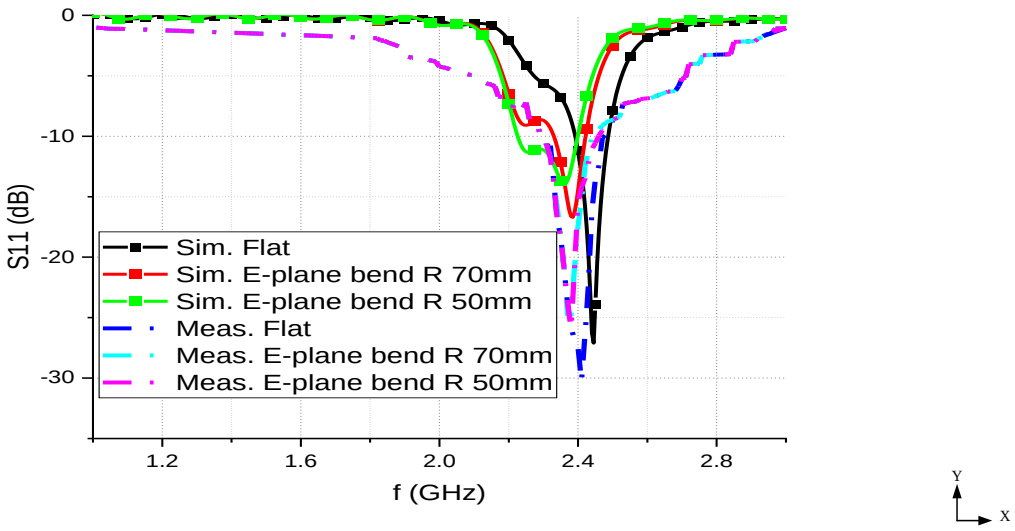

(a)

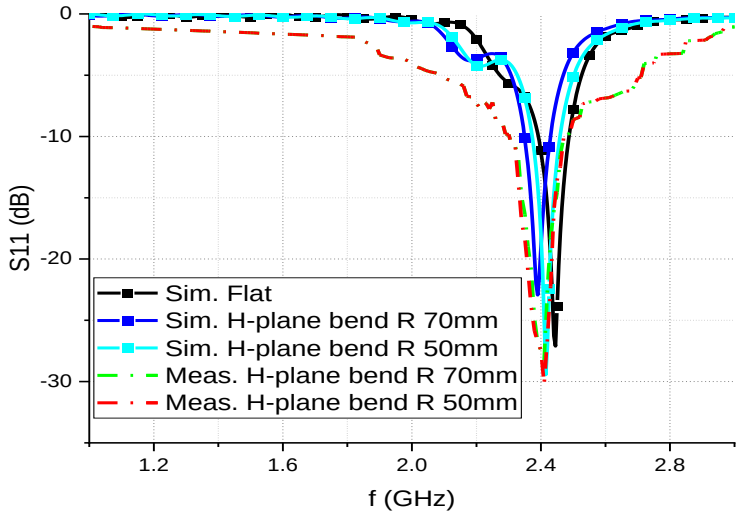

(b)

Fig.3.5. Effect of bending on the anticipated antenna under various bending scenarios (a) E-plane bending (b) H-plane bending

3.3.3. Radiation characteristics

Generally, wearable antennas are intended to have forward radiation or directive patterns instead of omnidirectional patterns. This is considered to keep the health standards of humans due to the unwanted radiation into the human body. Regularly, the radiation pattern is described in two principal planes, namely E-plane and H-plane. In this paper, the antenna is positioned in the X-Y plane facing +Z-direction, so the Y-Z plane, i.e., $Ø=90^0$ in the E-plane and X-Z plane, represents the H-plane where $Ø=0^0$. All investigations on radiation patterns are done in the same manner throughout the paper. The simulated E and H-plane patterns under flat and bent scenarios are shown in Fig.3.6 (a), (b). At 2.45 GHz, the antenna shows a forward gain of 5.76 dBi under flat conditions, whereas a slightly different gain is observed under the bend scenario. The gain reduction is due to the appearance of discontinuity of the antenna upon deformation. Although E and H-plane patterns seem alike, the small back radiation is observed. It is concluded that the radiation pattern is also affected when the antenna undergoes deformation. Yet, the safety of this antenna is still verified, and the SAR level estimated is in the following sections.

The prototype antenna has a directed radiation pattern having a forward gain of 6.12 dBi at 2.45 GHz. A slight change in the back radiation is detected when the antenna is bent in a particular direction. Fig.3.6 (c), (d) illustrates the measured far-field radiation pattern. Confirming the simulation predictions, the measurement shows nearly close values. The proposed antenna shows a slightly high gain when the antenna is under deformation significantly, either in E-plane or H-plane. This is due to the increased current densities at the discontinuity formed when deformation or bending [75]. The back lobes in the measured patterns account for the measurement setup limitations.

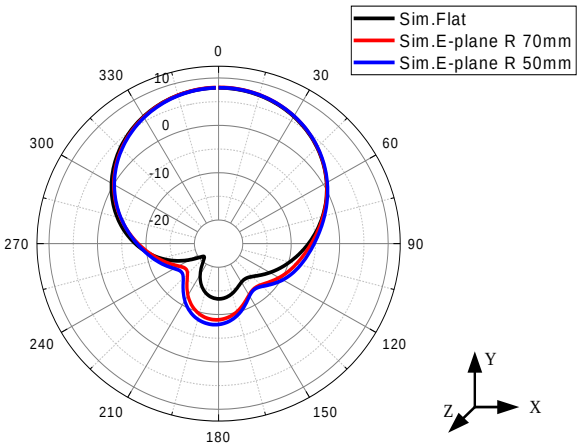
Sim.Flat
Sim.E-plane R 70mm
Sim.E-plane R 50mm
0
30
60
90
120
150
180
210
240
270
300
330
10
0
-10
-20
Y
Z
X

(a)

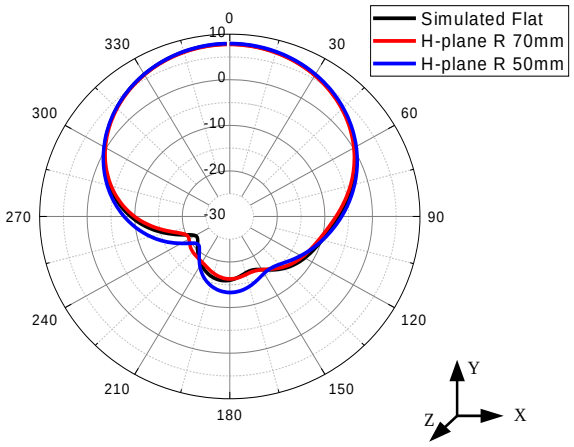
Simulated Flat
H-plane R 70mm
H-plane R 50mm
0
30
60
90
120
150
180
210
240
270
300
330
10
0
-10
-20
-30
Y
Z
X

(b)

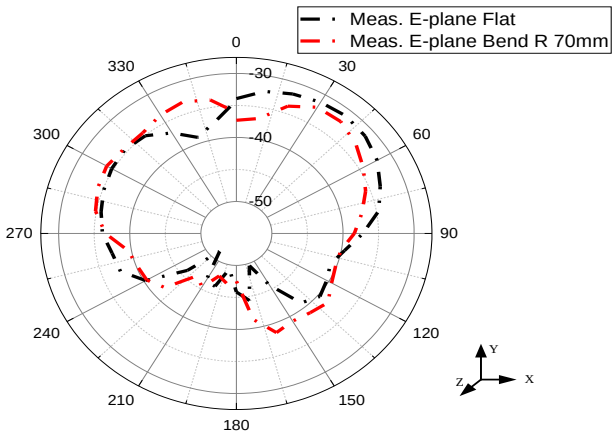
Meas. E-plane Flat
Meas. E-plane Bend R 70mm
0
30
60
90
120
150
180
210
240
270
300
330
-30
-40
-50
Y
Z
X

(c)

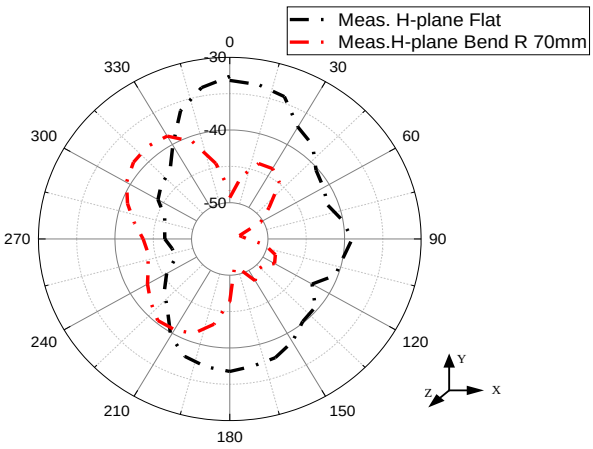

(d)

Fig.3.6. Simulated Radiation patterns (dB) along (a) E-plane (b) H-plane, Measured radiation patterns (dBm) along (c) E-plane (d) H-plane

Fig.3.7 depicts the measurement setup inside the anechoic chamber for radiation pattern. The far-field radiation patterns under flat and bending scenarios are measured at the middle frequency of 2.45 GHz. Due to the consistency of the simulated radiation patterns, a single measurement is taken into consideration for measurement under a bent scenario. The antenna is placed on an automatic rotating platform in an anechoic chamber. The pattern is observed at three discrete frequencies. The patterns are measured in dBm in both E and H-planes to observe accurate antenna gain variations. Overall the anticipated antenna demonstrates advantageous performance considering the deformations.

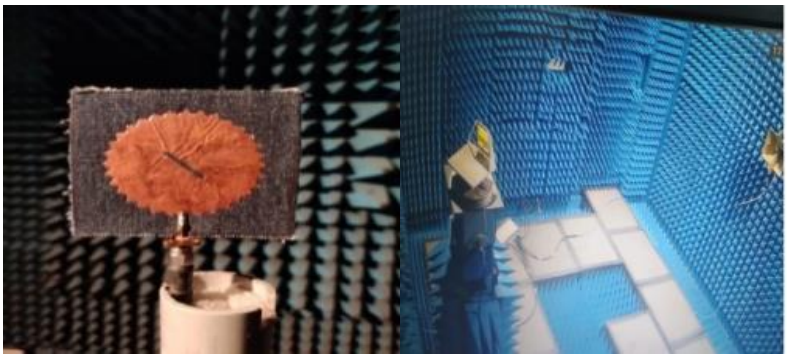

(a) (b)

Fig.3.7. Measurement setup inside the anechoic chamber for radiation pattern

3.4. Gain measurement

The gain transfer method is implemented to measure the gain of the antenna since it gives simple and accurate solutions for antenna gain measurements. A known gain standard, such as a Horn antenna operating from 1 GHz to 18 GHz broad frequency range, is utilized to determine the gain of the antenna under test (AUT) in conjunction with the following equation.

$$G_{AUT} = \frac{P_{R2}}{P_{R3}}.G_{\text{ref}} \tag{3.4}$$

Where P_{R2} is the power received by the reference antenna, P_{R3} is the power received by the antenna under test, G_{ref} is the reference antenna gain, and G_{AUT} is the gain of the antenna under test.

The transmitter and the receiver antennas are separated by a distance of 1.5 m, with the transmitted power 13 dBm to 15 dBm for the measurement. After replacing the gain standard, the AUT is rotated in the principal plane, and the received power is converted to an antenna gain estimate at each angle, with a transmitter power constant across all measurements. Fig.3.8 shows the comparison of simulated and measured gain values.

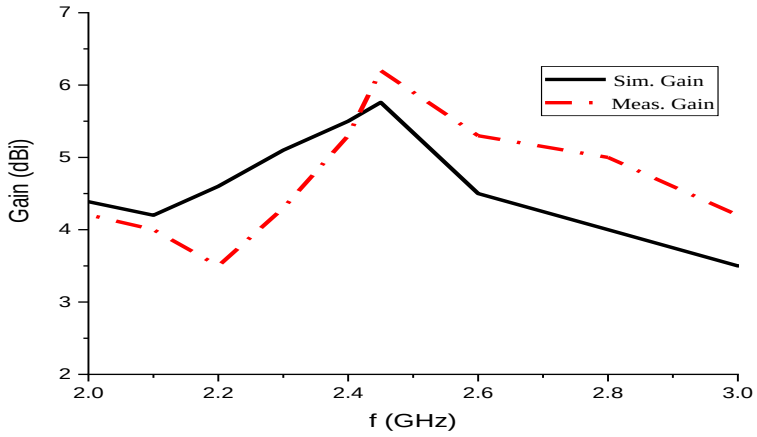

Fig.3.8. Simulated and measured peak gain of the anticipated antenna

3.5. Antenna performance on human tissue loading

Practically, it is necessary to make sure of the performance of the wearable antenna on the body. Numerical simulations are conducted by CST MW studio.

3.5.1. Electromagnetic Features of Human Tissue

The human body can be approximated using physical phantoms made of solid, liquid, or gel materials, or numerical phantoms embedded in numerical electromagnetic codes. Obtaining samples is a difficult task, and it is awkward to take measurements directly from the tissue as it has to contact with the tissue [77], [78]. Table.3.2 demonstrates the properties of the human tissues at 2.45 GHz.

Table.3.2. Electromagnetic Properties of Some Human Tissues at 2.45 GHz [79]

Property	**Skin**	**Fat**	**Muscle**	**Bone**
Thickness (mm)	2	5	20	13
Density (Kg/m3)	1001	900	1006	1008
Σ (S/m)	1.49	0.11	1.77	0.82
εr	37.95	5.27	52.67	18.49

3.5.2. Numerical phantoms

For computational analysis, numerical phantoms are utilized and studied by many researchers [80]. Usually, it is a simple theoretical phantom that can be used to analyze the effect of interaction betwixt the antenna and the tissue [81]. Though, in order to achieve more accurate results, realistic voxel phantoms are utilized [83]. Spherical models were mainly used as the human head, eyes, and whole-body models. These models just confirm the results from numerical simulations [82], and the method of moments (MoM) [81]. Other canonical models, such as a

chest and arm are impersonated by a cuboid of 150X150X40 mm^3, and a cylinder with a diameter of 80 mm and length of 150 mm, respectively, have been used [64].

3.6. Inferences from Results

The proposed antenna is situated on the four-layer phantom model, developed to impersonate the chest and arm of the human body as in Fig.3.9. The chest and arm are impersonated by a cuboid of 150X150X40 mm^3, a cylinder with a diameter of 80 mm and length of 150 mm, respectively.

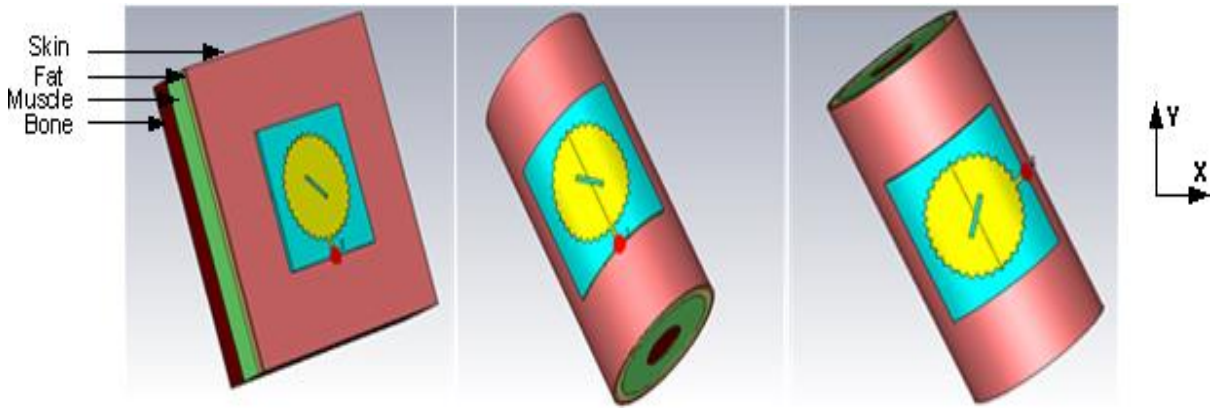

(a) (b) (c)

Fig. 3.9.Positioning of the anticipated antenna on (a) Chest, (b) arm along the Y-axis, (c) arm along the X-axis

The prototype antenna is measured on the chest, arm, and back of a male volunteer of height 161 cm and weight of 75 Kg, as demonstrated in Fig.3.10. This investigation provides extra reliability to the proposed work by instigating the real human volunteer instead of simulation models.

As described in Fig.3.10, the proposed antenna S_{11} is slightly shifted from 2.45 GHz to lower frequencies when situated on the chest and back of the human body. This is because of the effectiveness of the ground plane and the availability of large areas on the human chest and back. When the proposed antenna bent on the arm along the X and Y-axis, S_{11} shifted to even lower

frequencies due to the impedance mismatch caused by both bending and the presence of the high dielectric nature of the human body. Except for the small variations, the simulated and measured S_{11} curves agree. It demonstrates that the full ground plane isolates the antenna and the human body.

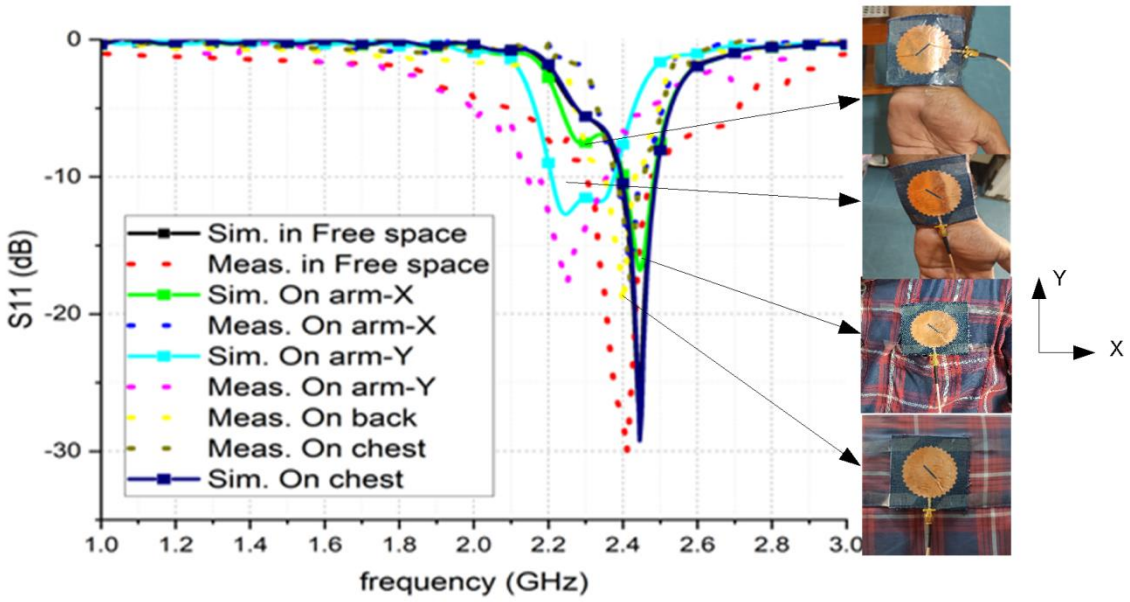

Fig.3.10. S_{11} curves of the anticipated antenna when located on the chest and arm

Fig.3.11 demonstrates the radiation characteristics of the proposed antenna when placed on the chest and arm. The results illustrate that the radiation characteristics are comparable with the free space and the human body. It can also uphold its pattern shape as in free space with negligible differences that don't disturb the radiation performance. The realized gain of the anticipated antenna loaded with human tissue is increased slightly with respect to free space as a result of reflection from the human body, and the radiation efficiency decreased due to lossy tissue.

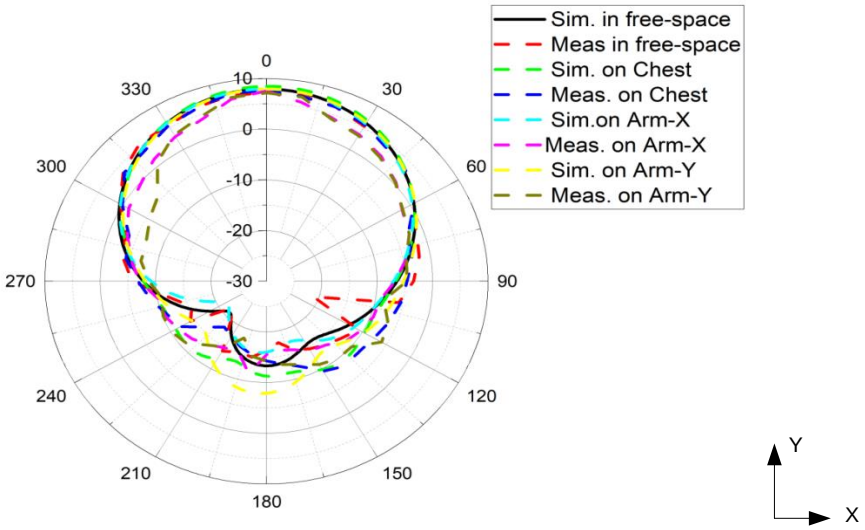

Fig.3.11. Radiation patterns of the proposed antenna when placed on the human body

There are many difficulties allied with the wearable antenna operating near the human body, particularly the change of characteristic performance of the antenna due to the absorption of electromagnetic energy. This context was enumerated by measuring the electromagnetic exposure limit. However, the proposed antenna has a full ground plane that will isolate and resist radiation penetration into the human body. This will tend to reduce the SAR levels. To estimate SAR, the anticipated antenna was positioned on a four-layered phantom of overall size 150X150X40 mm^3. The phantom model comprises four layers, namely skin (thickness 2 mm), Fat (Thickness 5 mm), muscle (Thickness 20 mm), and bone (Thickness 13 mm). The characteristics of each of the layers are listed in Table.3.6. The simulated maximum SAR value for 1 g and 10 g of average tissue for the input power of 100 mW are listed in Table.3.3.

Table.3.3. Simulated SAR value

Averaged Value	Realized SAR (W/Kg)	Standard SAR (W/Kg)
1g	1.1198	<1.6
10g	0.3025	<2

It is witnessed from Table.3.3 that the evaluated SAR is at an acceptable level and obeys both standards. A comparison of the anticipated work with the most recent methods is presented

in Table 3.8. Observing Table.3.4, the proposed antenna is significantly different from the previously reported designs because it enables a more compact footprint with superior performance in terms of gain and SAR. Therefore it is determined that the anticipated antenna is a potential candidate for wearable applications in WBAN.

Table.3.4. Comparison of the proposed antenna with the state art designs

S. No	substrate	Method Followed	Size	Gain (dBi)	SAR (w/kg)		Frequency of operation (GHz)	Remarks
					1g	10g		
[84]	RO3003	Metasurface	$0.5\lambda_0$x$0.3\lambda_0$x $0.028\lambda_0$	6.2	0.79	-	2.38	Complex geometry
[85]	Felt & Taconic	Folded ring antenna	$0.5\lambda_0$x$0.5\lambda_0$x $0.038\lambda_0$	5.1	0.2	-	2.45	The rigid substrate is used
[86]	RT 5880 (thickness 0.787mm)	Partial ground plane	$0.2\lambda_0$x$0.29\lambda_0$x$0.009\lambda_0$	2.5	-	-	2.4	Semi-flexible substrate used
[87]	polyimide	Artificial magnetic conductor plane	$0.67\lambda_0$x$0.67\lambda_0$x$0.04\lambda_0$	7.53	-	1.42	2.45	Too thick
[88]	RT 5880 (thickness 1.57mm)	Fractal technology	$0.58\lambda_0$x$0.58\lambda_0$x$0.013\lambda_0$	7	-	-	2.45	Not suitable for wearable applications
[89]	RT 5880 (thickness 1.57mm)	Loading stubs and slots	$0.46\lambda_0$x$0.46\lambda_0$x$0.01\lambda_0$	4.5	-	-	2.1	Complex design, rigid substrate
[90]	RT 5880 (thickness 1.57mm)	EBG	$0.33\lambda_0$x$0.26\lambda_0$x$0.01\lambda_0$	7.3	0.55	0.23	2.4	Too thick
This work	**Jeans**	**Fractal technology**	**$0.583\lambda_0$X$0.583\lambda_0$X$0.02\lambda_0$**	**5.76**	**1.11**	**0.302**	**2.45**	**Simple and robust**

3.7. Wearable step-shaped Sierpinski Fractal antenna

Wearable Wireless Body Sensor Networks (W-WBSN) is the best substitute for traditional healthcare systems by effectively monitoring patients within or remotely from the hospitals. Quite a few tiny sensors linked with one another on the body can efficiently observe the functional

status of the human body. Therefore, the W-WBSN has created a high demand for rapidly growing wearable and flexible antennas. Particularly the Medical Body Area Networks (MBAN) (2.36- 2.38 GHz), Industrial, Scientific, and Medical (ISM) band (2.4-2.485 GHz, 5.15-5.35 GHz, 5.75-5.85 GHz), and WI-Max band (3.3-3.79 GHz) are used to connect to wearable sensor nodes, which are equipped with system unit consists of sensing element, memory unit, transceiver and an antenna [91], [92]. In addition, compact, lightweight, conformable, and deformable antennas without compromising their performance when operating near the human body are necessary as the sensor nodes are attached to the garments [93]–[95].

It is important to choose the antenna topology that must provide high isolation and satisfactory performance in the near-human environment. In general, the antenna specifications for W-WBSN [77] are

1. The frequency range (GHz) is (3.3-3.79) GHz, (5.15-5.35) GHz, and (5.75-5.85) GHz, which covers WI-Max and ISM band frequencies.
2. S_{11} in the operating range (dB) is ≤-10dB
3. Radiation efficiency in the human body is ≥ 5%
4. The radiation pattern is unidirectional
5. The minimum Front-to-Back ratio (dB) is ≥10
6. Peak 10g average SAR (W/Kg) is ≤ 2

3.7.1. Anticipated antenna structure

The proposed wearable fractal antenna consists of a Sierpinski carpet fractal radiator on one side of the substrate and a partial ground on the other side of the substrate, as shown in Fig.3.12 (a). The Sierpinski carpet fractal is the principle of a square metallic radiator divided into four equal sub-squares in a 2-by-2 grid, in which the top left corner square is removed. After then, the process is repeated up to three times on the remaining three squares and the resulting element. With the removal of the upper left corner square every time in up to three iterations, the available patch area is greatly reduced by up to 75 %. For example, in iteration 1, one square removal contributes to a 25 % size reduction. For iteration 2, the remaining three squares, again dividing each square into four equal squares and removing the top left corner, contribute to a 50 % size reduction, and so on. A Jeans material of thickness 2.5 mm is used as a substrate, as it is a potential candidate for wearable applications. Simulations are carried out in CST MW Studio 2019. To enhance the bandwidth and match the proposed antenna to a 50Ω SMA connector, a

partial ground plane with a Hilbert fractal of 2nd order slot is inserted, as shown in Fig.3.12 (b). The length and width of the Hilbert slot are important while matching the impedance and obtaining the required reflection coefficient and bandwidth of the proposed antenna. The length of the Hilbert slot is calculated from eq. (3.5) and (3.6) [96].

$$d = \frac{L}{2^n - 1} \tag{3.5}$$

$$s = \left(2^n + 1\right) L \tag{3.6}$$

Where L is the total length of the Hilbert slot, n is the number of iterations, d is the length of the line segment, and 's' is the sum of the line segments.

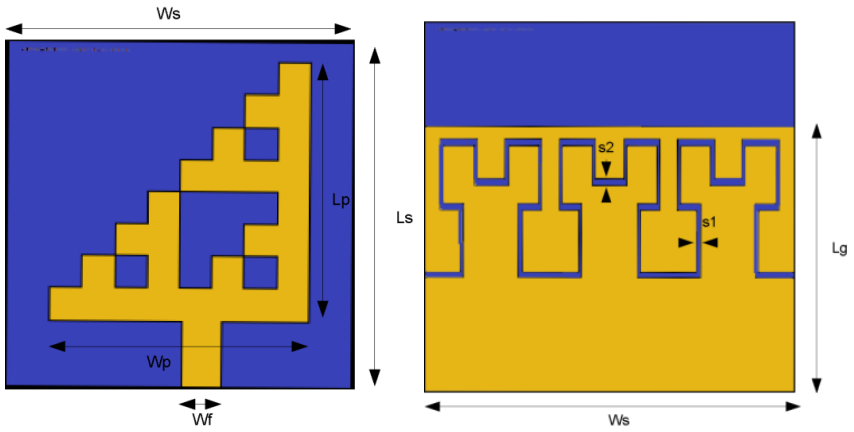

(a) (b)

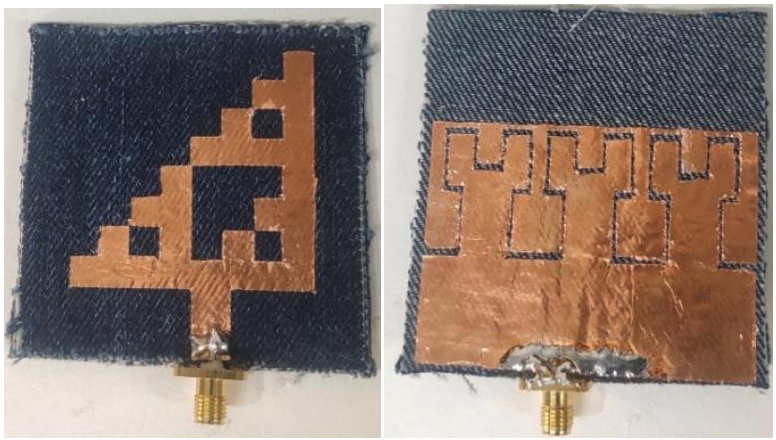

(c) (d)

Fig.3.12.The geometrical view of the anticipated antenna (a) Front (b) Back (c) Photograph of the fabricated prototype (c) Front (d) Back

As a consequence of electromagnetic coupling achieved with the Hilbert slot, a reduction in frequency results, which contributes to the antenna miniaturization, all the optimized dimensions are tabulated and presented in table 3.5. Fig.3.12 (c), (d) shows the front and back views of the fabricated prototype.

Table.3.5. Optimized dimensions of the proposed antenna

Parameter	W_s	L_s	W_p	L_p	W_f	L	L_g
Value (mm)	60	60	45	45	7	11	10

3.7.2. Free space analysis

The simulated and measured reflection coefficient of the proposed antenna in free space is compared and can be seen in Fig.3.13. The fabricated prototype antenna covers the impedance bandwidth (S_{11}≤-10 dB) of 6%, 7%, and 10.1% covering (3.237 GHz- 3.477 GHz), (5.135 GHz- 5.517 GHz), (5.474 GHz- 6.081 GHz) with a peak reflection coefficient of -18.565 dB, -32.497 dB, and -23.08 dB at 3.3 GHz, 5.2 GHz and 5.8 GHz, respectively. There is a sensible agreement between the simulated and measured reflection coefficient below -10dB level for the proposed antenna. The small shift in the resonant frequency is accredited to the fabrication faults.

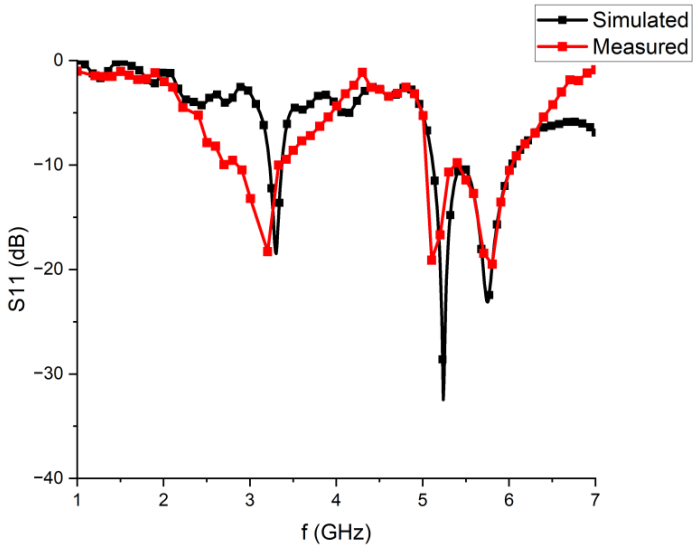

Fig.3.13. Comparison of the simulated and measured S_{11} curves of the proposed antenna

To further understand the contribution of Hilbert patterned slots on the ground, Fig.3.14 shows the simulated surface current distributions at various frequencies. All the current distributions at the three resonant frequencies are different. In all three frequencies, the current distribution is mainly concentrated at the slots and the feed line. Thus, Fractal slots on the radiator and ground can control the resonant frequency and improve the antenna performance.

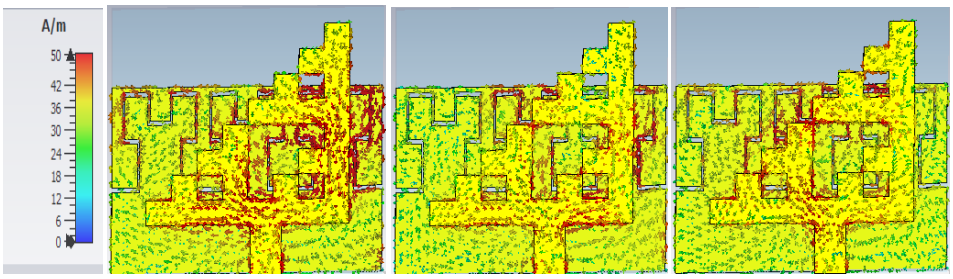

(a) (b) (c)

Fig.3.14. Surface current dispersal at (a) 3.3 GHz, (b) 5.2 GHz, (c) 5.8 GHz

Fig.3.15 demonstrates the proposed antenna's normalized numerical and experimental radiation patterns in free space at 3.3 GHz, 5.2 GHz, and 5.8 GHz. A directional pattern is preferred for wearable applications. It is seen from the Figure that the maximum radiation is along the positive Z-direction and relatively low back radiation. The anticipated antenna has a maximum gain of 2.57 dBi, 3.608 dBi, and 4.19 dBi, and radiation efficiency of 54.19%, 52.5%, and 54.8% at 3.3 GHz, 5.2 GHz, and 5.8 GHz, respectively in free space. The simulated and measurement results agree well and are close to each other.

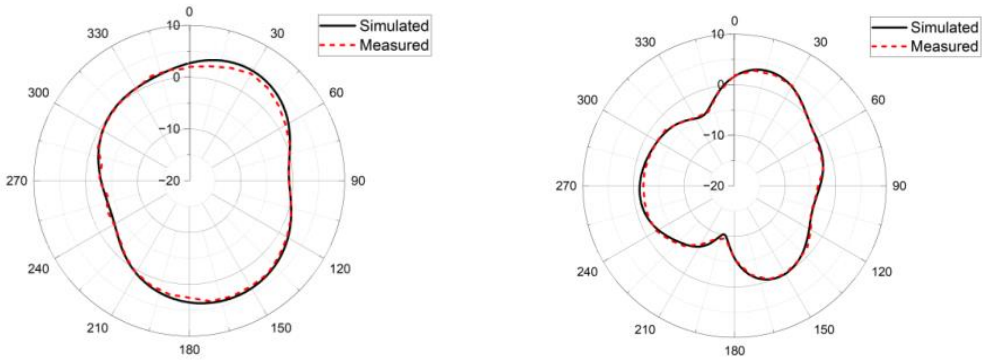

(a) (b)

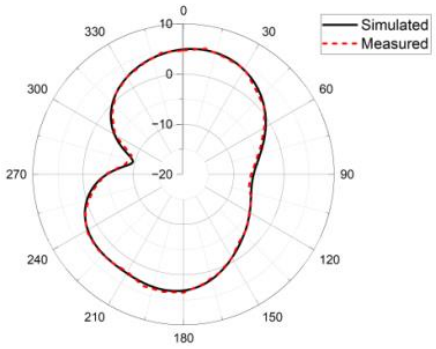

(c)

Fig.3.15. Radiation patterns of the proposed antenna in free space at (a) 3.3 GHz, (b) 5.2 GHz, (c) 5.8 GHz

3.7.3. On-Body Analysis

Due to the high dielectric and lossy nature of the human body, the antenna characteristics are influenced when it operates in the vicinity of the human body. For this purpose, a four-layer Human phantom model this resembles the human chest is considered, as depicted in Fig.3.16. The numerical simulations are conducted using CST MW Studio 2019. The electrical properties, such as permittivity, conductivity, and density of each layer, are provided in [97] for the desired frequencies. The thickness of each layer is depicted in the figure 3.16. An average frequency shift of 50 MHz is observed at the desired resonant frequencies compared to the free space simulations. The shift in the resonance frequency is due to the high dielectric and lossy nature of the human body.

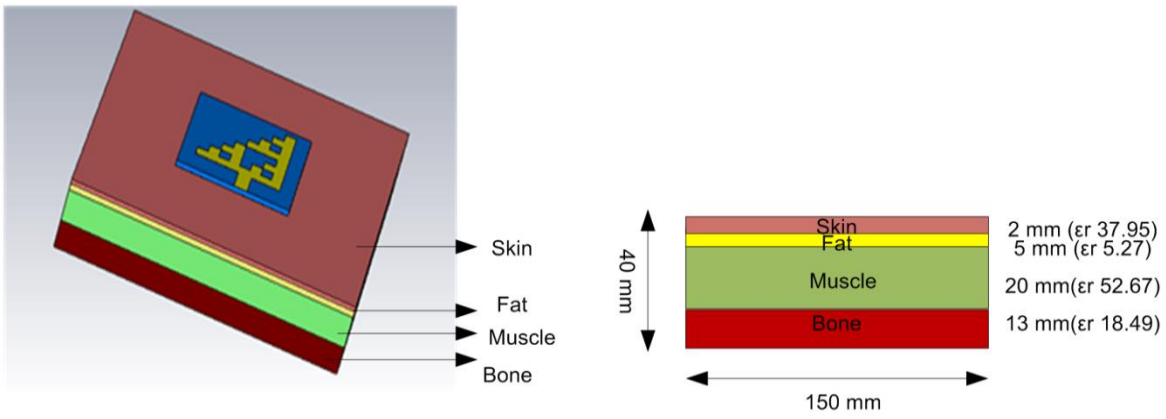

Fig.3.16. Model of the four-layered human phantom with the proposed antenna along with specified dimensions

Instead of relying on the simulation models, the proposed antenna is tested on a real human subject. A female volunteer, whose height and weight are 151 cm and 56 Kg, respectively, is considered for the measurement purpose and to locate the proposed antenna on the chest and arm, as shown in Fig.3.17. For simplicity, measurement is taken only on the chest part of the human subject. The result depicts that the S_{11} is reasonably stable and still covers the desired frequencies. This indicates that the proposed antenna is suitable for potential applications in wireless body sensor networks.

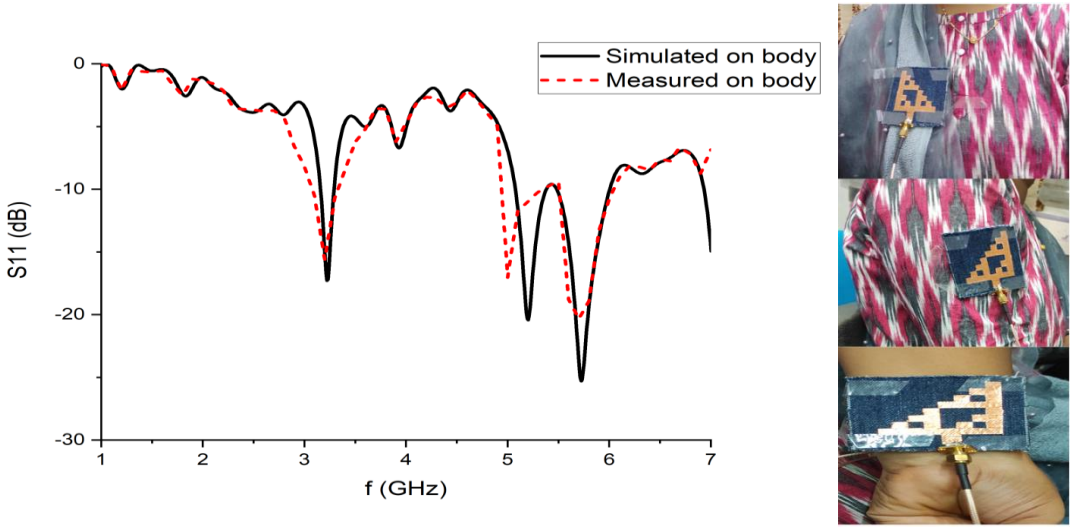

(a) (b)

Fig.3.17 (a) Simulated and measured S_{11} on the Human body (b) Proposed design on chest and arm

Apart from S_{11} measurements, the far-field radiation patterns measurements are also carried out for the proposed antenna in both free space and on-body scenarios. To understand the influence of the human subject, the radiation patterns are compared with the free space phenomena and presented in Fig.3.18. It is observed from the Figure that the patterns are strongly influenced by the human subject and became more directional compared to the free space [98], [99].

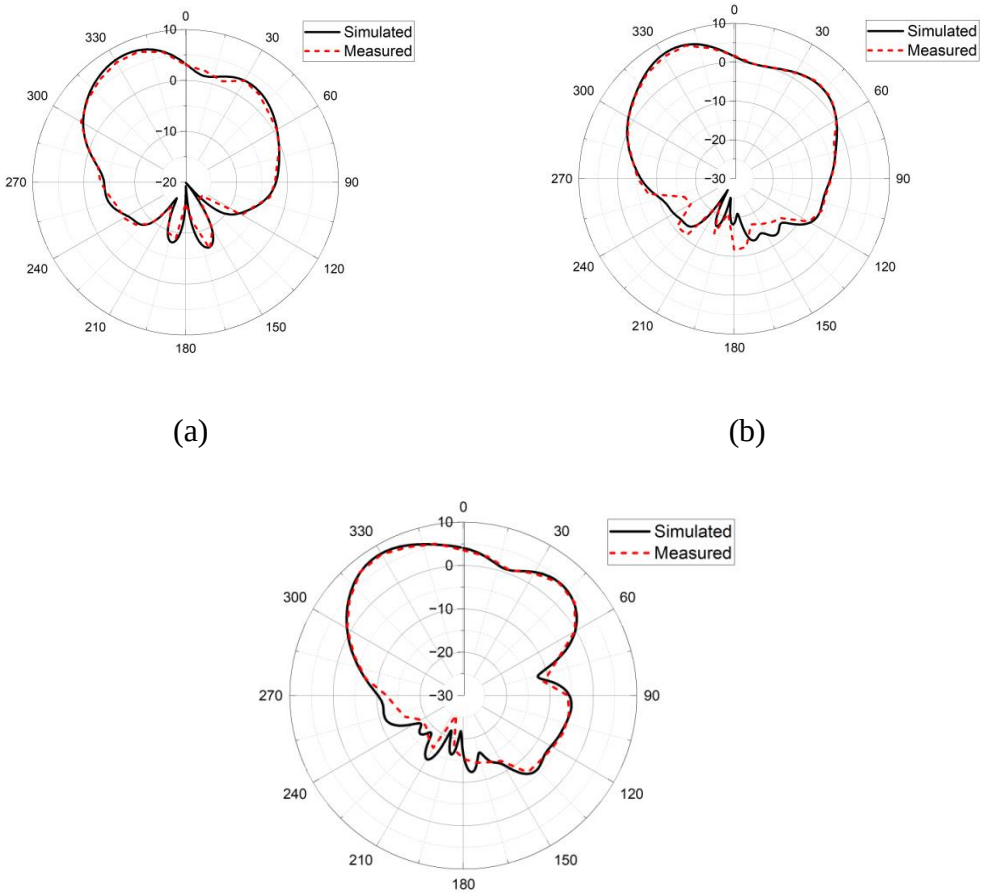

(a) (b)

(c)

Fig.3.18. Simulated and measured radiation patterns on the body at (a) 3.3 GHz, (b) 5.2 GHz, (c) 5.8 GHz

3.7.4. SAR simulations

When the antenna operates near the human body, the side and back lobe radiations penetrate and are absorbed by the human tissue. The amount of absorbed power per unit mass of human tissue can be evaluated in terms of a Specific Absorption Rate (SAR). The SAR value of the proposed antenna can be estimated by considering the human chest model as the most comfortable and wearable position. The power absorbed by the wearer can be evaluated from the induced electric field intensity (E) in the human biological tissue. The total absorbed power and SAR can be estimated as

$$P_{abs} = \frac{1}{2}\int_{v} \sigma |E|^2 \, dV \tag{3.7}$$

$$SAR = \frac{\sigma |E|^2}{2\rho} \tag{3.8}$$

Where σ and ρ are the electrical conductivity and mass density of the human tissue

The simulated SAR of the proposed antenna on the human phantom is listed in Table.3.6 for a distance of $0.22\lambda_0$ is kept between the antenna and the body to accommodate for the thickness of the fabric if the antenna is worn on the body. The simulated SAR for an average of 1g tissue is 0.891 W/ Kg and 0.422 W/ Kg for an average of 10g tissue at 5.8 GHz. It is observed from the table.2 that the simulated SAR for the desired frequencies is within the standards. A small amount of power is absorbed by the human tissue, which is acceptable. It is shown in Fig.3.19 (a)-(c) that the suggested antenna is a suitable contender for wearable applications in Wireless body sensor networks.

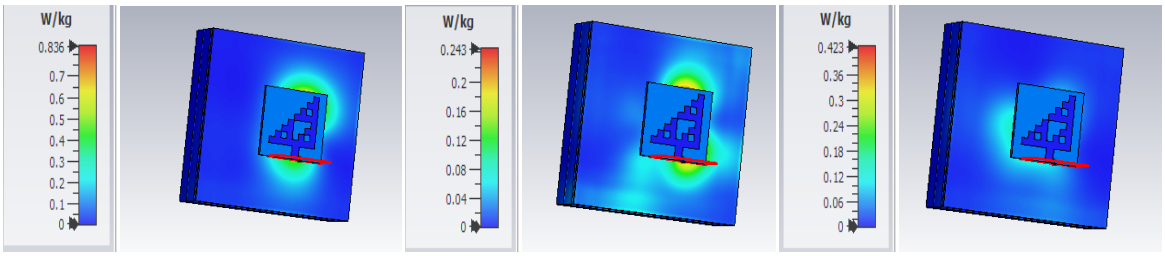

(a) (b) (c)

Fig.3.19. SAR of the proposed antenna for 10g of average Human tissue at (a) 3.3 GHz, (b) 5.2 GHz, (c) 5.8 GHz

Table.3.6. Simulated SAR values of the proposed antenna

Frequency (GHz)	SAR (W/Kg)	
	1g	10g
3.3	1.296	0.836
5.2	0.470	0.243
5.8	0.891	0.422

3.8. Summary

To start with, a few compact, flexible wearable antennas using the fractal geometry are designed, fabricated, and validated experimentally

- A compact (0.583λX0.583λ X0.02λ), fully flexible high gain sawtooth shaped boundary fractal wearable patch antenna for WBAN applications is designed with the highest gain of 5.76 dBi at 2.45 GHz center frequency.

- A compact, multi-band Sierpinski fractal antenna on a Hilbert patterned ground for Wearable-Wireless Body Sensor Networks (W-WBSN) applications is designed with maximum bandwidth and gain of 6%, 7%, 10.1%, and 2.57 dBi, 3.608 dBi, and 4.19 dBi, at 3.3 GHz/ 5.2 GHz/ 5.8 GHz, respectively.

Later, in the subsequent chapters, the Electromagnetic Bandgap structures are introduced beneath the patch/monopole antennas to improve the isolation between the antenna and the human body and to improve the gain of the antenna by suppressing the surface wave excitation.

- Mallavarapu, S., & Lokam, A. (2022). A fully flexible, high-gain saw-tooth-shaped boundary fractal wearable patch antenna for WBAN applications. International Journal of Microwave and Wireless Technologies, 1-10. http://doi:10.1017/S1759078722000836 **(SCIE)**
- M. Sandhya, L.Anjaneyulu , " Flexible, Compact Sierpinski Fractal Antenna on a Hilbert patterned ground for W-WBSN '' in MOTL indexed in (SCI) **(Under Review)**

Chapter 4.

Flexible Monopole Antenna Incorporated with Electromagnetic Bandgap (EBG) structures

This chapter introduces the Electromagnetic Bandgap (EBG) structures and proposes a fractal monopole antenna integrated with the EBG plane. The suspended transmission line method and dispersion diagram approach is used to evaluate the characteristics of the EBG structure. The performance of the fabricated antenna is compared with and without the EBG plane. The effect of deformations and human tissue loading is evaluated and also compared with the existing antennas.

4.1. Introduction

The design and development of wearable antennae experienced massive progress in the old spans, still experiencing enormous improvements. Various novel techniques have appeared in

modern antenna design, and one stimulating innovation is the design and development of EBG structures. The applications of EBG structures in antenna designs have become one of the thrilling topics for antenna scientists and engineers. The EBG structures are interpreted as "Artificial periodic/aperiodic structures that can prevent the propagation of the electromagnetic wave in a specified band of frequencies for all the incident angles and all the polarization states." EBG surfaces are also referred to as high-impedance structures because of their surface wave restriction features. Usually, these structures working on the principle of total internal reflection and also optical bandgap phenomena are also considered for certain periodic structures. For instance, microwave cavities and waveguides can permit propagation below the threshold frequency.

Usually, the EBG surfaces comprise of periodic/aperiodic arrangement of metal patches on dielectric substrates. Employing EBG structures in the antenna design opens new paradigms for novel designs. The properties of EBG structures include stopping surface waves for particular frequencies, reflecting the incident wave with zero reflection phases, and improving the gain and isolation. These are also used to lessen the noise and reduction of EMI in high-speed circuits. They can be classified into three types based on their geometric profile:

- 3 Dimensional volume structures.
- 2 Dimensional planar surfaces.
- 1 Dimensional transmission lines.

Fig.4.1. displays the sample 3-D woodpile EBG structure and the mushroom type and uniplanar 2-D EBG structures. The advantage of 3-D EBG structures is that the comprehensive band gaps that will not allow propagation states in any direction. However, fabrication and integration is the major problem associated with these structures. On the other hand, the 2-D EBG surfaces are utilized due to their advantages of compactness, lightweight, and low fabrication cost made their widespread use in antenna engineering.

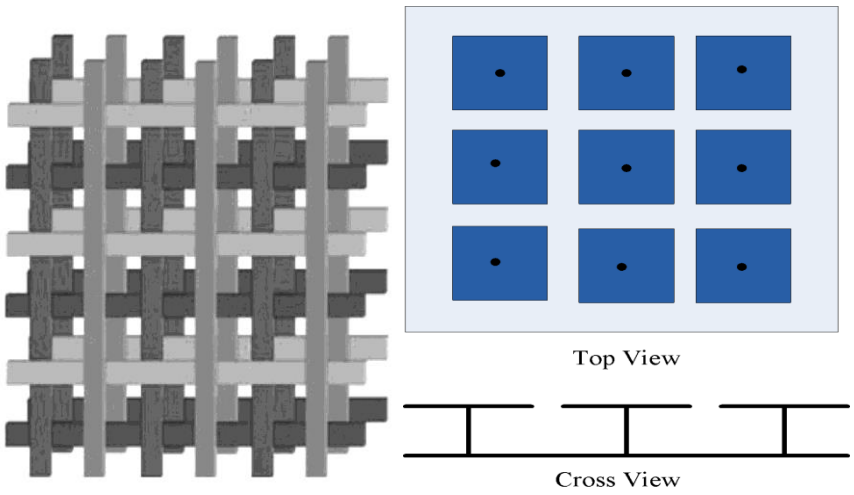

(a) (b)

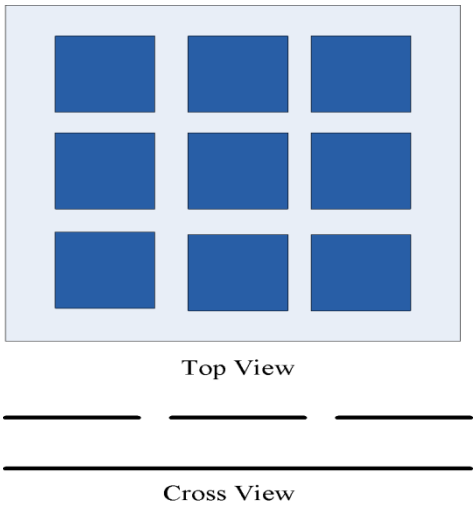

(c)

Fig.4.1. (a) A woodpile 3-D EBG structure (b) A mushroom 2-D EBG surface (c) A Uniplanar (UC-EBG) structure [100]

The uni-planar electromagnetic bandgap (EBG) structures demonstrate typical electromagnetic properties with regard to incident electromagnetic waves:

- When the incident wave is a surface wave, the EBG structures show a frequency band gap through which the surface wave cannot propagate for any incident angles and polarization states. A typical dispersion diagram is shown in Fig. 4.2 (a)

- When the incident wave is a plane wave, the reflection phase of the EBG structures varies with frequency, as shown in Fig. 4.2 (b). The reflection phase is 0 degrees at a particular frequency, like a perfect magnetic conductor that does not exist in nature.

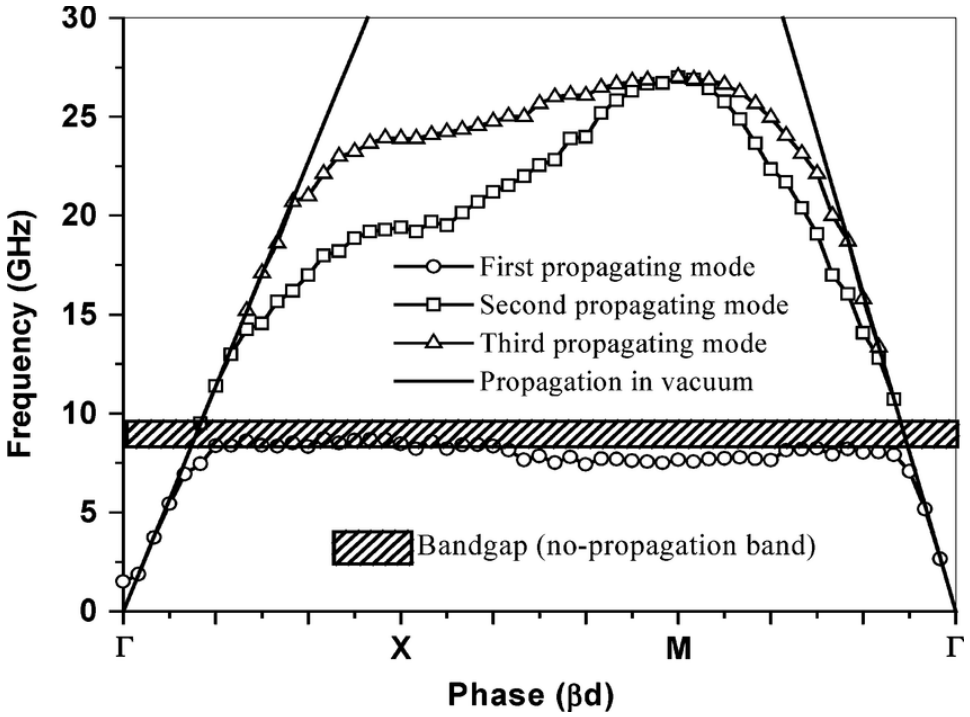

(a)

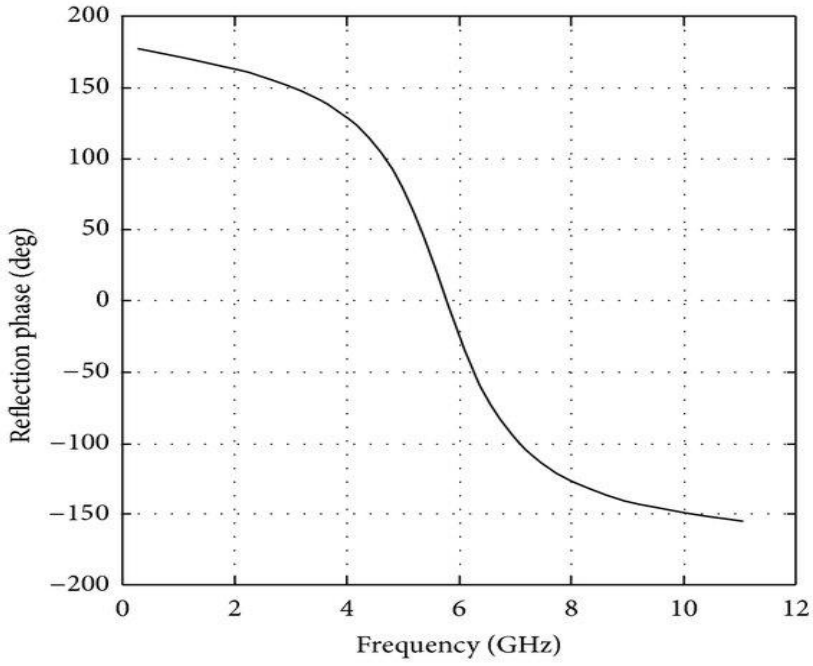

(b)

Fig.4.2. Identifying bandgap of EBG surface using (a) Dispersion diagram (b) Reflection phase [101], [102]

The presence of vias in the configuration of traditional mushroom EBG surfaces while dealing with the fabric substrates makes the fabrication process perplexing. Therefore, the vias are removed and become via-less, called the uniplanar EBG (UC-EBG). Many antenna designs have been fabricated and tested for their suitability to wearable applications in the open literature, including designing microstrip patch antennas [103], [104], PIFA [105], a vertical monopole antenna, and fractal slots loaded monopole antenna[106]. However, all these antenna designs suffer from narrow bandwidth, low gain, and high FBR. New structures called UC-EBG planes were incorporated in the recent antenna designs to overcome all such difficulties. The UC-EBG planes can act as a reflective surface and protect the human body from radiation, giving high isolation and a small SAR [55]. However, some structures are electrically large, too thick, and have reduced performance.

4.2. Design considerations and operating principles of EBG

Surface wave propagation is a severe problem in microstrip antenna design. It can cause the reduction of gain, and antenna efficiency, increase end-fire radiation and cross-pol levels and limit the bandwidth. To prevent the surface wave, one of the best solutions is to utilize high-impedance structures, such as electromagnetic bandgap (EBG) surfaces. There are numerous designs available for developing an EBG structure. A mushroom-shaped structure with metallic patches attached to a ground plane by shorting posts is one of the most widely used topologies, as seen in Fig. 4.1(b). Sievenpiper proposed the first mushroom-type EBG, which has the highest surface impedance [107]. The Mushroom EBG structures that were first proposed by Sievenpiper have greater surface impedance. At the resonant frequency, the EBG structure acts as a Perfect Magnetic Conductor (PMC) that reflects all the electric fields. Generally, the EBG surface comprises a periodic arrangement of maximum and minimum dielectric regions, which can create a band gap depending on their periodicity. In the bandgap region, no surface wave is propagated, leading to the reduction of back radiation by reflecting in the forward direction to contribute to improving the gain.

As demonstrated in Fig. 4.3, an LC filter array or a parallel resonant circuit can also be exploited to describe working of EBG structure. The electromagnetic waves travel along the EBG structure, and currents are induced on the top conducting patch. The field components of the EM wave induce charge at the edges of the patches. The inductance and capacitance appeared due to the formation of current loops and the gap between the two adjacent patches, respectively. If vias are removed, the effective inductance has reduced and still results due to the closeness of ground to the array of patches [108].

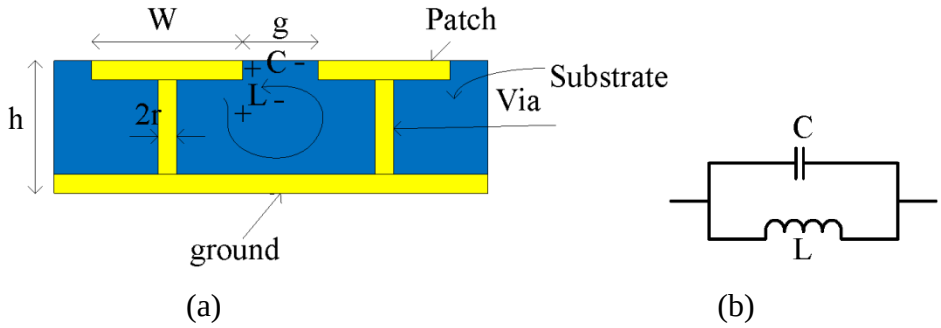

Fig.4.3. (a) Parameters of via-EBG (b) Equivalent circuit of EBG unit cell

The values of inductance (L), capacitance (C), bandwidth (BW), and resonant frequency are given by

$$L = \mu_0 h \tag{4.1}$$

$$C = \frac{W\varepsilon_0\left(1+\varepsilon_r\right)}{\pi}\cosh^{-1}\left(\frac{W+g}{g}\right) \tag{4.2}$$

$$BW = \frac{1}{\eta_0}\sqrt{\frac{L}{C}} \tag{4.3}$$

$$f_r = \frac{1}{2\pi\sqrt{LC}} \tag{4.4}$$

Where μ_0, ε_0, η_0 are the permeability, permittivity, and impedance in free space, correspondingly, g= the gap between adjacent patches, and W = width of the patch.

At resonance, the surface impedance is given by

$$Z_s = \frac{j\omega L}{1-\omega^2 LC} \tag{4.5}$$

By observing the above equations, it is found that the performance of the EBG design depends on the substrate's thickness, dielectric constant, periodicity of cells, and width of the patch [109].

At low frequencies, the unit cell is typically inductive, and the transverse magnetic field (TM) is supported by this surface. At high frequencies, the unit cells first show a resonant behavior and later show a capacitive nature with the dominant TE mode. In the band surrounded by the resonance frequency ω_0, it exhibits a high impedance behavior. Consequently, the surface waves are blocked within the band of frequencies, and due to the mismatch, a maximum proportion of the energy is returned to the system.

4.3. Characterizations of EBG

Because of the complexity associated with the EBG structures, it is difficult to characterize them through purely analytical methods. Instead, the analysis is based on the full wave simulators which are based on advanced numerical methods. The reflection phase diagram, suspended transmission line method, and dispersion diagram are revealed for the proposed EBG structures.

4.3.1. Reflection phase method

The "reflection coefficient" is an indispensable parameter unfolding the reflection characteristics of an object. The phase of the reflected electric field in the reflection plane is identified as the reflection phase. It is normalized to the phase of the incident electric field at the reflecting surface. Generally, the PEC (perfect electric conductor) and PMC (perfect magnetic conductor) surfaces represent 0^0 and 180^0 reflection phases correspondingly to the incident wave. However, the reflection phase of EBG continually varies in the range of -180^0 to $+180^0$ [107].

Notoriously, if the radiating elements are positioned parallel and near the conducting surface, the radiation resistance tends to decrease because of producing original and image

currents. While if the antenna is located at a distance less than λ/4 from the metal surface, as displayed in Fig. 4.4 (a), the phase of the incoming wave is reversed, contributing to destructive interference in the forward plane. Further, it leads to poor radiation efficiency of the antenna. To overcome this difficulty, a distance of λ/4 is used betwixt the radiating element and the ground plane, as displayed in Fig. 4.4 (b). Now, the original and image currents are in phase and contribute to constructive interference at the cost of thickness. To keep minimum thickness without compromising the radiation efficiency, an EBG surface is located behind the antenna, as in Fig. 4.4 (c). As a result of in-phase reflection, whole power is returned constructively leading to high radiation efficiency.

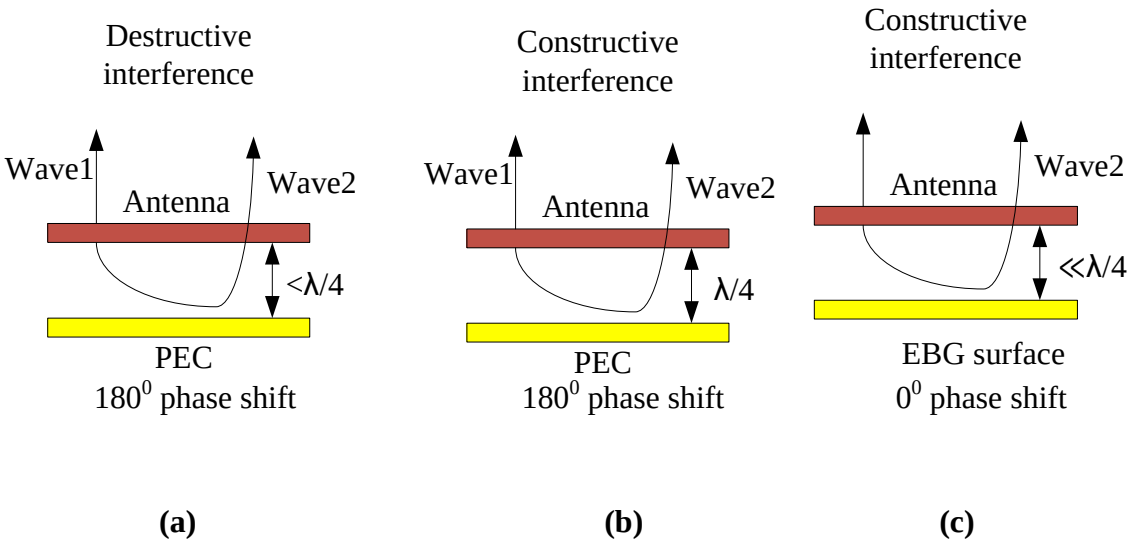

Fig.4.4. (a) Antenna situated near to ground plane (b) Antenna situated far from the ground plane (c) Antenna integrated with EBG surface in vicinity of the ground plane [101], [107]

4.3.2. Suspended transmission line method

The transmission characteristics of the EBG structure are obtainable through the suspended line method. This approach is comparable to using EBG as a filter. In this method, a microstrip line is placed above the EBG surface, soldering two SMA connectors at the two ends of the strip line as shown in Fig. 4.5. One port is excited with a plane wave and acts as a source, other port terminated with a matched load. The band of frequencies with attenuation loss less than -10 dB or -20 dB is the bandgap region. The amount of attenuation is based on the number of unit cells. The depth of attenuation in the bandgap region increased with the number of unit cells.

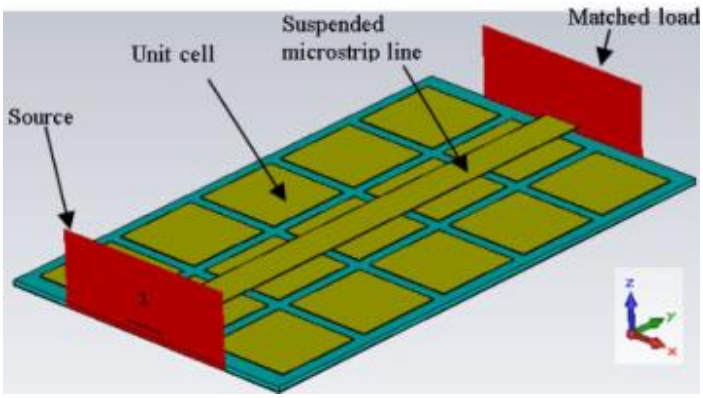

Fig. 4.5. Suspended transmission line method of EBG [64], [107]

4.3.3. Dispersion diagram

In this method, a single unit cell of EBG structure is simulated to model an infinite periodic structure in CST MW studio. The dispersion diagram is frequently used to determine the band gap of the EBG structure and is thought to be an accurate representation of surface wave property. For correct EBG design, it is essential to distinguish between the reflection and dispersion response of a structure. The dispersion diagram can be drawn to determine the bandgap of the EBG structure, which is analyzed from the Bloch-Floquet theorem. It describes the wave propagation of EM wave in an infinite media consisting of periodic repetition of a unit cell, as illustrated in Fig.4.6.

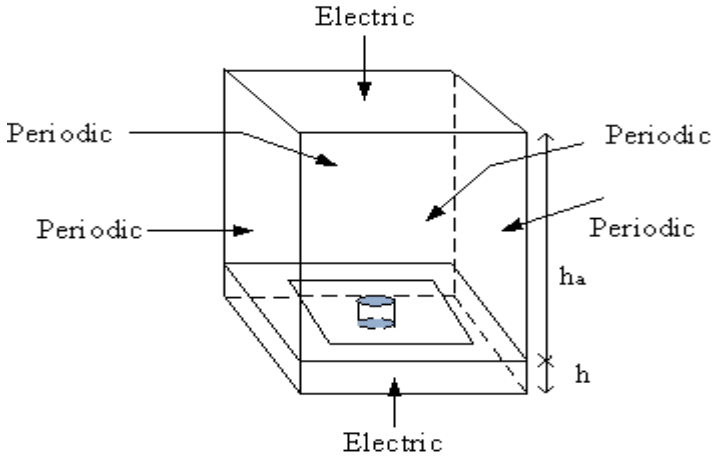

Fig. 4.6. Dispersion diagram calculation set up in CST design environment [64], [110]

The dispersion diagram has the advantage of estimating the bandgap without calculations and measurements for the entire EBG structure. Therefore the calculation time is less. To plot the dispersion diagram, the Eigenmode solver with unit cell boundary is used in CST MW studio. The EM wave is allowed at these solutions. The dispersion diagram shows the relation between the wave number and the frequency for the propagating modes. There are three regions in the diagram which can have different phase shifts. In the first region Γ-X, the boundary phase of the x-axis varies from 0^0 to 180^0, and the y-axis is kept at 0^0; in the second region, X-M, the x-axis is fixed at 180^0, and the y-axis is varied from 0^0 to 180^0. The region M- Γ, both the x-axis and y-axis, varies from 0^0 to 180^0.

4.4. Fractal Enabled EBG Incorporated Wearable Antenna

4.4.1. Design and configuration

An evolution of the proposed design is exposed in Fig.4.7 (a)-(c). The initial shape of the monopole antenna is inspired by an equilateral triangular shape. To enhance the parameters such as size and impedance bandwidth, the Koch fractal geometry is used on the boundary of the triangular-shaped monopole antenna, which is a self-similar design to increase the outer perimeter to achieve better performance with reduced size. The geometry is built on the 39X39 mm^2 flexible vinyl polymer-based PTFE, commercially known as Rogers 5880 (permittivity 2.2, Thickness 0.508 mm).

The dimensions of the anticipated antenna structure are determined by equations (4.6), and (4.7)

$$a = \frac{2C}{3 f_r \sqrt{\varepsilon_r}} \tag{4.6}$$

$$h = \frac{\sqrt{3}}{2} a \tag{4.7}$$

Where a = side length, C = speed of light, h is the height of the equilateral triangle, f_r = resonant frequency, and ε_r = permittivity.

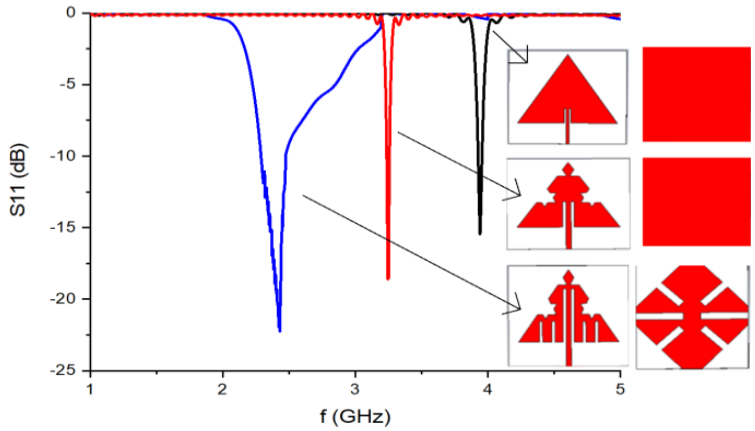

(a)

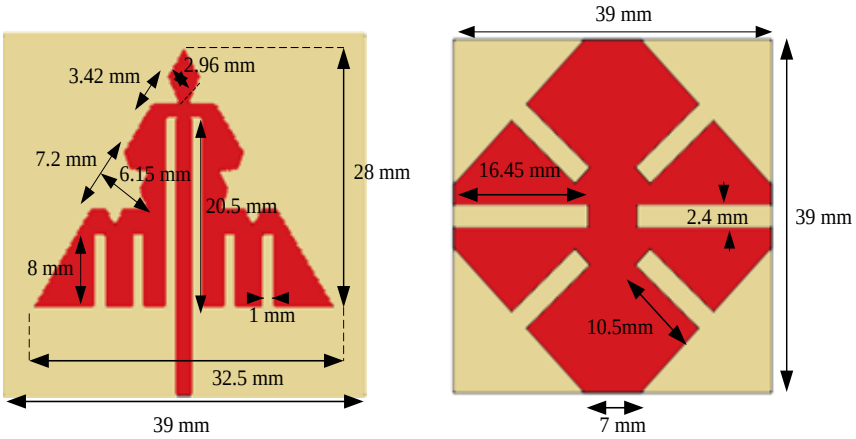

(b) (c)

Fig. 4.7. (a) S_{11} of evolution process (b) Front view (c) Back view of the anticipated geometry of the monopole antenna

To improve the mechanical flexibility and conformability of the antenna, a meander line slits parallel to the feed line is introduced, and a compact antenna resonating at the desired frequency band of center frequency 2.45 GHz can be achieved by introducing the Koch fractal geometry. Further, a defective ground was designed to improve the impedance bandwidth. Fig. 4.8 (a), (b) shows the prototype and the measured and simulated reflection coefficient curves. It is observed that both are in close agreement with each other and converge to the specified bandwidth.

(a)

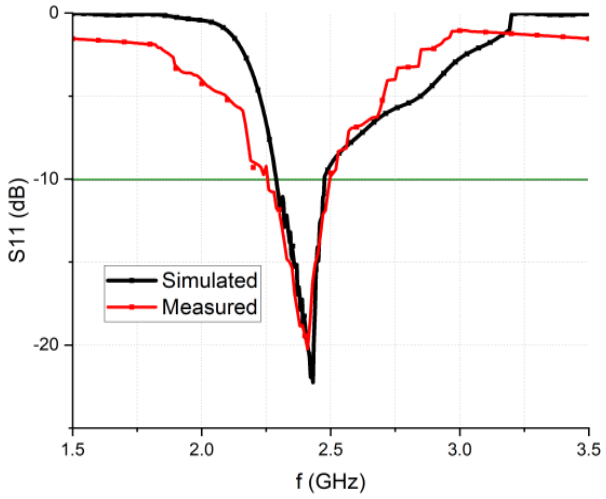

(b)

Fig.4.8. (a) Fabricated prototype (b) S_{11} evaluation of simulated and measured antenna.

4.4.2. Electrical Equivalent

To get more intuition into the behavior of the anticipated antenna, it can be represented in its lumped electrical equivalent circuit. It is well known that any conducting element represents the series combination of resistance (R) and inductance (L), and a gap between the elements is represented by a parallelly connected capacitance and conductance[43]. The proposed design used a Koch fractal on the periphery and meander line slits at the base of the equilateral triangle. The

monopole antenna without slots and notches can be represented by a parallel RLC resonant circuit, as revealed in Fig.4.9 (a). and the elemental values can be given as [111].

$$R = \frac{Q}{\omega_r^2 C} \tag{4.8}$$

$$L = \frac{1}{\omega_r^2 C} \tag{4.9}$$

$$C = \frac{LW\varepsilon_0\varepsilon_e}{2L}\cos^2\left(\frac{\pi Y_0}{L}\right) \tag{4.10}$$

$$Z = \frac{1}{\frac{1}{R} + j\omega C + \frac{1}{j\omega L}} \tag{4.11}$$

Where L, W = length and width of the radiator, L_1 = inductance, ε_e = effective permittivity of the medium, ε_0 = free space permittivity, Y_0 = admittance in free space, ω_r = resonance frequency, Z is the total input impedance and Q = quality factor.

The proposed design used a Koch fractal on the periphery and meander line slits at the base of the equilateral triangle. It involved the loading of notches at the outer boundary of the patch. From the circuit point of view, the increment in the current path accounts for the increased inductance, which tends to decrease the resonant frequency, as shown in Fig.4.9 (b). Therefore the addition of series inductance and capacitance can change the circuit parameters, and new L C along with the equivalent impedance are given by

$$L_{eq} = \nabla L_1 + \nabla L_2 + L \tag{4.12}$$

$$\frac{1}{C_{eq}} = \frac{1}{\nabla C_1} + \frac{1}{\nabla C_2} + \frac{1}{C} \tag{4.13}$$

$$Z_n = \frac{1}{\frac{1}{R_{eq}} + j\omega C_{eq} + \frac{1}{j\omega L_{eq}}} \tag{4.14}$$

Where ∇L_1, ∇L_2, ∇C_1, and ∇C_2 are additional inductance and capacitance, Z_n is the equivalent impedance.

The final electrical equivalent of the proposed antenna estimated from ADS is shown in Fig.4.9 (d). The final impedance can be obtained as

$$Z_{Total} = \frac{Z_m + Z}{Z_m Z} + Z_n + Z_L \qquad (4.15)$$

Where Z_m is the mutual impedance, Z_n is the notch-loaded impedance, and Z_L is the impedance of the line feed.

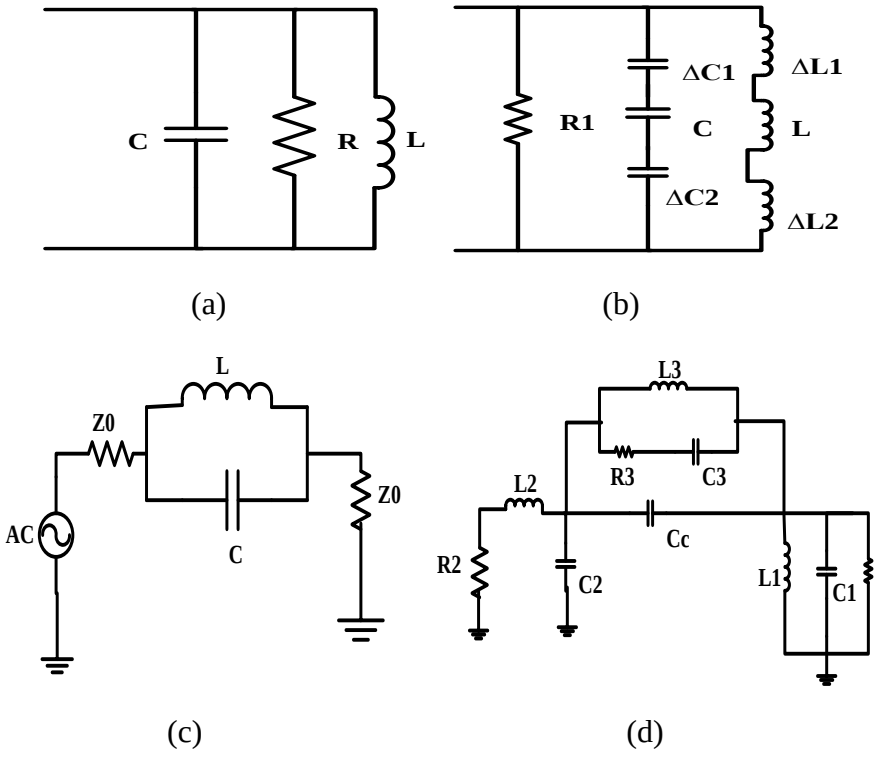

Fig.4.9. Equivalent circuit of (a) Simple monopole patch (b) notch loaded patch (c) DGS equivalent (d) proposed antenna

4.4.3. Proposed EBG Design and Electrical Equivalent

The Uni-planar EBGs are most suitable for wearable applications because of the comfortable non-via structures. In the proposed design, a 35X35 mm^2 square unit cell is designed, in which a slot of size $1/3^{rd}$ of the original square's length and width is introduced. The process is repeated for the second iteration of the fractal. This simplifies the proposed design, as displayed in

Fig. 4.10 (a). The unit cell is designed and optimized on the same substrate as the antenna but with a thickness of 1.57 mm. The equivalent circuit modeled and optimized by ADS software is shown in Fig.4.10 (b), where the capacitance comes from the gaps between the patch elements and space between the slots, and inductance comes from the metallic patch. The working of the Sierpinski square fractal EBG unit cell is elucidated by the in-phase reflection phase diagram shown in Fig 4.10 (c). Fig.4.10 (d) illustrates the dispersion diagram of the proposed EBG unit cell, where a bandgap at 2.45 GHz is exhibited.

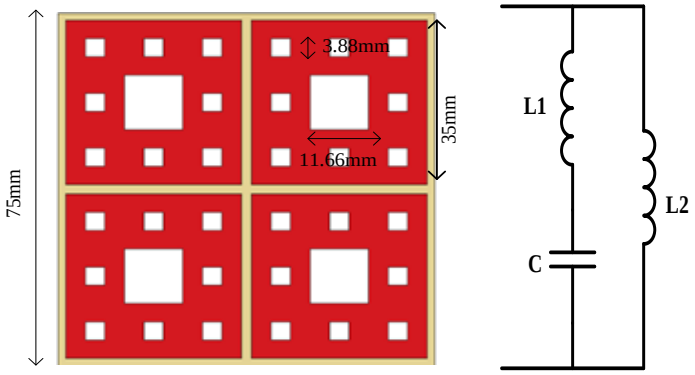

(a) (b)

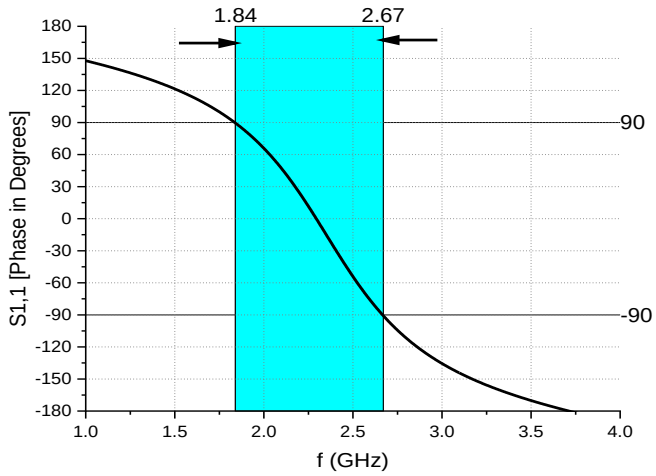

(c)

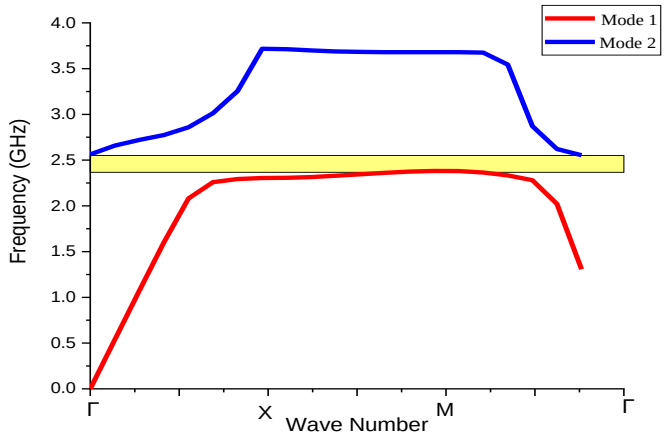

(d)

Fig.4.10. (a) The layout of the EBG array of unit cells (b) Equivalent circuit (c) Reflection phase diagram (d) Dispersion diagram of the proposed EBG unit cell

4.5. EBG incorporated antenna in free space

4.5.1. Reflection coefficient

The proposed Koch fractal-shaped monopole antenna is positioned over the EBG plane, as shown in the inset of Fig.4.11 (a). A foam layer of 1 mm is employed betwixt the antenna and EBG plane to keep away from the short circuit and improve matching. It is seen that the EBG-incorporated antenna ensures the impedance match which meets the requirement. Further, the simulated bandwidths for the antenna without EBG and with EBG are 0.35 GHz and 32 MHz, respectively is found to be in close agreement with measured bandwidths of 0.38 GHz and 48 MHz. Regardless of the shrink in bandwidth, the EBG-incorporated antenna shows a better match and still covers the specified ISM band. It is because the bandwidth typically depends on the periodicity provided in between the EBG unit cells[110]. A significantly less surface current is observed for the antenna alone, whereas maximum current density is focused on the proposed antenna incorporated with EBG. This implies that EBG also acts as a resonator and can resonate to contribute to reducing the overall size of the antenna.

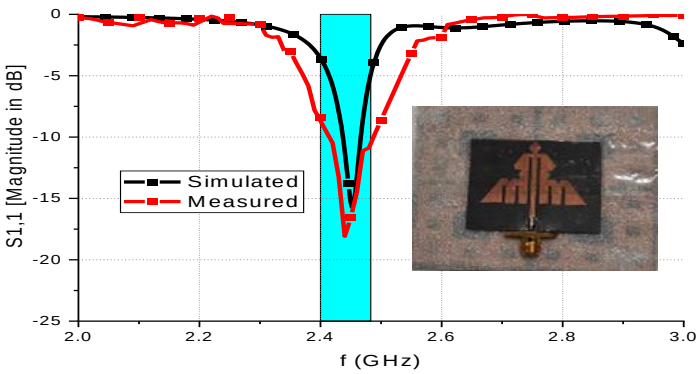

(a)

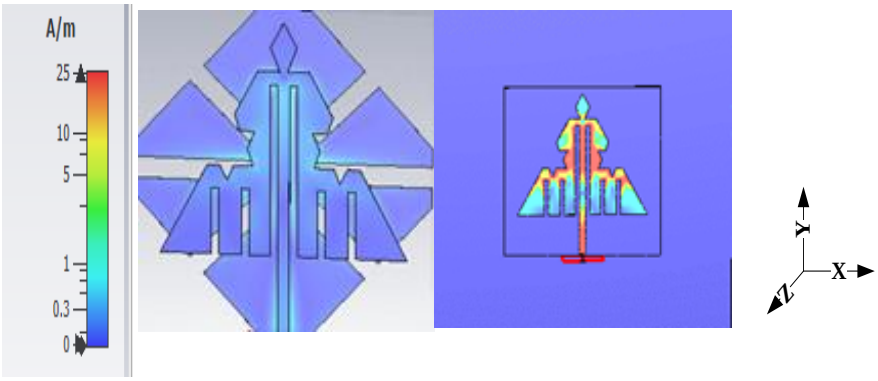

(b)

Fig.4.11. (a) Reflection coefficient of EBG integrated antenna, (b) The current distribution of antenna alone, (c) Current distribution of EBG integrated antenna

4.5.2. Radiation pattern

Fig.4.12 shows the radiation patterns of the proposed antenna plotted along the x-z and y-z planes. It is proved that the fractal-modified antenna shows a broadside pattern and an omnidirectional pattern along the x-z plane and y-z plane, respectively. However, it is always safe to consider maximum forward radiation, especially for wearable applications, which operate in the juxtaposition of the human body. This is because radiation into the body presents health risks. Therefore a directive pattern is always preferred, and the EBG integrated antenna shows maximum radiation in the x-z and y-z planes. Consequently, high isolation was achieved, and it is measured in terms of FBR, which is 13 dB for the proposed antenna. Additionally, EBG incorporated antenna offers a forward gain of 7.86 dBi and an efficiency of 90.35 %.

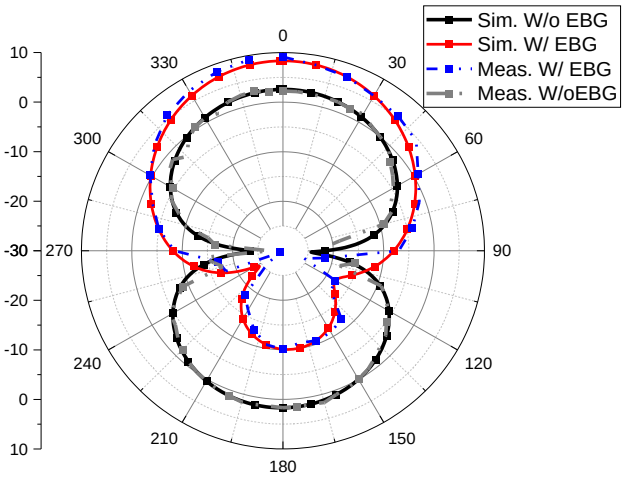

(a)

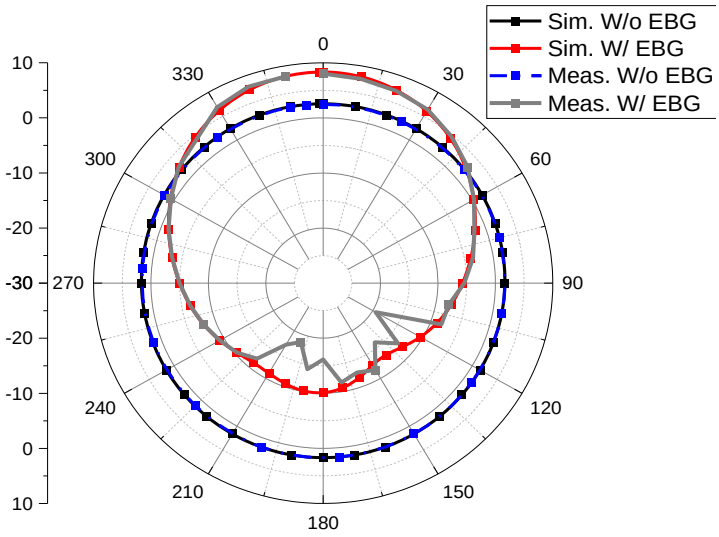

(b)

Fig.4.12. Radiation properties of the proposed antenna along (a) y-z (b) x-z plane at 2.45 GHz

4.5.3. Bending effects

The investigations are done for the deformation effects on the EBG-incorporated antenna placed on foam cylinders of diameters 80 mm, 100 mm, and 140 mm, along with length and width directions. The diameters were carefully picked to represent the model hand, arm, and chest of the human body. Fig.4.13 (a), (b), and (c) illustrates the reflection coefficient variation of the antenna

on various bend diameters along with length and width directions, namely on the x-z and y-z planes. It is seen that there is an almost negligible effect on resonant frequency when bent. Though there is a small disparity in resonant frequency, it still covers the specified ISM band frequencies.

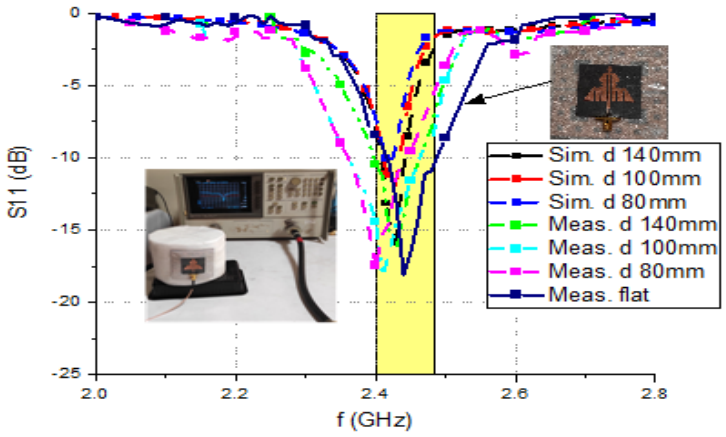

(a)

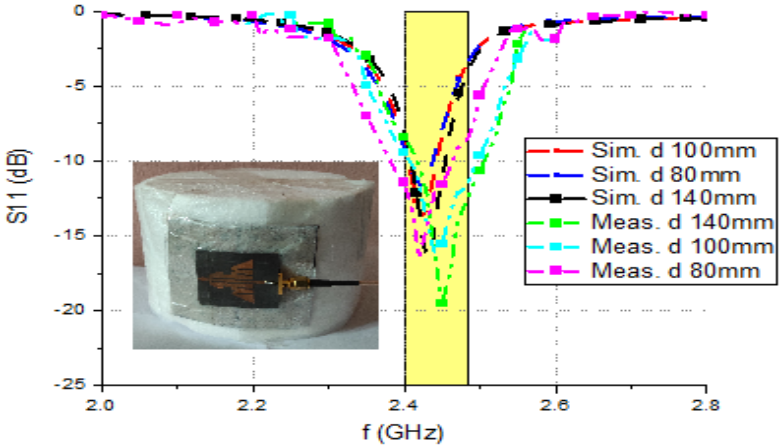

(b)

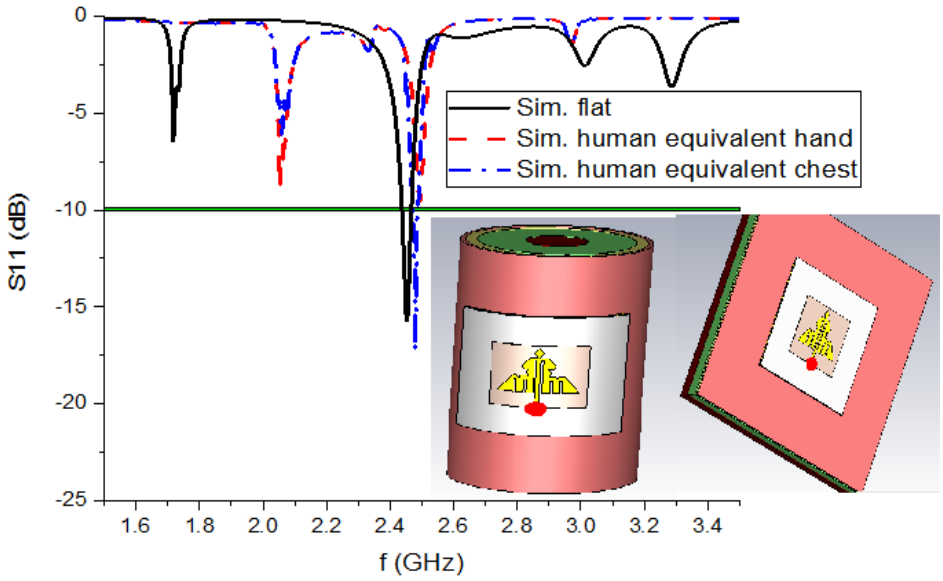

(c)

Fig.4.13. S_{11} variations of the anticipated antenna on various bend diameters along (a) x-z, (b) y-z planes, (c) On Human equivalent hand and chest tissue

Further, the radiation patterns for various bending situations are investigated and depicted in Fig.4.14. Observing the bent scenario patterns, the proposed antenna performs well. It is acceptable with a gain variation from 7.86 dBi to 6.92 dBi, 6.05 dBi, and 5.3 dBi for bending diameters 140 mm, 100 mm, and 80 mm, respectively. Also, efficiency experiences a drop from 90.36 % to 84.85 % when deformed on 80 mm diameter. This analysis demonstrates that the designed antenna is appropriate for conformal and wearable applications.

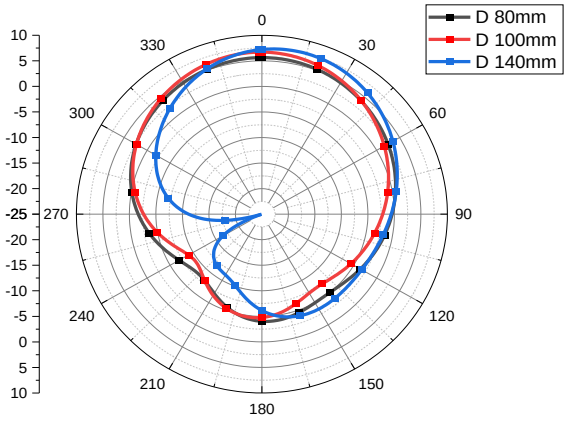

(a)

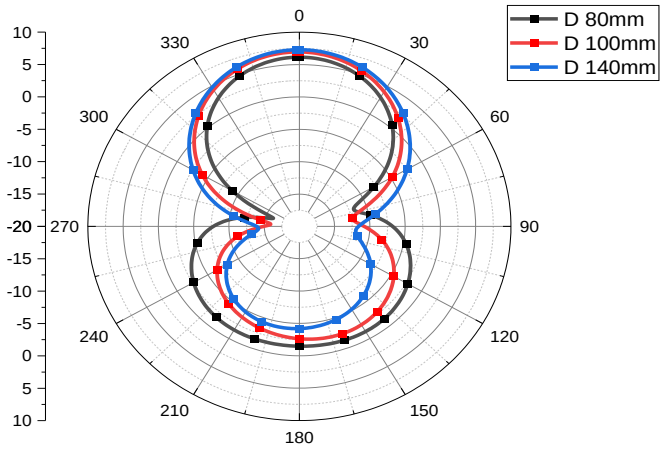

(b)

Fig.4.14. Radiation patterns of the proposed antenna under various banding situations along (a) x-z (b) y-z planes at 2.45 GHz

4.6. Performance of the integrated antenna on the human body

The robustness of the proposed model is verified with the simulations and measurements performed on a real human. The simulation human model takes a standard four-layer model, whose properties are specified in Table.3.6. To verify the merits of the anticipated antenna, it is confirmed on a female whose height and weight are 151 cm and 51 Kg, respectively. The reflection coefficient performance for this scenario is plotted in Fig.4.15 (a) for simulated and measured cases. It is seen that the resonant frequencies are shifted to lower frequencies since the human body is a big lossy cylinder that acts as a sizeable dielectric layer.

The radiation properties are portrayed in Fig.4.15 (b) for the human tissue loading of the anticipated antenna. As seen from Fig.4.15 (b), the radiation pattern became more directive because of the large permittivity offered by the human body than the substrate used. Fig.4.15 (c) displays the gain variation of the anticipated antenna with/without the EBG plane. It is witnessed that the gain of the EBG incorporated antenna upgraded to 7.86 dBi compared to the antenna alone and maintains stability within the specified frequency band, and is in close agreement with the measured values of gain.

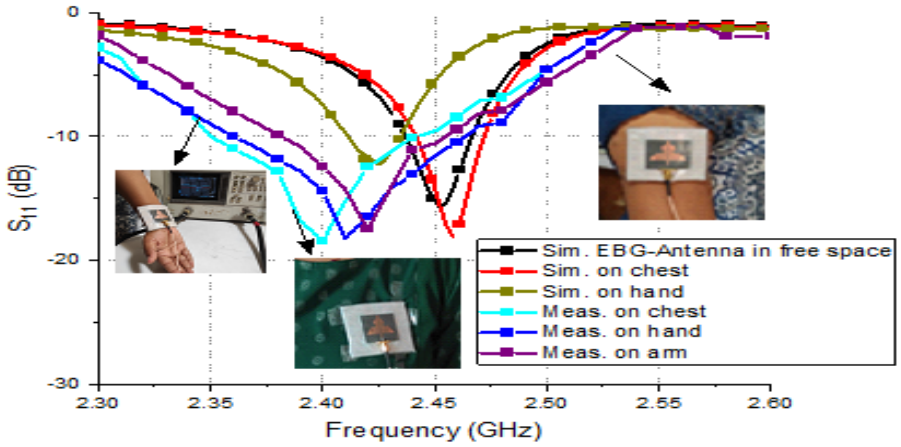

(a)

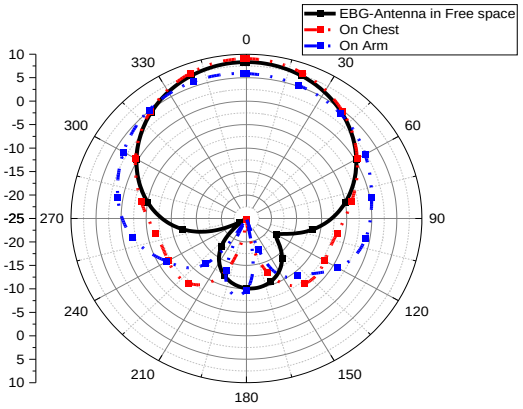

(b)

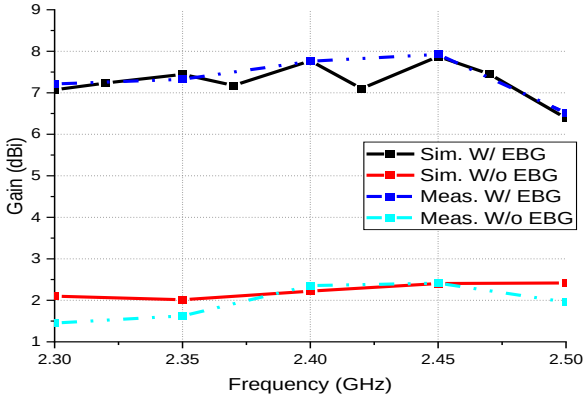

(c)

Fig.4.15. (a) Variation of S_{11} on the human body (b) radiation pattern at 2.45 GHz (c) Variation of gain along with the frequency for the anticipated antenna

4.7. SAR analysis

The wearable equipment creates biological effects on the human body when worn/ operating near the human body. The electromagnetic exposure to the human body parts, namely the chest and arm, are evaluated for the anticipated antenna as revealed in Fig.4.16 and presented values in Table.4.1.

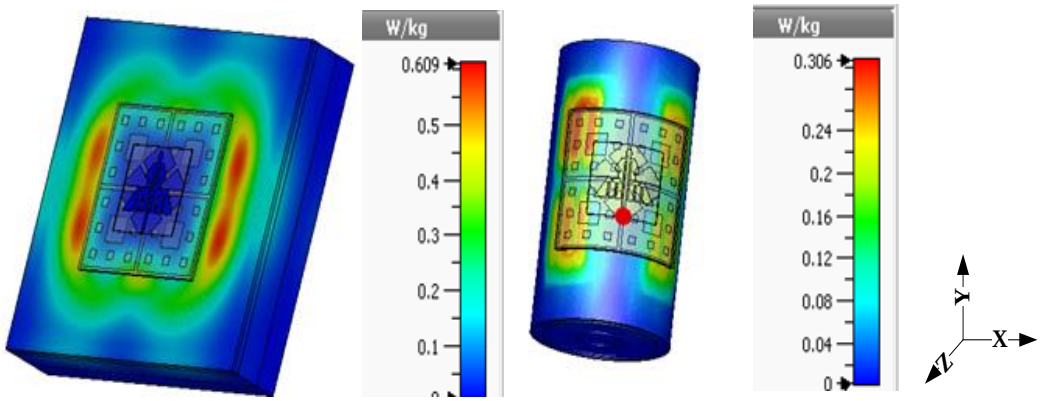

(a) (b)

Fig.4.16. Evaluation of SAR for 10 g of tissue on (a) Chest, (b) Arm

Table.4.1. SAR evaluation for chest and Arm models

Distance from phantom (mm)	On Chest		On Arm bent-X-axis		On Arm bent-Y-axis	
	1g	10g	1g	10g	1g	10g
0	1.291	0.608	1.499	0.305	1.506	0.305
2	1.290	0.608	0.044	0.021	0.545	0.256
4	0.302	0.142	0.405	0.198	0.406	0.199
6	0.041	0.027	0.360	0.170	0.044	0.021

4.8. Summary

A compact, high-efficiency, and robust antenna incorporated with EBG is designed and tested successfully in this chapter. The electrical equivalent circuits are also obtained for

investigating the matching potentials. Very good isolation and SAR performance is achieved by the use of the EBG surface beneath the monopole antenna. The EBG acts as a shield that can disengage the antenna from the human body, reducing the size of the antenna. The flexibility to deformations is tested with the use of foam cylinders, which will mimic the human body parts. The accomplished compactness, high flexibility, and deformation susceptibility make the proposed antenna suitable for wearable applications in WBAN standards.

Table. 4.2 show some of the results of the proposed antenna in comparison with the already existing EBG-based antennas. The proposed antenna offers the best compromise in terms of size, bandwidth, gain, and SAR levels.

Table.4.2. Comparison of the anticipated antenna against the available literature

Ref	**No. of unit cells**	**Overall size (mm^2)**	**Gain (dBi)**	**Radiation efficiency (%)**	**FBR (dBi)**	**SAR (W/Kg) /Distance from body**		**Frequency (GHz)**
						1 g	10 g	
[112]	3X3	150X150	NA	NA	15	NA	0.016/1	2.45
[113]	4X4	100X100	2.4	>40	12	NA	0.0464/1	2.45
[114]	3X3	60X60	6.69	>70	NA	0.612/1	0.330/1	2.45
[115]	3X2	75X50	8.2	44	NA	0.86/1	0.414/1	2.45
[116]	2X2	83X83	7.8	78.4	NA	0.64/1	0.359/1	2.38
[117]	3x3	55x43	8	>80	17.33	NA	NA	5.8
[118]	3x3	89x83	6.2	NA	NA	0.29/1	NA	2.4
Proposed	**2X2**	**75X75**	**7.86**	**90.35**	**13**	**0.302/1**	**0.1423/1**	**2.45**

- M. Sandhya, L. Anjaneyulu, "Robust, Efficient, and Low Profile Fractal Enabled EBG Incorporated Wearable Antenna for WLAN Standards. Defence Science Journal, 72(3), 429-440. https://doi.org/10.14429/dsj.72.17674 **(SCIE)**

Chapter 5.

Dual-band, EBG-DGS Wearable antenna for WBAN Applications

This chapter introduces the concept of Electromagnetic bandgap structures combined with Defected ground structures and proposes a dual-band wearable antenna for emergency services and responses in WBAN. The performance is compared with the existing literature.

5.1. Introduction

Wireless technologies have evolved into an enabler, uplifting public safety and emergency response agencies. Wireless technology for development (W4D) has devised unique network methodologies for usages in rural areas with limited infrastructure to confront emergencies and facilitate swift reply and immediate relief. With an accelerated uptick in the number of unfortunate events worldwide and the inability of traditional emergency response systems in these events, emergency response system adjustment is inevitable. Because the 'wireless' option is a promising alternative, it can assist public safety organisations in selecting the appropriate technology and system based on scenario prerequisites. Some of the most popular and emerging wireless technologies are Wi-Fi, Bluetooth, ZigBee, WiMAX, Satellite and wireless optical technologies, etc. Table.5.1 listed out the comparison of wireless technologies in terms of throughput, channel bandwidth, and the maximum number of nodes allowed.

Table.5.1. Assessment of modern wireless technologies

Technology	**Frequency Band**	**Throughput (Mbps)**	**Range**	**Channel Bandwidth**	**Success Metrics**

Wi-Fi (802.11a/b/g/n)	2.4, 5 GHz	11, 54–600	10–100 meters	20/40 MHz	Flexibility, Speed
Bluetooth (802.15.1)	2.4 GHz	3	10 meters	1 MHz	Cost, convenience
Zigbee (802.15.4)	868,915 MHz 2.4 GHz	250	10–100 meters	0.3,0.6,2 MHz	Reliability, Power and cost
WiMAX (802.16)	2.4 GHz 5.1–66 GHz	35–70	0.3–49 kilo-meters	10,20 MHz	Throughput, speed, range
UWB	3.1–10 GHz	480	10–102 meters	More than 500 MHz	Throughput, power, cost
3G/4G	400–2100 MHz(3G) 2–8 GHz(4G)	2(3G)-200(4G)	-	1.25,5–20 MHz(3G) 100 MHz(4G)	Data Rate, Range, Speed
RFID	860–960 MHz	10–100 kbps	1–100 meters	-	Cost, Power
Satellite	24–36 GHz	16 kbps–64 Mbps (downlink) 16 kbps–2 Mbps (uplink)	500–1400 kilo-meters (altitude range) 100 kilo-meters (radius)	On-demand	Coverage, Cost
Optical Wireless	300 GHz–30 PHz	622	More than 10000 kilo-meters	10–200 MHz	Cost, Robustness Throughput

In the systems associated with remote health monitoring, front-line workers, and emergency services applications, the antenna systems utilized should pinpoint the location of the

wearer. These systems gather the data from on-body devices and collectively transmit the user data to external rescue or data analysis centers. Therefore, the wearable antenna can be designed in such a way that it can satisfy the requirements of rescue operations along with prominent performance. There are many limitations associated with conventional microstrip antenna designs. To increase the impedance bandwidth of microstrip antennas, techniques like stacking patch antennas, inserting shortening pins, using different feeding mechanisms, etc, and to enhance the gain and SAR, techniques like Frequency selective surface (FSS), EBG, DGS structures, and metamaterial and so forth can be used.

Nevertheless, for a good design, the EBG unit cell must be designed so that the resonant frequency of the antenna situated in the band gap region of the EBG structure. Electromagnetic Bandgap (EBG) planes are utilized at the back of the monopole antenna to achieve the required gain and efficiency. The EBG structures offer high impedance and prevent surface wave propagation inside the substrate for certain frequencies [119], [120]. On the other hand, the integrated antennas with EBG become too thick, large in size, and sometimes less efficient with a low Front-to-Back Ratio (FBR) [100], [121], [122]. To further increase the isolation and radiation features of the flexible antenna, a novel method of integrating the antenna with an array of EBG unit cells and an etched Defects at the backplane of EBG is utilized [123]. The EBG not only improves isolation but also diminishes the effect of electromagnetic exposure on the human body. The DGS improves cross-polarization and co-polarization by changing the fields in the ground plane at the back of EBG.

5.2. Antenna Geometry

The dual-band nature of the proposed monopole antenna on a flexible substrate can be investigated by utilizing the brunching technique [40]. The fabricated antenna has two parts of U-shaped radiators on the upper side and a partial ground on the bottom of the substrate, as shown in Fig. 5.1. The antenna is mounted on a low-cost, flexible jeans substrate, having a dielectric constant of 1.7 and thickness of 0.7 mm. The large U-shaped patch generates lower resonance at 2.45 GHz, and the smaller U-shaped patch generates higher resonance at 5.85 GHz. However, both patches have a mutual influence on their resonance. The dimensions are calculated with the traditional formulae [66] and tabulated as in Table 5.2.

Table.5.2.Optimized Dimension of the Dual-Band Monopole Antenna

Parameter	W_S	L_S	W_p	L_p	W_{p1}	L_{p1}	L_f	L_g
Value (mm)	0.35 λ_0	0.36 λ_0	0.125 λ_0	0.125 λ_0	0.083 λ_0	0.066 λ_0	0.183 λ_0	0.025 λ_0

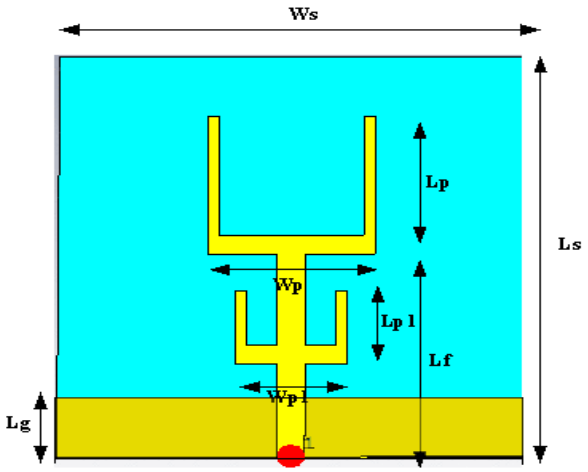

Fig.5.1. Geometry of the anticipated dual band antenna

The adjustable spacing between the top and lower U patches and the extent of the ground plane are the major parameters in controlling the S_{11} curve. The fabricated prototype is exposed in Fig. 5.2 (a), (b). Fig. 5.2 (c) demonstrates the simulated and measured S_{11} of the proposed antenna. It is observed that the reflection curve has resonance dips at 2.45 GHz and 5.85 GHz with a return loss of –12.5 dB and –18.6 dB and impedance bandwidth of 116 MHz and 398.06 MHz, respectively. The deviation in the measured values is due to faults in fabrication as parallax errors while cutting the edges of the substrates, and loss factors are associated with the substrates.

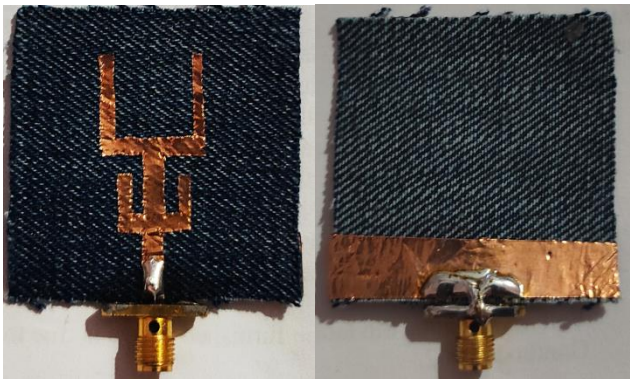

(a) (b)

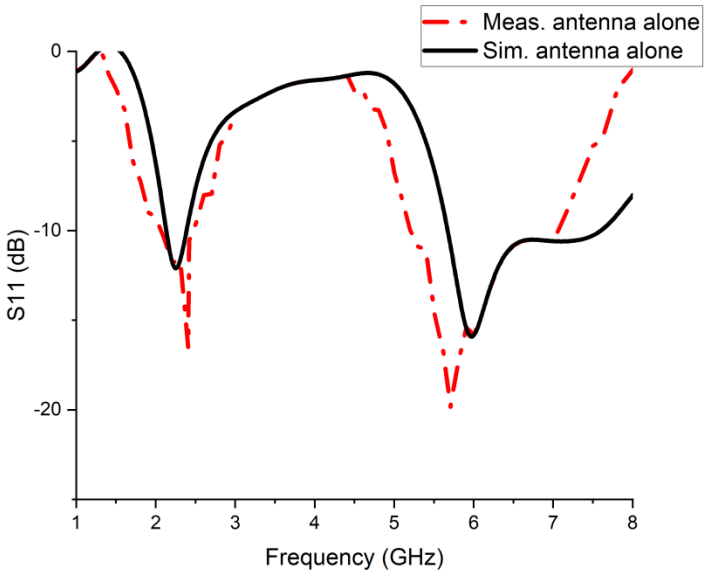

(c)

Fig.5.2. Prototype of the anticipated antenna (a) Front view (b) Backward view (c) Comparison between simulated and measured S_{11} curves.

5.3. Design of EBG structure

The EBG structure is built on a jeans substrate of thickness h_s = 1.4 mm, as presented in Fig. 5.3. The dimensions of the EBG unit cell are calculated using the equations mentioned in [124], analyzed and optimized through parametric simulations using CST Microwave Studio, and tabulated in Table 5.3.

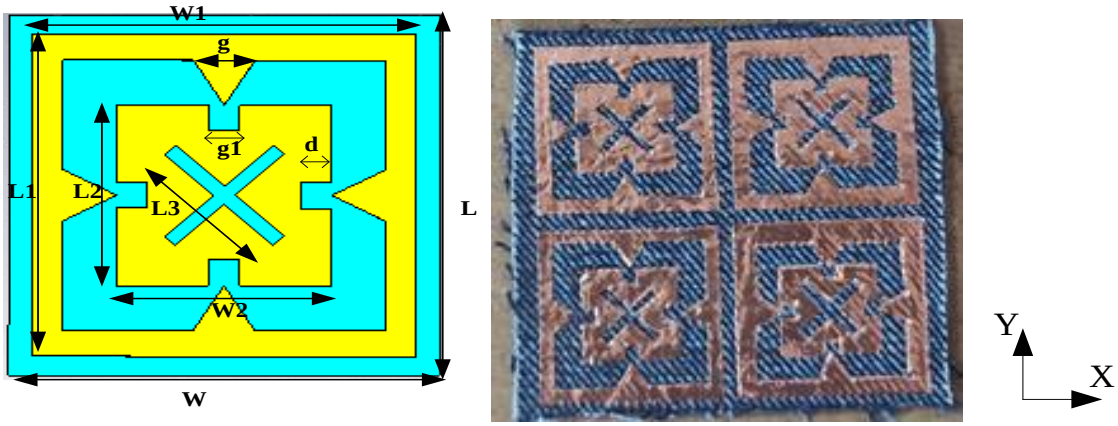

(a) (b)

Fig.5.3. (a) Proposed configuration of the EBG unit cell (b) Fabricated EBG array

Table. 5.3. Detailed parameters of the anticipated EBG unit cell

Parameters	Value, mm	Parameters	Value, mm
W	28	L_3	10
W_1, L_1	25	g	4
W_2, L_2	14	g_1	2
L	28.5	d	2

5.3.1. Reflection phase characteristics

Fig. 5.4 illustrates the reflection phase characteristics of the anticipated EBG unit cell. It is observed that there is a 0-degree reflection phase that appeared at 2.45 GHz and 5.85 GHz and behaved like a perfect magnetic conductor. The reflection phase characteristics are obtained by simulating the unit cell with periodic boundaries in both X and Y directions using the software CST microwave studio. The structure is excited by a plane wave source placed at a distance of ten times the height of the substrate (10 h_s) on top of the EBG unit cell.

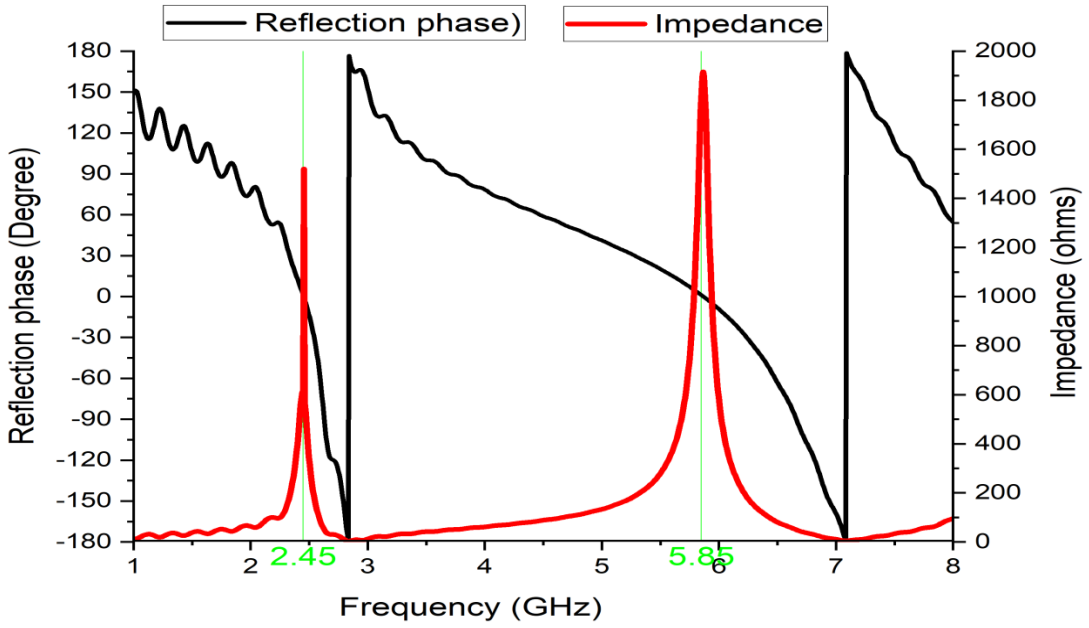

Fig.5.4. Reflection phase and impedance diagram of proposed EBG unit cell

5.3.2. Transmission characteristics

Fig. 5.5 demonstrates the transmission characteristics, where the anticipated EBG suppresses the surface waves at the specified frequencies. The EBG planes are mostly integrated into the monopole antennas that can suppress the surface by properly designing and optimizing the unit cell of EBG. This phenomenon can be visualized by simulating the array of unit cells with the suspended transmission line method. In this method, the unit cells are arranged periodically, and a microstrip line is placed above the structure. The proposed high impedance structure can suppress the surface waves at desired frequency bands, also referred to as stop bands of EBG. This surface offers a high impedance of order 1.6 kΩ and 2 kΩ approximately at the specified frequencies, as observed from Fig.5.5.

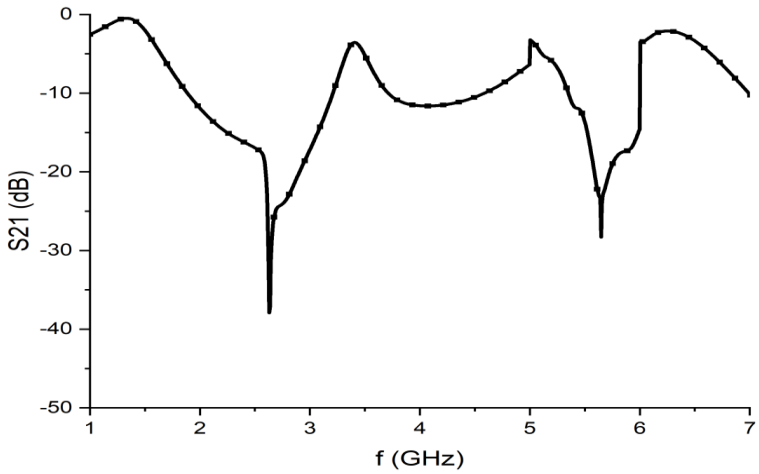

Fig.5.5. Transmission characteristics of the proposed EBG surface

5.4. Defected Ground Structures (DGS)

Engraved slots or defects on the ground plane of microstrip circuits are denoted to as Defected Ground Structures. DGS can be utilized in the field of microstrip antennas for improving the bandwidth, gain, to suppress the higher order harmonics, reducing the mutual coupling, cross-polarization levels and to upgrade the radiation characteristics.

5.4.1. Characteristics of DGS

The DGS structure has two key characteristics, namely slow wave propagation in Passband & Band Stop Characteristics in microwave circuits.

5.4.1.1. Slow wave Propagation in Pass Band

In general, the defects in the ground of the microstrip antenna can be equivalent to a parallel combination of the inductor and capacitor. With the introduction of slots etched in the ground, the equivalent inductance par increases, leading to an increase in the effective dielectric constant, which is the slow wave property. It implies that for the same physical length, the DGS line has a relatively long electrical length than the usual microstrip line. Mostly, the slow-wave factor is defined by λ_0/λ_g, where λ_g is the guided wavelength and λ_0 is the free space wavelength.

5.4.1.2. Band Stop Characteristics

The effect of bandgap of the etched DGS can be described by studying the equivalent circuit model. The series inductance is the result of DGS sections, which will increase the reactance of the microstrip line with frequency. Consequently, the rejection of a certain frequency ranges can be started. The parallel capacitance with the series inductance provides the attenuation pole location, which is the resonance frequency of the parallel LC resonator. As the operating frequency increases, the capacitive reactance decreases and the bandgap between the propagating frequency bands can occur. Usually, the microstrip line has an impedance of 100–130 Ω. With the defective structures, the impedance increases even more.

Any wearable antenna design requires reducing the power loss due to back lobes and improving the radiation in the forward direction. Otherwise, they may be hazardous to humans who wear them. Therefore, a critical parameter in wearable antenna design is the front-to-back ratio (FBR). In general, the FBR is the ratio of power radiated in the front/main radiation lobe and the power radiated in the opposite direction (180^0 from the main beam). To improve the FBR of the wearable antenna, an EBG structure is situated at the back of the antenna. Most of the EBG structures suffer from the large size, narrow bandwidth, less radiation efficiency, and cross-polarization levels. Therefore, a novel DGS array is etched on the same substrate of EBG to alleviate the high resonant frequency, narrowband and cross-polarization level.

5.4.2. Advantages of defected ground structures

The defective ground structures in the antenna design can be useful for

1. Size reduction
2. Higher-order harmonic reduction
3. Cross-polarization reduction
4. Mutual coupling reduction in arrays
5. One of the design approach for generating circular polarization
6. Broadband RCS reduction
7. Elimination of scan blindness in antenna arrays

8. Radiation properties enhancement

5.4.3. Proposed DGS array

A novel DGS is printed on the same substrate of EBG. The shape of the DGS is inspired by the traditional Dumbbell shape. Cutting a rectangular slot with four branches on all sides on the ground plane of the EBG substrate forms one DGS unit cell. The characteristics of the proposed DGS array can be verified by the suspended microstrip line method, where a microstrip line is placed on the top of the substrate, and the DGS array is placed on the bottom of the substrate as the ground plane as shown in Fig.5.6.

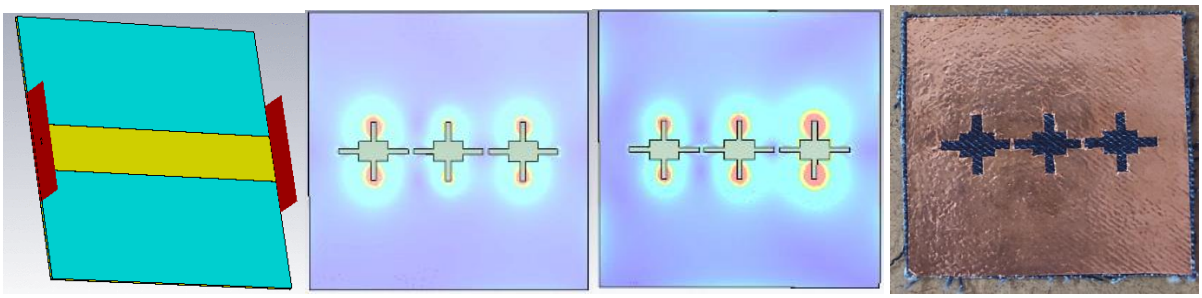

(a) (b) (c) (d)

Fig.5.6. (a) Suspended line method of DGS; Surface current dispersal of the anticipated DGS array at (b) 2.45 GHz, (c) 5.85 GHz, (d) DGS array etched on the ground plane of EBG structure.

From Fig.5.6 (b), (c), the current distributions strongly distract the electromagnetic fields in the ground plane. In general, the slots in the ground plane distract the shielding electromagnetic fields and increase the effective permittivity of the medium. Different attributes of DGS, including shape and dimension, can affect the wave propagation inside the substrate.

5.5. Performance of the integrated antenna in free space

The monopole antenna is situated in the middle of the EBG-DGS structure, and the overall dimension of the structure is 56 mm × 57 mm × 1.4 mm. An isolated layer of foam with a 2 mm thickness is inserted between the monopole antenna and DGS-loaded EBG structure to provide isolation, reducing the shorting and mismatch effects.

5.5.1. Reflection coefficient

The integration of the monopole antenna with the DGS-loaded EBG surface prototype is displayed in Fig.5.7 (a), (b). The S-parameters of the monopole antenna alone, monopole antenna with EBG, and DGS-loaded EBG structure are displayed in Fig. 5.7 (c). It is marked in Fig. 5.7 (c) that the S11-parameters of monopole antenna with DGS-loaded EBG structure have a better reflection coefficient at resonant frequencies of 2.45 GHz and 5.85 GHz. It is seen that an impedance bandwidth of 115.9 MHz and 398 MHz are obtained at 2.45 GHz and 5.85 GHz, respectively. With the use of the DGS structure, the bandwidth of the final antenna is increased compared to the monopole antenna with the EBG structure. A small deviation of 1.22 % is detected between the simulated and measured reflection coefficient curves, which are due to the inhomogeneity of the flexible substrate, soldering errors, and fabrication inaccuracies.

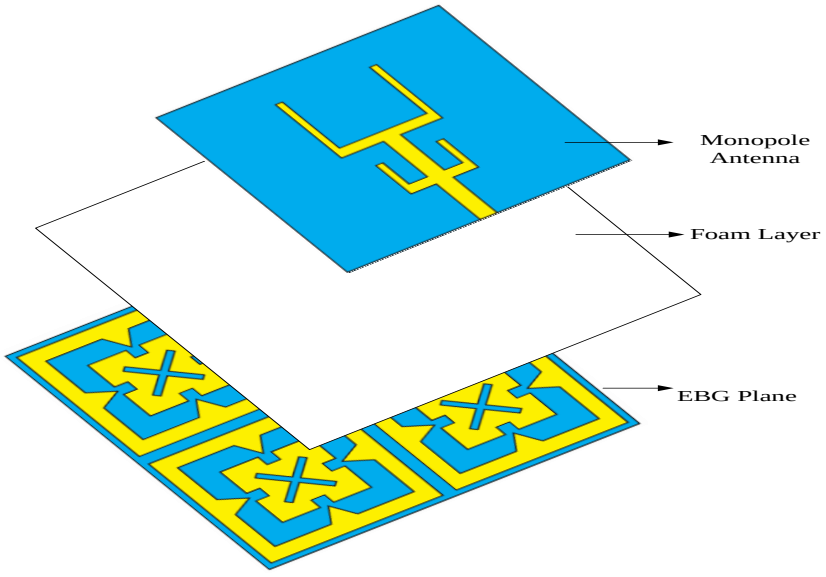

(a)

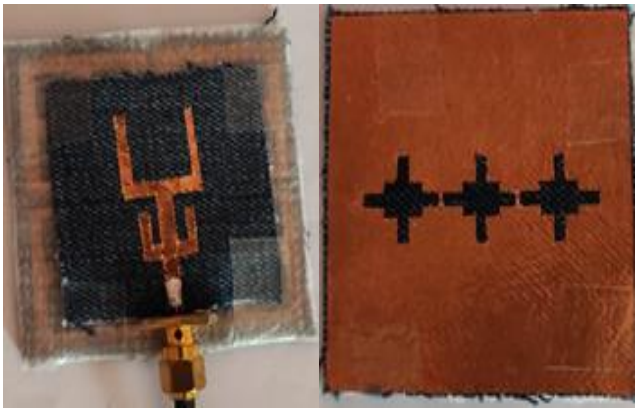

(b)

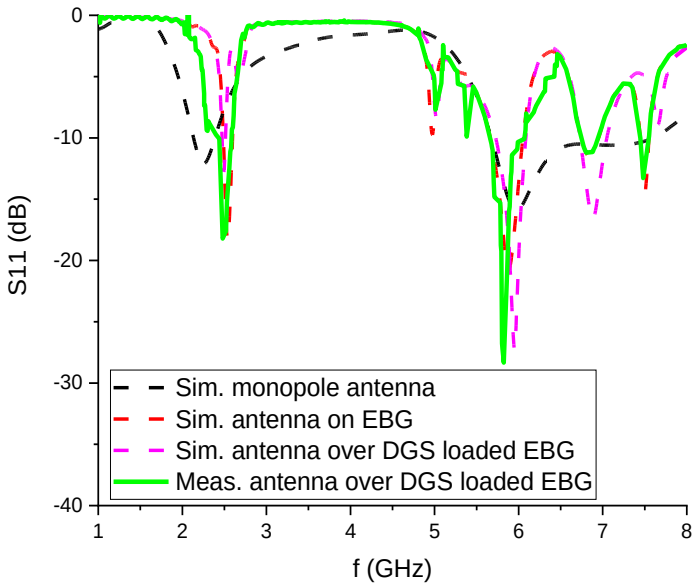

(c)

Fig.5.7 (a) The configuration of the proposed antenna; (b) Fabricated prototype front and back view; (c) Reflection coefficient of the anticipated antenna

5.5.2. Radiation pattern

Fig. 5.8 demonstrates the E-plane and H-plane radiation patterns at 2.45 GHz and 5.85 GHz; for conventional monopole antenna, the monopole antenna is integrated with EBG, and the monopole antenna with DGS loaded EBG structure, respectively. The results illustrate that the

E-plane radiation pattern has maximum radiation in ±Z directions; H-plane has omnidirectional patterns at 2.45 GHz and 5.85 GHz for the monopole antenna, indicating backward radiations and poor front-to-back ratio. On the other hand, backing the monopole antenna with an EBG plane, the maximum radiation is in the +Z direction and less back lobe, leading to an improved front-to-back ratio of the antenna to 10.52 dB, 28.46 dB at 2.45 GHz and 5.85 GHz, respectively. With the introduction of DGS on the ground plane of EBG, the FBR further improved to 16.77 dB and 32.72 dB at 2.45 GHz and 5.85 GHz, respectively. This is clear evidence that the radiated power in the back hemisphere of the antenna pattern is less than 6 % and 3 % at 2.45 GHz and 5.85 GHz, respectively. A substantial reduction in the back radiation is observed when integrating the antenna with EBG-DGS planes; hence, the gain is considerably improved in the broadside direction, which is most desirable in wearable applications.

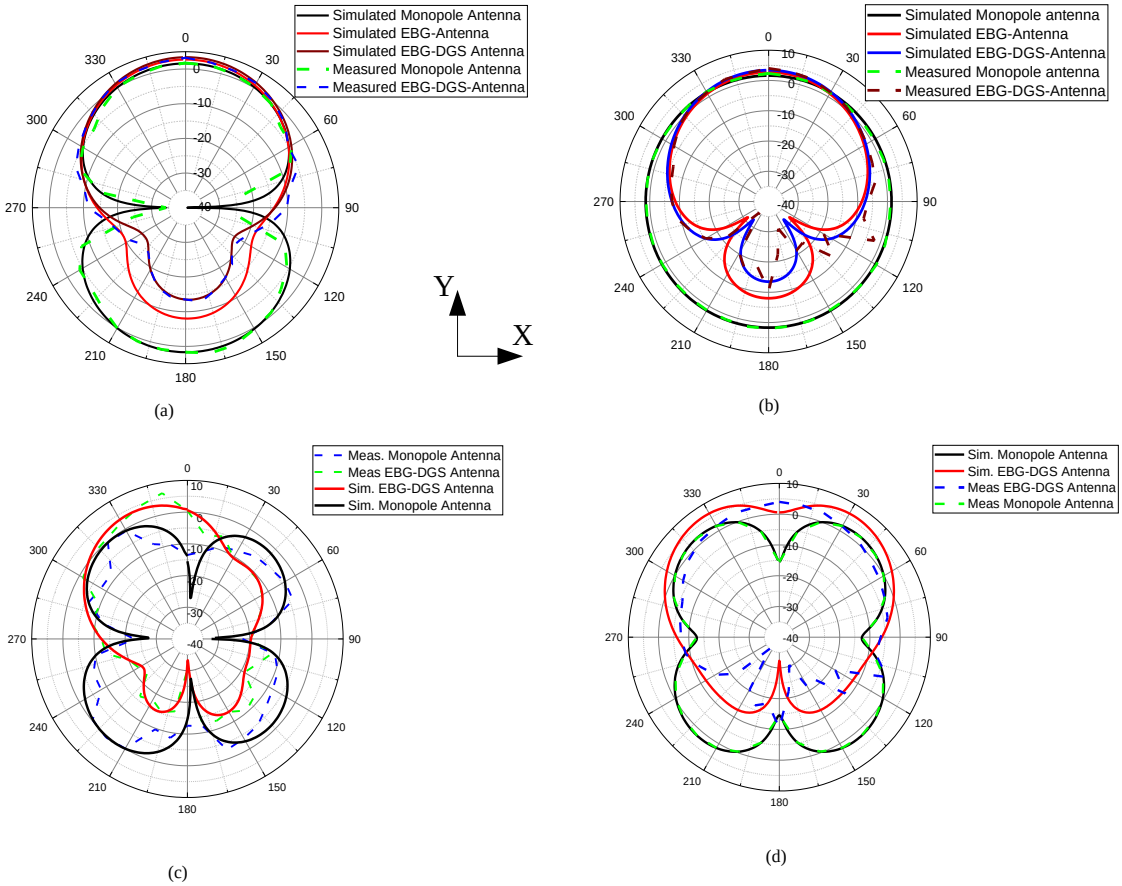

Fig.5.8. Radiation patterns (a) E-plane; (b) H-plane at 2.45 GHz; (c) E-plane; (d) H-plane at 5.85 GHz.

5.5.3. Gain and Radiation efficiency

The proposed DGS disturbs the current distribution in the ground of the EBG structure and reduces surface wave propagation. As the surface wave is reduced, the losses acquired due to surface waves are reduced, and hence the gain and radiation efficiency increase. Table 5.3 shows the comparison of the gain and radiation efficiency of the monopole antenna alone and the DGS-loaded EBG structure. In Table 5.4, the gain of the antenna increased to 3.37 dBi and 6.47 dBi from 1.68 dBi and 2.51 dBi, respectively, thus indicating a 50.23 % of improvement, practically doubling the gain with the usage of the DGS-loaded EBG planes beneath the monopole antenna.

Table.5.4. Comparison of Gain and Radiation Efficiency of a Monopole Antenna, EBG Based Monopole Antenna, Monopole Antenna with DGS Loaded EBG Structure

	Gain, dBi		**Radiation Efficiency, %**	
Operating frequency	2.45 GHz	5.85 GHz	2.45 GHz	5.85 GHz
Monopole antenna alone	1.68	2.51	96.60	93.11
EBG-based monopole antenna	2.72	6.92	32.58	74.03
Monopole antenna with DGS loaded EBG	3.37	6.47	37.15	77.13

5.5.4. Co-polarization and cross-polarization

In particular rescue and emergency search and response applications, the polarization of the antenna can be useful for the different polarizations at the transmitter and receiver ends. This can be improved by introducing the array of defects in the ground plane of the EBG structure. As the antenna is placed on X-Y (phi plane) plane, the X-Z plane is the H-plane, and the Y-Z plane becomes the E-plane. Therefore, the Gain-phi plane is the co-polarization, and the Gain-theta plane is the cross-polarization. Fig. 5.9 shows the simulated co- and cross-polarization for the proposed antenna on the E, and H-plane at 2.45 GHz and 5.85 GHz, respectively. It is observed

from Fig. 5.9 that the cross-polarization level meets the low acceptable level for better antenna performance and co-polarization has the maximum main lobe magnitude in the forward direction. Also, better isolation is observed between the co- and cross-polarization on E-plane and H-plane, respectively.

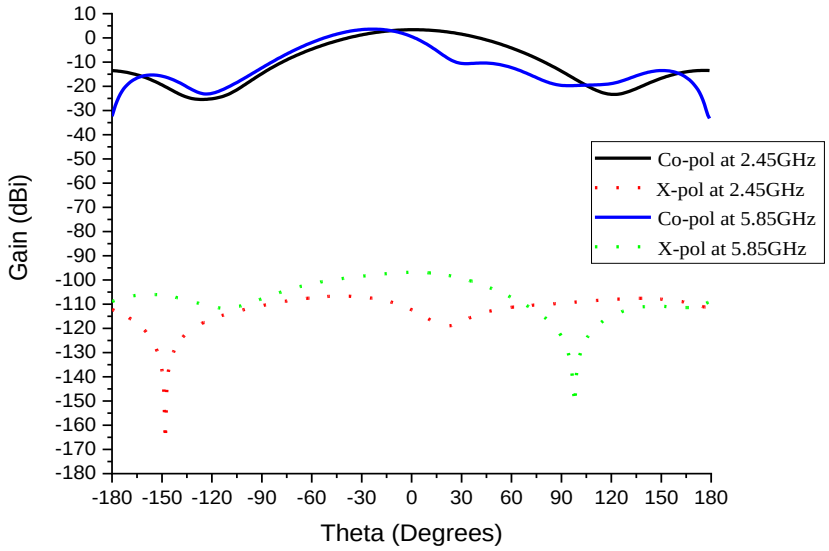

(a)

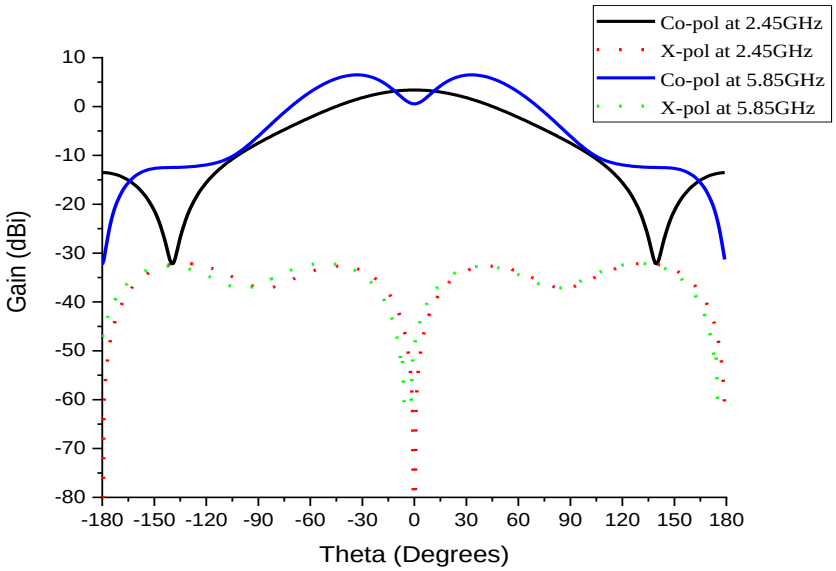

(b)

Fig.5.9. Simulated co- and cross-polarization of the proposed antenna in (a) H-plane; (b) E-plane at 2.45 GHz, 5.85 GHz, respectively.

5.6. Deformation effects

The proposed design is experimentally confirmed with a few radii of curvature to make certain of its flexibility and conformability. The influence of bending is verified with foam cylinders of radii 70 mm and 50 mm along the E-plane and H-plane, as demonstrated in Fig. 5.10.

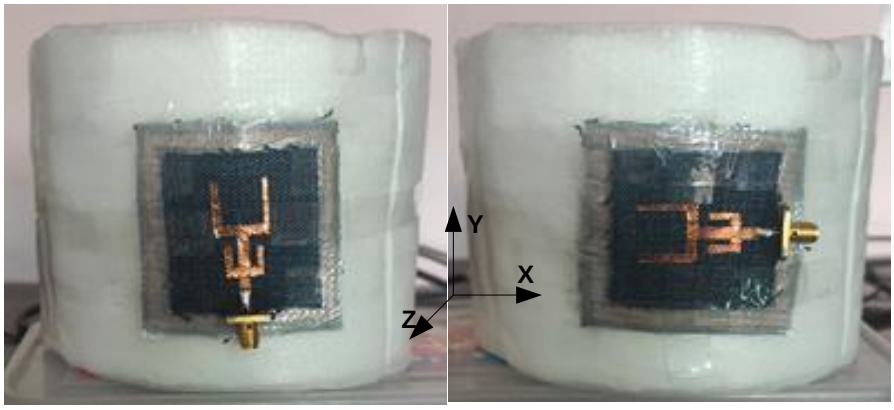

(a) (b)

Fig. 5.10. Photograph of the proposed antenna when wrapped around the foam cylinders of different radii R along (a) E-plane and (b) H-plane

5.6.1. On reflection coefficient

Fig. 5.11 shows the reflection coefficient of the proposed design under the bending scenario. The –10 dB impedance bandwidth matching is maintained in the entire bending scenario with a slight shift in the resonant frequency. It is marked in Fig. 10 that the resonant frequency is slightly shifted under the influence of bending, still covering the desired frequencies.

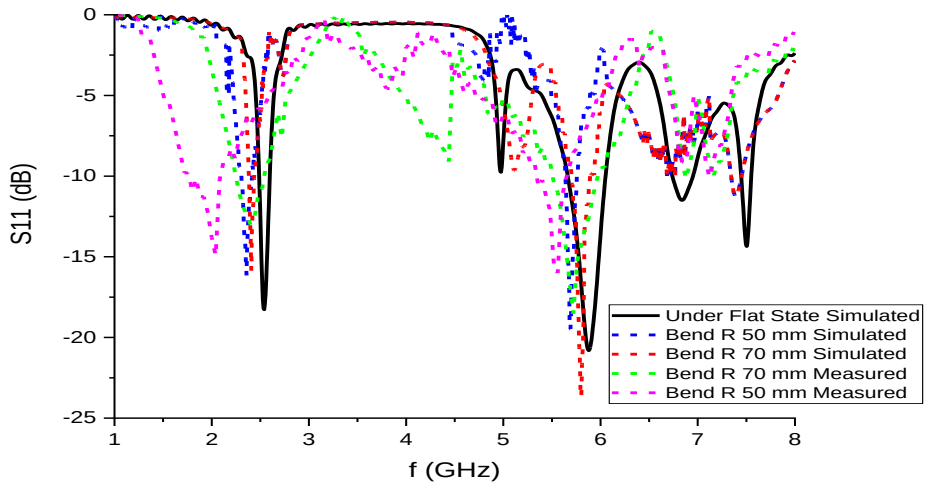

(a)

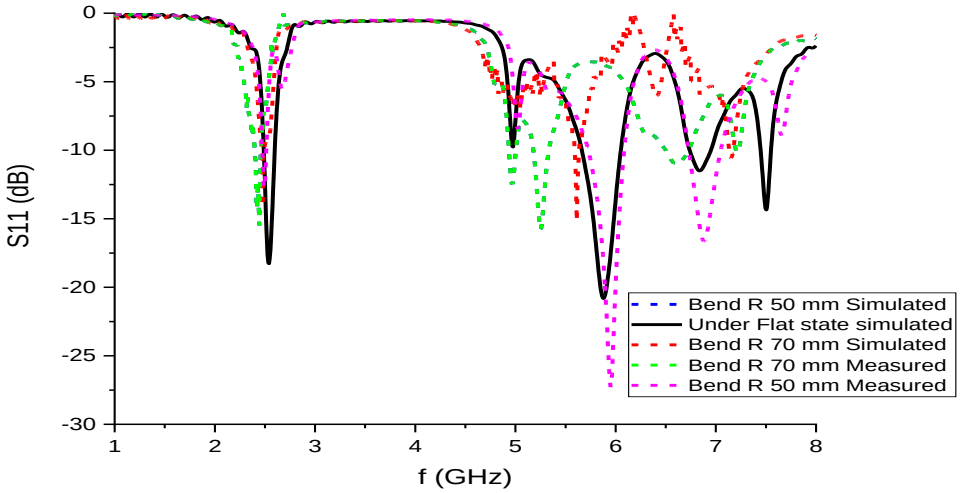

(b)

Fig. 5.11. Bending performance of the anticipated antenna on reflection coefficient (a) E-plane; (b) H-plane

5.6.2. On radiation pattern

The radiation pattern is also verified, and the proposed design maintains approximately the same result as that of a flat scenario, except for small variations. The patterns are presented in Fig. 5.12. This investigation explores the validity of the proposed antenna under various circumstances

and confirms that the anticipated antenna is useful for wearable and conformal applications in WLAN standards.

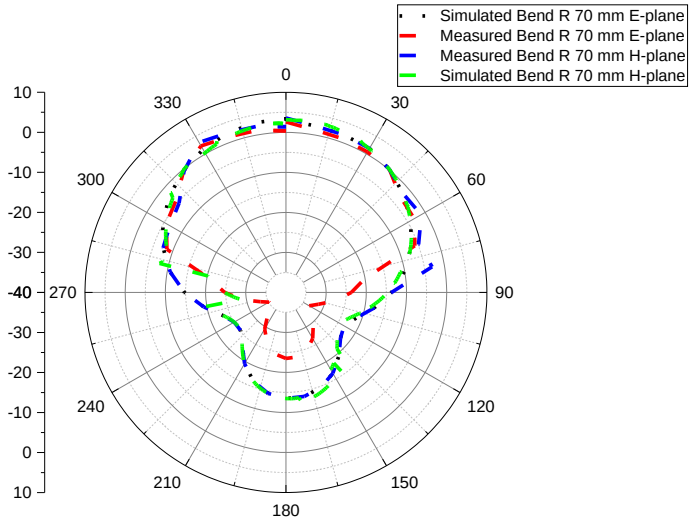

(a)

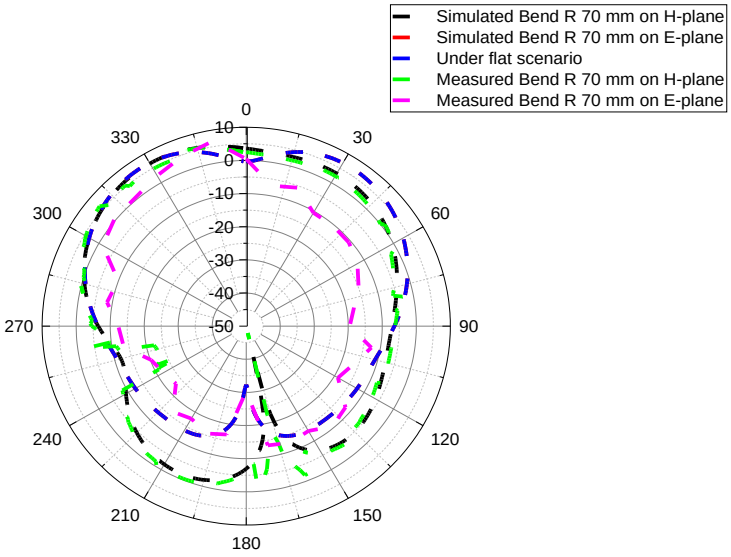

(b)

Fig.5.12. Influence of bending on radiation pattern at © 2.45 GHz; (d) 5.85 GHz

5.7. Summary

A compact and thin, flexible textile antenna integrated with DGS loaded EBG structure is presented in this chapter to cover the WLAN bands (2.4–2.485 GHz and 5.1–5.8 GHz) for emergency rescue applications. The use of DGS structures in wearable antenna designs can

improve the antenna parameters like bandwidth, radiation efficiency, and cross-pol levels. The EBG-DGS integrated antenna exhibits a compact textile design, a thin, simple antenna with excellent isolation, cross-polarization level, great gain, and bandwidth coverage for the two specified bands compared to the reported configurations in the literature listed in Table 5.5.

Table.5.5. Comparison of the Proposed Work against the Previously Published Literature

Ref	**Band of operation (GHz)**	**Method**	**Gain (dBi)**	**Bandwidth (%)**	**FBR (dB)**	**Overall Size (mm^3)**	**Substrate**
[53]	1.8, 2.4	Layered EBG	NA	NA	NA	119X119X4.62	Duroid 5880
[125]	2.45, 5.5	EBG	NA	4, 16	15	55X55X4.48	Felt fabric
[126]	1.8, 2.45	Fractal EBG	NA	6.94, 11.1	15	150X150X2.35	Jeans fabric
[115]	2.45, 5.8	AMC	8.2, 9.95	NA	NA	75X50X6	Felt fabric
[127]	2.5, 4.2	DGS	3.5, 5.5	NA	NA	50X40X0.8	FR4
Proposed	**2.45, 5.85**	**EBG-DGS**	**3.37, 6.47**	**4.73,16.2**	**16.7, 32.7**	**56X57X1.4**	**Jeans fabric**

- M. Sandhya, L.Anjaneyulu, ‘‘ DUAL-BAND Aperiodic EBG-DGS Wearable Antenna for Emergency Search Services in WBAN, in Electrical, Control and Communication Engineering, 1-10, http://doi.org/10.2478/ecce-2022-0001 **(ESCI)**

Chapter 6.

Improved wearable, breathable triple band antenna integrated with porous EBG

This chapter presents a novel, triple-band wearable, breathable, and flexible wearable antenna design with a CPW feedline for WBAN applications. A prototype is fabricated, measured, and validated experimentally. Introducing a new porous EBG by inserting a huge total of holes in the ground plane of EBG improves flexibility and breathability. Bending and on-body measurements are also performed with the prototype and achieve the most favourable results compared to the recently published ones. An assessment of the anticipated antenna with the previously published antennas is also included.

6.1. Introduction

With the expanding cross-integration of fabric materials, electronics, and information technology, there is an ultimatum for wearable-breathable e-textiles and smart apparel in the Wireless Body Area Networks (WBAN) [128]. Devising a compact, flexible, and breathable antenna is perplexing because of the incompatibility and inhomogeneity of the mechanical and electromagnetic attributes of conductive and soft textile materials. Wearable antennas are usually designed in the ideal flat state. Still, when integrated into clothing and worn, they are likely to be subjected to deformations such as bending, stretching, crumpling [129], temperature, and moisture [130] which cause variations in the resonance frequency of the antennas [95]. Additionally, textile material utilized as a substrate in the design of wearable antennas may transport the moisture/humidity from the body to the surroundings and absorb part of it due to the hydrophilic

nature of the textiles. When the substrate absorbs the moisture/humidity, the dielectric characteristics such as relative permittivity and loss tangent tend to increase, as water has a high dielectric constant [131]. The moisture content absorbed by the textile also depends on the environmental conditions and geographic region. Generally, the dielectric constant of all textile substrates is in the range of 1-2. When the substrate absorbs the moisture, the dielectric constant becomes higher than 1, and the dependent resonant frequency of the design shifts to a lower frequency. To mitigate the effect of moisture, many researchers used water-resistant materials as substrates or restrained coating on the final design making the antenna brittle and not flexible [132]. Therefore, the selected textile substrate should at least have the ability to transport moisture to the environment. A wearable, breathable fabric antenna can be the only solution to combat the above-mentioned effects more efficiently. The breathability depends on the recurrence of porosity. The greater the porosity of the material utilized in the construction of the antenna, the more the antenna converts to breathable [37].

6.2. Triple band CPW fed wearable antenna

6.2.1. Geometrical evolution

The typical geometry and design considerations of the anticipated antenna are displayed in Fig.6.1. The reference antenna is a simple decagon ring that resonates at 2.44 GHz. The concentric decagon rings loaded on the radiating structure follow the self-similarity property of the fractals. The process is repeated in up to two iterations. The jeans material (permittivity 1.7, loss tangent 0.025) of 1 mm thickness is chosen as a substrate. A proper impedance matching is achieved with the calculation of the length of the ground Lg and the gap between the feedline and the ground ‘g,’ and the optimized dimensions are as presented in Table.6.1.

Table.6.1. Parameters of the proposed antenna

Parameter	W	L	R3	R2	R1	s	s1	g	g1	g2	Lg	S2	S3	w_f
Value(mm)	40	41	14	10.5	6	1.5	3	0.5	1	1	10	2.5	2	5

Initially, the resonance frequency of the decagon ring is calculated using the conventional circular ring resonance as follows [133]

$$f = \frac{C}{\lambda} = \frac{C}{\pi(l_1 + l_2)\sqrt{\varepsilon_{eff}}} \tag{6.1}$$

Where l_1 and l_2 are the radii of outer and inner rings, C is the speed of light, and ε_{eff} is the effective permittivity of the substrate.

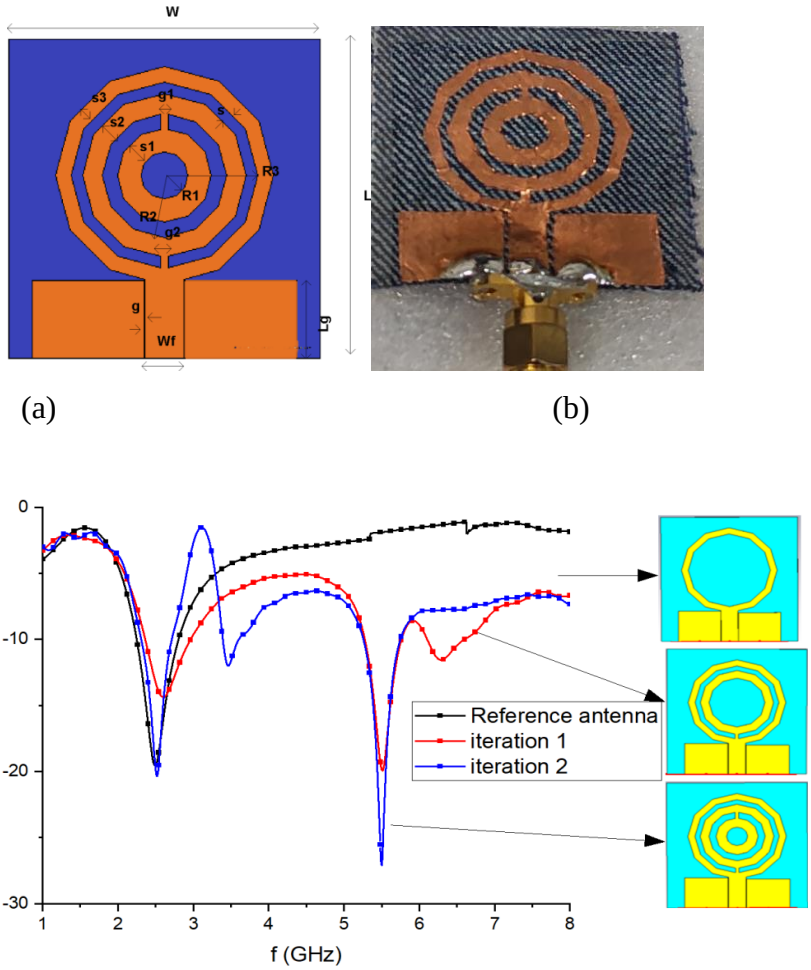

Fig.6.1. (a) Geometrical configuration (b) Fabricated prototype (c) Evolution of the proposed design in terms of reflection characteristics

6.3. Triple band porous EBG (P-EBG) design

A noteworthy advantage of uniplanar EBG design is the easy fabrication process and comfortable with conformal applications. Though, the intricate EBG structures hold its challenges

in prototyping even if the vias are excluded. Additionally, fabricating on thin textile substrates makes the task even more difficult and leads to inaccuracies. Yet, they have a narrow reflection phase band compared to conventional EBGs. The dimensions of the EBG structure decide the frequency at which zero reflection phases occur. Therefore dimensions are chosen carefully and accordingly for the desired operating frequencies. To obtain the compact and desired bandgap from UC-EBG, the circular periodic defects are introduced on the ground plane of EBG structures. Consequently, one of the design objectives is to minimalize the structural complication while attaining extreme gain and low SAR from the EBG. Hence, a novel porous type uniplanar EBG structure is designed to solve these difficulties. The P-EBG structure is realized by the construction of a periodic/non-periodic radiating element on top of the structure and perorated circular holes of 2 mm diameter behind the substrate as in Fig.6.2. The holes in the ground plane of the EBG structure, whose size is small compared to the wavelength of the propagation, generate an inductive behavior, whereas the gap between the holes generates the capacitive behavior.

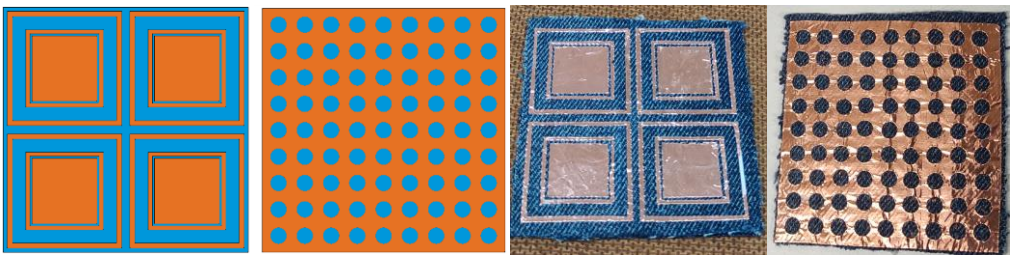

(a) **(b)** **(c)** **(d)**

Fig.6.2. Schematic of P-EBG Structure (a) Front view (b) Backward view, photo graph of the fabricated prototype (c) Front view (d) Backward view

6.3.1. Reflection phase characteristics

The optimal EBG array comprised of 2X2 unit cells is chosen and computed using CST MW Studio on a jeans substrate with dimensions 60X60X1 mm^3. The reflection phase characteristics of the anticipated EBG structure are presented in Fig.6.3. The center frequency is the point where the reflection phase achieves 0^0, and the considerable bandwidth is the interval

between $+90^0$ and -90^0. It is seen that the proposed EBG covers three frequencies 2.45 GHz, 3.5 GHz, and 5.5 GHz.

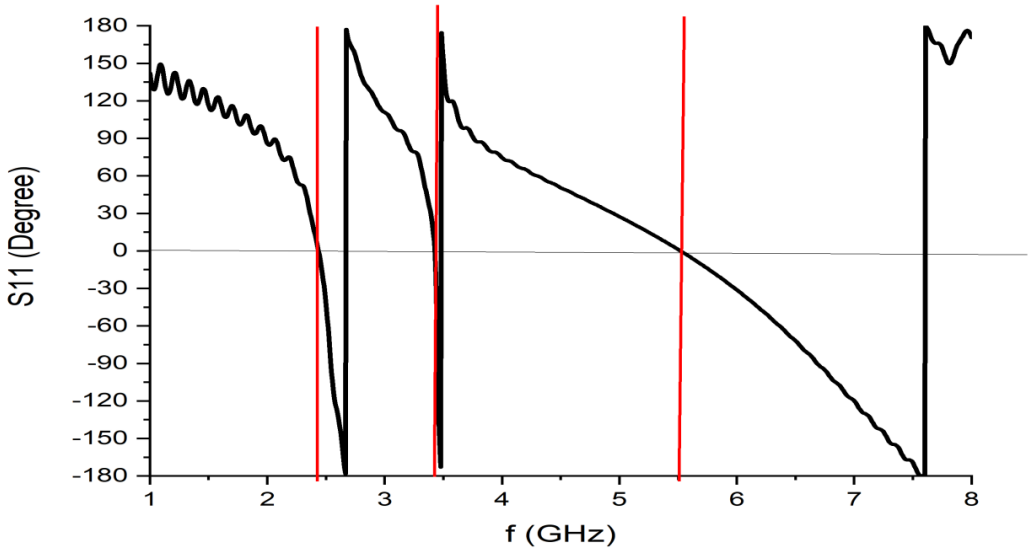

Fig.6.3. Simulated Reflection phase characteristics of Porous EBG unit cell

It is assumed that the electromagnetic wave incident perpendicularly from the top metal layer of the EBG structure. The incident wave frequency is at 2.45 GHz/3.5 GHz/5.5 GHz, respectively, which are also the frequencies that correspond to the zero reflection phase of the incident wave. The same scenario is verified by the corresponding current distributions revealed in Fig.6.4 (a), (b), and (c).

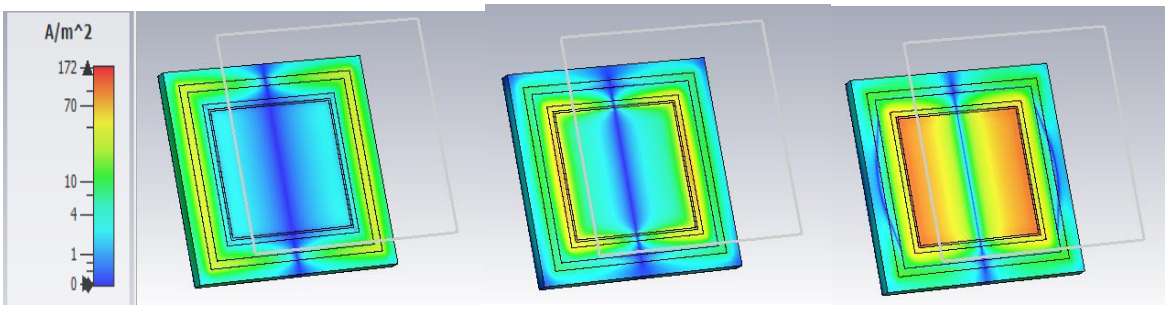

(a) **(b)** **(c)**

Fig.6.4. Surface current dispersal on EBG unit cell at (a) 2.45 GHz, (b) 3.5 GHz, (c) 5.4 GHz

6.4. Performance of P-EBG Loaded CPW Antenna

The CPW antenna is carefully positioned on the 2X2 array of P-EBG, as shown in Fig.6.5. A foam layer of 5 mm thickness is employed between the CPW antenna and EBG array to prevent any unexpected short circuit and mismatch problems. The overall size of the anticipated antenna is 60X60X7 mm^3. The integrated antenna is tested on VNA (Agilent N5247A) for reflection coefficient under the required range of frequencies.

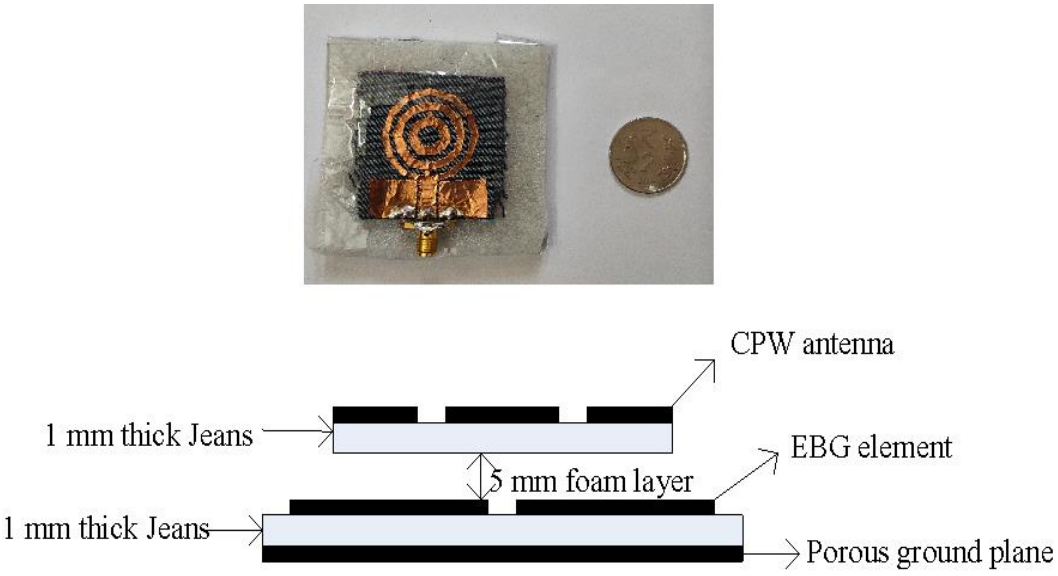

Fig.6.5. Fabricated prototype of the proposed antenna

6.4.1. Under Flat state

The measured and simulated S_{11} (dB) plots of the integrated antenna in free space are shown in Fig.6.6 (a). It is demonstrated from the figure that the realized S_{11} is reasonably stable and covers the desired frequencies of 2.45 GHz, 3.5 GHz, and 5.5 GHz. It is found that the impedance bandwidth of the proposed antenna is 264 MHz/100 MHz/153 MHz at 2.45 GHz/3.5 GHz/ 5.5 GHz, respectively. The integrated antenna resonates within the ISM band ranges from (2.4 GHz-2.485 GHz), (3.4 GHz-3.6 GHz), (5.53 GHz-5.57 GHz), which covers the minimum required bandwidth of 83.5 MHz/100 MHz/ 150 MHz, respectively. It should be noted that an additional benefit of a P-EBG integrated antenna is that the holes in the ground plane of EBG

allow the air and sweat to pass through/be absorbed by the substrate, which helps to increase the breathability of the anticipated antenna.

The radiation patterns of the integrated antenna measured at 2.45 GHz, 3.5 GHz, and 5.5 GHz are displayed in Fig.6.6 (b), (c), and (d) for both the CPW antenna and the integrated antenna. The CPW antenna has eight shaped bidirectional radiation patterns without P-EBG. With the presence of P-EBG at the back of the CPW antenna, there is a considerable reduction in the back lobe while improving the gain performance. The gain of the integrated antenna is measured as 2.18 dBi at 2.45 GHz, 6.75 dBi at 3.5 GHz, and 9.50 dBi at 5.5 GHz, respectively, compared to 1.653 dBi at 2.45 GHz, 2 dBi at 3.5 GHz, 3.74 dBi at 5.5 GHz for the CPW antenna. There is no discernible difference between the measured and simulated radiation patterns.

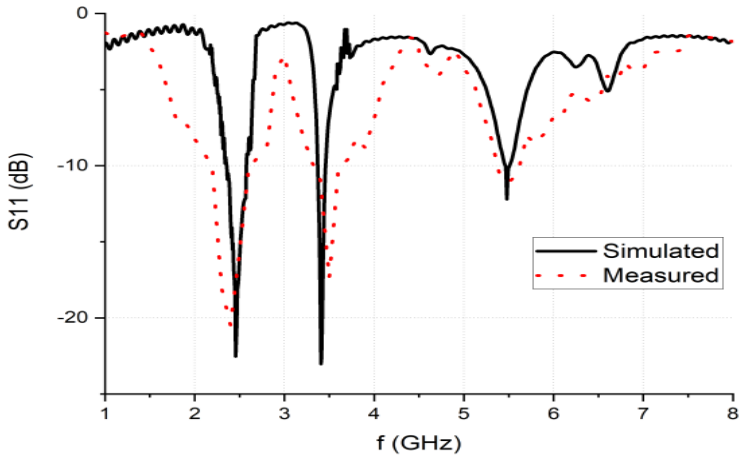

(a)

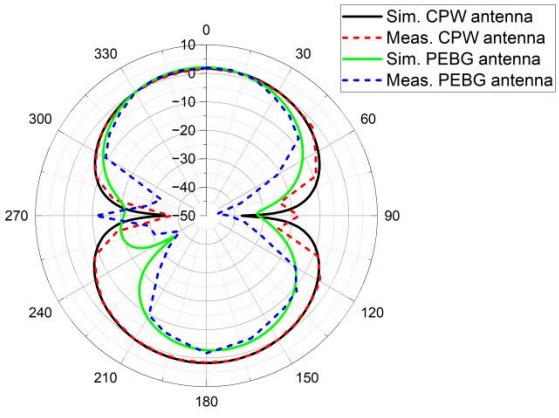

(b)

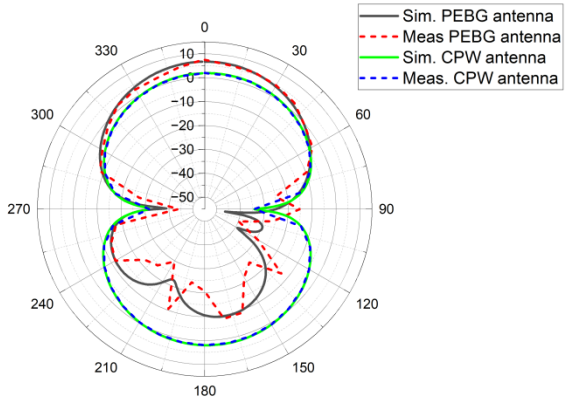

(c)

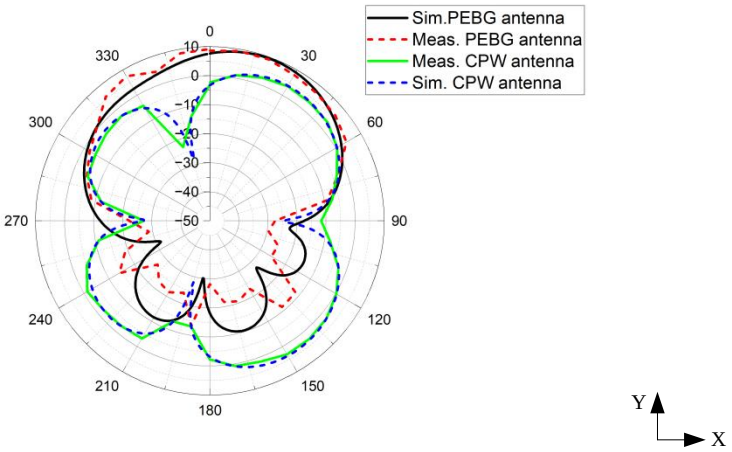

(d)

Fig.6.6 (a) Measured and simulated S_{11} of the anticipated antenna, Radiation patterns comparison of the CPW antenna and PEBG antenna in free space at (b) 2.45 GHz (c) 3.5 GHz (d) 5.5 GHz

6.4.2. Under Deformations

The reflection coefficient and radiation patterns are measured to assess the performance of bending along both x-, and y-axis. Fig.6.7 depicted the bending performance of the integrated antenna and compared it with the performance in the ideal flat state. It is seen from the figure that the bending along the y-axis nearly has no significant effect on the integrated antenna. In contrast, a slight shift in the resonance frequencies is witnessed for the bend along the x-axis.

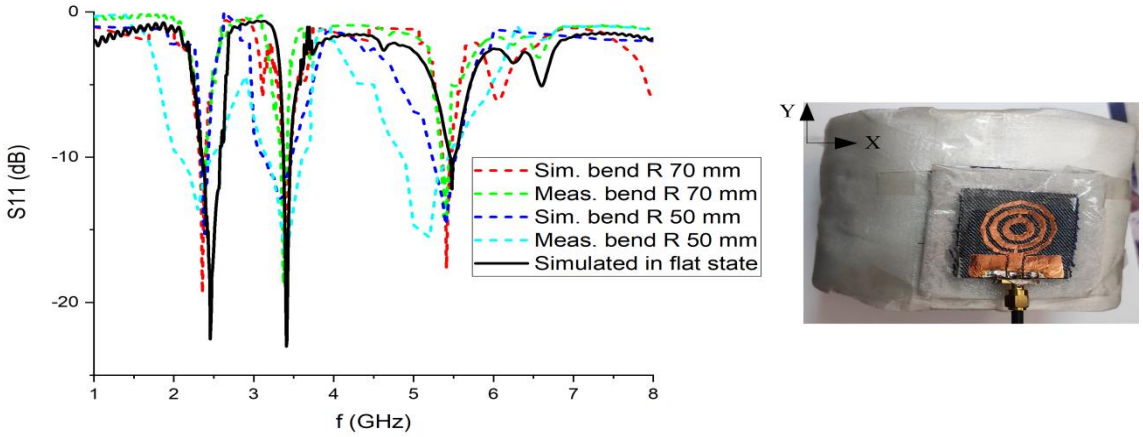

(a)

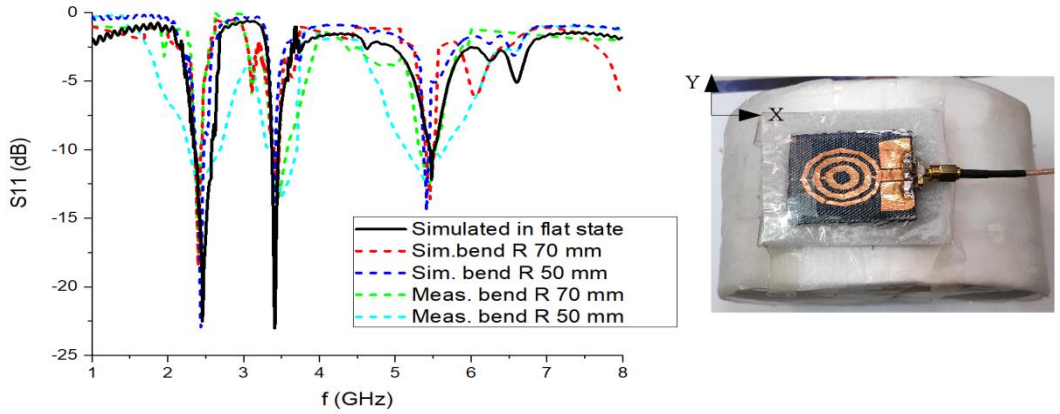

(b)

Fig.6.7. (a) S_{11} curves of the deformed integrated antenna under bending for various radii along (a) y-axis, (b) x-axis

Fig. 6.8 demonstrates the simulated and measured radiation patterns along the y-axis for a bend radius of 70 mm only for simplicity. The radiation patterns measured at 2.45 GHz, 3.5 GHz, and 5.5 GHz shows little variation over the simulated, except for the back radiations.

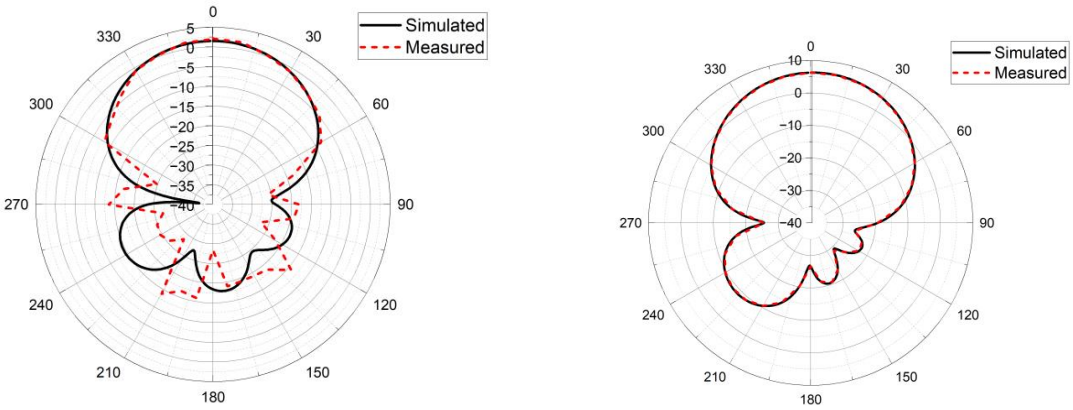

(a) (b)

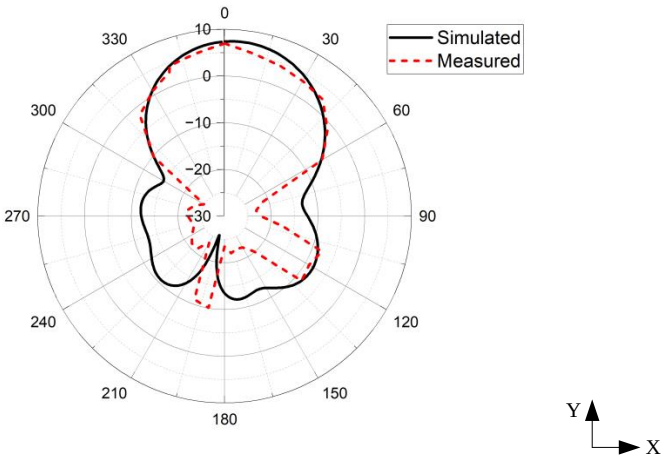

(c)

Fig.6.8. Radiation patterns of the integrated antenna under bending of radius 70 mm along the y-axis (a) 2.45 GHz, (b) 3.5 GHz, (c) 5.5 GHz

6.5. Integrated antenna performance on-body

The models are developed in the CST MW Studio environment, where the chest is emulated as a cuboid of 150X150X40 mm^3, and the arm is emulated as a cylinder of 80 mm diameter with a length of 150 mm respectively. Here, the chest part of the human model is simulated, as represented in Fig. 6.9 (a). To give more practicality, the integrated antenna is situated directly on the T-shirt of the wearer and measured for the reflection coefficient, as seen in Fig.6.9 (b). Fig.6.9 (b) demonstrates that the resonant frequency slightly shifted to lower frequencies but still covers the desired frequencies for the measured chest, hand, and thigh cases. This is caused by the occurrence of a high dielectric human body, which is viewed as an additional substrate layer.

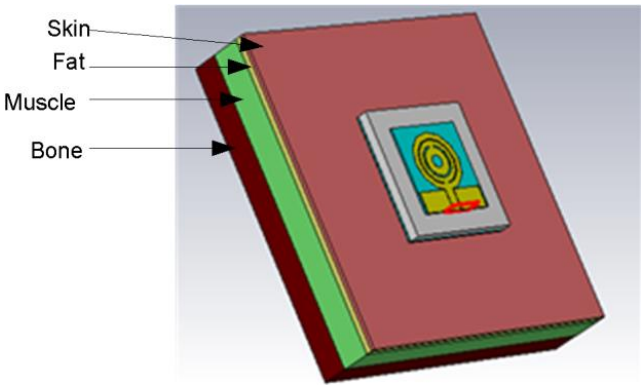

(a)

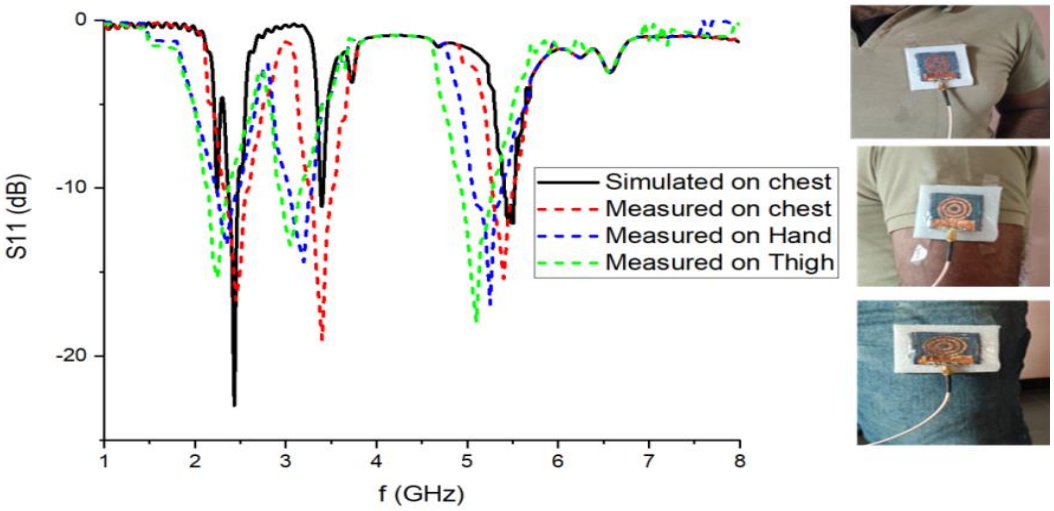

(b)

Fig.6.9. (a) Numerical model of chest developed in CST (b) S_{11} curves of the integrated antenna on real human

Fig.6.10 depicts the comparison of on-phantom radiation patterns with free space simulated at the intended frequencies. It should be noticed that the integrated antenna has preserved the radiation pattern's shape with nearly the same gain as in free space. However, the reasonable back radiation is observed because of the holes presented in the ground plane of EBG.

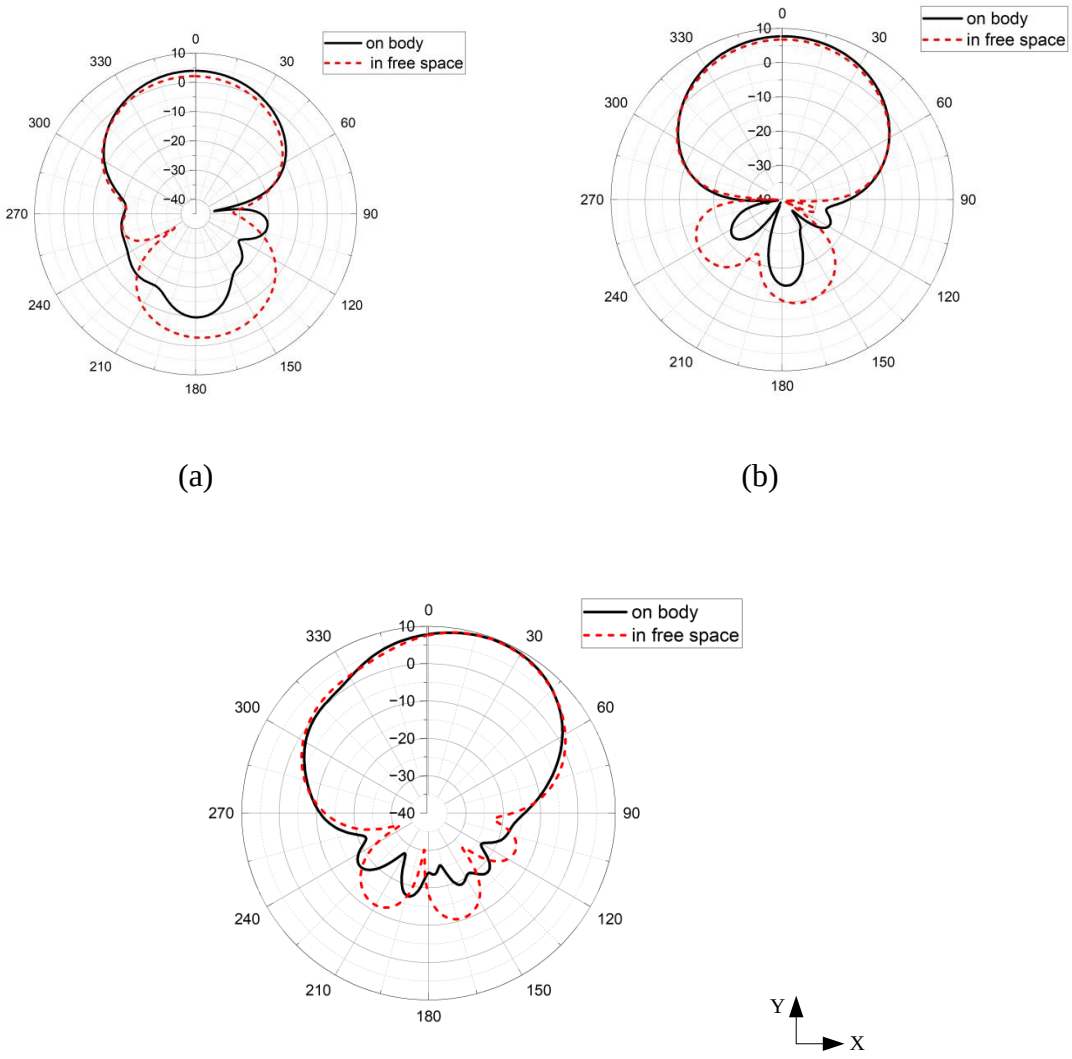

Fig.6.10. Comparison of Radiation performance of the integrated-antenna on the phantom at (a) 2.45 GHz, (b) 3.5 GHz, (c) 5.5 GHz

6.6. SAR

The same four-layer model specified above is used for SAR assessment. The prototype is distanced from the human body by 10 mm. The SAR calculation is performed in CST MW Studio, in which the IEEE C95.1 standard is followed, providing an input power of 100mW. The estimated SAR values at 2.45 GHz/3.5 GHz/5.5 GHz are tabulated and presented in Table.6.2.

Table.6.2. Simulated SAR of the anticipated antenna

Peak SAR value in W/Kg				
	EBG integrated antenna		CPW antenna	
Frequency (GHz)	1g	10g	1g	10g
2.45	1.099	0.591	10.92	5.69
3.5	0.2128	0.0961	20.7	10.02
5.5	0.3081	0.1326	21.25	7.11

Fig. 6.11 shows the simulated result from the human tissue model. Implementing the PEBG structure results in a notable reduction in SAR, as the integrated antenna reduces the SAR levels by > 95%, meeting the required level.

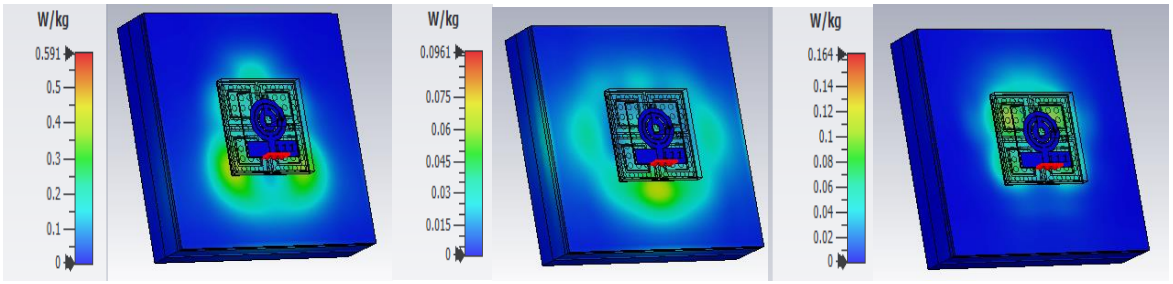

(a) (b) (c)

Fig.6.11. SAR analysis for an average 10g tissue at (a) 2.45 GHz, (b) 3.5 GHz, (c) 5.5 GHz

6.7. Summary

A compact textile antenna with a miniaturized P-EBG structure for wearable applications is effectively presented in this chapter. The proposed wearable antenna has the ability to support three different frequencies with highly improved wearability and breathability. The porous nature of the proposed EBG enhances breathability and, thereby comfort. The integrated antenna is highly radiation safe, while improved breathability finds applications in WLAN bands.

The antenna projected in this chapter is compared to some recent wearable antennas designed in different technologies in terms of size, impedance bandwidth, gain, and specific absorption rate (SAR), as demonstrated in table 6.3. The suggested antenna offers the optimal

compromise in regards to size, gain, and SAR, as can be evident from the table. Moreover, the antenna maintains a triple-band nature.

Table.6.3 Comparison of wearable breathable antenna against previously published literature

Ref	EBG type	Overall Size (mm3)	Gain (dBi)	SAR (W/Kg)/distance from the body (mm)		Substrate	Frequency of operation (GHz)
				1g	10g		
[71]	Defected ground EBG	60X60X2.4	6.45	0.983/2	0.258/2	Jeans	2.4
[134]	EBG	62X97X2.6	-	0.6	0.056	Denim	5.8
[135]	Square ring EBG	69X69X10	7.0,9.1	0.123, 0.212	0.0452, 0.0563	Rogers	2.45,5.8
[36]	Simple EBG	69X69X5	5.11/6.43/7.41	-	0.47/0.86/0.14	Wool felt	2.4,3.5,5.8
Proposed work	Perforated EBG	60X60X7	2.18/6.75/9.50	1.099, 0.212, 0.308	0.591, 0.096, 0.132	Jeans	2.45,3.5,5.5

- M. Sandhya, L.Anjaneyulu, "An Improved wearable, breathable, triple band EBG loaded CPW fed fractal textile antenna for WBAN applications'' in Journal of Electromagnetic Waves and Applications indexed in **(SCIE) (Under Review)**

Chapter 7

Conclusions and Future scope

7.1. Conclusion

The Wireless Body Area Networks (WBAN) are the most attractive research area and the most repeated words throughout the thesis. Its applications in real-time healthcare monitoring systems, military, entertainment, glamour industry, safety and security, space applications, and specific occupations made body-centric communications one of the essential and fast-growing areas for research. Nevertheless, the system operates near or integrated with the human body and is sensitive to deformations. Consequently, the system gets more complicated. Hence, the design and deployment phases must pay particular attention to each component of the system.

The primary objective of this thesis is to exhibit designs of single and multi-band wearable antennas that are made of textile jeans material (as substrate), which is suitable for wearable applications. A systematic approach is taken to demonstrate this research. To start with, a few designs of Koch fractal, saw-tooth shaped fractal, and Sierpinski fractal boundary patch antennas, the inset fed and aperture coupling, EBG structure, and DGS structure techniques offering high impedance bandwidth and gain are modeled and evaluated for their capabilities in connection with their operating characteristics for WBAN applications. The core of this research work presented in this thesis is the established methodology applicable for the realization of compact, flexible, high gain, and radiation-safe wearable antennas.

The aspects of concern in the thesis were on-body and off-body communications in the ISM, Wi-Max, and 5GHz bands. To conform to user demands (unobtrusiveness and aesthetical acceptability), planar microstrip antennas on flexible jeans substrates were taken as a logical

choice for the analysis and design. In the course of the research for this thesis and the evaluation of the specific characteristics of the body-centric environment, several antenna prototypes have been proposed and measured in free space, on the human body phantom and the body of human male and female volunteers. The issues that have received particular attention throughout this thesis are as follows:

1. Design of wearable fractal antennas with less complexity for their effective usage in several wireless devices.
2. Implemented and measured the dielectric properties of the textile substrates.
3. By using suitable materials and production techniques, the overall cost is kept to a minimum while maintaining a certain level of robustness.
4. Evaluating the influence of mechanical deformations like bending on the characteristics of the antenna.
5. A design strategy for wearable antennas is to minimize the radiation into the human body for safety concerns and also to ensure maximum on-body radiation efficiency.
6. A concept to improve the wearability and breathability of the designed antennas

7.2. Future Scope

The findings of the thesis can serve as a basis for future work, with the following directions:

1. **Tests of durability:** The antenna and conductive textile realizations need to be tested for durability due to other issues that arise in the real world (e.g., washing, scratching, freezing, etc.)

2. **Improvements in the antenna design**: Based on the findings of the thesis and the strategy followed, the research could move towards other frequency ranges, such as UWB, and millimeter wave antennas.

3. **Utilizing other textile substrates:** The use of advanced artificial substrates in designing wearable antennae rather than the commonly available substrates can reduce the impact of humidity (using hydrophobic substrates) or bend (using less flexible substrates). However, the comfort level and overall price of the product are a concern when worn on the body.

4. To boost channel capacity and combat spectral shortage, MIMO antennas can be designed in the future.

5. **Implementing other fabrication methods:** In order to reduce human errors and improve the accuracy while fabrication, methods other than PCB technologies, embroidery or sewing methods can be incorporated.

List of publications out of this research work

International Journals

[1] M. Sandhya, L.Anjaneyulu, "Robust, Efficient, and Low Profile Fractal Enabled EBG Incorporated Wearable Antenna for WLAN Standards. Defence Science Journal, 72(3), 429-440. https://doi.org/10.14429/dsj.72.17674 **(SCI)**

[2] Mallavarapu, S., & Lokam, A. (2022). A fully flexible, high gain saw-tooth-shaped boundary fractal wearable patch antenna for WBAN applications. International Journal of Microwave and Wireless Technologies, 1-10. http://doi:10.1017/S1759078722000836 **(SCIE)**

[3] S. Mallavarapu and A. Lokam, "Circuit Modeling and Analysis of Wearable Antennas on the Effect of Bending for Various Feeds," Eng. Technol. Appl. Sci. Res., vol. 12, no. 1, pp. 8180–8187, Feb. 2022.https://doi.org/10.48084/etasr.4699 **(ESCI)**

[4] M. Sandhya, L.Anjaneyulu, '' DUAL-BAND Aperiodic EBG-DGS Wearable Antenna for Emergency Search Services in WBAN, in Electrical, Control and Communication Engineering Journal indexed in **(ESCI) (Accepted)**

[5] M. Sandhya, L.Anjaneyulu, "An Improved wearable, breathable, triple band EBG loaded CPW fed fractal textile antenna for WBAN applications'' in Journal of Electromagnetic Waves and Applications indexed in **(SCIE) (Under Review)**

[6] M. Sandhya, L.Anjaneyulu, "Flexible, Compact Sierpinski Fractal Antenna on a Hilbert patterned ground for W-WBSN '' in MOTL indexed in **(SCI) (Under Review)**

International Conferences

[1] M.Sandhya, L.Anjaneyulu, "A critical survey on fractal wearable antennas with enhanced gain and bandwidth for WBAN'', in International Conference on Inventive Communication and Inventive Technologies (ICICCT2020). Lecture Notes in Networks and Systems, vol 145. Springer, Singapore. https://doi.org/10.1007/978-981-15-7345-3_63, indexed in **SCOPUS**

[2] M.Sandhya, L.Anjaneyulu, "Design and analysis of Wearable step-shaped Sierpinski Fractal Antenna for WBAN applications," in International conference on communications, Signal processing and VLSI (IC2SV). Lecture notes in Electrical engineering, Vol 722. Springer, Singapore. https://doi.org/10.1007/978-981-334058-9_11.

[3] M.Sandhya, L.Anjaneyulu, "A Compact, Flexible, Circularly polarized wearable antenna for wireless applications", in IEEE international symposium on smart electronic systems (iSES) conference. **(Accepted)**

References

[1] A. Ometov *et al.*, "A Survey on Wearable Technology: History, State-of-the-Art and Current Challenges," *Comput. Networks*, vol. 193, no. December 2020, p. 108074, 2021.

[2] T. I. of S. H. and The College of Optometrists and [Online] Where Glasses May Have Begun, 2019, "No Title." [Online]. Available: https://www.encyclopedia.com/science/encyclopedias-almanacs-transcripts-and-maps/invention-spectacles.

[3] "Abacus Ring was Used During the Qing Dynasty to Help Traders, Daily Mail (2014)." [Online]. Available: https://www.dailymail.co.uk/sciencetech/article-2584437/Is-wearable-computer-300-year-old-Chinese-abacus-ring-used-Qing-Dynasty-help-traders.html. [Accessed: 19-Nov-2022].

[4] D. Hinhs, "Walkie Talkie." [Online]. Available: http://www.dlhings.ca/walkietalkie.html.

[5] "The 'Invention' of the Wristwatch." [Online]. Available: https://www.vintagewatchstraps.com/wristwatchinvention.php. [Accessed: 19-Nov-2022].

[6] E. O. Thorp, "Beat the Dealer: A Winning Strategy for the Game of Twenty-One - Edward O. Thorp," pp. 1–220, 1966.

[7] T. Emerson, "Mastering the art of vr: On becoming the hit lab cybrarian," *Electron. Libr.*, vol. 11, no. 6, pp. 385–391, 1993.

[8] Hewlett Packard, "Watch calculators." [Online]. Available: https://www.oldcalculatormuseum.com/hp-01.html.

[9] R. Want, A. Hopper, V. Falcao, and J. Gibbons, "The Active Badge System," *ACM Trans. Inf. Syst.*, vol. 10, no. 1, pp. 91–102, 1992.

[10] "Plantronics, An Industry Pioneer Reflects on a Decade'S Worth of Achievements To Honour the 10th Anniversary of Bluetooth Headsets, 2010." [Online]. Available: https://newsroom.poly.com/press-release/consumer/plantronics-celebrates-10-years-bluetooth-headset-innovation/. [Accessed: 19-Nov-2022].

[11] C. Evers, "Researching action sport with a GoPro™ camera." [Online]. Available: https://www.taylorfrancis.com/chapters/edit/10.4324/9781315761121-12/researching-action-sport-gopro™-camera-clifton-evers. [Accessed: 19-Nov-2022].

[12] C. Marshall, "The story of Fitbit: How a wooden box was bought by Google for $2.1bn." [Online]. Available: https://www.wareable.com/fitbit/story-of-fitbit-7936. [Accessed: 19-Nov-2022].

[13] T. BAJARIN, "The Real Reason Apple Made the Apple Watch." [Online]. Available: https://time.com/4323318/apple-watch-steve-jobs-health/. [Accessed: 19-Nov-2022].

[14] C. Hertleer, H. Rogier, L. Vallozzi, and L. Van Langenhove, "A textile antenna for off-body communication integrated into protective clothing for firefighters," *IEEE Trans. Antennas Propag.*, vol. 57, no. 4 PART. 1, pp. 919–925, 2009.

[15] S. Agneessens, S. Lemey, T. Vervust, and H. Rogier, “Wearable, Small, and Robust: The Circular Quarter-Mode Textile Antenna,” *IEEE Antennas Wirel. Propag. Lett.*, vol. 14, pp. 1482–1485, 2015.

[16] H. I. Azeez, W. S. Chen, C. K. Wu, C. M. Cheng, and H. C. Yang, “A simple resonance method to investigate dielectric constant of low loss substrates for smart clothing,” *Sensors Mater.*, vol. 30, no. 3, pp. 595–608, 2018.

[17] C. A. Balanis, “Antenna Theory - Analysis And Design (Constantine A Balanis) (2Nd Ed).pdf.” 1997.

[18] E.C. jordan and K.G. Balmin, “Electromagnetic Waves and Radiating Systems Prentice.” Printice Hall 2000.

[19] “Antenna Basics.” [Online]. Available: https://www.antenna-theory.com/basics/main.php.

[20] “Federal Communication Commission.” [Online]. Available: https://www.fcc.gov/.

[21] “ICNIRP guidelines.” [Online]. Available: https://www.icnirp.org/en/activities/news/news-article/rf-guidelines-2020-published.html.

[22] H. R. Khaleel, *Innovation in Wearable and Flexible Antennas*. WIT Press, 2015.

[23] J.James and P.Hall, “Handbook of Microstrip Antennas,” *Inst. Eng. Technol.*, vol. 2, 1989.

[24] K. P. R. Girish kumar, *Antennas, Broadband Microstrip*. .

[25] D. M. Pozar, “Microstrip Antennas,” *Proc. IEEE*, vol. 80, no. 1, pp. 79–91, 1992.

[26] D. M. Pozar, “A review of aperture coupled microstrip antennas: History, operation, development, and applications,” *Univ. Massachusetts Amherst*, no. May, pp. 1–9, 1996.

[27] I. B. and A. . G. Ramesh, P. Bhatia, *Microstrip Antenna Design Handbook*. Artect House Inc., 2001.

[28] L. Song and Y. Rahmat-Samii, “A Systematic Investigation of Rectangular Patch Antenna Bending Effects for Wearable Applications,” *IEEE Trans. Antennas Propag.*, vol. 66, no. 5, pp. 2219–2228, 2018.

[29] X. Y. Zhang, H. Wong, T. Mo, and Y. F. Cao, “Dual-Band Dual-Mode Button Antenna for On-Body and Off-Body Communications,” *IEEE Trans. Biomed. Circuits Syst.*, vol. 11, no. 4, pp. 933–941, 2017.

[30] A. Arif, M. Zubair, M. Ali, M. U. Khan, and M. Q. Mehmood, “A Compact, Low-Profile Fractal Antenna for Wearable On-Body WBAN Applications,” *IEEE Antennas Wirel. Propag. Lett.*, vol. 18, no. 5, pp. 981–985, 2019.

[31] A. Arif, M. R. Akram, K. Riaz, M. Zubair, and M. Q. Mehmood, “Koch Fractal Based Wearable Antenna Backed with EBG Plane,” *Proc. 2020 17th Int. Bhurban Conf. Appl. Sci. Technol. IBCAST 2020*, pp. 642–646, 2020.

[32] S. Velan *et al.*, “Dual-Band EBG Integrated Monopole Antenna Deploying Fractal Geometry for Wearable Applications,” *IEEE Antennas Wirel. Propag. Lett.*, vol. 14, pp. 249–252, 2015.

[33] G. Gao, R. Zhang, C. Yang, H. Meng, W. Geng, and B. Hu, “Microstrip monopole antenna

with a novel UC-EBG for 2.4 GHz WBAN applications," *IET Microwaves, Antennas Propag.*, vol. 13, no. 13, pp. 2319–2323, 2019.

[34] A. Chauraya, R. Seager, W. Whittow, S. Zhang, and Y. Vardaxoglou, "Embroidered Frequency Selective Surfaces on textiles for wearable applications," *2013 Loughbrgh. Antennas Propag. Conf. LAPC 2013*, no. November, pp. 388–391, 2013.

[35] C. Huang, C. Ji, X. Wu, J. Song, and X. Luo, "Combining FSS and EBG Surfaces for High-Efficiency Transmission and Low-Scattering Properties," *IEEE Trans. Antennas Propag.*, vol. 66, no. 3, pp. 1628–1632, 2018.

[36] W. El May, I. Sfar, J. M. Ribero, and L. Osman, "Design of low-profile and safe low SAR tri-band textile EBG-based antenna for IoT applications," *Prog. Electromagn. Res. Lett.*, vol. 98, no. May, pp. 85–94, 2021.

[37] P. V. T. 3 Abdul Wahab Memon 1, 2,* , Igor Lima de Paula 3, Benny Malengier 1 , Simona Vasile 4 and and L. V. L. 1, "Breathable Textile Rectangular Ring Microstrip Patch Antenna at 2.45 GHz for Wearable Applications," *sensors*, pp. 1–17, 2021.

[38] B. Zoubiri, A. Mayouf, F. Mayouf, S. Abdelkebir, and T. Devers, "Enhancement of front-to-back ratio and gain of rectangular microstrip antenna using novel elliptical EBG structure," *Microsyst. Technol.*, vol. 24, no. 8, pp. 3241–3244, 2018.

[39] B. Sugumaran, R. Balasubramanian, and S. K. Palaniswamy, "Reduced specific absorption rate compact flexible monopole antenna system for smart wearable wireless communications," *Eng. Sci. Technol. an Int. J.*, vol. 24, no. 3, pp. 682–693, 2021.

[40] M. Wang *et al.*, "Investigation of SAR Reduction Using Flexible Antenna With Metamaterial Structure in Wireless Body Area Network," *IEEE Trans. Antennas Propag.*, vol. 66, no. 6, pp. 3076–3086, 2018.

[41] D. Dhanasekaran, N. Somasundaram, and R. Rengasamy, "A compact decagon ring-shaped multiband antenna for WLAN/WiMAX/WAVE/satellite applications," *J. Appl. Sci. Eng.*, vol. 24, no. 5, pp. 757–761, 2021.

[42] D. Guha, C. Kumar, and S. Pal, "Improved cross-polarization characteristics of circular microstrip antenna employing arc-shaped defected ground structure (DGS)," *IEEE Antennas Wirel. Propag. Lett.*, vol. 8, pp. 1367–1369, 2009.

[43] M. G. Siddiqui, A. K. Saroj, D. Tiwari, and S. S. Sayeed, "Koch–Sierpinski Fractal Microstrip antenna for C/X/Ku-band applications," *Aust. J. Electr. Electron. Eng.*, vol. 16, no. 4, pp. 369–377, 2019.

[44] M. El Atrash, O. F. Abdalgalil, I. S. Mahmoud, M. A. Abdalla, and S. R. Zahran, "Wearable high gain low SAR antenna loaded with backed all-textile EBG for WBAN applications," *IET Microwaves, Antennas Propag.*, vol. 14, no. 8, pp. 791–799, 2020.

[45] H. Yang, W. Yao, Y. Yi, X. Huang, S. Wu, and B. Xiao, "A Dual-Band Low-Profile Metasurface-Enabled Wearable Antenna for WLAN Devices," vol. 61, no. September 2015, pp. 115–125, 2016.

[46] Y. Tao, Y. Tao, L. Wang, B. Wang, Z. Yang, and Y. Tai, "High-reproducibility, flexible conductive patterns fabricated with silver nanowire by drop or fit-to-flow method,"

Nanoscale Res. Lett., vol. 8, no. 1, pp. 1–5, 2013.

[47] L. Corchia, G. Monti, and L. Tarricone, "Wearable Antennas: Nontextile Versus Fully Textile Solutions," *IEEE Antennas Propag. Mag.*, vol. 61, no. 2, pp. 71–83, 2019.

[48] B. Mohamadzade, R. M. Hashmi, R. B. V. B. Simorangkir, R. Gharaei, S. U. Rehman, and Q. H. Abbasi, "Recent advances in fabrication methods for flexible antennas in wearable devices: State of the art," *Sensors (Switzerland)*, vol. 19, no. 10. 2019.

[49] S. F. Jilani, Q. H. Abbasi, and A. Alomainy, "Inkjet-Printed Millimetre-Wave PET-Based Flexible Antenna for 5G Wireless Applications," *2018 IEEE MTT-S Int. Microw. Work. Ser. 5G Hardw. Syst. Technol. IMWS-5G 2018*, vol. 1, pp. 5–7, 2018.

[50] A. Angelucci *et al.*, "Smart textiles and sensorized garments for physiological monitoring: A review of available solutions and techniques," *Sensors (Switzerland)*, vol. 21, no. 3. pp. 1–23, 2021.

[51] S. S. Dhanabalan *et al.*, "Flexible compact system for wearable health monitoring applications," *Comput. Electr. Eng.*, vol. 102, no. May, p. 108130, 2022.

[52] S. M. Shah *et al.*, "A compact dual-band semi-flexible antenna at 2.45 GHz and 5.8 GHz for wearable applications," *Bull. Electr. Eng. Informatics*, vol. 10, no. 3, pp. 1739–1746, 2021.

[53] X. W. and Y. Hao, "DUAL-BAND OPERATION OF AN ELECTROMAGNETIC BAND-GAP PATCH ANTENNA," *Microw. Opt. Technol. Lett.*, vol. 49, no. 11, pp. 2562–2568, 2007.

[54] P. Saha, D. Mitra, and S. K. Parui, "Control of Gain and SAR for Wearable Antenna Using AMC Structure," *Radioengineering*, vol. 30, no. 1, pp. 81–88, 2021.

[55] U. Ali *et al.*, "Design and SAR analysis of wearable antenna on various parts of human body, using conventional and artificial ground planes," *J. Electr. Eng. Technol.*, vol. 12, no. 1, pp. 317–328, 2017.

[56] A. I. Garg, Ramesh, Prakash Bhartia, Inder Bath, "Microstrip antenna design handbook," *Artech House antennas and propagation library*. pp. 761–762, 2001.

[57] J. A. Ansari, S. K. Dubey, P. Singh, R. U. Khan, and B. R. Vishvakarma, "Analysis of U-slot loaded Patch for Dualband Operation," *Int. J. Microw. Opt. Technol.*, vol. 3, no. 2, pp. 80–84, 2008.

[58] H. Maros and S. Juniar, *Innovation in Wearable Flexible Antennas*. 2016.

[59] H. I. Azeez, W.-S. Chen, C.-K. Wu, C.-M. Cheng, and H.-C. Yang, "A Simple Resonance Method to Investigate Dielectric Constant of Low Loss Substrates for Smart Clothing," *Sensors Mater.*, vol. 30, no. 3, p. 595, 2018.

[60] M. R. Resonator, P. J. Low, F. Esa, K. Y. You, and Z. Abbas, "Estimation of Dielectric Constant for Various Standard Materials using Estimation of Dielectric Constant for Various Standard Materials using Microstrip Ring Resonator," no. January 2018, 2017.

[61] K. P. Lätti, J. M. Heinola, M. Kettunen, J. P. Ström, and P. Silventoinen, "A review of microstrip T-resonator method in determination of dielectric properties of printed circuit

board materials," *Conf. Rec. - IEEE Instrum. Meas. Technol. Conf.*, vol. 1, no. 5, pp. 62–66, 2005.

[62] A. Rashidian, M. T. Aligodarz, and D. M. Klymyshyn, "Dielectric characterization of materials using a modified microstrip ring resonator technique," *IEEE Trans. Dielectr. Electr. Insul.*, vol. 19, no. 4, pp. 1392–1399, 2012.

[63] S. Sankaralingam and B. Gupta, "Determination of dielectric constant of fabric materials and their use as substrates for design and development of antennas for wearable applications," *IEEE Trans. Instrum. Meas.*, vol. 59, no. 12, pp. 3122–3130, 2010.

[64] A. Y. I. Ashyap *et al.*, "Compact and Low-Profile Textile EBG-Based Antenna for Wearable Medical Applications," vol. 16, pp. 2550–2553, 2017.

[65] M. I. Ahmed, M. F. Ahmed, and A. A. Shaalan, "Novel Electrotextile Patch Antenna on Jeans Substrate for Wearable Applications," vol. 83, no. April, pp. 255–265, 2018.

[66] B. C.A, "Antenna Theory_ Analysis and Design (1996).pdf." .

[67] S. Ramdani, I. Pratama, and Basari, "Single Coaxial Feed Microstrip GPS Antenna Aimed at Wearable Device Application," *Proc. - CAMA 2019 IEEE Int. Conf. Antenna Meas. Appl.*, pp. 247–250, 2019.

[68] K. R. Rathod and B. K. Mishra, "Performance evaluation of linearly polarized, circularly polarized corner cut square using coaxial feed and rectangular slot textile antenna using CPW FEED at 2.45 GHz," *IET Conf. Publ.*, vol. 2016, no. CP700, pp. 37–44, 2016.

[69] F. Boeykens, L. Vallozzi, and H. Rogier, "Cylindrical bending of deformable textile rectangular patch antennas," *Int. J. Antennas Propag.*, vol. 2012, 2012.

[70] L. C. Ping, "Circuit Model of Curved Ultra Wideband (UWB) Antenna," *MATEC Web Conf.*, vol. 95, 2017.

[71] A. Y. I. Ashyap *et al.*, "Robust and efficient integrated antenna with EBG-DGS enabled wide bandwidth for wearable medical device applications," *IEEE Access*, vol. 8, pp. 56346–56358, 2020.

[72] L. Zheng Tung, G. Amouzed Mahdiraji, and L. Chia Ping, "Comparative Study between Planar and Bent Antenna Characterization," *MATEC Web Conf.*, vol. 152, p. 03002, 2018.

[73] K. Falconer, *FRACTAL Second Edition*. 2003.

[74] D. H. Werner and S. Ganguly, "An overview of fractal antenna engineering research," *IEEE Antennas Propag. Mag.*, vol. 45, no. 1, pp. 38–57, 2003.

[75] L. Zhou, S. Fang, and X. Jia, "A Compact Dual-Band and Dual-polarized Antenna Integrated into Textile for WBAN Dual-Mode Applications," vol. 91, no. March, pp. 153–161, 2020.

[76] S. I. Mondal and R. P. Ghosh, "Multiband wearable antennas," *2016 Int. Conf. Microelectron. Comput. Commun.*, pp. 1–5.

[77] G. Atanasova and N. Atanasov, "Small antennas for wearable sensor networks: Impact of the electromagnetic properties of the textiles on antenna performance," *Sensors (Switzerland)*, vol. 20, no. 18. pp. 1–21, 2020.

[78] R. Augustine, “Electromagnetic modelling of human tissues and its application,” no. July 2009, 2010.

[79] R. A. Valenzuela, *Antennas and propagation for wireless communications*. 2002.

[80] M. Nikolovski, “Detailed Modeling of the Human Body in Motion to Investigate the Electromagnetic Influence of Fields in a Realistic Environment,” 2018.

[81] M. Ur-Rehman, Q. H. Abbasi, X. Chen, and Z. Ying, “Numerical modelling of human body for Bluetooth body-worn applications,” *Prog. Electromagn. Res.*, vol. 143, no. August, pp. 623–639, 2013.

[82] D. Mandal and S. S. Pattnaik, “FDTD based Analysis of Input Impedance of a Wearable Patch Antenna with Milli Bends,” vol. 10, no. August, pp. 1–5, 2017.

[83] J. Wang and O. Fujiwara, “Comparison and Evaluation of Electromagnetic Absorption Characteristics in Realistic Human Head Models of Adult and,” vol. 51, no. 3, pp. 966–971, 2003.

[84] Z. H. Jiang, D. E. Brocker, S. Member, P. E. Sieber, S. Member, and D. H. Werner, “A Compact , Low-Pro fi le Metasurface-Enabled Network Devices,” *IEEE Trans. Antennas Propag.*, vol. 62, no. 8, pp. 4021–4030, 2014.

[85] T. T. Le and T. Y. Yun, “Miniaturization of a Dual-Band Wearable Antenna for WBAN Applications,” *IEEE Antennas Wirel. Propag. Lett.*, vol. 19, no. 8, pp. 1452–1456, 2020.

[86] amor Smida, amjad Iqbal, abdullah J. alazemi, M. I. Waly, R. Ghayoula, and S. Kim, “Wideband Wearable antenna for Biomedical Telemetry applications,” *IEEE Access*, vol. 8, pp. 15687–15694, 2020.

[87] Y. Wang, J. Bao, Y. Tian, Z. Wang, and N. Li, “Design of High Gain Wearable Antenna Based on Wireless Body Area Network Communications,” *J. Phys. Conf. Ser.*, vol. 1971, no. 1, 2021.

[88] M. P. Joshi, V. J. Gond, and J. J. Chopade, “Saw-Tooth Shaped Sequentially Rotated Fractal Boundary Square Microstrip Patch Antenna for Wireless Application,” vol. 94, no. November, pp. 109–115, 2020.

[89] R. Mishra, R. Dandotiya, A. Kapoor, and P. Kumar, “Compact High Gain Multiband Antenna Based on Split Ring Resonator and Inverted F Slots for 5G Industry Applications,” *ACES J.*, vol. 36, no. 8, pp. 999–1007, 2021.

[90] G. P. Gao, B. Hu, S. F. Wang, and C. Yang, “Wearable Circular Ring Slot Antenna with EBG Structure for Wireless Body Area Network,” *IEEE Antennas Wirel. Propag. Lett.*, vol. 17, no. 3, pp. 434–437, 2018.

[91] J. Buckley, B. O’Flynn, P. Haigh, C. O’Mathuna, and K. G. McCarthy, “Antenna tuning for wearable wireless sensors,” *Proc. IEEE Sensors*, pp. 1990–1993, 2011.

[92] D. C. Ranasinghe, R. L. S. Torres, and A. Wickramasinghe, “Automated activity recognition and monitoring of elderly using wireless sensors: Research challenges,” *Proc. 2013 5th IEEE Int. Work. Adv. Sensors Interfaces, IWASI 2013*, no. November 2018, pp. 224–227, 2013.

[93] B. Mohamadzade, R. M. Hashmi, R. B. V. B. Simorangkir, R. Gharaei, S. U. Rehman, and Q. H. Abbasi, "Recent advances in fabrication methods for flexible antennas in wearable devices: State of the art," *Sensors (Switzerland)*, vol. 19, no. 10, 2019.

[94] S. Karthikeyan, Y. Venu Gopal, V. Giri Narendra Kumar, and T. Ravi, "Design and Analysis of Wearable Antenna for Wireless Body Area Network," *IOP Conf. Ser. Mater. Sci. Eng.*, vol. 590, no. 1, 2019.

[95] S. Mallavarapu and A. Lokam, "Circuit Modeling and Analysis of Wearable Antennas on the Effect of Bending for Various Feeds," *Eng. Technol. Appl. Sci. Res.*, vol. 12, no. 1, pp. 8180–8187, 2022.

[96] A. Shehni *et al.*, "Using Hilbert Curve Slot for Bandwidth Enhancement of Microstrip Patch Antenna To cite this version : Using Hilbert Curve Slot for Bandwidth Enhancement of Microstrip Patch Antenna," *IEEE-BTH Student Pap. Contest 2011-12*, pp. 0–2, 2019.

[97] T. T. Le, Y.-D. Kim, and T.-Y. Yun, "A Triple-Band Dual-Open-Ring High-Gain High-Efficiency Antenna for Wearable Applications," *IEEE Access*, vol. 9, pp. 118435–118442, 2021.

[98] S. Varma, S. Sharma, M. John, R. Bharadwaj, A. Dhawan, and S. K. Koul, "Design and Performance Analysis of Compact Wearable Textile Antennas for IoT and Body-Centric Communication Applications," *Int. J. Antennas Propag.*, vol. 2021, 2021.

[99] R. Bharadwaj and S. K. Koul, "Experimental analysis of ultra-wideband body-to-body communication channel characterization in an indoor environment," *IEEE Trans. Antennas Propag.*, vol. 67, no. 3, pp. 1779–1789, 2019.

[100] F. Yang and Y. Rahmat-Samii, "EBG characterizations and classifications," *Electromagn. Band Gap Struct. Antenna Eng.*, pp. 59–86, 2010.

[101] M. S. Alam, N. Misran, B. Yatim, and M. T. Islam, "Development of electromagnetic band gap structures in the perspective of microstrip antenna design," *Int. J. Antennas Propag.*, vol. 2013, 2013.

[102] B. Mohajer-Iravani, S. Shahparnia, and O. M. Ramahi, "Coupling reduction in enclosures and cavities using electromagnetic band gap structures," *IEEE Trans. Electromagn. Compat.*, vol. 48, no. 2, pp. 292–303, 2006.

[103] S. Hussain, S. Hafeez, S. A. Memon, and N. Pirzada, "Design of Wearable Patch antenna for wireless body area networks," *Int. J. Adv. Comput. Sci. Appl.*, vol. 9, no. 9, pp. 146–151, 2018.

[104] R. Singh, N. Narang, D. Singh, and M. Gupta, "Compact wideband microstrip patch antenna design for breast cancer detection," *Def. Sci. J.*, vol. 71, no. 3, pp. 352–358, 2021.

[105] Q. Bai and R. Langley, "Textile PIFA antenna bending," *LAPC 2011 - 2011 Loughbrgh. Antennas Propag. Conf.*, no. November, pp. 1–4, 2011.

[106] A. Arif, M. Zubair, M. Ali, M. U. Khan, and M. Q. Mehmood, "A Compact, Low-Profile Fractal Antenna for Wearable On-Body WBAN Applications," *IEEE Antennas Wirel. Propag. Lett.*, vol. 18, no. 5, pp. 981–985, 2019.

[107] D. Sievenpiper, L. Zhang, R. F. Jimenez Broas, N. G. Alexöpolous, and E. Yablonovitch,

"High-impedance electromagnetic surfaces with a forbidden frequency band," *IEEE Trans. Microw. Theory Tech.*, vol. 47, no. 11, pp. 2059–2074, 1999.

[108] S. Zhu, "Wearable antennas for personal wireless networks," no. January, p. 164, 2008.

[109] F. Yang and Y. Rahmat-Samii, "Reflection Phase Characterizations of the EBG Ground Plane for Low Profile Wire Antenna Applications," *IEEE Trans. Antennas Propag.*, vol. 51, no. 10 I, pp. 2691–2703, 2003.

[110] G. Goussetis, A. P. Feresidis, and J. C. Vardaxoglou, "Tailoring the AMC and EBG characteristics of periodic metallic arrays printed on grounded dielectric substrate," *IEEE Trans. Antennas Propag.*, vol. 54, no. 1, pp. 82–89, 2006.

[111] S. E. S. Hakimi, "An Equivalent Circuit Model for Broadband Modified Rectangular Microstrip-Fed Monopole Antenna," pp. 1363–1375, 2014.

[112] E. F. Sundarsingh, S. Velan, M. Kanagasabai, A. K. Sarma, C. Raviteja, and M. G. N. Alsath, "Polygon-shaped slotted dual-band antenna for wearable applications," *IEEE Antennas Wirel. Propag. Lett.*, vol. 13, pp. 611–614, 2014.

[113] S. Yan, P. J. Soh, and G. A. E. Vandenbosch, "Low-profile dual-band textile antenna with artificial magnetic conductor plane," *IEEE Trans. Antennas Propag.*, vol. 62, no. 12, pp. 6487–6490, 2014.

[114] A. Afridi, S. Ullah, S. Khan, A. Ahmed, A. H. Khalil, and M. A. Tarar, "Design of dual band wearable antenna using metamaterials," *J. Microw. Power Electromagn. Energy*, vol. 47, no. 2, pp. 126–137, 2013.

[115] A. Mersani, L. Osman, and J. M. Ribero, "Performance of dual-band AMC antenna for wireless local area network applications," *IET Microwaves, Antennas Propag.*, vol. 12, no. 6, pp. 872–878, 2018.

[116] A. Arif, M. R. Akram, K. Riaz, M. Zubair, and M. Q. Mehmood, "Koch Fractal Based Wearable Antenna Backed with EBG Plane," *Proc. 2020 17th Int. Bhurban Conf. Appl. Sci. Technol. IBCAST 2020*, no. March, pp. 642–646, 2020.

[117] B. Bahaa Qas Elias, P. Jack Soh, A. Abdullah Al-Hadi, C. Hodgkinson, and S. K. Podilchak, "Design of a Compact Textile Crown Antenna Integrated with AMC for Wearable IoT Applications," *15th Eur. Conf. Antennas Propagation, EuCAP 2021*, pp. 1–4, 2021.

[118] S. M. Saeed *et al.*, "Wearable Flexible Reconfigurable Antenna Integrated With Artificial Magnetic Conductor," *IEEE Antennas Wirel. Propag. Lett.*, vol. 1225, no. c, pp. 1–4, 2017.

[119] H. Yalduz, B. Koç, L. Kuzu, and M. Turkmen, "An ultra-wide band low-SAR flexible metasurface-enabled antenna for WBAN applications," *Appl. Phys. A Mater. Sci. Process.*, vol. 125, no. 9, pp. 1–11, 2019.

[120] C. Mao, P. L. Werner, D. H. Werner, Di. Vital, and S. Bhardwaj, "Dual-polarized armband embroidered textile antenna for on-/off-body wearable applications," *2019 IEEE Int. Symp. Antennas Propag. Usn. Radio Sci. Meet. APSURSI 2019 - Proc.*, pp. 1555–1556, 2019.

[121] E. L. M. Wissem, I. Sfar, L. Osman, and J. M. Ribero, "A textile EBG-based antenna for future 5G-IoT millimeter-wave applications," *Electron.*, vol. 10, no. 2, pp. 1–12, 2021.

[122] V. P. Kudumu and V. S. P. Mokkapati, “Reduction of surface waves in arrays using uni-planar EBG,” *Int. J. Recent Technol. Eng.*, vol. 8, no. 3, pp. 8065–8069, 2019.

[123] H. Liu, Z. Li, X. Sun, and J. Mao, “Harmonic suppression with photonic bandgap And defected ground structure for a microstrip patch antenna,” *IEEE Microw. Wirel. Components Lett.*, vol. 15, no. 2, pp. 55–56, 2005.

[124] D. Sievenpiper, L. Zhang, R. F. J. Broas, E. Yablonovitch, and N. G. Alexopolous, “Corrections to ‘High-Impedance Electromagnetic Surfaces with a Forbidden Frequency Band,’” *IEEE Trans. Microw. Theory Tech.*, vol. 48, no. 4, p. 620, 2000.

[125] S. Zhu and R. Langley, “Dual-band wearable textile antenna on an EBG substrate,” *IEEE Trans. Antennas Propag.*, vol. 57, no. 4 PART. 1, pp. 926–935, 2009.

[126] S. Velan *et al.*, “Dual-band EBG integrated monopole antenna deploying fractal geometry for wearable applications,” *IEEE Antennas Wirel. Propag. Lett.*, vol. 14, no. c, pp. 249–252, 2015.

[127] B. P. Nadh, B. T. P. Madhav, and M. S. Kumar, “Design and analysis of dual band implantable DGS antenna for medical applications,” *Sadhana - Acad. Proc. Eng. Sci.*, vol. 44, no. 6, pp. 1–9, 2019.

[128] Q. Liu *et al.*, “Flexible, breathable, and highly environmental-stable Ni/PPy/PET conductive fabrics for efficient electromagnetic interference shielding and wearable textile antennas,” *Compos. Part B Eng.*, vol. 215, no. February, p. 108752, 2021.

[129] R. Sanchez-Montero, P. L. Lopez-Espi, C. Alen-Cordero, and J. A. Martinez-Rojas, “Bend and moisture effects on the performance of a U-shaped slotted wearable antenna for off-body communications in an industrial scientific medical (ISM) 2.4 GHz band,” *Sensors (Switzerland)*, vol. 19, no. 8, 2019.

[130] C. Hertleer, A. Van Laere, H. Rogier, and L. Van Langenhove, “Influence of Relative Humidity on Textile Antenna Performance,” *Text. Res. J.*, vol. 80, no. 2, pp. 177–183, 2010.

[131] and J. S. J. Hasan Shahariar1, Henry Soewardiman2, Clifford A. Muchler3, Jacob J. Adams3 and Ipt, “Porous Textile Antenna Designs for Improved Wearability,” *IOP Sci.*, no. 111, pp. 0–13, 2018.

[132] S. Kim and M. M. Tentzeris, “Parylene coated waterproof washable inkjet-printed dual-band antenna on paper substrate,” *Int. J. Microw. Wirel. Technol.*, vol. 10, no. 7, pp. 814–818, 2018.

[133] H. Z. Sheng Peng, “Design of Coplanar-Waveguide-Feed Antenna,” *Int. J. Eng. Res. Technol.*, vol. 4, no. 7, pp. 1171–1177, 2015.

[134] V. R. Keshwani, P. P. Bhavarthe, and S. S. Rathod, “Eight shape electromagnetic band gap structure for bandwidth improvement of wearable antenna,” *Prog. Electromagn. Res. C*, vol. 116, no. July, pp. 37–49, 2021.

[135] C. Wang, L. Zhang, S. Wu, S. Huang, C. Liu, and X. Wu, “A Dual-band Monopole Antenna with EBG for Wearable Wireless Body Area Networks,” *Appl. Comput. Electromagn. Soc. J.*, vol. 36, no. 1, pp. 48–54, 2021.